Effets des incertitudes et de la variabilité spatiale des propriétés des sols et des structures sur le dimensionnement des semelles filantes et des conduites enterrées

Saber Imanzadeh

HAL Id: tel-00803563
https://theses.hal.science/tel-00803563

Submitted on 10 Apr 2013

N° d'ordre : 4761

Thèse de Doctorat

Présentée à

L'UNIVERSITE BORDEAUX 1

ECOLE DOCTORALE DES SCIENCES PHYSIQUES ET DE L'INGENIEUR (ED 209)

Par

Saber IMANZADEH

Pour obtenir le grade de docteur

Spécialité: Mécanique

Effects of uncertainties and spatial variation of soil and structure properties on geotechnical design. Cases of continuous spread footings and buried pipes

Soutenue le 15 février 2013

Devant le jury composé de:

M. Pierre BREUL	Professeur - Université Blaise Pascal, Clermont-Ferrand	Rapporteur
M. Djamel NEDJAR	Professeur - Université des Science et de la Technologie d'Oran	Rapporteur
Mme Sylvie YOTTE	Professeur - Université de Limoges, Egletons	Présidente
M. Sidi Mohammed ELACHACHI	Maître de Conférences HDR - Université Bordeaux 1	Examinateur
M. Alain DENIS	Professeur - Université Bordeaux 1	Directeur de thèse
M. Antoine MARACHE	Maître de Conférences - Université Bordeaux 1	Co-directeur de thèse

Résumé:

Le sol présente une variabilité spatiale des propriétés physiques et mécaniques dont les effets sur des structures légères avec semelles filantes et sur les conduites enterrées ne sont pas bien pris en compte dans leur dimensionnement. Cette variabilité naturelle peut être très importante dans le cas de ces ouvrages car elle induit des tassements différentiels, dont les conséquences peuvent être dommageables : fissures dans les murs, les poutres ou encore des fuites dans les réseaux d'assainissement. La variabilité naturelle du sol et l'incertitude liée à la connaissance imparfaite des propriétés du sol et/ou du béton ou de l'acier de la structure sont les principales sources d'incertitude dans le choix des paramètres de calcul pour le dimensionnement de ces structures. Dans cette thèse, une approche analytique avec les méthodes probabilistes (FOSM et SOSM) et le modèle de Winkler, puis numérique avec le couplage de la méthode des éléments finis avec des approches géostatistiques ont été successivement menées pour modéliser le comportement des semelles filantes et des conduites enterrés lorsque les incertitudes sur les propriétés mécaniques du sol et de la structure sont prises en compte dans leur dimensionnement. Il apparait ainsi, l'importance du comportement longitudinal de ces ouvrages et du poids des incertitudes dans leur dimensionnement.

Mots clés: incertitude, variabilité spatiale, module de réaction du sol, semelle filante, conduite enterrée, interaction sol-structure, approches analytique et numérique, géostatistique.

Abstract:

Soil exhibits spatial heterogeneities resulting from the history of its deposition and aggregation processes that occur in different physical and chemical environments. This inherent or natural variability can be very important in the case of the superficial geotechnical works inducing differential settlements, whose consequences on structural response can be harmful: local failures, cracking in beams or walls, leakage in sewers. Natural variability of soil and uncertainty related to imperfect knowledge in soil properties and/or of concrete or steel of the structure, are the major source of uncertainty in the choice of the design parameters. In this thesis the probabilistic methods in geotechnical engineering, the analytical Winkler model and the coupling of the finite element method with geostatistical approaches were successively used to model the behavior of shallow foundations and buried pipe networks when soil and structure uncertainties are considered in their design.

Keywords: uncertainty, spatial variability, subgrade reaction modulus, spread footing, buried pipe, soil-structure interaction, analytical and numerical methods, geostatistic.

Acknowledgment

This thesis would not have been possible without the guidance and the help of several individuals who in one way or another contributed and extended their valuable assistance in the preparation and completion of this study; to only some of whom it is possible to give particular mention here.

By participating in the European exchange project of ERASMUS MUNDUS EM8, I had a chance to meet and have discussion with Prof. Alain Denis, Prof. Denys Breysse and Dr. Antoine Marache. From there, they offered me to do the interesting PhD research. As this thesis, finally, met its end, I would like to extend my deep appreciation to the people that made this possible.

First and foremost, I would like to express my sincerest gratitude to my supervisor Alain Denis and my co-supervisor Dr. Antoine Marache for the continuous support of my PhD study and research, for their patience, motivation, enthusiasm, and immense knowledge. Their guidance helped me in all the time of research and writing of this thesis and their encouragement gave me a strong motivation to learn the French language. They taught me how to question thoughts and express ideas. I hope that one day I would become as good an advisor to my students as they have been to me. I could not imagine anyone else as better advisors and mentors for my PhD study other than them.

I would like to thank the jury members for their willing review, valuable and helpful suggestions to improve my thesis.

Special thanks as well to Prof. SylvieYotte, Dr. Sidi-Mohammed Elachachi and Dr. Halidou Niandou. Their help and good ideas were always useful and constructive. They gave me lots of positive energy and during difficult parts of the work they were a real support.

During these three years of living in France and working in GCE department of Bordeaux University which was full of ups and downs, I met many friends and colleagues. Their support and care helped me overcome setbacks and stay focused on my thesis. I greatly value their friendship and I deeply appreciate their belief in me.

And most importantly, I am thanking my parents. They brought me forth, raised me, supported me, taught me, loved me and still loving me. To them I whole-heartedly dedicate this thesis.

Lastly, I offer my regards and blessings to all of those who supported me in all respect during the completion of my thesis.

Saber Imanzadeh
February 2013

Table of contents

List of tables

List of figures

Résumé étendu en français

Résumé étendu en français

Les propriétés physiques et mécaniques d'un sol présentent toutes des hétérogénéités spatiales dont l'origine vient de la complexité des processus géologiques naturels mis en jeu (érosion, transport, dépôt, compaction, transformation physico-chimique…) qui mènent à la constitution d'un sol. A cette variabilité se rattache une incertitude sur chacun des paramètres usuellement utilisés pour quantifier la variabilité naturelle: moyenne, variance et fonction de covariance dans le cas d'une approche spatialisée de la variabilité naturelle. Ces incertitudes existent également dans le cas des matériaux de structure.

La variabilité naturelle des propriétés mécaniques des sols de fondations peut être, dans le cas des ouvrages géotechniques superficiels tels que des semelles filantes pour les bâtiments légers ou des conduites enterrées (en béton et en acier) à faible profondeur, à l'origine de tassements différentiels dont les conséquences peuvent être dommageables: fissures dans les murs et les poutres ou fuites dans les réseaux d'assainissement.

Dans les calculs usuels de dimensionnement de ces ouvrages géotechniques superficiels, le comportement n'est modélisé que dans une section droite pour représenter le comportement transversal de l'élément de structure où l'hétérogénéité (variabilité spatiale) et les incertitudes sur les paramètres de calcul ne sont pas prises en compte.

L'objectif principal de cette thèse est d'étudier, en considérant le comportement longitudinal des semelles filantes et des conduites enterrées, l'influence des incertitudes des paramètres de calcul et de la variabilité spatiale des propriétés du sol sur le dimensionnement de ces ouvrages. Le modèle de Winkler a été choisi comme modèle d'interaction sol-structure. Ce modèle, d'un point de vue pratique, est approprié pour le dimensionnement des ouvrages géotechniques superficiels. Il a l'avantage de ne prendre en compte qu'un seul paramètre (coefficient de réaction du sol k_s) pour caractériser les réponses d'un sol élastique et de la structure sous chargement. Grâce à sa simplicité, le modèle de Winkler a été largement utilisé pour résoudre de nombreux problèmes d'interaction sol-structure et a donné des résultats satisfaisants pour de nombreux problèmes pratiques. Le coefficient de réaction du sol (k_s) n'est pas un paramètre intrinsèque du sol, il dépend de plusieurs paramètres (paramètres mécaniques du sol et de la structure, paramètres géométriques de la structure) qui possèdent chacun des incertitudes propres et qui sont la source majeure des incertitudes sur le coefficient de réaction.

Les objectifs spécifiques de notre recherche sont les suivants:

- Modélisation de l'interaction sol-structure dans la direction longitudinale des ouvrages superficiels en prenant en compte les incertitudes sur les paramètres du sol et de la structure afin de déterminer les incertitudes sur le tassement différentiel et le moment fléchissant. Cela nous permettra d'effectuer une analyse de sensibilité, une analyse probabiliste et une analyse globale de l'incertitude,

- Etude de l'effet de la variabilité spatiale des propriétés du sol sur le comportement des ouvrages superficiels à partir de données expérimentales issues d'un site d'étude,

- Application de la méthodologie aux ouvrages superficiels.

Afin de répondre à ces objectifs, des méthodes probabilistes (First Order Second Moment (FOSM) et Second Order Second Moment (SOSM)) appliquées au modèle de Winkler et des approches numérique et géostatistique (couplage de la méthode des éléments finis avec l'approche géostatistique) ont été utilisées pour modéliser le comportement longitudinal des semelles filantes et des conduites enterrées lorsque les incertitudes sur les paramètres mécaniques et géométriques sont prises en compte dans leur dimensionnement.

Huit modèles semi-empiriques, qui donnent la valeur du coefficient de réaction du sol, sont étudiés en prenant en compte les incertitudes sur les paramètres du sol et de la structure. Les méthodes FOSM et SOSM sont utilisés à partir de ces modèles semi-empiriques pour déterminer le coefficient de variation du module de réaction du sol. Les résultats obtenus avec la méthode FOSM pour les semelles filantes montrent l'effet majeur des incertitudes du module d'Young du sol, de la largeur de la semelle filante et du coefficient de Poisson du sol sur l'incertitude du coefficient de réaction du sol. Dans le cas des conduites enterrées en acier et en béton les paramètres les plus influents sur l'incertitude du module de réaction du sol sont le module d'Young du sol, le diamètre de la conduite et le coefficient de Poisson du sol. L'utilisation de la méthode SOSM n'apportant pas une précision significative par rapport à la méthode FOSM, l'utilisation unique de cette dernière apparaît suffisante pour estimer de manière satisfaisante l'incertitude sur le coefficient de variation de k_s. Pour chacun des modèles semi-empiriques, des expressions simplifiées peuvent être proposées en prenant en compte le minimum de paramètres pour

une détermination du coefficient de variation de k_s. Ces différentes expressions peuvent permettre aux praticiens d'estimer simplement et rapidement l'incertitude du module de réaction du sol.

Dans l'approche analytique, l'incertitude de k_s, obtenue en utilisant les expressions simplifiées, est introduite dans le modèle analytique de Winkler (sans prendre en compte les variabilités spatiales des paramètres du modèle d'interaction sol-structure). L'influence de l'incertitude de k_s sur le tassement différentiel et le moment fléchissant est étudiée à partir de l'utilisation de la méthode FOSM sur la solution analytique du modèle de Winkler selon différentes conditions limites.

Les résultats obtenus avec la méthode FOSM pour les semelles filantes montrent que les incertitudes du tassement différentiel et du moment fléchissant sont très différentes en fonction de la longueur de la semelle filante et des conditions limites considérées. Pour le tassement différentiel et le moment fléchissant, les résultats obtenus concernant la probabilité de l'état limite de service montrent l'importance du choix du modèle semi-empirique et des conditions limites. Lorsque les incertitudes sur les valeurs du coefficient de réaction du sol sont importantes, la probabilité correspondant à l'état limite de service peut être dépassée même pour des sols possédant de bonnes caractéristiques mécaniques.

Les résultats obtenus dans le cas des conduites enterrées (en acier et en béton) montrent, dans un premier temps, que les incertitudes du tassement différentiel et du moment fléchissant sont très différentes en fonction de la longueur de la zone de faibles propriétés mécaniques du sol se situant en dessous de la conduite enterrée et de la valeur du module d'Young du sol. Dans un deuxième temps, les incertitudes du tassement différentiel et du moment fléchissant sont plus influencées par l'incertitude de la longueur de la zone de faibles propriétés mécaniques du sol que par l'incertitude du module de réaction du sol. Cela met en évidence que cette longueur de la zone de faibles propriétés mécaniques du sol est aussi importante à caractériser que les propriétés propres du sol lui-même. Ceci montre tout l'intérêt de réaliser une bonne reconnaissance de sol pour estimer au mieux la longueur d'une zone de faibles propriétés mécaniques du sol présente sur un site de construction.

Dans le cas où le choix d'un modèle semi-empirique approprié pour l'estimation de l'incertitude sur k_s est difficile, une approche globale de l'incertitude est proposée. Cette approche inclue les incertitudes de chaque modèle semi-empirique et peut être utilisée pour

vérifier si les valeurs maximales du tassement différentiel ou du moment fléchissant excèdent les valeurs de l'état limite de service.

Une comparaison de la méthode FOSM avec des simulations à partir de la méthode de Monte Carlo a été réalisée en vue de valider la méthode FOSM pour ce genre d'analyse. On montre que cette méthode est bien adaptée à l'étude de ce type problème et qu'elle pallie certains des défauts de la méthode de Monte Carlo.

Dans l'approche analytique proposée, la variabilité spatiale du module d'Young du sol n'a pas été prise en compte. Afin de prendre en compte cette variabilité, il est proposé de coupler la méthode des éléments finis avec l'approche géostatistique. Cette application a été réalisée à partir de mesures faites sur un site réel de 25000 m^2 pour lequel nous disposons de 12 forages pressiométriques (donnant 12 valeurs de module pressiométrique) et de 272 valeurs de résistivité électrique du sol. Les 12 valeurs de module pressiométrique n'étant pas suffisantes en nombre pour obtenir une carte satisfaisante de ce paramètre, l'utilisation de la méthode de cokrigeage colocalisé a été employée afin d'utiliser les informations géophysiques pour l'estimation du module du sol (une relation physique existant entre résistivité et module du sol) sur une grille à maille 10*10 m². Cette taille de maille étant trop grande pour une modélisation éléments finis d'une structure comme une fondation, des simulations conditionnelles ont été effectuées afin d'obtenir n cartes de module (pour un même modèle de structuration spatiale) avec une maille de 0,5*0,5 m². A partir de ces réalisations, l'étude du comportement de trois semelles filantes (longueur de dix mètres) et d'une conduite enterrée (longueur de cent mètres) localisées sur le site d'étude a été conduite par la méthode des éléments finis afin d'obtenir les tassements différentiels et les moments fléchissants correspondants pour les n simulations conditionnelles. Le post-traitement statistique des résultats permet d'obtenir des probabilités d'occurrence et de prendre des décisions quant au dimensionnement des structures.

Une comparaison des résultats obtenus par ces approches numérique et géostatistique avec l'approche analytique est ensuite réalisée. Elle montre l'influence importante de la variabilité spatiale du module du sol sur l'incertitude du tassement différentiel et du moment fléchissant pour des semelles filantes et des conduites enterrées.

L'ensemble des résultats montre que le comportement longitudinal des ouvrages superficiels comme des semelles filantes et des conduites enterrées nécessiterait d'être pris

en compte dans leur dimensionnement dès lors que la présence de zones de faibles propriétés mécaniques ou une variabilité spatiale des propriétés mécaniques des sols de fondations est supposée sur un site de construction.

Introduction

Introduction

Soil exhibits spatial heterogeneities resulting from the history of its deposition and aggregation processes, which occur in different physical and chemical environments. This inherent or natural variability can be very important in the case of superficial geotechnical works inducing differential settlements, which can have harmful consequences on the structure. For example in individual houses with continuous spread footings, damage can range from sticking doors and hairline plaster cracks to complete destruction. In the case of continuous buried steel or concrete pipes, such as sewer networks or oil and gas transmission networks, these differential settlements can induce cracking and consequently liquid leakages which, in their turn, by modifying the characteristics of the surrounding medium, can induce additional settlements. Moreover, when there is a crack in a buried waste water pipe, there is a tendency for the water outside the pipe (underground water) to enter. This will then be added to waste water, increasing the cost of treatment processes.

In a conventional design, geotechnical systems are always designed on the basis of the deterministic approaches and modeled in a cross section to represent the transverse behavior of the structural element (spread footings and buried pipes), where the heterogeneity of soil in their longitudinal directions is usually not considered. These effects need to be taken into account and studied in order to perform an accurate analysis leading to a correct design, which is the main topic of this work.

In this thesis we are interested in studying the influence of soil heterogeneity and uncertainties in structural parameters on the longitudinal behavior of these superficial geotechnical designs (continuous spread footing and continuous buried steel or concrete pipes). We will go on to determine how uncertainties in the mechanical properties of soil and structure are propagated on the uncertainties of differential settlement and bending moment.

First, a constitutive model has to be chosen. Two questions need to be answered to justify this choice, particularly for geomaterials:

1- When considering the particular class of engineering problem under study, is the model accurate enough in reproducing mechanical behavior?

2- Using the available experimental data, is it possible to carry out a satisfactory calibration of the material parameters of the model?

To answer the first question a systematic study of different classes of engineering problems would be required. It is not easy to find such studies in the technical literature. In recent years some analyses have been performed in order to assess the capability of many classes of constitutive models to predict, for example, exact ground movements around excavations.

The second question is much more difficult. Experimental tests in situ or in a laboratory are expensive; therefore, it is often difficult to find the reliable measurements or test data that would be used to carry out a proper identification of the constitutive parameters using the FEM and a massive soil model such as Mohr-Coulomb or Cam-Clay.

Because of these complex constitutive models and the difficulty of obtaining experimental data, Winkler's analytical approach is used to model the soil-structure interaction, instead of modeling the subsoil in all its complexity, which seems, from a practical point of view, to be appropriate for superficial geotechnical designs. Thanks to its simplicity and with the advantage of taking into account only one parameter (the coefficient of subgrade reaction) to characterize elastic soil and structure responses under loading, the Winkler model has been extensively used to solve many soil-structure interaction problems and has given satisfactory results for many practical problems. The soil reaction modulus is not an intrinsic parameter of soil; it depends on the mechanical parameters of soil and mechanical and geometrical parameters of the structure. All of these parameters are uncertain and represent the major source of uncertainty in the output model.

The specific objectives of our research are as follows:

- model the soil-structure interaction along the longitudinal direction of the superficial geotechnical systems by taking into account the uncertainties of soil and structure parameters in order to estimate the uncertainty in differential settlement and bending moment,
- propose a simplified approach for uncertainty analysis,
- understand the effects of inherent random soil spatial variability on the behavior of these geotechnical systems using data from a real construction site.

In order to satisfy these objectives, we use probabilistic methods (FOSM, SOSM) with Winkler's model and a numerical approach that couples the finite element method with

geostatistical methods in order to model the longitudinal behavior of continuous spread footings and buried pipes when uncertainties of mechanical and geometrical parameters are taken into account in their design.

Chapter 1 presents the main concepts of uncertainties in geotechnical designs. In order to prevent any misunderstanding or confusion in the following parts of this thesis, the main modeling method of spatial variability (basic random variables, random field theory and geostatistics) will be precisely defined to prepare for the use of geostatistics in chapter 4. The tools and techniques of probabilistic methods used in geotechnical engineering for propagating uncertainty will be introduced. We will introduce the soil-structure interaction concept and the different analytical models that take it into account along with their advantages and drawbacks. Finally, we will describe the superficial geotechnical systems studied in this thesis.

In Chapter 2, the modulus of subgrade reaction k_s and its uncertainty are explained in detail. The chapter begins by explaining the modulus of soil reaction and suggested expressions or semi-empirical models used to determine this modulus as a function of the studied applications. After explaining the nature and origin of uncertainties, the first order (FOSM) and the second order (SOSM) of the Taylor series are developed in order to estimate the influence of soil and structure parameters on the coefficient of variation of k_s. Finally, we propose simplified equations that compute the coefficients of variation of k_s in the case of spread footings and buried pipes. These simplified models will be used in the following chapters.

In Chapter 3, we discuss the effect of the uncertainty of the subgrade reaction modulus and the existence of a low stiffness zone on the behavior of the superficial geotechnical works. Reliability analyses for a continuous spread footing and a buried steel or concrete pipe are presented in order to avoid exceeding the serviceability limit state. A simplified uncertainty analysis is proposed. Finally, a comparison between FOSM and Monte Carlo analysis results is performed to validate the use of the FOSM method.

Chapter 4 focuses on the application of this methodology to a real construction site. Settlements, bending moments and their uncertainties are obtained by geostatistical approaches coupled with the finite element method in order to perform a statistical analysis that describes the behavior of superficial geotechnical designs. Finally a comparison between analytical and numerical results for these superficial geotechnical systems is

performed to show that the spatial variability of soil properties adds a significant part of uncertainty in differential settlements and bending moments. A general conclusion and future research directions are provided in Chapter 5.

Chapter 1

Dealing with uncertainties in

geotechnical designs

1. Dealing with uncertainties in geotechnical designs

1.1. Uncertainties in geotechnical designs

Most of the parameters used in geotechnical analyses, physical and soil mechanical properties, are uncertain. Therefore an essential but new aspect of geotechnical engineering is to deal with uncertainty. In fact, the uncertainties can usually be divided into two groups: aleatory or active uncertainty and epistemic or passive uncertainty (Lacasse and Nadim, 1996; Uzielli et al., 2008). Aleatory uncertainty mainly includes natural variability of a property (spatial and temporal variability).The knowledge of experts cannot be expected to reduce this uncertainty although their knowledge may be useful in quantifying the uncertainty. Thus, this type of uncertainty is sometimes referred to as irreducible uncertainty. Epistemic uncertainty consists of statistical uncertainty, model uncertainty and measurement uncertainty (possible differences between the measured and true, but unknown, values of the relevant parameter), which are all classified as a type of uncertainty associated with limited, insufficient or imprecise knowledge. This uncertainty can, in theory, be reduced by obtaining additional information on the process to be modeled on the measured variable or by increasing the number of data in order to reduce the statistical uncertainty. Epistemic uncertainty leads to unawareness or ignorance of the potential risks for the foreseen constructions (Phoon and Kulhawy, 1999a, 1999b; Baecher and Christian, 2003).

Engineering judgment and reliance on factors of safety have been the conventional tools for dealing with soil heterogeneity in geotechnical practice and then the geotechnical engineer tries to deal with the uncertainties by choosing reasonably conservative parameters for the deterministic stability evaluation (Griffiths & Fenton, 2007). However in this approaches, variability is not addressed explicitly as in uncertainty-based approaches.

Recent theoretical developments and advances in probabilistic methods and computational methods have improved uncertainty analysis in geotechnical and related fields. The characterization and reduction of uncertainties is still an area where only few researchers have worked until a few years ago, even though as early as 1982 Einstein and Baecher stated the following words of wisdom:

In thinking about sources of uncertainty in engineering geology, one is left with the fact that uncertainty is inevitable. One attempts to reduce it as much as possible, but it must ultimately be faced. It is a well recognized part of life for the engineer. The question is not whether to deal with uncertainty, but how?

Combining actual data, knowledge about the quality of the data, knowledge on the geology and, most importantly, engineering judgment help the engineer to evaluate the uncertainty.

The geotechnical engineer processes testing data to obtain parameters for characterization and design. In geotechnical works, there are lack of information in quantity and accuracy. Geomaterials, moreover, are naturally complex and variable at all scales, ranging from the microstructure to regional scale. This lack of uniformity and information must be considered in parameterizing and modeling. Furthermore the level of explicitness with which this occurs depends upon the selected approach.

In the technical literature and geotechnical engineering is no exception- the terms variability and uncertainty are often employed interchangeably. Variability is an observable manifestation of heterogeneity of one or more physical parameters and/or processes. Uncertainty pertains to the modeler state of knowledge and strategy, and reflects the decision to recognize and address the observed variability in a qualitative or quantitative manner (Huang and An-bin, 2008).

Deterministic methods lie at the basis of virtually every technological science, and geotechnical engineering doesn't make exception. However, the importance of explicitly modeling and assessing the variability of geotechnical parameters (i.e. quantifying, processing and reporting the associated uncertainty) is increasingly recognized in geotechnical design and characterization. Most evolutionary design codes operate in an uncertainty-based perspective, requiring explicit quantification not only of most suitable values (usually termed characteristic or nominal), but also of the level of uncertainty and confidence in the selection of such values.

The progressive shift towards an uncertainty-based perspective may be motivated by the fact that this may be more convenient in terms of safety, performance and costs. Providing more complete and realistic information regarding the level of risk associated with design will be possible by the explicit parameterization of uncertainty. Addressing uncertainty does not in itself increase the level of safety, but allows the engineer to rationally calibrate

his decisions on desired or required reliability or performance level of geotechnical system. Being able to select the performance level and reduce undesired conservatism, in turn, is generally beneficial in the economic sense. The results of uncertainty-based analyses can be used confidently for engineering purpose only if preceded, accompanied and followed by geotechnical expertise and expert judgment.

The techniques commonly used to analyze geotechnical data, and to estimate its uncertainties, include traditional probabilistic and statistical methods (Einstein and Baecher, 1983; Emeriault et al., 2004; Dubost et al., 2007; Villavicencio et al., 2011), spatial statistical methods, such as that based on random field theory (Vanmarcke, 1980, 1983), and geostatistics (Chilès and Delfiner, 1999; Mendes and Lorandi, 2008; Marache et al., 2009a, Bourges et al., 2012). Numerous finite element studies have been carried out in understanding the effect of uncertainty on the stability of geotechnical systems. For example, Fenton et al. (2005) and Zevgolis and Bourdeau (2010) analyzed the reliability of a retaining wall, Elachachi et al. (2004, 2011, 2012) and Buco et al. (2006, 2008a, 2008b) studied soil–pipe interactions. Park et al. (2005) and Srivastava et al. (2010) studied rock and soil slope stability respectively. Niandou and Breysse (2007) carried out reliability analysis of a piled raft. Dubost et al. (2011) analyzed soil-pile interaction. Foundation settlements on spatially random soil have been studied by Fenton and Griffiths (2002) and Srivastava and Sivakumar Babu (2009). Note that in these numerical studies, mostly the variability in the transverse direction of the structure elements is considered.

Analytical approaches can also be used to study the effect of uncertainty on the stability of geotechnical systems (Houy et al., 2005; Deck and Singh, 2012).

This chapter provides general information to quantify and integrate the uncertainties into the geotechnical designs concerning the modeling of soil properties: basic random variables, random field theory and geostatistics, the most commonly probabilistic methods in geotechnical engineering: Taylor series approach, Monte Carlo simulation and reliability based design. Finally, soil-structure interaction and chosen superficial geotechnical designs are introduced.

1.2. Modeling of soil properties

Soils are geological materials formed by weathering processes and, save for residual soils, transported by physical means to their present locations. They have been subject to various stresses, pore fluids, and physical and chemical changes. Thus, it is hardly surprising that the physical properties of soils vary from place to place within resulting deposits. The scatter observed in soil data comes both from this natural spatial variability and from errors in testing. Each of these exhibits a distinct statistical signature, which can be used to draw conclusions about the character of a soil deposit and about the quality of testing. In the following, we consider different approaches to modeling of soil properties: basic random variables, random field theory and geostatistical approaches.

1.2.1. Basic random variables

Here, we will introduce a tool that is useful for evaluating the probability of an event: the random variable. First, we will provide graphical and numerical methods to represent understand and quantify variability. Next, we will present the random variable as a theoretical tool for modeling variability. Finally, common models for continuous random variables are breifly introduced.

1.2.1.1. Graphical analysis of variability

Variability often leads to uncertainty. In the following, we will briefly present five graphical methods for analyzing variability: histograms, frequency plots, frequency density plots and cumulative frequency plots.

Histogram: A histogram is obtained by dividing the data range into bins, and then counting the number of values in each bin. The histogram conveys important information about variability in the data set. It shows the range of the data, the most frequently occurring values, and the amount of scatter about the middle values in the set.

Frequency plot: The frequency of occurrence in each histogram interval is obtained by dividing the number of occurrences by the total number of data points. A bar-chart plot of the frequency of occurrence in each interval is called a frequency plot. Note that the histogram and frequency plots have the same shape and convey the same information. The frequency plot is simply a normalized version of the histogram. Because it is normalized, the frequency plot is useful in comparing different data sets.

Frequency density plot: Another plot related to the histogram is the frequency density plot. The frequency density is obtained by dividing the interval frequencies by the interval widths. A bar-chart plot of the frequency density is called the frequency density plot. The objective in dividing the frequency by the interval width is to normalize the histogram, further the area below the frequency density plot (obtained by multiplying the bar heights by their widths) is equal to 100%. This normalization will be useful in fitting theoretical random variable models to the data.

Cumulative frequency plot: The cumulative frequency plot is the final graphical tool that we present for variability analysis. Cumulative frequency is the frequency of data points that have values less than or equal to the upper bound of an interval in the frequency plot. The cumulative frequency is obtained by summing up (or accumulating) the interval frequencies for all intervals below the upper bound. A plot of cumulative frequency versus the upper bound is called the cumulative frequency plot.

1.2.1.2. Quantitative Analysis of Variability

In addition to graphical analyses, the variability in a data set can also be analyzed quantitatively. The statistics of a data set (also known as the sample statistics where the data set is the sample) provide quantitative measures of variability. Features of interest include the central tendency of the data, dispersion or scatter in the data, skewness and kurtosis in the data and correlation or dependence between data points.

- **Central Tendency**

The most common measure for the center of a data set is the average value, which is also called the sample mean. The sample mean is obtained as follows (Equation 1-1):

$$\mu_x = \frac{1}{n}\sum_{i=1}^{n} x_i$$

Equation 1-1

where μ_x is the sample mean x_i is each data value, and n is the total number of data points.

- **Dispersion or Scatter**

The amount of scatter in a data set is most easily measured by the sample range. The maximum value in the data set minus the minimum value is defined as sample range. A

measure of dispersion around the mean value of the data set is defined as the sample variance. The sample variance is obtained as follows (Equation 1-2):

$$\sigma_x^2 = \frac{1}{n-1}\sum_{i=1}^{n}(x_i - \mu_x)^2$$

Equation 1-2

where σ_x^2 is the sample variance. The sample variance is the average of the square of the distance between individual data points and the sample mean. Its value will always be greater than or equal to zero.

The square root of the sample variance is defined as the sample standard deviation σ_x while the sample coefficient of variation *CV* is the standard deviation divided by the mean value (Equation 1-3):

$$CV = \frac{\sigma_x}{\mu_x}$$

Equation 1-3

Since the standard deviation has the same units as the mean value, the coefficient of variation is a dimensionless measure of dispersion.

- **Skewness and Kurtosis**

Skewness is a measure of distributional asymmetry. Conceptually, skewness describes which side of a distribution has a longer tail. A skewness coefficient of zero means that the data values are distributed symmetrically about the mean value (distribution is perfectly Gaussian). A positive skewness coefficient indicates that the data are skewed about the mean to the right (toward larger values) while a negative skewness coefficient indicates that the data are skewed to the left (toward smaller values).

The term kurtosis refers to the degree to which a curve is peaked or flat. A Kurtosis coefficient for the Gaussian distribution is equal to three.

Skewness and kurtosis will be used for the second order second moment (SOSM) in the ensuing sections.

1.2.1.3. Theoretical random variable models

A random variable is a mathematical model to represent a quantity that varies. Specifically, a random variable model describes the possible values that the quantity can

take on and the respective probabilities for each of these values. Since the frequency plot for a data set indicates the probability of different values occurring, a random variable model is just a mathematical representation of the information contained in a frequency plot.

For two reasons a theoretical random variable model is needed to describe a data set: first, a data set is limited in size and second, in most engineering problems we are interested in combinations of variable quantities. For example, a pile foundation will undergo large displacements if the applied load exceeds the pile capacity. We need to consider variability both in the load and the capacity to design this foundation. Random variable models provide a mathematical framework for working with and combining multiple quantities that vary.

Discrete and continuous models for random variables are discussed in the following sections.

- **Discrete random variables**

Discrete random variables can only take on discrete values within the sample space. The probability mass function (PMF) for a discrete random variable (X) is denoted by the following mathematical form for notational convenience:

$$P[X = x] = p_X(x)$$

Equation 1-4

The cumulative distribution function (CDF) describes the probability that the random variable takes on a value less than or equal to a given value. It is obtained as follows (Equation 1-5):

$$F_X(x) = P[X \leq x] = \sum_{all\ x_i \leq x} p_X(x_i)$$

Equation 1-5

The mean value is an important tool when working with random variables. The expectation of a quantity is the weighted average of that quantity, where the possible values are weighted by their corresponding probabilities of occurrence. For example, the expected value of X, denoted *E[X]*, is given by the following (Equation 1-6):

$$E[X] = \sum_{all\ x_i} x_i\, p_X(x_i)$$

Equation 1-6

Note that the mean of X is equal to its expected value E[X]. The expected value of any function of X, denoted *g(X)*, can be obtained similarly (Equation 1-7):

$$E[g(X)] = \sum_{all\ x_i} g(x_i) p_X(x_i)$$

Equation 1-7

Similarly, the variance is obtained as follows (Equation 1-8):

$$\sigma_X^2 = \sum_{all\ x_i} (x_i - \mu_X)^2 \cdot p_X(x_i)$$

Equation 1-8

where σ_X is the standard deviation of X.

- **Continuous random variables**

Continuous random variables can take on any value within the sample space. Total unit weight is an example of a continuous random variable; it can take on any value greater than zero. The probability density function (PDF) for a continuous random variable describes its probability distribution.

While the PDF is similar to the PMF in the information that it conveys, there is significant difference in these two functions. For a continuous random variable, there is infinite number of possible values within the sample space. Hence, unlike a discrete random variable, it is not possible to define the probability of the event that X is equal to a given value x, since this probability is vanishingly small. Instead, we can define the probability that X is within a very small interval. This probability is proportional to the PDF.

The cumulative distribution function (CDF) for a continuous variable describes the probability that the variable takes on a value less than or equal to a given value. It is obtained as follows (Equation 1-9):

$$F_X(x) = P[X \le x] = \int_{-\infty}^{x} f_X(\xi)d\xi$$

Equation 1-9

Note that the CDF is the area under the PDF. Since the probability of the sample space is equal to 1.0, the area under the PDF must equal 1.0. Recall that the area under a frequency density plot for a data set is also equal to 1.0. Therefore, theoretical PDFs can be fit to model a data set by overlaying a theoretical PDF on top of a frequency density plot.

The expectation for a continuous random variable is defined in the same way as for a discrete random variable; it is a weighted average, in which values are weighted by their likelihood. However, since there are an infinite number of possible values in the sample space, the process of summing up values weighted by their likelihoods is an integration (Equation 1-10):

$$E[X] = \int_{-\infty}^{\infty} x f_X(x)dx$$

Equation 1-10

Similarly, variance, skewness and kurtosis for a continuous random variable are found as follows:

$$\sigma_X^2 = E\left[(X - \mu_X)^2\right] = \int_{-\infty}^{\infty} (x - \mu_X)^2 f_X(x)dx$$

Equation 1-11

$$Skewness = \frac{E\left[(X - \mu_X)^3\right]}{\sigma_X^3} = \frac{\int_{-\infty}^{\infty} (x - \mu_X)^3 f_X(x)dx}{\sigma_X^3}$$

Equation 1-12

$$Kurtosis = \frac{E\left[(X - \mu_X)^4\right]}{\sigma_X^4} = \frac{\int_{-\infty}^{\infty} (x - \mu_X)^4 f_X(x)dx}{\sigma_X^4}$$

Equation 1-13

1.2.1.4. Common models for continuous random variables

Different probability distribution models such as normal, lognormal, beta, uniform, triangular, exponential, Weibull and gamma have been implemented by different authors to curve fit the results of field data. This implies that these distributions are probably site and parameter specific and that there is no generic distribution pattern for soil properties. Where observations are scarce or absent, parametric distributions can be assumed from the literature. Studies have estimated coefficients of variation and probability density functions of soil properties (Lumb 1966; Chowdhury 1984; Harr 1987; Kulhawy et al. 1991; Lacasse and Nadim 1996). Based on several studies reported in the literature, soil properties can follow different probability distribution functions (PDF's) for different types of soils and sites. Furthermore in the reliability analysis, the input soil parameters are modeled as continuous random variables defined by their probability density functions (PDFs) and the parameters of distributions.

Care should be exercised, however, to ensure that the minimum and maximum values of the selected distribution are consistent with the physical limits of the parameter being modeled. For example, shear strength parameters should not take negative values. If the selected distribution implies negative values, then the distribution is truncated at a practical minimum threshold.

Jimenez et al. (2009) have investigated the effects of using different types of statistical distributions (lognormal, gamma, and beta) to characterize the variability of Young's modulus of soils in random finite element analyses of shallow foundation settlement. Results indicated the type of distribution considered for characterization of the random field of Young's modulus could have a significant impact on computed settlement results.

Usually, in geotechnical practice, the input soil parameters are either modeled as normally distributed or log-normally distributed continuous random variables (Baecher and Christian, 2003). The parameters of the normal and lognormal probability distribution function (PDF) are directly related to the unbiased estimates of statistical moments i.e. sample mean and variance of the measured data set. These two distributions will be used in this study. They are briefly discussed in this following.

- **Normal Distribution**

The normal distribution (also known as the Gaussian distribution) is the classic bell-shaped curve that arises frequently in data sets. The probability density function of a normal random variable is defined by Equation 1-14:

$$f_X(x) = \frac{1}{\sigma_X \sqrt{2\pi}} e^{\frac{-1}{2}\left(\frac{x-\mu_X}{\sigma_X}\right)^2} \qquad -\infty \langle x \langle +\infty \qquad\qquad \textit{Equation 1-14}$$

In which μ_X is mean value and σ_X is standard deviation. The normal distribution has several interesting properties. First, it is a symmetrical distribution (skewness is zero for a normal distribution). Secondly, its tails decay in an exponential manner. There is a 68% chance that a normal variable will be within ±1 standard deviation from the mean value, a 95% chance that it will be within $\mu_X \pm 2\sigma_X$, and a 99.7% chance that it will be within $\mu_X \pm 3\sigma_X$. Therefore, it is very unlikely (less than 1% chance) to observe a value outside of 3 standard deviations from the mean value. The two-parameter normal distribution has theoretically a range from -∞ to +∞. Since geotechnical parameters should not take negative values, a normal distribution truncated below zero is a more suitable assumption. Finally, a linear function of a normally distributed variable also has a normal distribution. It can be shown that a linear combination of normal random variables, have normal distributions. If $Y=aX+b$ and X has a normal distribution, then Y also has a normal distribution with mean $\mu_Y = a\mu_X + b$ and standard deviation $\sigma_Y = a\sigma_X$.

- **Lognormal Distribution**

The lognormal distribution has often been suggested in lieu of the normal distribution, which is in engineering science widely used for the description of random material parameters. Since the lognormal distribution ranges between zero and infinity, skewed to the low range, and is therefore particularly suited to parameters that cannot take negative values (Limpert et al. 2001). The probability density function of a lognormal random variable is defined by assuming the natural logarithm of the random variable as normally distributed (Equation 1-15):

$$f_X(x) = \frac{1}{x\sigma_{ln\,X}\sqrt{2\pi}}\,e^{\frac{-1}{2}\left(\frac{ln\,x - \mu_{ln\,X}}{\sigma_{ln\,X}}\right)^2} \qquad x \geq 0$$

Equation 1-15

Lognormal distribution has simple relationship with normal distribution (Fenton and Griffiths 2003). Once the mean and standard deviation are expressed in terms of the dimensionless coefficient of variation (CV), defined as $CV = \sigma_X/\mu_X$ then the distribution parameters μ_{lnX} and σ_{lnX} can be obtained from the mean value X and the variance σ_X^2 as (Equation 1-16):

$$\sigma_{ln\,X} = \sqrt{ln\{1 + CV_X^2\}}, \qquad \mu_{ln\,X} = ln\,\mu_X - 0.5\sigma_{ln\,X}^2$$

Equation 1-16

The distribution parameters μ_{lnX} and $\sigma_{ln\,X}^2$ are respectively equivalent to the mean value and variance of the logarithmised observations, which are assumed to be normally distributed.

The lognormal distribution has been widely employed to model variations of the Young's modulus of soils (Paice et al. 1996; Nour et al. 2002; Fenton et al. 2005). This choice is motivated by the fact that the elastic modulus is a positive parameter, and the lognormal distribution enables analyzing its large variability.

1.2.2. Random field theory and geostatistics

Generally, four mathematical techniques are used to model the spatial variability of geotechnical parameters. These are (i) regression analysis; (ii) random field theory; (iii) geostatistics; and (iv) fractal theory. Regression analysis offers limited application to spatial variability models; primarily because it neglects the fact that soil properties exhibit autocorrelation, that is, neighbouring samples indicate stronger correlation than distant ones. Jaksa and Fenton (2002) demonstrated that fractal, or self-similar, behaviour is exhibited by some soils, but is generally absent in most. As a result, soil profiles can be well modelled stochastically using a finite-scale correlation structure, such as the Markov correlation function, which is exponentially decaying with separation distance. Consequently, random field theory and geostatistics are most often applied to the modelling of the spatial variability of soil profiles. These approaches facilitate

incorporation of measurement results obtained at individual locations within the area of interest and it is these that will apply in the present study. These are each treated briefly below.

1.2.2.1. Random field theory

Random field theory is an extension of time series analysis (Vanmarke, 1983; Jaksa, 1995; Brockwell and Davis, 1987). In geotechnical engineering to study the spatial variability of geomaterials, the time domain is replaced by the domain distance.

Random field theory is important for two reasons: first, it provides powerful statistical results which can be used to draw inferences from field observations and plan spatial sampling strategies; secondly, it provides a vehicle for incorporating spatial variation in engineering and reliability models. Random field theory is part of the larger subject of stochastic processes, of which we will only touch a small part. For more detailed treatment, see Adler (1981), Christakos (1992, 2000), Christakos and Hristopoulos (1998), Parzen (1964), or Vanmarcke (1983).

Let X denotes a soil variable such as the soil strength within a soil volume. X exhibits natural variability and therefore varies from point to point within the soil volume. X is said to form a random field over the soil volume. The natural variability from point to point within a soil volume is a result of the natural formation of soil in different depositional environments. This variation can exist even in apparently homogeneous soil units.

The autocorrelation function for X is defined as the coefficient of correlation between the values of X in two points located a distance r apart within the soil volume (Equation 1-17)

$$\rho(r) = \frac{Cov[X(s), X(s')]}{Var[X]}$$

Equation 1-17

where s and s' are the location coordinates of the two points, $r = |s - s'|$ denotes the distance between them, $Cov[X(s), X(s')]$ the covariance between two points and $Var[X]$ variance of a soil variable X. The autocorrelation function reflects the connectivity in the soil properties and tells something about how the variation of X from point to point is. An autocorrelation function typically decreases for increasing lag r.

A commonly applied model for the autocorrelation function for soil properties is quadratic exponential decay model (Equation 1-18):

$$\rho(r) = exp\left(-\frac{r^2}{R^2}\right)$$

Equation 1-18

in which R is a correlation length which expresses the scale of fluctuation in the random field X. Random fields of soil properties are usually anisotropic. The vertical correlation length R_V is usually smaller than the horizontal correlation length R_H (Det Norske Veritas as, 2007). This difference reflects the geological processes that lead to the formation of soil deposits by sedimentary depositing and may amount to as much as an order of magnitude.

Let r have components Δx in the horizontal plane and Δz in the vertical direction. For the anisotropic case that $R_V \neq R_H$, the quadratic exponential decay model can then be expressed as (Equation 1-19):

$$\rho(\Delta x, \Delta y) = exp\left(-\left(\frac{\Delta x}{R_H}\right)^2 - \left(\frac{\Delta z}{R_v}\right)^2\right)$$

Equation 1-19

Example of quadratic exponential and exponential models of autocorrelation function as is shown in Figure 1-1.
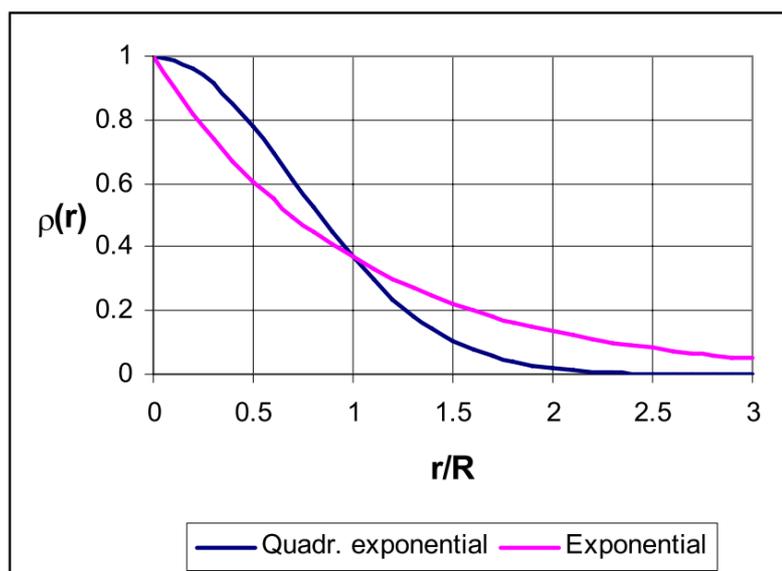
Figure 1-1: Example of autocorrelation function models (Det Norske Veritas as, 2007)

The theoretical limit of the autocorrelation function as the lag r approaches zero is unity ($\rho(r) \rightarrow 1$ for $r \rightarrow 0$). However, when $\rho(r)$ is inferred from data, one may observe that $\rho(r) \rightarrow b$ for $r \rightarrow 0$ with $0 < b < 1$

The difference $(1-b)$ is known as nugget effect. The nugget effect is in most cases due to measurement uncertainty, which by nature does not exhibit any spatial correlation structure. By considering a nugget effect the quadratic exponential decay model becomes changed to (Equation 1-20):

$$\rho(r) = b.exp\left(-\frac{r^2}{R^2}\right) \qquad for \quad r \geq 0 \qquad \qquad \textit{Equation 1-20}$$

1.2.2.2. Geostatistics

Geostatistics are proved to be reliable and well adapted methods when dealing with gridding tasks and risk analysis in the geotechnical engineering (Marache et al., 2009a-2009b). Compared to classical statistics, geostatistical methods take into account the spatial variability of the target parameter, in order to provide realistic spatial estimates together with a quantification of the associated uncertainty. A lot of applications can be found for liquefaction potential for example (Dawson and Baise, 2005; Lenz and Baise, 2007; Sitharam and Samui, 2007). Any geostatistical process begins with data quality control and analysis, thus allowing an understanding of the data prior to any further step. The variographic analysis is then performed in order to measure the spatial variability of the data (continuous, discontinuous behaviour, stationarity, non-stationarity…) leading to a variogram computation. Afterwards, geostatistical modelling such as kriging, cokriging and simulation can be performed using this spatial information (variogram). The geostatistical methods are discussed in the following sections.

1.2.2.2.1.   Variogram

In the geostatistical approach, such analysis is made to evaluate the dependence of a variable in relation to itself and separated by a vector distance h. The magnitude of dependence can be detected by means of correlation coefficients and spatial covariance that can be expressed by a function called variogram. The variogram is a basic graphic tool to support geostatistical techniques which allows quantitative representation of the variability of a regionalized phenomenon spatially (Huijbregts, 1975).

Figure 1-2 shows a variogram with nugget effect (C_0), range (*a*) and sill *(C_0+C)*. In theory the variogram value at the origin (0 lag) should be zero. If it is significantly different from zero for lags very close to zero, then this variogram value is referred to as the nugget. This value represents the variability is due to measurement errors or errors of location of measures, either to the existence of a microstructure (small scale variability) (Chilès and Delfiner, 1999). The range is a distance beyond which the variogram essentially remains constant and reaches the sill value. Presumably, autocorrelation is essentially zero beyond the range. The sill is the plateau the variogram reaches at the range. If the variogram reaches a sill, the variable is stationary (its mean and variance are constant whatever the location in the space). If the variogram keeps increasing, the variable is non-stationary (the variable presents a trend, for instance its mean varies regarding the location in the space).
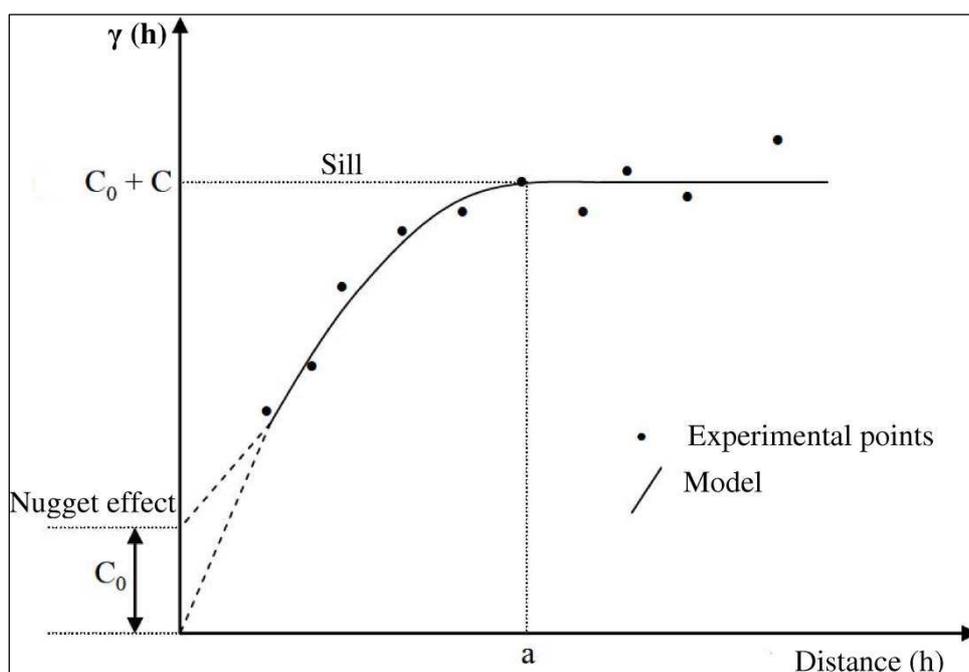
Figure 1-2: Diagram of a stationary variogram

Assume two regionalized variables, *X* and *Y*, where *X=Z(x)* and *Y=Z(x+h)* with reference to the same attribute that has been measured at two different spatial positions: *x* represents a bidimensional position with components (x_i, y_i) and *h* is a distance lag that separates the two spatial positions and expressed as a vector (module and direction). The

magnitude of dependence between the two regionalized variables, *X* and *Y*, can be expressed by a variogram function *γ(h)* given by Equation 1-21:

$$\gamma(h) = \frac{1}{2} E\left\{ [Z(x+h) - Z(x)]^2 \right\} = \frac{1}{2} Var\left\{ Z(x+h) - Z(x) \right\}$$

Equation 1-21

The quantity *γ(h)* is known as the semivariance: it is half the expected squared difference between two values. Variogram and covariance functions are correlated through the variance of field data, σ^2, in the form (Equation 1-22):

$$\gamma(h) = \sigma^2 - C(h)$$

Equation 1-22

It should be emphasized that the above variogram and covariance relations are only valid for stationary random fields where both the mean and standard deviation are constants across the domain of interest.

Taking a sample $Z(x_i)$ where $i=1, 2, ..., n$; an experimental variogram is defined as half the average squared difference between values separated by a given lag *h* as follows (Equation 1-23):

$$\gamma_e(h) = \frac{1}{2N(h)} \sum_{i=1}^{N(h)} [Z(x_i + h) - Z(x_i)]^2$$

Equation 1-23

where $\gamma_e(h)$ experimental variogram, *N(h)* number of pairs of measured values separated from one another by vector *(h)*, and $Z(x_i)$ and $Z(x_i+h)$ are observed values of the regionalised variable at different positions x_i and x_i+h *(i=1,..., n)*, also separated from one another by vector (*h*).

Journel, 1977 (citing Bacconnet, 1991) recommends a number of couples of points more than 30 in mining practice. However, the available data in geotechnic generally do not always satisfy this condition and a less number of couples of points can be considered (Bacconnet, 1991). It gives more weights to the calculated variogram points with many pairs (*N (h)*> 30), and less to others. If the number of pairs is very low (*N (h)* <10), it is impossible to consider the point.

These recommendations lead to emphasize the importance of the data structure. The sampling distribution in plan can follow three schema of theoretical sampling (Bacconnet,

1991). Systematic sampling (Figure 1-3a) with a regular mesh is the only schema able to provide a correct inference of the variogram. Second pattern is structured aleatory, in this case the sample is supposed to randomly located in a cell of a regular mesh (Figure 1-3b). The third pattern is pure aleatory, this case is very theoretical but can correspond to the majority of the geotechnical investigations for which the location of sample in fact is guided by the geometry and nature of the problem to treat (Figure 1-3c). In the same idea, there is no guarantee that the data structure is isotropic.

| a) Regular | b) Structured aleatory | c) Pure aleatory |
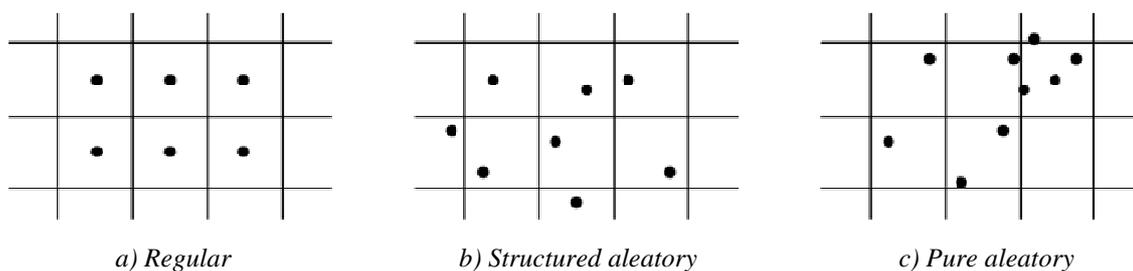
Figure 1-3: Sample configurations

We can also calculate the variogram in certain specific directions (Equation 1-24):

$$\gamma_e(h,\theta) = \frac{1}{2N(h,\theta)} \sum_{i=1}^{N(h,\theta)} \left[Z(x_i + h) - Z(x_i) \right]^2$$

Equation 1-24

where $N(h, \theta)$ = number of pairs separated by h in the direction θ.

In practice it is generally a tolerance on h and θ in order to have enough pairs for each h and each θ. The first step in the geostatistical estimation process is the building-up of the experimental variogram. After building-up a number of experimental variograms, a global mathematical model must be adjusted or fitted in order to best represent the spatial behavior of the variable being studied. It is important that such mathematical model could express any prevalent tendency of the variogram $\gamma(h)$ in relation to lag distance h. Once the model adopted, any further calculations are done with the values of the model and not with the experimental values.

When the variogram is the same in all directions, it is said to be isotropic or omnidirectional. When the variogram differs depending on the direction, it is anisotropic;

also range and sill are different. The variograms can have special forms. Significant spatial variations of the random variable analysis are:

- Stepped variogram shows the existence of several structures of different scales. (Figure 1-4a)

- Periodic variogram can correspond to periodic variation of the variable. It is better to verify the reality or at least physical likelihood of such phenomenon. The presence of hole effect in a variogram shows a tendency for high values areas are surrounded by low values areas, or vice versa (Figure 1-4b).

a) Stepped variogram   *b)Periodic variogarm*
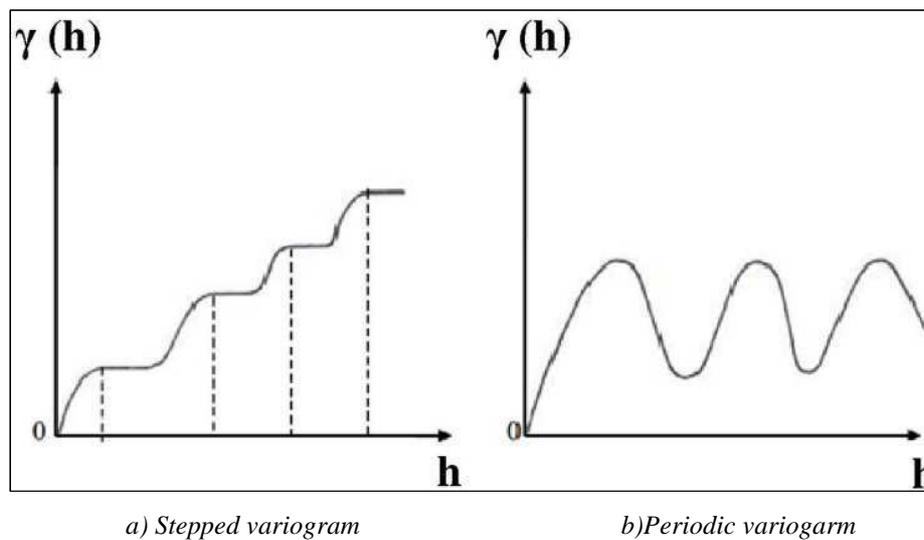
Figure 1-4: Different forms of variograms (Magnan, 1982)

The experimental variograms must be represented by convenient models (i.e. that provide a positive variance of random variables). In geological and geotechnical engineering, the most common models are (Figure 1-5 and Table 1-1):

- Pure nugget
- Power model (special case: the linear model)
- Spherical model
- Gaussian model
- Exponential model
- Cubic model
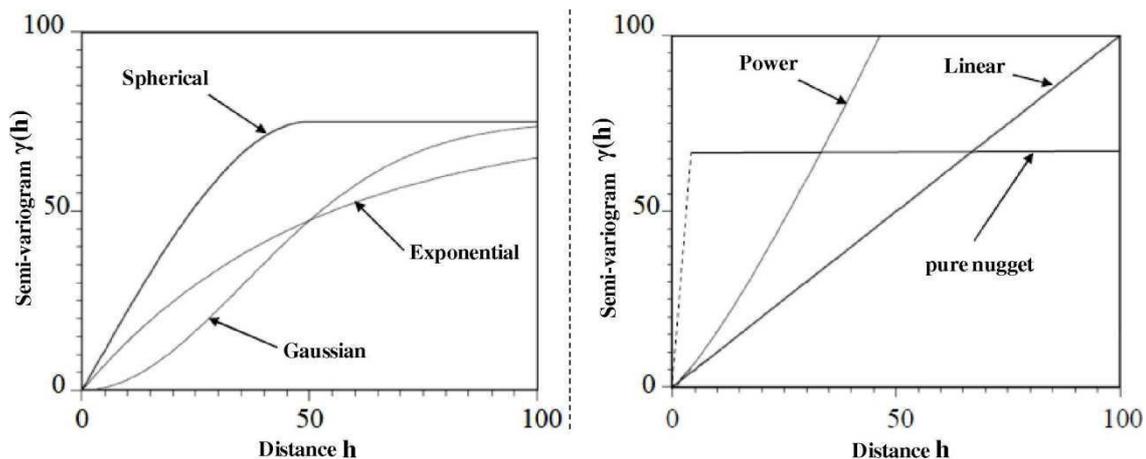
Figure 1-5: Commonly used semi-variogram models with C_0 set to zero (Jaksa 1997)

Table 1-1: Commonly used mathematical functions of semi-variogram models (Jaksa 1997)

Model	Mathematical functions	
Pure nugget	$\gamma(h) = C_0$	C_0= nugget effect
Spherical	$\gamma(h) = C\left(\dfrac{3h}{2a} - \dfrac{h^3}{2a^3}\right) + C_0$	for $h \leq a$, a=range
	$\gamma(h) = C + C_0$	for $h \geq a$, $C_0 + C$=sill
Exponential	$\gamma(h) = C(1 - e^{\frac{-3h}{a}}) + C_0$	
Gaussian	$\gamma(h) = C(1 - e^{-\left(\frac{\sqrt{3}h}{a}\right)^2}) + C_0$	
linear	$\gamma(h) = ph + C_0$	p=slope
Power	$\gamma(h) = ph^\alpha + C_0$	$0 < \alpha < 2$
Cubic	$\gamma(h) = C\left[7\left(\dfrac{h}{a}\right)^2 - \dfrac{35}{4}\left(\dfrac{h}{a}\right)^3 + \dfrac{7}{2}\left(\dfrac{h}{a}\right)^5 - \dfrac{3}{4}\left(\dfrac{h}{a}\right)^7\right]$	for $h \leq a$
	$\gamma(h) = C + C_0$	for $h \geq a$

The nugget model represents the discontinuity at the origin due to small scale variation and the pure nugget model would represent a purely random variable, with no spatial correlation. The power model does not reach a finite sill and does not have a corresponding covariance function.

The spherical model actually reaches the specified sill value at the specified range. The exponential and Gaussian approach the sill asymptotically, with a representing the practical range, the distance at which the semi-variance reaches 95% of the sill value.

The Gaussian model, with its parabolic behavior at the origin, represents very smoothly varying properties at small scales (However, using the Gaussian model alone without a nugget effect can lead to numerical instabilities in the kriging process). The spherical and exponential models exhibit linear behavior the origin, appropriate for representing properties with a higher level of short-range variability. Also we can combine several of these models by simple summation.

In the fitting models, the first points of the variogram (small h) are the values that have the greatest impact in the geostatistical calculations. When $h \geq (d_{max}/2)$ we ignore the values of the variogram (d_{max} is the size of the study area).

1.2.2.2.2.   Spatial estimation – kriging

One of the most important uses of regionalized variable theory is for local estimation by the method known as kriging. The purpose of kriging, also known as Best Linear Unbiased Estimator (BLUE), is to provide a best estimate of soil properties between known data. Krige (1951, 1966) developed the method empirically for estimating amounts of gold in bodies of rock from fragmentary information in the mines of South Africa. Kolmogorov's (1941) method of optimum interpolation is, however, the first recognizable formulation of kriging. Kriging is a general term that embraces several estimation procedures (Krige et al., 1989). What makes kriging unique and highly commendable compared with other methods of estimation is that its estimates are unbiased and have minimum variances. In this sense it is optimal. In fact kriging enables the interpolation errors to be minimised if the variogram model is of good quality.

Furthermore the estimation variances themselves can be estimated, and so the technique can be used with known confidence. Kriging is also an exact interpolator, i.e. the kriged value at a sampling point is the measured value there and the variance is zero. Laslett et al. (1987) compared kriging with other techniques of interpolation and showed that kriging was the only one that performed reliably in all circumstances.

When the data have a known, constant, mean value throughout the study area, we speak of simple kriging, otherwise ordinary kriging. As a result, simple kriging can be less

accurate than ordinary kriging, but it generally produces a result that is "smoother" and more aesthetically pleasing. Kriging is not an option since data is not available over the domain in question.

Supposing that the goal is to estimate the value of the variable Z at the point x_0, the unknown value of $Z(x_0)$ can be estimated from a linear combination of n observed values added to the parameter λ_0 (Journel, 1989) as follows (Equation 1-25):

$$Z_{x_0}^* = \lambda_0 + \sum_{i=1}^{n} \lambda_i \times Z(x_i)$$

Equation 1-25

Considering that the intended estimate should be unbiased as much as possible, which means $E\left[Z_{X_0} - Z_{X_0}^*\right] = 0$, it is then assumed that the two means must be equal and so from Equation 1-26:

$$E\left[Z_{x_0}\right] = E\left[\lambda_0 + \sum_{i=1}^{n} \lambda_i \times Z(x_i)\right] \Rightarrow \mu = \lambda_0 + \sum_{i=1}^{n} \lambda_i \times \mu$$

Equation 1-26

The ordinary kriging does not require previous knowledge of the mean μ. In this case, in order to satisfy Equation 1-26 it is necessary that:

$$\lambda_0 = 0 \ \ and \ \ \sum_{i=1}^{n} \lambda_i = 1$$

Equation 1-27

Therefore, the ordinary kriging estimate is given by Equation 1-28:

$$Z_{x_0}^* = \sum_{i=1}^{n} \lambda_i \times Z(x_i) \ with \ \sum_{i=1}^{n} \lambda_i = 1$$

Equation 1-28

Journel (1989) demonstrated that error variance $Var\left[Z_{X_0} - Z_{X_0}^*\right] = 0$ is minimized to obtain the weights λ_j from Equation 1-29:

$$\sum_{j=1}^{n} \lambda_j \times C(x_i, x_j) - \alpha = C(x_i, x_0), \ to \ i = 1,...,n \ \ and \ \ \sum_{j=1}^{n} \lambda_j = 1$$

Equation 1-29

where $C(x_i, x_j)$ and $C(x_i, x_0)$ are the covariance between points x_i and x_j and between points x_i and x_0 respectively; α is the Lagrange coefficient that is needed to minimise error variance.

The theoretical development of geostatistical methods is available from a number of publications including Journel and Huijbregts (1978), Journel (1989), and Isaaks and Srivastava (1989). Largueche (2006) studied estimating soil contamination with kriging interpolation method and recommended advantages and disadvantages for kriging based on personal experiences.

In practice, applications of geostatistic in geotechnic remains, despite the available softwares, complicated to use and often unemployable for lack of sufficient data. It is most often used in geostatistics for the establishment of geological and geotechnical models. There are two scales:

- The model treats a large area, and then we find general applications in risk analysis or feasibility of the project. For example, the project RIVIERA (Thierry et al., 2006) proposing an underground model of the Bordeaux urban community with several applications: geotechnical, treatment of waste water and archeology.
- The model is used to a particular site (or project), then we find further geotechnical applications, the estimations from the models are used in dimensions of the work. For example, Chilès and Blanchin, 1995 and El Gonnouni et al., 2005 used geostatistics in tunnel projects, respectively the tunnel under Manche and the Lyon metro, see also Elkadi and Huisman (2002) and Dubost et al. (2011).

Another part of the application is evaluation or the definition of geotechnical campaigns (Bacconnet, 1991; Parsons and Frost, 2002; Khalfaoui and Mezghache, 2005). There are also examples of simple descriptions of the site variability without precise presentation of the study aimes (Auvinet et al., 2005, Yoon et al., 2007).

1.2.2.2.3. Cokriging-collocated cokriging

The cokriging procedure is a natural extension of kriging when a multivariate variogram or covariance model and multivariate data are available. A variable of interest is cokriged at a specific location from data about itself and about auxiliary variables (or secondary variables) in the neighborhood. The data set may not cover all variables at all sample locations. Depending on how the measurements of the different variables are scattered in

space we distinguish between isotopic and heterotopic data-sets. The measurements available for different variables $Z_i(x)$ in a given domain may be located either at the same sample points or at different points for each variable as illustrated on Figure 1-6. The following situations can be distinguished:

- entirely heterotopic data: the variables have been measured on different sets of sample points and have no sample locations in common,
- partially heterotopic data: some variables share some sample locations (Figure 1-6b),
- isotopy: data is available for each variable at all sampling points (Figure 1-6a).

 primary data   secondary data

a) Isotopic data (sample sites are shared)   **b)** Heterotopic data (sample sites may be different)
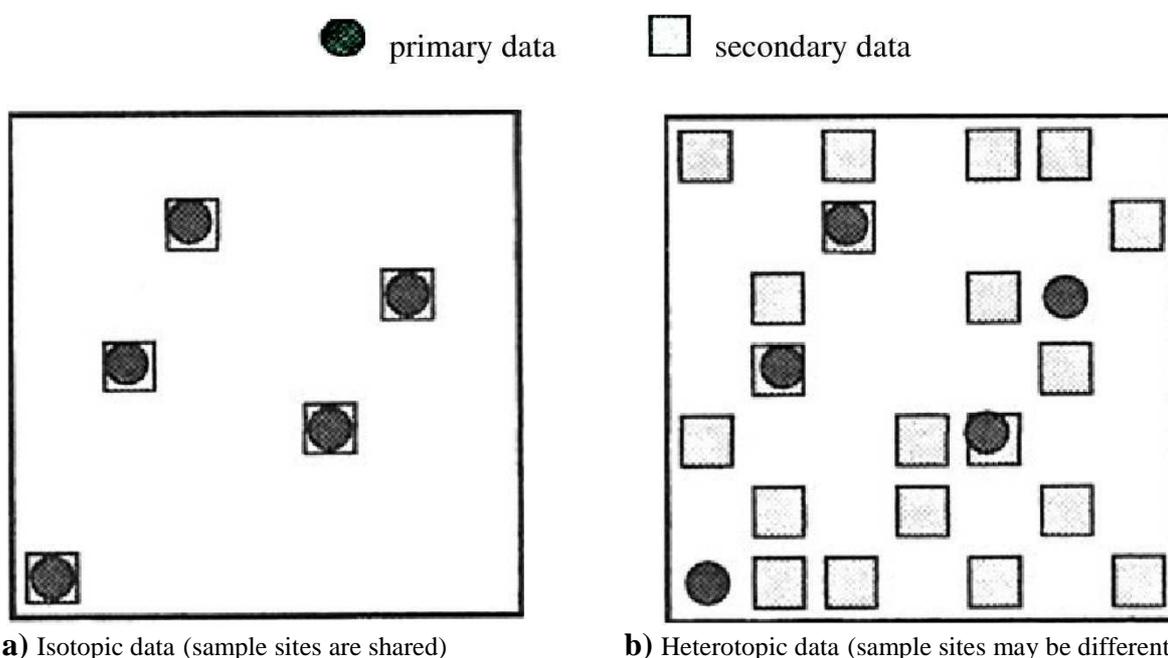
Figure 1-6: a) Isotopic and b) Partially heterotopic data, Wackernagel (2006)

Cokriging in the heterotopic case is explained in the following. For cokriging in the isotopic case, one can refer to Wackernagel (2006).

The ordinary cokriging estimator is a linear combination of weights w_α^i with data from different variables located at sample points in the neighborhood of a point x_0. Each variable is defined on a set of samples of (possibility different) size n_i and the estimator is defined as (Equation 1-30)

$$Z_{i0}^*(x_0) = \sum_{i=1}^{N} \sum_{\alpha=1}^{n_i} w_\alpha^i \, Z_i(x_\alpha)$$

Equation 1-30

where the index i_0 refers to a particular variable of the set of N variable. The number of samples n_i depends upon the index i of the variables, so as include into the notation the possibility of heterotopic data.

In the framework of a joint intrinsic hypothesis we wish to estimate a particular variable of a set of N variables on the basis of an estimation error which should be nil on average. This condition is satisfied by choosing weights which sum up to one for the variable of interest and which have a zero sum for the auxiliary variables (Equation 1-31).

$$\sum_{\alpha=1}^{n_i} w_\alpha^i = \delta_{ii0} = \begin{cases} 1 & if \ i = i_0 \\ 0 & otherwise \end{cases}$$

Equation 1-31

Ordinary cokriging has no meaning when no data is available for the variable of interest in a given neighborhood. On the other hand, simple kriging leans on the knowledge of the means of the variables, so that an estimation of a variable can be calibrated without having any data value for this variable in the cokriging neighborhood.

The simple cokriging estimator is made up of the mean of the variable of interest (m_i) plus a linear combination of weights w_α^i with the residuals of the variables (Equation 1-32):

$$Z_{i0}^*(x_0) = m_{i0} + \sum_{i=1}^{N} \sum_{\alpha=1}^{n_i} w_\alpha^i (Z_i(x_\alpha) - m_i)$$

Equation 1-32

In cokriging problems with heterotopic data we can distinguish between sparsely and densely sampled auxiliary variables. In the second case, when an auxiliary variable is available everywhere in the domain, particular technique like collocated cokriging can be of interest. This technique is explained in the following.

1.2.2.2.4. Collocated cokriging

A particular heterotopic situation encountered in practice is when we have a variable of interest known at a few points and an auxiliary variable known everywhere in the domain (or at least at all nodes of a given estimation grid and at the data locations of the variable of interest). With plenty of data available for the auxillary variable the question at hand is how to choose a parsimonious neighbourhood.

Cokriging with many variables using all data easily generates a very large linear system to solve. This means that the choice of a subset of data around a given estimation location, called a neighborhood, is a crucial step in cokriging. It is of particular importance to know when, due to the particular structure of a coregionalization, the full cokriging with all data is actually equivalent to a cokriging using a subset of data, so that the neighborhood can be reduced a priori and the cokriging system simplified accordingly, thus reducing in the end the numerical effort to a considerable extent. Concerning heterotopic data, we will focus on a case that has attracted most attention recently as it is increasingly frequently encountered in applications: the case of a dense secondary variable.

Figure 1-7 sketches three different neighborhoods for a given central estimation location (denoted by a star), primary data (denoted by full circle) as well as three alternate subsets of data from a secondary variable (denoted by squares). The neighborhood:

- (A) uses all data available for the secondary variable,
- (B) restricts the secondary information to the subset of locations where primary data is available as well as to the estimation location,
- (C) merely includes a sample value of the secondary variable at the estimation location.

Case (A) can be termed the full neighborhood, while case (C) was called a collocated neighborhood by Xu et al., (1992) as the secondary data is collocated with the estimation location. Whereas case (B) was termed a multicollocated neighborhood by Chilès and Delfiner (1999) as additionally the secondary data is also collocated with the primary data.

Using the full neighborhood (A) with secondary data dense in space will easily lead to linear dependencies for neighboring samples in the cokriging system, causing it to be singular. The size of the system can also be numerically challenging. Vargas-Guzman and Yeh (1999) suggest a way out of numerical difficulties by starting from a small

neighborhood and progressively extending the neighborhood in the framework of what they call a sequential cokriging.
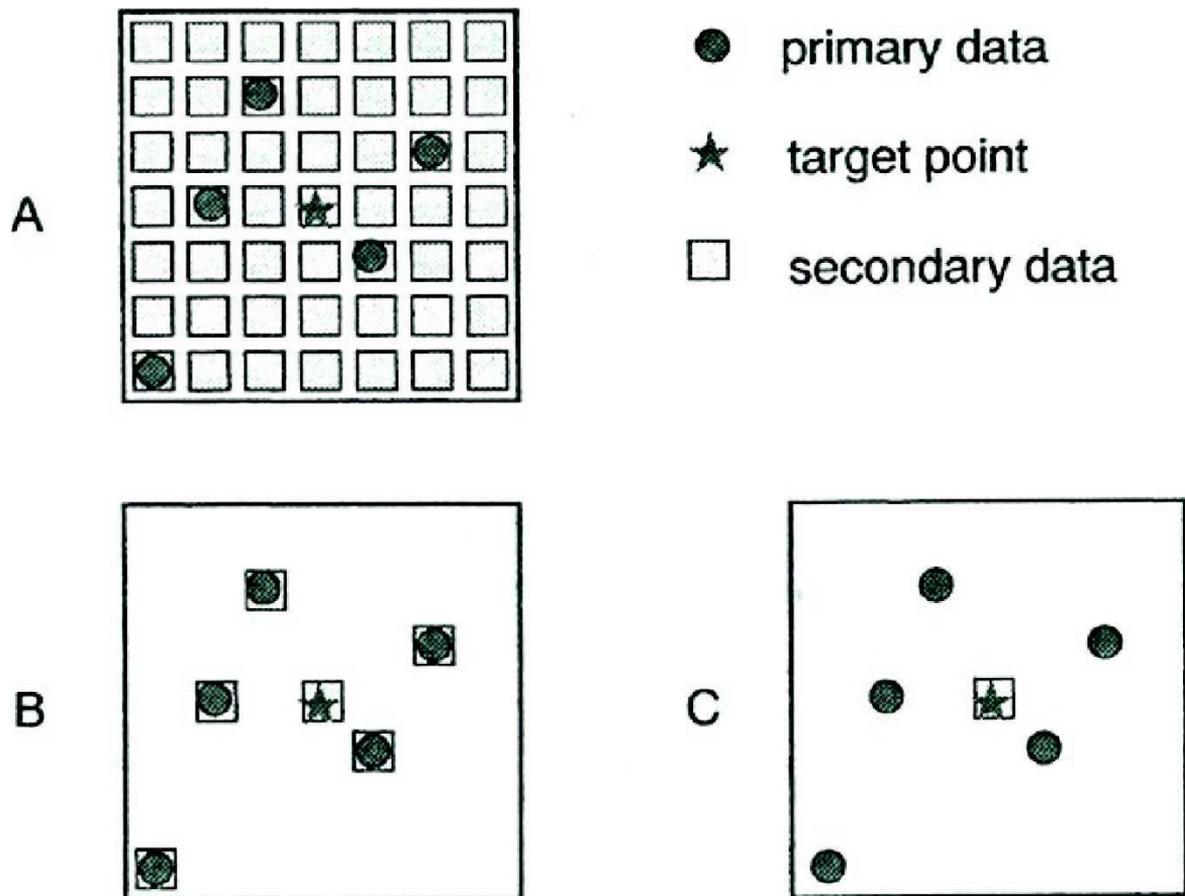
Figure 1-7: Three possible neighborhoods with a dense secondary variable

With reference to Xu et al., (1992), we call collocated simple cokriging a neighborhood definition strategy in which the neighborhood of the auxiliary variable ($S(x_0)$) is arbitrarily reduced to only one point: the estimation location. The value $S(x_0)$ is said to be collocated with the target point of $Z(x)$. The collocated simple cokriging estimator is (Equation 1-33):

$$Z^*(x_0)=m_z + w_0(S(x_0)-m_s)+ \sum_{\alpha=1}^{n} w_\alpha(Z(x_\alpha)-m_z)$$

Equation 1-33

The collocated neighborhood used for simple cokriging would yield a trivial result if applied in ordinary cokriging: because of the constraint that the weights of the auxiliary variable should sum up to zero, the weight w_0 is zero and the auxiliary variable does not come into play.

An ordinary cokriging needs to use more data together with the value $S(x_0)$. If the values $S(x_\alpha)$ that are collocated with the sample points of the main variable are also included we get a multicollocated neighborhood. The collocated ordinary cokriging estimator is then (Equation 1-34)

$$Z^*(x_0) = w_0\, S(x_0)+ \sum_{\alpha=1}^{n} (w_z^\alpha\, Z(x_\alpha)+ w_s^\alpha\, S(x_\alpha))$$

Equation 1-34

One can start the study of non-stationary methods with a multivariate method that is applicable to auxiliary variables that are densely sampled over the whole domain and related to the principal variable. Such auxiliary variables can be incorporated into a kriging system as external drift functions. More detailed information can be found elsewhere (Wackernagel, 2006).

1.2.2.2.5.   Simulation

Kriging estimates the average value of a parameter with minimal error at a point where we did not measure. Generally, the geostatistic allows us to model a spatially continuous field values with conserving the measured values, then a random function would simulate a value at a known point. It can be useful to simulate different regionalized fields that represent several possible cases, but not better than kriging.

There are two kind of simulation: conditional and non-conditional simulations. In the event that data is available at the site being simulated, conditional simulation should be employed to ensure that the random field realizations match the data at the data locations exactly. Furthermore all realizations pass through the known data but are random between

the data sites. An unconditional simulation ignores this additional information and will lead to higher variability in the response quantities.

There are many simulation methods that can be grouped into Gaussian methods (matrix decomposition method, sequential methods, frequency, autoregressive, turning bands method, etc.) and non-Gaussian (annealing simulations, using methods in the probability field, etc.). Chilès and Delfiner (1999) gave a fairly complete description of these methods. Examples of the simulation algorithms used in practice are the sequential Gaussian, the sequential indicator simulations (Deutsch, 2002) and the local average subdivision technique (Fenton and Vanmarcke 1990).

The sequential Gaussian simulation (SGS) is the most commonly used technique, especially in the field of petroleum engineering. The basic idea of this technique is illustrated in Figure 1-8. Input random variables are transformed into standardized normally distributed random variables with zero means and unit variances for which different variogram characteristics are assessed. Simulated values of a standardized variable, Z, can be determined at any node of the simulation grid according to the relationship (Equation 1-35):

$$Z_s(x_0) = Z^*(x_0) + R(x_0)$$

Equation 1-35

where $Z_s(x_0)$ is the simulated value of the variable Z at location x_0, $Z^*(x_0)$ is the krigged estimate of the variable Z at location x_0; and $R(x_0)$ is a random residual.

The random residual $R(x_0)$ follows a normal distribution with zero mean and a variance equal to the krigging variance (Deutsch, 2002). A different value of $R(x_0)$ is obtained in each realization using Monte Carlo Simulation resulting in a variation of the simulated value of the random variable ($Z(x_0)$ from one realization to another). A random path is followed to assess the value of the standardized random variable at each node of the numerical simulation grid. The simulated values across the analysis domain are then back transformed to their original probability distribution. By repeating the above procedure, several realizations of soil spatial variation across the analysis domain can be obtained.

An example of simulations cited by Chilès & Delfiner (1999) and Marcotte (2003) is the case a submarine cable which must be deposited at the bottom and one seeks to estimate the best length (Alfaro, 1979). The estimated length by kriging (104.2 km) is less

than the real length (110 km). This is due to the average of the kriging estimation (Figure 1-9a). Diagrams b and c in Figure 1-9 show two examples of simulation, and diagrams d for 1000 simulations. The estimated values by simulation are closer to the real length; but some simulated points are locally far away from reality. The 95% confidence interval obtained for the simulations is [108.8, 113.5]. The kriging value which is small, because of smoothing effect, is not in the confidence interval. Another application in the same example is the search for possible natural slopes. Estimated values by kriging are lower than observed values. The simulations allow better modeling of possible anomalies, without being more accurate compare to the real profile. By using more simulation, it will be accurate compare to the real profile.

```
┌──────────────────────────────────────────────────────────────────┐
│  ┌──────────────────────────────────────────────────────────┐    │
│  │ Transform input random variable into a standardized        │    │
│  │ normally distributed (Gaussian) random variable of zero    │    │
│  │ mean and unit variance.                                     │    │
│  └──────────────────────────────────────────────────────────┘    │
│                              ↓                                     │
│     ┌──────────────────────────────────────────────────┐          │
│     │ Assess variogram characteristics for the           │          │
│     │ standardized variable.                              │          │
│     └──────────────────────────────────────────────────┘          │
│                              ↓                                     │
│  ┌──────────────────────────────────────────────────────────┐    │
│  │ Implement Monte Carlo simulation to estimate a simulated   │    │
│  │ value of the standardized variable at a certain node in    │    │
│  │ the simulation grid.                                        │    │
│  └──────────────────────────────────────────────────────────┘    │
│                              ↓                                     │
│    ┌────────────────────────────────────────────────────┐        │
│    │ Choose a random path through all nodes of the        │        │
│    │ simulation grid.                                      │        │
│    └────────────────────────────────────────────────────┘        │
│                              ↓                                     │
│  ┌──────────────────────────────────────────────────────────┐    │
│  │ For each node, search for nearby simulated nodes and use   │    │
│  │ them to estimate a new simulated value of the random       │    │
│  │ variable.                                                   │    │
│  └──────────────────────────────────────────────────────────┘    │
│                              ↓                                     │
│  ┌──────────────────────────────────────────────────────────┐    │
│  │ Check that new simulated values of the random variable     │    │
│  │ satisfy variogram characteristics.                          │    │
│  └──────────────────────────────────────────────────────────┘    │
│                              ↓                                     │
│  ┌──────────────────────────────────────────────────────────┐    │
│  │ Back-transform all simulated values from its standardized  │    │
│  │ form to its original probability distribution.             │    │
│  └──────────────────────────────────────────────────────────┘    │
└──────────────────────────────────────────────────────────────────┘
```

Figure 1-8: The basic idea of the sequential Gaussian simulation (Elkateb et al., 2003)
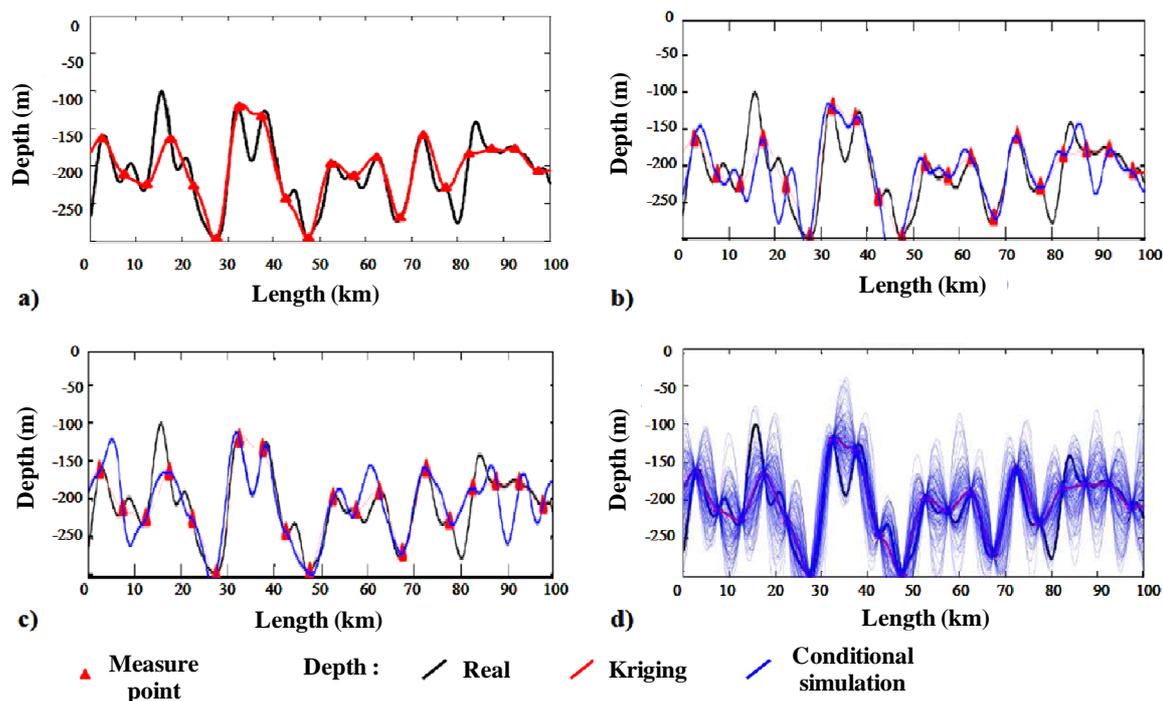
Figure 1-9: Cable length estimation by using conditional simulations (Marcotte, 2003)

1.2.2.3. Concept of correlation length: different related approaches

The autocorrelation function has been widely used for investigating spatial variability in the context of geotechnical engineering (Baecher and Christian, 2003; Jaksa et al., 1997; Phoon and Kulhawy, 1999 a, b and Sivakumar et al., 2006). For the spatial variability modeling, a parameter i.e. an autocorrelation distance (v_0) is defined as the distance within which the soil property exhibits relatively strong correlation. To obtain the numeric value of autocorrelation distance (v_0), it is taken as the distance at which autocorrelation coefficient $\rho_h = C(h)/C(0)$ decays to $1/e$, where e is the base of natural logarithms. In a physical sense, it is the same as the scale of fluctuation (δ), although the methodologies of obtaining scale of fluctuation (δ) and autocorrelation distance (v_0) are different (Vanmarcke, 1977). In the other words, the scale of fluctuation has the same meaning as the autocorrelation distance but differs in numeric value. The scale of fluctuation estimates the distance within which soil properties show relatively strong correlation and data become either above or below the mean value.

Vanmarcke (1977) described the random field theory. It defined the scale of fluctuation (δ), in order to describe a random field in terms of first and second-order moments. It corresponds to the area under the autocorrelation function, namely (Equation 1-36):

$$\delta = \int_{-\infty}^{+\infty} \rho_h \, d(h) = 2 \int_{0}^{+\infty} \rho_h \, d(h)$$

Equation 1-36

A large autocorrelation distance value implies that the soil property is highly correlated over a large spatial extent, resulting in a smooth variation within the soil profile. On the other hand, a small value indicates that the fluctuation of the soil property is large. Although an isotropic correlation structure is often assumed in works reported in the literature, correlations in the vertical direction tend to have much shorter distances than those in the horizontal direction due to the geological soil formation process for most natural soil deposits. A ratio of about 1 to 10 for these autocorrelation distances is common (Baecher and Christian, 2003).

Given practical difficulties with the characterization of spatial variability in real applications, however, some authors perform sensitivity analyses to identify the most unfavorable scale of fluctuation (Fenton and Griffiths, 2003) which can then be (conservatively) employed in subsequent analysis. An extensive literature review was conducted to estimate the typical scales of fluctuations for a variety of common geotechnical parameters. The results of this review are summarized in Table 1-2. Full details are given elsewhere (Phoon et al. 1995). The scales of fluctuation are generally calculated using the method of moments. Information on the soil type and the direction of fluctuation also are included in the table.

Table 1-3 shows the difference between the approaches for two commonly mathematical models (exponential and Gaussian models). We note that autocorrelation distance, fluctuation scale and practical range, vary widely from one approach to another and these three terms have distinct significations.

Table 1-2: Summary of scale of fluctuation of some geotechnical properties (Phoon et al. 1995).

Property[a]	Soil type	No. of studies	Scale of fluctuation (m) Range	Mean
Vertical fluctuation				
s_u	Clay	5	0.8–6.1	2.5
q_c	Sand, clay	7	0.1–2.2	0.9
q_T	Clay	10	0.2–0.5	0.3
s_u(VST)	Clay	6	2.0–6.2	3.8
N	Sand	1	—	2.4
w_n	Clay, loam	3	1.6–12.7	5.7
w_L	Clay, loam	2	1.6–8.7	5.2
$\bar{\gamma}$	Clay	1	—	1.6
γ	Clay, loam	2	2.4–7.9	5.2
Horizontal fluctuation				
q_c	Sand, clay	11	3.0–80.0	47.9
q_T	Clay	2	23.0–66.0	44.5
s_u(VST)	Clay	3	46.0–60.0	50.7
w_n	Clay	1	—	170.0

a: S_u and S_u(VST), undrained shear strength from laboratory tests and vane shear tests, respectively; $\bar{\gamma}$, effective unit weight.

Table 1-3: Significance of the correlation length according to the considered approach (Jaksa, 1995)

Model	Random field theory $F_{ac}(h)$	v_0	δ	Geostatistic $\gamma(h)$	a	v_0/δ	v_0/a	δ/a
Exponential	$F_{ac}(h)=C.e^{\frac{-|h|}{b}}$	b	$2b$	$\gamma(h)=C\left(1-e^{-\left(\frac{h}{b}\right)}\right)+C_0$	$3b$	$\frac{1}{2}$	$\frac{1}{3}$	$\frac{2}{3}$
Gaussian	$F_{ac}(h)=C.e^{-\left(\frac{|h|}{b}\right)^2}$	b	$\sqrt{\pi}.b$	$\gamma(h)=C\left(1-e^{-\left(\frac{h}{b}\right)^2}\right)+C_0$	$\sqrt{3}.b$	$\frac{1}{\sqrt{\pi}}$	$\frac{1}{\sqrt{3}}$	$\frac{\sqrt{\pi}}{\sqrt{3}}$

b: correlation length, a: practical range, δ: scale of fluctuation and v_0: autocorrelation distance

1.3. Probabilistic methods in geotechnical engineering for propagating uncertainty

The reluctance of practicing engineers to apply probabilistic methods is attributed to four factors. First, engineers' training in statistics and probability theory is often limited to basic information during their early years of education. Hence, they are less comfortable dealing with probabilities than they are with deterministic factors of safety. Second, there is a common misconception that probabilistic analyses require significantly more data, time, and effort than deterministic analyses. Third, few published studies illustrate the implementation and benefits of probabilistic analyses. Lastly, acceptable probabilities of unsatisfactory performance (or failure probability) are ill-defined, and the link between a probabilistic assessment and a conventional deterministic assessment is absent. This creates difficulties in comprehending the results of a probabilistic analysis. All of these issues are addressed in detail in El-Ramly, 2001.

In the following, the probabilistic methods for propagating uncertainties, most commonly, used in geotechnical engineering are described.

1.3.1. Taylor series approach

Model uncertainties can be quantified by standard deviation (square root of variance) around the mean of modeled outputs (Hwang et al., 1998). The Taylor series approach is based on evaluating the derivatives of the output function with respect to the independent input variables. The Taylor series formulae are defined for a continuously differentiable function $f(x)$. The Taylor's formula for expansion of a function $f(x)$ is given by Equation 1-37 (Harr, 1987):

$$f(x) = f(\bar{x}) + f'(\bar{x})(x - \bar{x}) + \frac{f''(\bar{x})}{2!}(x - \bar{x})^2 + ... + \frac{f^{(n-1)}(\bar{x})}{(n-1)!}(x - \bar{x})^{(n-1)} + Rn \qquad \text{Equation 1-37}$$

where $\bar{x}$ is the mean of the input variable and $f^n(\bar{x})$ is the nth derivative of the studied function evaluated at $\bar{x}$ and Rn is the remainder.

In many modeling applications a first order approximation of variance from the Taylor series expansion is used to describe uncertainty in the modeled result (Tiktak et al., 1999; Graettinger and Dowding, 1999; Seefeld and Stockwell, 1999).The first order

approximation for the variance, FOSM method, is given by the following equation (Harr, 1987) Equation 1-38 in the case of no correlation between parameters:

$$V[f(x)] = \left[f'(\bar{x})\right]^2 V[x]$$ *Equation 1-38*

where $f'(\bar{x})$ is the first derivative of the studied function, $V[x]$ is the variance of the input variable and $V[f(x)]$ is the variance of the studied function. The obtained variances for each variable can be summed up to calculate the variance of function, which depends on all the input variables. The variances of the input variables are obtained from experimental data or from expert judgment.

When the function $f(x)$ is non-linear, the higher order terms of Taylor series are necessary to more accurately estimate the variance. In this case, the second-order approximation for variance, SOSM method, is given by Equation 1-39 (Harr, 1987, Dettinger and Wilson, 1981):

$$V[f(x)] = \left[f'(\bar{x})\right]^2 V[x] + \frac{1}{4}\left[f''(\bar{x})\right]^2 V^2[x][\beta(2)-1] + \beta(1)V^{1.5}[x]f'(\bar{x})\left[f''(\bar{x})\right]$$ *Equation 1-39*

where $f''(\bar{x})$ is the second derivative of function $f(x)$, $\beta(1)$ and $\beta(2)$ are the coefficients of skewness and kurtosis, respectively. When the probability distribution is symmetrical, then $\beta(1) = 0$. Let $\lambda = \beta(2) - 1$ then Equation 1-39 becomes:

$$V[f(x)] = \left[f'(\bar{x})\right]^2 V[x] + \frac{1}{4}\left[f''(\bar{x})\right]^2 V^2[x]\lambda$$ *Equation 1-40*

The parameter of λ depends on the probability distribution, for example the coefficient of kurtosis for the normal distribution is equal to three ($\beta(2) = 3$), so $\lambda = 2$.

1.3.2. Monte Carlo Simulation method

Sometimes the system being designed is too complicated (non-linearity) to allow the calculation of the variance of the studied function. Fortunately there is a simple, albeit computer intensive, solution; simulate realizations of the random field and analyze each to produce realizations of the response. From a set of response realizations, one can build up a picture of the response distribution from which probability estimates can be derived. This

is called Monte Carlo Simulation (MCS), reference is made to Madsen et al., 1986. Although various stochastic methods have been proposed in the literature, the only currently available universal method for accurate solution of geotechnical problems is this technique, mainly due to the large variability and strong non-linearity of soil properties (Popescu et al., 2005). Moreover it involves strong non-linearities and large variations of non-Gaussian uncertain system parameters.

This method involves the generation of n random numbers of input soil parameters with given probabilistic characteristics. These n sample points for output response are used to obtain required sample statistics, which is incorporated in probabilistic calculations. The minimum value of number n depends on percentage (%), acceptable error in the estimation of sample mean and variance as well as confidence level (Baecher and Christian, 2003).

In a Monte Carlo Simulation, a series of random fields are generated in a manner consistent with their probability distribution and correlation structure and the response is calculated for each generated set. Various statistical properties evaluated after the process of simulation, such as mean, variance, coefficient of skewness, probability density functions and cumulative probability distribution functions, can provide a broader perspective and a more comprehensive description of a given system.

In the last decade, a series of papers appeared in the literature where the effect of inherent random soil heterogeneity on the mechanical behavior of various problems in geomechanics was assessed quantitatively. The methodology used in essentially all these studies were Monte Carlo Simulation. Paice et al., 1996 studied settlements of foundations on elastic soil, Griffiths & Fenton, 2000 studied slope stability, Popescu et al., 1995-1997 and Koutsourelakis et al., 2002 studied seismically induced soil liquefaction. Nobahar and Popescu, 2000; Popescu et al., 2002; Fenton and Griffiths, 2003 and Nobahar, 2003 studied the bearing capacity of shallow foundations.

Furthermore studies applying Monte Carlo Simulation also rarely addressed the spatial variability of soil properties (Major et al., 1978; Tobutt, 1982; Nguyen and Chowdhury, 1985) because of difficulties in generating random values in ways that preserved their spatial correlations.

Monte Carlo simulation has its own limitations, which can be summarized as follows:

- The need to define a reliable input reference distribution, which requires a considerable number of field data. In addition, older versions of Monte Carlo Simulation algorithms used to deal only with parametric probability distribution functions, i.e., probability distributions that can be defined through mathematical relationships such as normal and lognormal distribution. Field data, however, do not necessarily fit into any of these parametric distributions. This problem has been overcome by recent versions of Monte Carlo Simulations, such as that of Deutsch and Journel, 1998 that are capable of dealing with nonparametric distribution functions directly inferred from field data.

- Clustering of the simulation outcome into a limited zone of the input probability distribution, as the drawn samples are more likely to be in areas of higher probability, as shown in Figure 1-10, This problem mainly arises in cases where an insufficient number of realizations (number of iterations in Monte Carlo algorithm) are used in the simulation process (Palisade Corporation, 1996). This may result in sampling values of the random variable away from the tails of the input probability distribution, which can be on the unsafe (non-conservative) side. This problem, however, can be overcome by using a number of realizations large enough to reproduce the input distribution.

- Monte Carlo Simulation cycles influences the accuracy of the results. These results are more accurate when sufficient iterations and sufficient sample size are used. Depending on the number of variables involved in the simulation process, Monte Carlo Simulation may require a significantly large number of iterations and consequently a considerable computational effort.
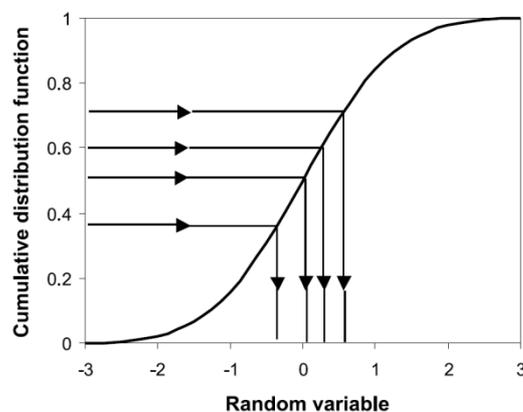
Figure 1-10: Clustering of the outcome of Monte Carlo Simulations resulting from an insufficient number of realizations (modified from Palisade Corporation, 1996)

Despite the fact that the mathematical formulation of the Monte Carlo Simulation is relatively simple and the method has the capability of handling practically every possible case regardless of its complexity, this approach has not received overwhelming acceptance due to the excessive computational effort required (Papadrakis et al., 1996). To improve the computational efficiency of the method, several sampling techniques known as variance reduction techniques have been developed in order to improve the computational efficiency of the method by reducing the statistical error inherent in Monte Carlo methods and keeping the sample size to the minimum possible. A detailed review can be found in Baecher and Christian, 2003. Among them Latin hypercube sampling may be viewed as a stratified sampling scheme designed to ensure that the upper or lower ends of the distributions used in the analysis are well represented. Latin hypercube sampling is considered to be more efficient than simple random sampling, that is, it requires fewer simulations to produce the same level of precision. Latin hypercube sampling is generally recommended over simple random sampling when the model is complex or when time is an issue.

The principal geotechnical applications are stability studies (Cho, 2007 and Low, 2008 for the slope stability; Low, 2005 and Fenton et al., 2005, for the retaining wall stability), analysis of foundation systems (Niandou and Breysse , 2007 for the piled raft design; Massih et al., 2008 for rupture of soil under shallow foundations) and some specific applications are also found as the study of buried networks (Elachachi et al., 2004). In cited examples were used FOSM or FORM methods, and often enriched by comparison with the results of calculations using the Monte Carlo Simulation method.

1.3.3. Reliability-Based Design

Reliability-based design approaches are becoming common in civil engineering. For example, U.S. codes for concrete and steel design are reliability-based. In addition, a reliability-based approach was adopted by the European Community in the new Eurocode standards. These approaches are referred to by the names Load and Resistance Factor Design (LRFD) in the U.S. and Limit State Design (LSD) in Europe.

The objective of a reliability-based design approach is to assure satisfactory system performance within the constraint of economy. Most designs are developed without the benefit of complete information and under conditions of uncertainty. What maximum load

will a structure experience over its lifetime? How will the strength of steel change as a function of time due to corrosion? Because of these uncertainties, there always exists a chance or risk of failure. In most cases, it is not practical or economical to eliminate this risk. All design approaches implicitly balance costs and benefits; a reliability-based approach attempts to achieve this balance in a more systematic and rational manner.

1.3.3.1. Traditional Design Approach

Conceptually, most problems can be described in terms of a load, S and a resistance, R. The load represents the load applied to the system (e.g., an axial load on a column, the volume of water entering a treatment facility, etc.), while the resistance represents the capacity of the system (e.g., the axial capacity of column, the capacity of a treatment plant, etc). Traditional design approaches are deterministic. We account for uncertainties in the load and resistance by requiring a resistance that is greater than the estimated load (Equation 1-41):

$$R_{reqd} \geq F_s.S \hspace{4cm} Equation\ 1\text{-}41$$

where F_s is a factor of safety. The factor of safety typically ranges between 1.0 and 3.0; however values as large as 10 or 100 may be used in some instances.

1.3.3.2. Decision making in geotechnical engineering-reliability based approche

One of the major challenges that faces geotechnical engineers is the need to make decisions regarding the soil parameter to be used in engineering analysis. These decisions have to be based on information that invariably has a certain degree of uncertainty.

Consequently, the decision making process is considered to be governed by two factors, the uncertainty in the decision variables and the risk level of the project. Several decision making algorithms have been used throughout the history of geotechnical engineering practice, such as the worst case and quasi worst case approaches and reliability-based techniques, details of these algorithms will be discussed in the following paragraphs.

The worst case approach aims at achieving the absolute safety of the project and relies on the notion of maximum loss and maximum expected hazards, often referred to as the maxi-max criterion (Ang and Tang, 1984). For example, if the range of the measured

friction angle of a sandy deposit at a certain site ranges from 30–40°, the design value will be assessed as 30°. This approach is over-conservative and rarely used in practice. On the other hand, the quasi worst case approach (Pate-Cornell, 1987) tries to apply some kind of engineering judgment into the above approach to provide an upper bound for the risk level. Revisiting the above example, the sandy soil at the site is classified (say medium dense sand) and the minimum value associated with such classification (say 33°) will be used as the design value. A common problem of the two approaches is that no information can be obtained about the risk level associated with the design value; in fact design value is a deterministic value.

The reliability-based approach relies on selecting design parameters that satisfy a desired degree of reliability or a certain probability of failure is defined a probability of safety of a system in a given environment and loading conditions. With a reliability-based approach, we attempt to account explicitly for uncertainties in the load and resistance. We can calculate the probability that the load exceeds the resistance as follow (Equation 1-42):

$$P(\,S > R\,) = P(\,R \leq S\,) = P(\,R - S \leq 0\,) = P(\,X \leq 0\,)$$

Equation 1-42

Recall that one objective in developing theoretical random variable models was to provide a mathematical framework for combining random variables. It can be shown that a linear combination of normal random variables, such as $X = R - S$, where R and S have normal distributions, will also have a normal distribution. Further, the mean and standard deviation for X are given as follows (Equation 1-43):

$$\mu_X = \mu_R - \mu_S, \qquad \sigma_X = \sqrt{\sigma_R^2 + \sigma_S^2 - 2\rho_{RS}.\sigma_R.\sigma_S}$$

Equation 1-43

in which ρ_{RS} is coefficient of correlation between R and S. Baecher and Christian, 2003 point out that this assumption (R and S have normal distributions) is rarely true, but it is a good approximation when the number of parameters which depend on R and S is more than four.

These distributions can be characterized by their mean values μ_R (resistance) and μ_S (load) and by their standard deviations σ_R and σ_S or their coefficients of variation (CV_R and

CV_S). If normal distributions of R and S are assumed, reliability index (β) can be calculated using Equation 1-44 (Benjamin and Cornell, 1970; Melchers, 2002):

$$\beta = \frac{\mu_X}{\sigma_X} = \frac{\mu_R - \mu_S}{\sqrt{\sigma_R^2 + \sigma_S^2 - 2\rho_{RS}.\sigma_R.\sigma_S}} \qquad \textit{Equation 1-44}$$

All the random variables can be regarded as independent as this assumption simplifies the computation and also gives conservative results (Li and Lumb, 1987). Then if S and R are statistically independent normal varieties (Equation 1-45):

$$\beta = \frac{\mu_R - \mu_S}{\sqrt{\sigma_R^2 + \sigma_S^2}} \qquad \textit{Equation 1-45}$$

The reliability index (β) value depends on the probability density functions of the resistance (R) and load (S). By assuming that R and S follow lognormal distributions, the Hasofer and Lind, (1974) reliability index β is defined by the following expression (Equation 1-46):

$$\beta = \frac{ln\left[\left(R/_S \right).\sqrt{(1+CV_S^2)/(1+CV_R^2)} \right]}{\sqrt{ln\,[(1+CV_S^2).(1+CV_R^2)]}} \qquad \textit{Equation 1-46}$$

where CV_S and CV_R are, respectively, associated coefficients of variation of S and R.

The reliability index (β) reflects both the mechanics of the problem and the uncertainty in the input variables, and it permits comparisons of reliability among different structures or modes of performance without having to calculate absolute failure probability values. Clear expositions of the underlying theory are found in various publications including Shinozuka, 1983; Ang and Tang, 1984; Madsen et al., 1986; Melchers, 2002; and U.S. Army Corps of Engineers, 1997.

The probability of failure P_f of the structure is then defined as follows (Equation 1-47):

$$P_f = \varphi(-\beta) = 1 - \varphi(\beta) \qquad \textit{Equation 1-47}$$

in which $\varphi(-\beta)$ is the standard normal cumulative distribution function (zero mean and unit variance). This value can be obtained from tables of the standard cumulative normal distribution function found in many textbooks or from built-in functions in most spreadsheets. Note that large value of β lead to small value of P_f.

The complementary probability $P_S = 1 - P_f$ is referred to as the reliability and is sometimes also denoted the probability of survival. In addition, the failure probability, the reliability, and the reliability index are all suitable measures of the structure safety with respect to the considered failure mode.

Historical failure probabilities for civil engineering facilities are between 10^{-3} to 10^{-4}, therefore, target failure probabilities for new designs are typically within this range (Griffiths and Fenton, 2007). Normally, a reliability index value in the range of 3.0–4.0 is accepted for good performance of the system (Baecher and Christian, 2003; U.S. Army Corps of Engineers, 1997). Harr (1977), has written that, in classical geotechnical problems, one often has $P_f > 10^{-3}$ ($\beta \approx 3$). However, Zhang and Tang, 2001 and Paikowsky 2002, proposed that redundant pile (stiff structures allowing transfer of load) could be accounted for by applying lower β values: i.e. $\beta = 2.33$ ($P_f \approx 10^{-2}$). Meanwhile, recommended has $P_f = 10^{-3}$ ($\beta \approx 3$) for non-redundant piles (Paikowsky, 2002). The target value of the reliability index β to be reached in the Eurocode 1 is equal to 1.5 for the serviceability limit state (SLS) [Eurocode 1, 1991]. The probability of the serviceability limit state (P_{SLS}) should be less than 0.067 to avoid exceed the serviceability limit state.

In summary, a reliability-based design approach consists of the following steps:

- Select a target probability of failure, P_f. This failure probability is established considering costs, consequences of failure, engineering judgment, politics and experience.
- Calculate the required reliability index (β) to achieve the target failure probability (Equation 1-48)

$$\beta = -\varphi^{-1}(P_f) \hspace{4cm} \text{Equation 1-48}$$

- Find the mean resistance required to achieve the target (β)

Note that this approach has been commonly used in slope stability analysis but there are some softly differences between the two approaches (reliability index approach and soil stability analysis approach). Wolff (1996), proposed soil design parameters to be associated with a reliability index (β) of 3 for routine slopes and 4 for critical slopes such as dams. The reliability index can be obtained through Equation 1-49:

$$\beta = \frac{m_{FS} - L}{\sigma_{FS}}$$

<div align="right">*Equation 1-49*</div>

where m_{FS} is the mean factor of safety; L is a limit state value usually equal to 1; and σ_{FS} is the standard deviation of the factor of safety.

The FORM approximation (First Order Reliability Method) (Hasofer and Lind, 1974) is the improving form of the FOSM method, based on a geometrical interpretation of the reliability index. In this approach, the performance function is transformed into a standard Gaussian space. The reliability index is distance between the origin and the design point, visually representing the intersection between the unsafe and safe areas (Figure 1-11).
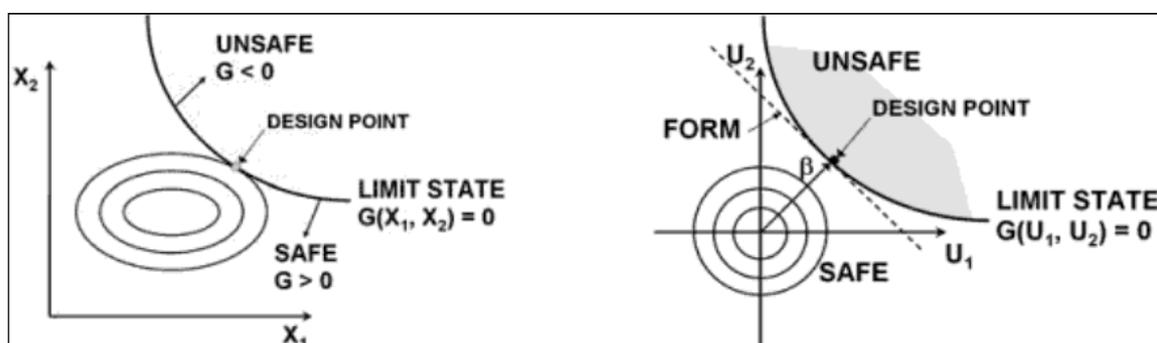
Figure 1-11: FORM approximation (Lacasse and Nadim, 2007)

1.3.3.3. Advantages and limitations of a reliability-based design approach

There are several advantages in using a reliability-based approach versus the traditional approach (Griffiths and Fenton, 2007):

- A factor of safety does not provide information on the level of safety in the design. The same factor of safety may produce two designs that have different reliabilities. A reliability-based approach allows us to quantify the reliability, and load and

resistance factors are developed to achieve consistent levels of reliability among different designs.

- Factors of safety are based on experience with similar designs. What if we don't have experience (e.g., a new construction material or a new environment)? What if our experience is not positive? A reliability-based approach provides the ability to develop new designs that achieve a specified reliability.

- Since a factor of safety has no real meaning in terms of reliability, it is difficult to select an optimum factor of safety. By quantifying reliability, we can perform cost-benefit analyses to balance construction costs against the risk of failure.

However, reliability-based approaches in their current form (e.g., LRFD) do have limitations. The code user does not have control over the target failure probability, and cannot directly incorporate the uncertainties associated with their specific design. Further, even a purely probabilistic approach cannot prevent poor engineering; it can only help to make good engineering better.

1.4. Model of soil-structure interaction

Most of the civil engineering structures involve some type of structural element with direct contact with ground. When the external forces act on these systems, neither the structural displacements nor the ground displacements, are independent of each other. The process in which the response of the soil influences the motion of the structure and the motion of the structure influences the response of the soil is termed as soil-structure interaction.

Different calculation methods can be used to study the soil-structure interaction. For example, the finite element method has been used in numerous studies (Elachachi et al. 2004, 2011, 2012, Niandou and Breysse, 2007 and Buco et al. 2006, 2008). However, in order to simplify the soil-structure interaction, analytical approaches can be used (Deck and Singh, 2010; Houy et al., 2005).

The search for a physically close and mathematically simple model to represent the soil-media in the soil-structure interaction problem shows a basic classical approach, such as Winklerian approach. At the foundation-supporting soil interface, contact pressure distribution is the important parameter. The variation of pressure distribution depends on the foundation behavior (such as rigid or flexible: two extreme situations) and nature of

soil deposit (clay or sand etc.). Since the philosophy of foundation design is to spread the load of the structure on to the soil, ideal foundation modeling is that wherein the distribution of contact pressure (Taylor, 1964) is simulated in a more realistic manner. From this viewpoint, this fundamental approach has some characteristic limitations. However, the mechanical behavior of subsoil appears to be utterly erratic and complex and it seems to be impossible to establish any mathematical law that would conform to actual observation. In this context, simplicity of model, many a time, becomes a prime consideration and it often yields reasonable results. Attempts have been made to improve upon this model by some suitable modifications to simulate the behavior of soil more closely from physical standpoint. In the recent years, a number of studies have been conducted in the area of soil-structure interaction modeling the underlying soil in numerous sophisticated ways. Details of these modelings are depicted in the following section.

1.4.1. Analytical approaches to solving soil structure interaction problems

1.4.2. Winkler's model

In the past, many researchers have worked on the soil-structure interaction which is referred to as beams and plates on elastic foundations. Most of the previous work began with the well known Winkler's model. This model is also frequently referred to as a one parameter model, which was originally developed for the analysis of railroad tracks (Winkler, 1867). This model is expressed by the following formula (Equation 1-50):

$$p(x) = k_S \cdot b \cdot w(x) \hspace{4cm} \textit{Equation 1-50}$$

where k_s is the coefficient of subgrade reaction (or constant of proportionality of Winkler in [F/L^3]), $w(x)$ vertical displacement (settlement), b width of the foundation and $p(x)$ the reactive pressure of the foundation. Figure 1-12 shows the physical representation of the Winkler foundation.
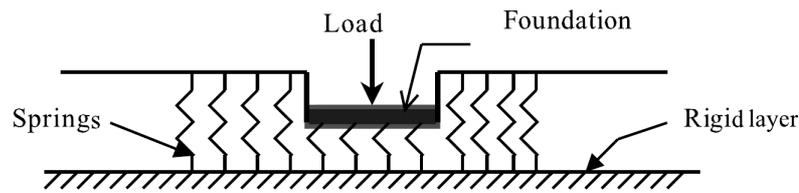
Figure 1-12: Winkler foundation (Dutta, 2000)

Winkler's idealization considers the soil as being a system of identical but mutually independent, closely spaced, discrete, linearly elastic springs. The simplifying assumptions which Winkler hypothesis is based on causes some deficiencies (Terzaghi 1955, Stavridis 2000, Avramidis and Morfidis, 2006). One of the most important deficiencies of the Winkler model is that a displacement discontinuity appears between the loaded and the unloaded part of the foundation surface and this model cannot transmit the shear stresses which are derived from the lack of spring coupling. In reality, the soil surface does not show any discontinuity (Figure 1-13).

a
b
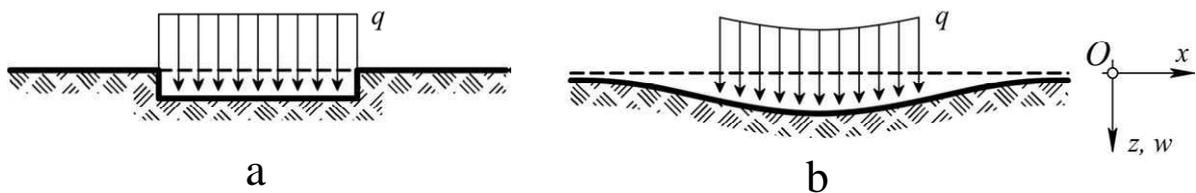
Figure 1-13: Deflections of elastic foundations under uniform pressure: a) Winkler foundation;
b) Practical soil foundation.

The differential equation governing the deflection, *w(x)*, of a homogeneous elastic bending beam with constant bending stiffness resting on a Winkler foundation and subjected to a transversal continuous load, *q(x)*, can be written as Equation 1-51 (Hetenyi, 1946):

$$E_c . I \frac{d^4 w(x)}{dx^4} + k_s . b . w(x) = q(x)$$

Equation 1-51

where $E_c I$ is the constant bending stiffness of the beam (E_c and I are respectively the Young's modulus of concrete and the moment of inertia of the cross section of the foundation). Equation 1-51 is a continuous differential equation whose general solution

$w(x)$ is the sum of the solution $w_0(x)$ of its homogeneous part and of a particular solution $w_q(x)$. The solution $w_0(x)$ has the following form (Equation 1-52) (Hetenyi, 1946):

$$w_0(x) = e^{\beta x}(C_1 \sin \beta x + C_2 \cos \beta x) + e^{-\beta x}(C_3 \sin \beta x + C_4 \cos \beta x) \qquad \textit{Equation 1-52}$$

where $\beta = \left[\dfrac{k_s.b}{4\,E_c.I}\right]^{\frac{1}{4}}$.

The expression of the particular solution $w_q(x)$ depends on the load $q(x)$ type. For example, if the load is constant, then w_q is constant too, and given by $w_q(x) = q/(k_s.b)$. The general solution $w(x)$ is completely defined once that the constants C_i (i=1 to 4) are evaluated by imposing the natural and essential boundary conditions. When the deflection $w(x)$ is known, the bending moment ($M(x)$) and the shear force ($V(x)$) can be determined (

$$M(x) = -E_c I \frac{d^2 w(x)}{dx^2}, V(x) = -E_c I \frac{d^3 w(x)}{dx^3}).$$

Hence, several attempts have been made to develop modified models to make the model more realistic by assuming some form of interaction among the spring elements that represent the soil continuum. These models are discussed in below.

1.4.3. Filonenko-Borodich foundation

Filonenko-Borodich developed a model that improved upon the Winkler model by connecting the top ends of the springs with a thin elastic membrane subjected to a constant tension T. Figure 1-14 shows the physical representation of this model (Filonenko-Borodich, 1940). Thus, the response of the model is mathematically expressed as follows (Equation 1-53 and Equation 1-54):

$$p(x, y) = k_s.b.w(x, y) - T.\nabla^2 w(x, y) \textit{ for rectangular or circular foundation} \qquad \textit{Equation 1-53}$$

$$p(x) = k_s.b.w(x) - T\frac{d^2 w(x)}{dx^2} \qquad \textit{for strip foundation} \qquad \textit{Equation 1-54}$$

where ∇^2 is the Laplace operator ($\nabla^2 \equiv \dfrac{\partial^2}{\partial x^2} + \dfrac{\partial^2}{\partial y^2}$) and all other terms were previously defined.

Hence, the interaction of the spring elements is characterized by the intensity of the tension T in the membrane. An essentially same foundation model consisting of heavy liquid with surface tension is also suggested in the literature (Schiel, 1942).
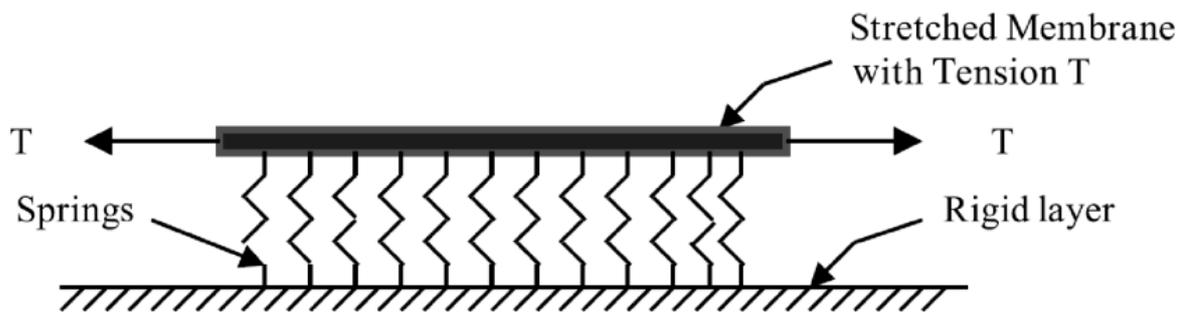
Figure 1-14: Filonenko-Borodich foundation (Kerr, 1965)

1.4.4. Hetenyi's foundation

In this model, the interaction among the discrete springs is accomplished by incorporating an elastic beam or an elastic plate, which undergoes flexural deformation only, as shown in Figure 1-15. Thus the pressure–deflection relationship becomes (Equation 1-55):

$$p(x, y) = k_s . b . w(x, y) + D . \nabla^4 w(x, y)$$

Equation 1-55

where D is the flexural rigidity of the elastic plate and $\nabla^4 \equiv \dfrac{\partial^4}{\partial x^4} + \dfrac{\partial^4}{\partial y^4} + 2\dfrac{\partial^4}{\partial x^2 \partial y^2}$.

Thus, it is seen that the flexural rigidity of embedded beam or plate characterizes the interaction between the spring elements of the Winkler model. Detailed descriptions of this model as well as some numerical examples are available in the literature (Hetenyi, 1946-1950).
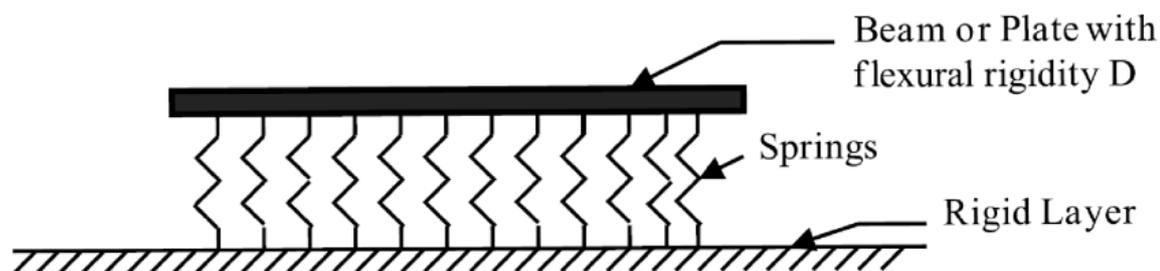
Figure 1-15: Hetenyi foundation (Winkler, 1867)

1.4.5. Pasternak foundation

In this model, existence of shear interaction among the spring elements is assumed which is accomplished by connecting the ends of the springs to a beam or plate that only undergoes transverse shear deformation (Figure 1-16). The load-deflection relationship is obtained by considering the vertical equilibrium of a shear layer. The pressure-deflection relationship is given by Equation 1-56:

$$p(x, y) = k_s.b.w(x, y) - G.\nabla^2 w(x, y)$$

Equation 1-56

where *G* is the shear modulus of the shear layer. As a special case, if this modulus (*G*) is neglected, the mechanical modeling of the foundation converges to the Winkler formulation.

Thus the continuity in this model is characterized by the consideration of the shear layer. A comparison of this model with that of Filonenko-Borodich implies their physical equivalency (*T* has been replaced by *G*). A detailed formulation and the basis of the development of the model have been discussed elsewhere (Pasternak, 1954). Analytical solutions for plates on Pasternak-type foundations with a brief of the derivation of the model have been reported in the literature (Kerr, 1964; Wang et al., 2001).
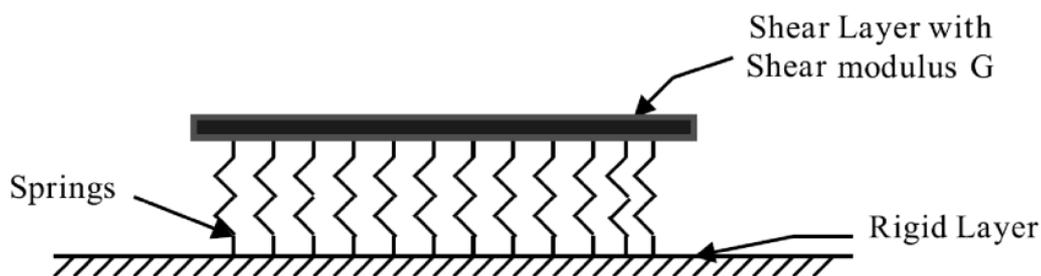
Figure 1-16: Pasternak foundation (Schiel, 1942)

1.4.6. Kerr foundation

A shear layer is introduced in the Winkler foundation and the spring constants above and below this layer is assumed to be different as per this formulation (Kerr, 1964). Figure 1-17 shows the physical representation of this mechanical model. The governing differential equation for this model may be expressed as follows (Equation 1-57):

$$\left(1 + \frac{k_2}{k_1}\right) . p(x, y) = \frac{G}{k_1 . b} . \nabla^2 p(x, y) + k_2 . b . w(x, y) - G . \nabla^2 w(x, y)$$

Equation 1-57

where k_1 is the spring constant of the first layer; k_2 is the spring constant of the second layer; $w(x)$ is the deflection of the first layer.
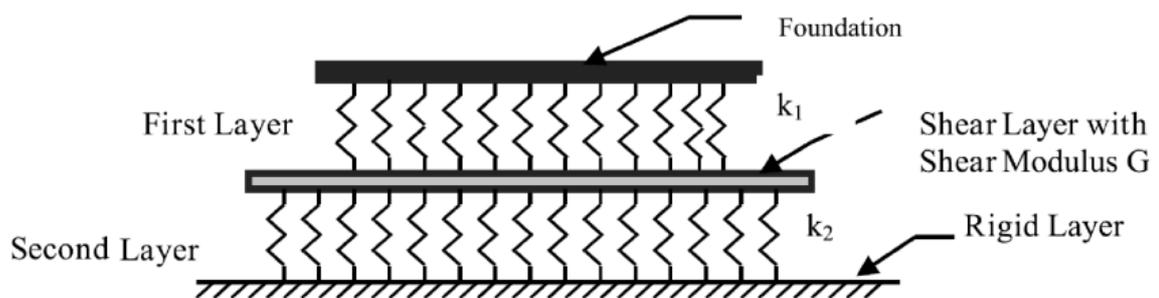
Figure 1-17: Kerr foundation (Gorbunov-Posadov, 1949)

1.4.7. Synthesis of different analytical approaches for soil-structure interaction modeling

Using these analytical approaches, the soil is modeled by a simple system called a subgrade reaction model instead of attempting to model the subsoil in all its complexity, i.e. its nonlinear, stress-dependent, anisotropic and heterogeneous nature. In the majority of proposed solutions, the foundation-supporting soil is represented using the well-known Winkler hypothesis, which assumes the soil to be made up of continuously distributed, non-connected discrete springs (Winkler, 1867). Due to its simplicity, the Winkler model has been extensively used to solve many soil-foundation interaction problems and has given satisfactory results for many practical problems. However, it is a rather crude approximation of the discontinuous mechanical behavior of ground material. This has

given rise to the development of a variety of two-parameter elastic foundation models, in which the continuity, i.e. the coupling effect between the discrete Winkler springs, is introduced by assuming that the springs are connected by a shear layer membrane or beam (Filonenko-Borodich, 1940; Pasternak, 1954). The two-parameter models describe soil behavior more accurately and yet remain simple enough for practical purposes. A third category of mechanical models comprises the so-called three-parameter models (Matheu and Suarez, 1996; SAP2000; Biot, 1937), which constitute a generalization of two-parameter models. Their main advantage is their ability to take into account the desired degree of continuity of the vertical displacements of the soil surface at the boundaries between its loaded and unloaded regions (Matheu and Suarez, 1996). Of particular interest are the three-parameter models devised by Reissner and Kerr. The former was the object of a study by Horvath (Council on tall buildings and urban habitat, 1993; Bowles, 1988; Vallabhan and Das, 1991). This established the superiority of Reissner's model even though it requires more parameters.

Since the second and third foundation parameters are difficult to estimate, we chose to use Winkler's analytical model which seems, from a practical point of view, to be appropriate for superficial geotechnical designs (Elachachi et al., 2004). While Winkler's model is one of the simplest models for a mathematical description of soil-structure interaction, it has the advantage of using only one parameter, the coefficient of subgrade reaction, to characterize soil and structure responses under loading. Taking into account fewer parameters brings less uncertainty to the model. One must choose between a very accurate model with many parameters - and consequently many uncertainties in the model - and a simple, less accurate model with fewer parameters and lesser uncertainties.

1.5. Superficial geotechnical designs

As heterogeneity can be very important in the case of superficial geotechnical designs, we chose the two kind of the superficial geotechnical designs, spread footings and and buried pipe networks, to study in this work. In the following, geometrical parameters of the spread footings and the buried pipes and the hypothesis for their loadings are presented. Additionally, the different kind of joints for connecting the buried pipes to each other will be discussed.

1.5.1. Spread footings

Continuous spread footings consist of concrete strips with a rectangular cross section, placed under masonry walls. In residential constructions with relatively lightly loaded walls, the dimensions of the concrete strip are typically 0.5 m in width (*b*) and 0.3 m in thickness (*h*), for a length (*L*) ranging between 5 and 20 m (Figure 1-18). The lowest level of the footing must be located deeper than the maximum frost penetration depth, to avoid the occurrence of frost heave. In France, this frost depth (*D*) lies typically between 0.6 and 1.2 m. Definitions of the differential settlement and the angular distortion for this kind of foundation are shown in Figure 1-18.
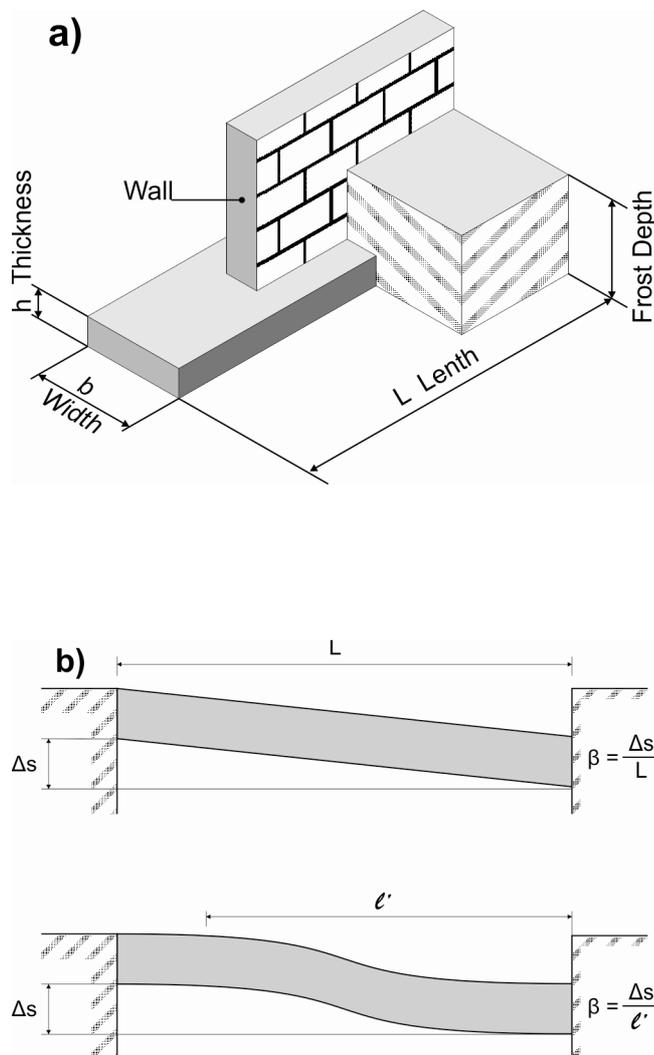
Figure 1-18: a) Continuous wall footing characteristics and b) Definition of the angular distortion β

(Δs: differential settlement)

1.5.2. Buried pipes

Buried pipelines are part of the so-called lifelines which play a vital role as infrastructure components conveying and/or distributing energy, fluids, waste water, oil products and gas in present-day's world. The pipelines in particular allow conveying water, fossil liquid fuels and liquid gas over long distances.

The pipe materials are varied: masonry, plain or reinforced concrete, cast iron or steel, PVC, etc (Balkaya et al., 2012a). The pipe diameter (d) varies in practice from 0.15 to 1.5 m for the non-visitable pipes and from 1.5 to 3 m for visitables ones (Figure 1-19).
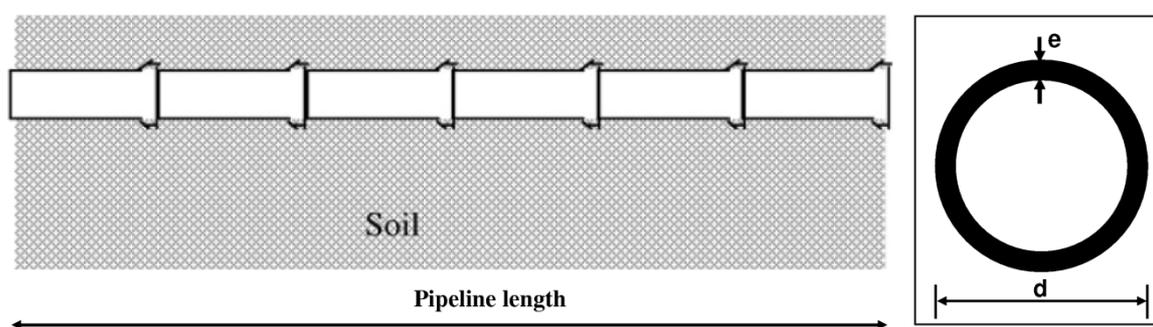
Figure 1-19: Buried pipe (e: thickness of the pipe, d: external diameter of the pipe)

The sealing between pipes is ensured by joints made of plastic, cement mortar or, more frequently, elastomer or by welding. The rigidity of these joints is as variable as technologies and geometries employed: it can be very weak (flexible joints), high (quasi rigid joints) or very high (rigid joints).

Concrete collar (norme NF P 16-341, 1990) and Spigot and socket joints are two kinds of flexible joints. Spigot and socket joint is also commonly called the Rubber Ring Joint (RRJ). RRJ provides the flexibility in concrete pipelines. A certain degree of linear deflection is allowed in this type of joint. For soft foundation, these two kinds of joints are recommended (Figure 1-20).

a)

b)
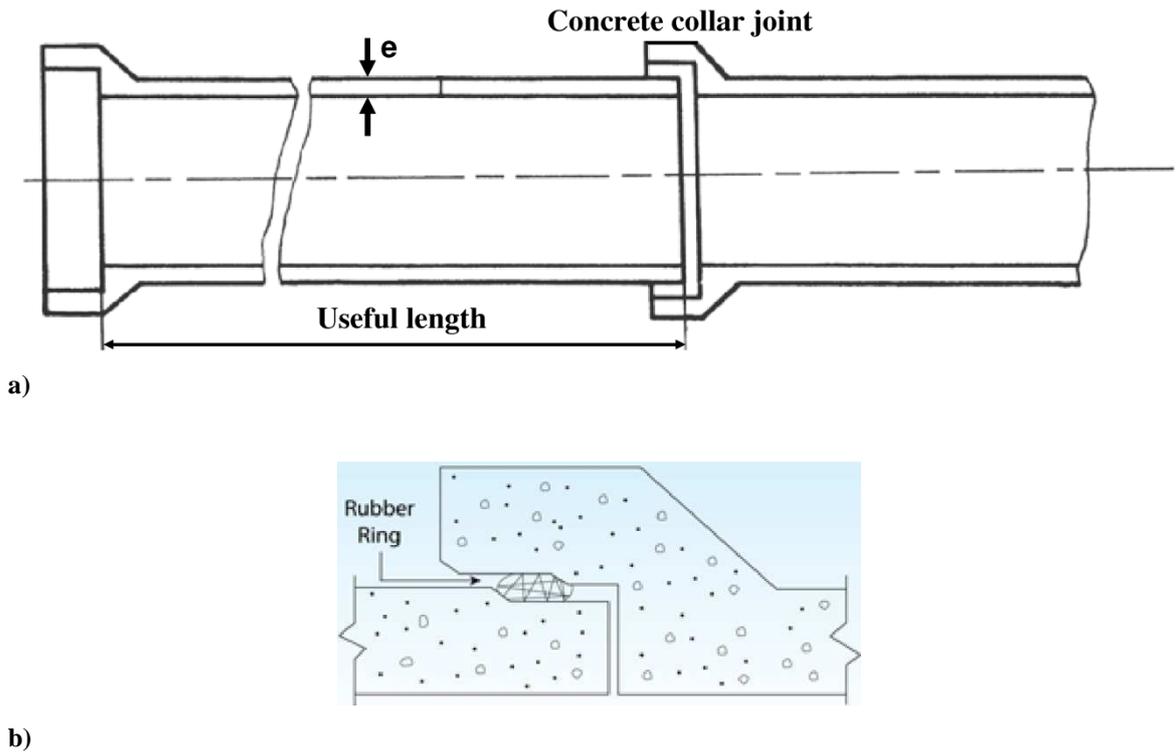
Figure 1-20: Two kinds of flexible joints a) Concrete collar joint and b) Rubber Ring Joint

e: thickness of the pipe

A kind of quasi rigid joint before and after embedding with details is shown in Figure 1-21.
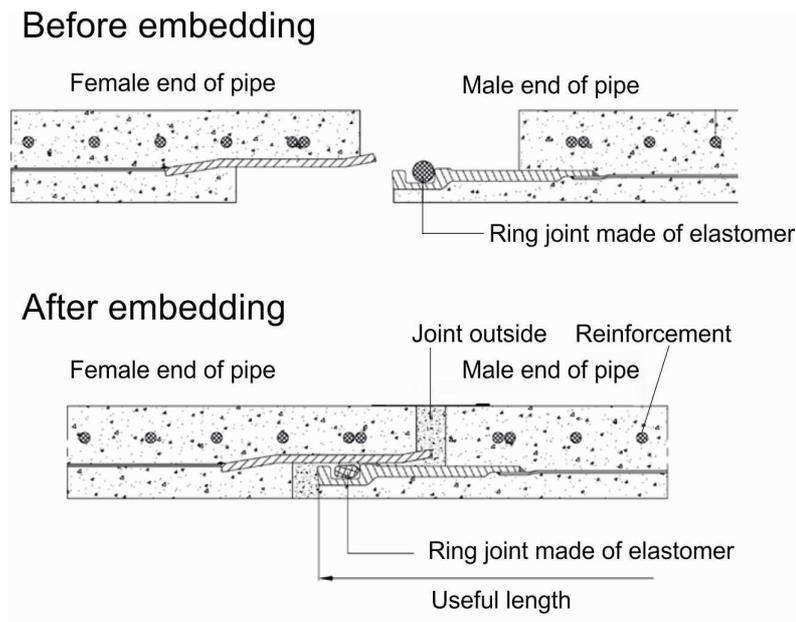
Figure 1-21: A kind of quasi rigid joint

61

Butt joint with collar and rebated joint are two kinds of the rigid joints. Butt joint with collar uses a precast or cast in-situ concrete collar to connect the pipes. This is a rigid joint and no flexibility is provided (Figure 1-22a). This joint is not recommended for soft foundation where deflection can occur. Rebated joint is also known as the Ogee joint or Flush joint. The internal rebated joint is used for pipes of diameters 675 mm and above while the external rebated joint is for pipes of diameters 600mm and below. Any deflection or movement occurs after leakage (Figure 1-22b).

a)

b)
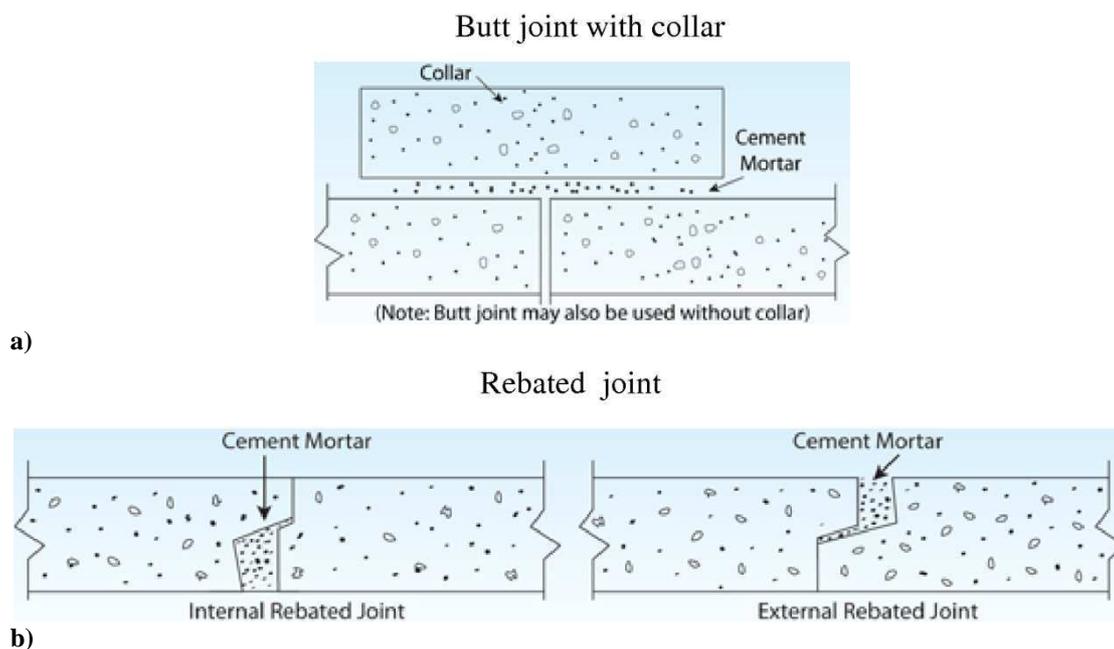
Figure 1-22: Two kinds of rigid joints a) Butt joint with collar and b) Rebated joint

Figure 1-23 shows embedded pipes with half thickness at the location of joints and pipes with the same thickness at the location of joints. These kinds of joints can be constructed as rigid or quasi rigid on a construction site (norme NF P 16-341, 1990).

a)
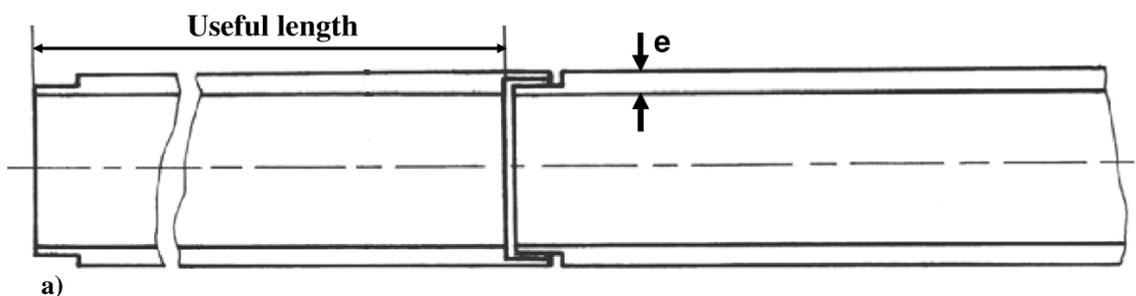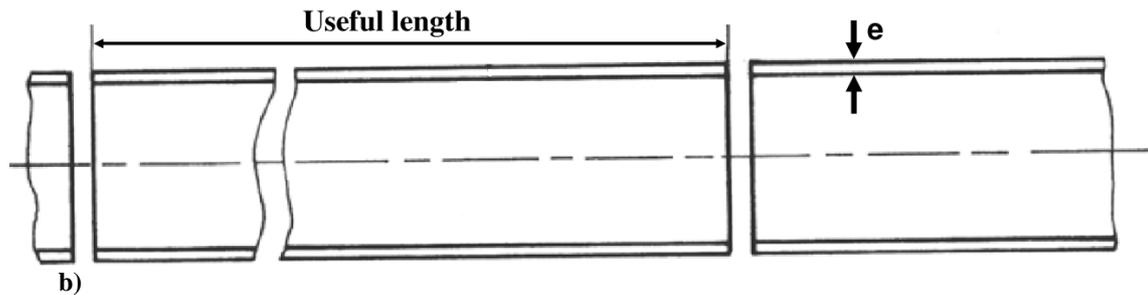
Figure 1-23: Two kinds of joints can be constructed as rigid or quasi rigid on the construction site a) Embedded pipes with half thickness at the location of joints b) Pipes with the same thickness at the location of joints (norme NF P 16-341, 1990)

Continuous buried steel pipes (such as oil and gas transmission pipelines) are constructed in great lengths without joints (Balkaya et al., 2012b). Concrete buried pipes with the quasi rigid joints and continuous buried steel pipes are chosen in this study with the simplication of the same rigidity all along the pipelines.

- **The loading**

In practice, it results from overhanging load, living load (due for example to vehicles), and hydrostatic pressure due to the water table, soil loading from weight of soil above pipe, horizontal pressure of soil and also from the internal actions of the conveyed fluid (pipe internal pressure) (Figure 1-24). In this study, we will assume that the loading applied consists of a uniform vertical action distributed, of intensity q (kN/m).
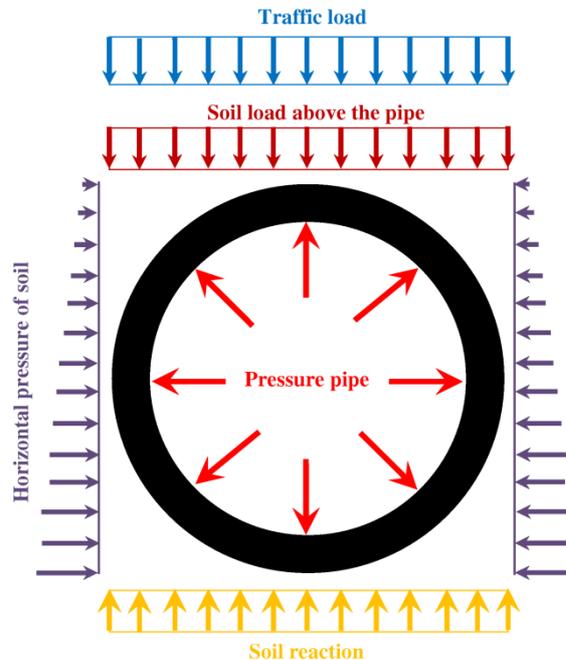
Figure 1-24: Schematic of the loads on a buried pipe

1.6. Summary and conclusion

In this chapter, the main concepts of the uncertainties in geotechnical designs were discussed. In order to prevent any misunderstanding or confusion in the following parts of this thesis, the main terms used in the modeling of soil properties (basic random variables, random field theory and geostatistics) were precisely defined. Geostatistics, a very practical and useful method that takes into account the spatial variability of soil, was highlighted in detail and will be used later on. Different available tools and techniques of probabilistic methods in geotechnical engineering for propagating uncertainty (such as Taylor series approach, Monte Carlo Simulation method and Reliability-Based Design) were introduced and will be used in the ensuing sections.

Next, the soil-structure interaction concept was explained and different available analytical models for taking it into account were introduced. Their advantages and drawbacks were briefly pointed out; the Winkler model was chosen to model soil-structure interaction for the considered superficial geotechnical designs in this study. Finally, the superficial geotechnical systems used in this study were briefly described.

Chapter 2

Modulus of subgrade reaction and its uncertainty

2. Modulus of subgrade reaction and its uncertainty

2.1. Introduction

Physical and mechanical properties of a soil have some natural variability which originates in the complexity of the natural geological processes (erosion, transport, deposition, compaction, physico-chemical…) that caused the soil formation. An uncertainty on each parameter is attached to this variability, commonly used to quantify the natural variability: the mean, the variance and the covariance function in the case of a spatial approach of the natural variability (Marache et al. 2009, Cho & Park 2010, Denis et al. 2011).

Uncertainties which also exist in the case of the materials of a structure, are taken into account by considering parameters of structures as aleatory variables. These variables are modeled by probability distributions which can be introduced in design calculation of structures in order to obtain the uncertainty attached to this design.

In the case of the design of spread footings and buried pipes, the analytical models with one or two parameters are used to study of soil-structure interaction on elastic soil (Winkler 1965, Pasternak 1954, Vlassov 1960). The common parameter for these models is the modulus of soil reaction (k_s).

Eight semi-empirical models, the most commonly used in spread footings and buried pipes designs, are chosen to determine a value of the subgrade reaction modulus (k_s). This modulus is not an intrinsic parameter of soil; it depends on the mechanical parameters of soil and mechanical and geometrical parameters of the structure.

The objective of this chapter is to estimate the variability of soil reaction modulus from the uncertainties in soil and structure parameters. Then Taylor series approach (FOSM (First Order Second Moment) and SOSM (Second Order Second Moment) methods) are successively used on these non-linear semi-empirical models to estimate the uncertainty of k_s from the uncertainties on the soil and the structure parameters and to determine the most influential parameters on this uncertainty.

2.2. Modulus of soil reaction and suggested expressions

Soil has very complex mechanical behavior, because of its nonlinear, stress- dependant, anisotropic and heterogeneous nature. Hence, instead of modeling the subsoil in all its complexity, the subgrade is often replaced by a much simpler system called a subgrade

reaction model. The value of subgrade modulus can be obtained in the following alternative approaches:

- Plate load test (Dutta and Roy 2002; Bowles 1998),
- Consolidation test (Dutta and Roy 2002; Bowles 1998),
- Triaxial test (Dutta and Roy 2002),
- CBR test (Nascimento and Simoes 1957) and
- Semi-empirical and theoretical relations that are proposed by researchers.

Among these methods, Plate load test and semi-empirical and theoretical relations are utilized more than the others. Plate load test is a direct method to estimate the modulus of subgrade reaction. There are numerous semi-empirical models, which can be used to determine the coefficient of subgrade reaction as function of Young's modulus, the Poisson coefficient of the ground and the parameters of the structure (Elachachi et al., 2004; Ziaie-Moayed and Janbaz 2009). Each of the authors wrote a different but suitable expression (some of formulas are given in Table 2-1), this fact underlining the uncertainty attached to the semi-empirical model of reaction (the same questions arise for the rigidity of the soil behind a flexible screen).

Biot (1937) and Vesic (1961) expressions are defined for infinite beams resting on an elastic soil continuum. Biot (1937) solved the problem for an infinite beam resting on a 3D elastic soil continuum. He found a correlation between continuum elastic theory and Winkler model, that the maximum moments in the beam are equated (Biot expression in Table 2-1). Vesic (1961) matched the maximum displacement of the beam in both models and tried to develop a value for k_s with matching bending moments. He obtained the equation for k_s to use in the Winkler model (Vesic expression in Table 2-1).

Table 2-1: Common relations suggested for k_s

Authors	Suggested expressions	Application
Biot, (1937)	$k_s = \dfrac{0.95}{b} \cdot \left(\dfrac{E_s b^4}{EI} \right)^{0.108} \cdot \dfrac{E_s}{1 - v_s^{\,2}}$	Infinite beams resting on an elastic soil continuum
Terzaghi, (1955)	$k_s = k_{s1} \dfrac{1}{b} \quad for\ clays$ $k_s = k_{s1} \left(\dfrac{b+1}{2b} \right)^2 \quad for\ sands$	Rigid slab placed on a soil medium
Vlassov, (1960, 1966)	$k_s = \dfrac{E_s (1 - v_s)}{(1 + v_s)(1 - 2v_s)} \cdot \left(\dfrac{\mu}{2b} \right)$	Beams and plates resting on elastic half space
Vesic, (1961)	$k_s = \dfrac{0.65}{b} \cdot \sqrt[12]{\dfrac{E_s b^4}{EI}} \cdot \dfrac{E_s}{1 - v_s^{\,2}}$	Infinite beams resting on an elastic soil continuum
Meyerhof & Baikie (1963)	$k_s = \dfrac{E_s}{(1 - v_s^{\,2}) \cdot b}$	Buried circular conduits
Kloppel & Glock (1979)	$k_s = \dfrac{2E_s}{(1 + v_s) \cdot b}$	Buried circular conduits
Selvadurai (1985)	$k_s = \dfrac{0.65}{b} \cdot \dfrac{E_s}{(1 - v_s^{\,2})}$	Buried circular conduits
Matsubara (2000)	$k_s = \dfrac{2\pi}{\log \lambda} \cdot \dfrac{E_s}{2(1 + v_s)} \cdot \dfrac{1}{b}$	Buried pipelines for seismic design
Ménard (Cassan, 1978)	$\dfrac{1}{k_s} = \dfrac{b}{9E_s} \cdot \lambda_c + \dfrac{2B_0}{9\alpha E_s} \cdot \left(\lambda_d \dfrac{b}{B_0} \right)^{\alpha}$	Beams and plates resting on elastic half space, different types of foundations ($E_{PMT} = \alpha \cdot E_s$, Cassan, 1978)

E_s and v_s: Young's soil modulus and Poisson's ratio of soil, μ: non-dimensional parameter, b: width of the foundation(external diameter in the case of buried pipe), EI: constant bending stiffness of the structure (E and I respectively Young's modulus of the structure and the moment of inertia of the cross section of the structure),B_0: reference width of the foundation, α: structural or rheological coefficient, E_{PMT}: Ménard's pressuremeter modulus, λ_c and λ_d: form factors of the foundation geometry, λ: the ratio between the distance to the point at which the displacement is regarded as null and the radius of pipe, k_{s1}: the coefficient of subgrade reaction for a plate 1 ft wide.

Terzaghi (1955) made some recommendations about k_s for 1×1 ft rigid slab placed on a soil medium (Terzaghi expression in Table 2-1). This equation is also relevant in analysis of plate load test results by substituting width of loading plate with 1ft, but some of the researchers instead of using these equations in plate load test suggest using of those modified by Arnold (Al-sanad et al., 1993).

Vlassov (1960, 1966) expression is introduced for beams and plates resting on elastic half space (Elachachi et al., 2004), but ambiguities of estimating μ (non-dimensional parameter) make the problem more complex (Elachachi et al., 2004; Sadrekarimi and Akbarzad, 2009).

Meyerhof (1963), Kloppel (1979) and Selvadurai (1985) expressions are proposed for computing the coefficient of horizontal subgrade reaction in buried circular conduits (Okeagu and Abdel-Sayed 1984) and are employed for evaluation of k_s in few limited cases (Elachachi et al., 2004).

One should note that the expression from Matsubara (2000) needs an additional parameter λ (λ: the ratio between the distance to the point at which the displacement is regarded as null and the radius of pipe). The magnitude of this parameter being non-defined, it is taken equal to 10 in this study.

If the site reconnaissance allows to acquire the deformation modulus E_{PMT}, we can use Ménard expression (Cassan, 1978) to determine the value of k_s.

The value of E_s can be obtained from in situ testing such as, the plate load test (Swiss test (V.S.S.), ASTM Standard Test, Westergaard test) (Cassan, 1978; ASTM, 1994; Ziaie Moayed and Naeini, 2006) and field-test drilling, such as pressuremeter testing (where $E_{PMT}=\alpha.E_s$, with E_{PMT} Ménard's pressuremeter modulus and α structural or rheological coefficient) (Cassan, 1978).

2.3. Nature and origin of uncertainties

As it was mentioned before (section 1.1) uncertainties can usually be divided into two groups: aleatory or active uncertainty and epistemic or passive uncertainty (Lacasse and Nadim, 1996; Uzielli et al., 2008). Soils are naturally variable because of the way they are formed and the random continuous processes of the environment that alter them. The uncertainty in the mechanical properties of soils (E_s and v_s) is due to the natural variability from point to point within a soil volume and from laboratory measurements. The uncertainty

in a length of low stiffness zone of soil beneath the pipe (L) comes from the natural spatial variability of soil on a site. Those in the width (b), height (h) and Young's modulus of the structure (E_c) and external diameter (d) might result in their construction.

One approach to estimating the soil parameters' uncertainties when sufficient data is not available is to use estimates based on published values, which are most conveniently expressed in terms of the coefficient of variation (CV). Values of the coefficient of variation for a number of geotechnical engineering parameters and in situ tests (such as soil strength properties, soil index parameters, field measurements and laboratory tests) have been compiled by Harr (1987), Kulhawy (1992), Lacasse and Nadim (1996, 1997), Phoon and Kulhawy (1999a,b) and Duncan (2000). However, few data exist in the literatures concerning the value of the coefficient of variation for soil modulus. Phoon and Kulhawy (1999a) determined the value of CV of soil modulus in sand from the direct methods (pressuremeter test and the dilatometer test) that was in the range of 15-70%. The CV of soil modulus in silt determined by standard penetration test below count was found to be in the range of 40-60% and the CV of soil modulus in clay was estimated to be highest (up to 85%) but from a correlation between soil modulus and standard penetration test values (Phoon and Kulhawy, 1999a).

From these different analyses a CV of soil modulus between 5 and 50% is considered in this study. The possible range of CV for the soil (v_s and L) and structure parameters (d and E_c) are based on statistical analyses and expert judgment, since there are no data available in the literatures concerning these parameters.

Concerning the uncertainties of b and h, we have studied a real experimental site located at Pessac (France) in order to estimate these uncertainties. This is described in the following.

- **Estimation of the uncertainties of b and h for a spread footing for a real individual house (experimental site of Pessac)**

The objective is to estimate the uncertainties on a width and a height of a spread footing for an individual house on the experimental site of Pessac for a preliminary evaluation of these uncertainties. As can be seen from Figure 2-1, a half of the individual house rests on the sandy soil and the other half rests on the clayey soil. The four spread footings of this house with the lengths of 6 m (for L_1 and L_3) and 10 m (for L_2 and L_4), width of 0.5 m and height of 0.3 m are also sketched in this figure. The spread footings (L_1) and (L_3) respectively rest on

the sandy soil and clayey soil while the half of the spread footings (L_2) and (L_4) rest on the clayey soil and the other half rest on the sandy soil.
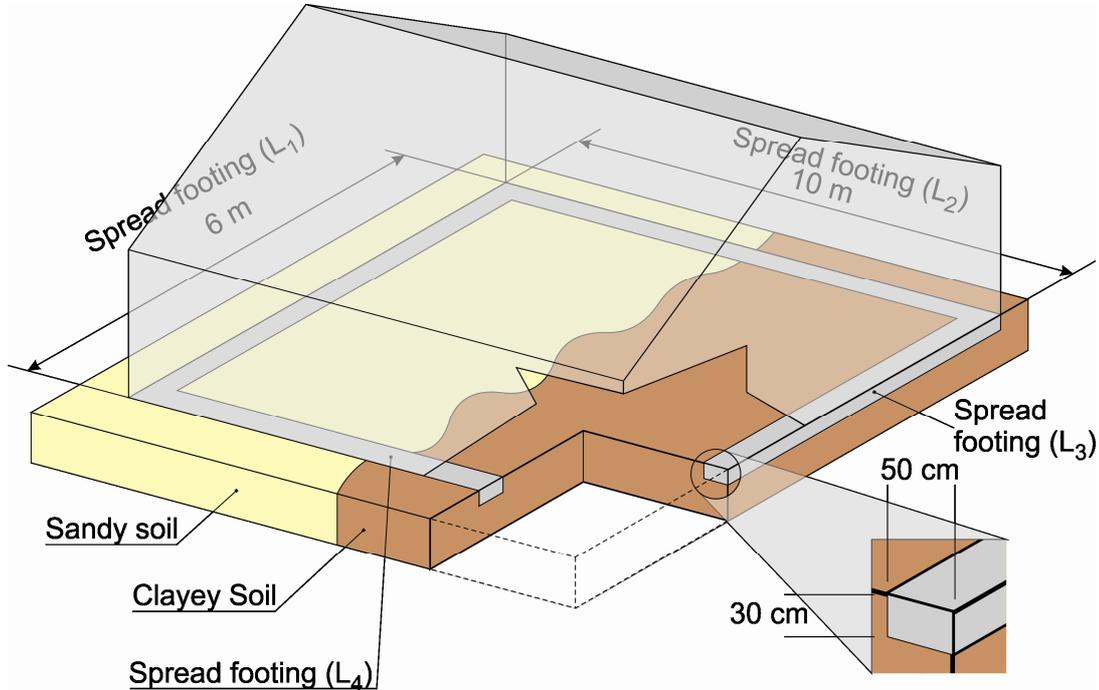
Figure 2-1: Constructed individual house with the four spread footings on the experimental site of Pessac

Different construction stages of these spread footings on the experimental site are shown in Figure 2-2. Figure 2-3 illustrates the measured widths and heights along the lengths of the spread footings during their constructions. This figure shows the natural spatial variability of these parameters along the spread footings during their construction on the experimental site.

Figure 2-2: Different construction stages of the spread footings on the experimental site of Pessac
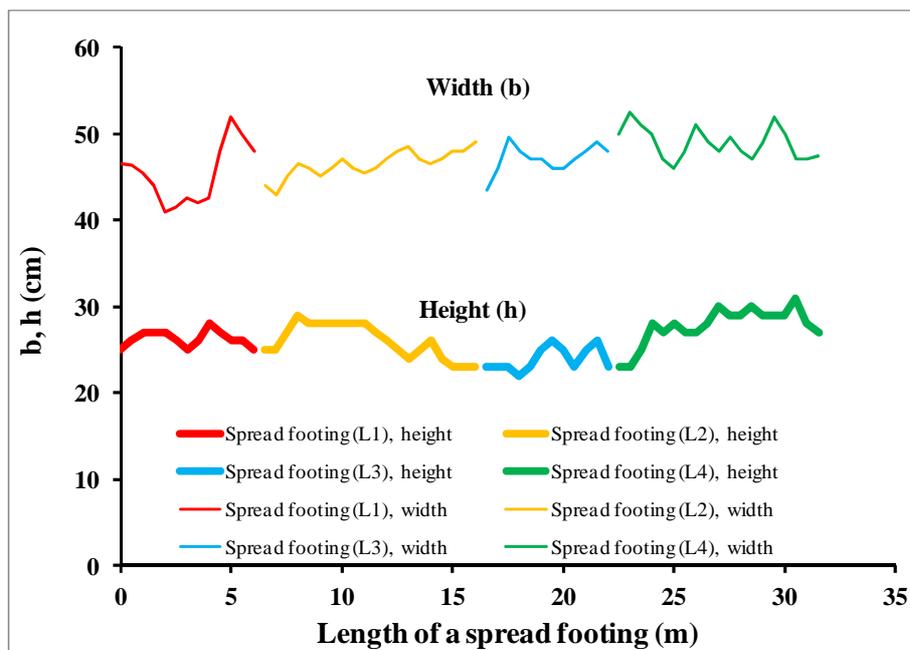
Figure 2-3: Measured widths and heights along the lengths of the spread footings during their construction

For the calculation of the coefficient of variations of *b* and *h* for each spread footing, we have considered the means of *b* and *h* for each spread footing (Figure 2-4a) which are not very different between spread footings. Note that these values are inferior to the expected values respectively 0.5 m and 0.3 m.

Figure 2-4b and Figure 2-4c shows the standard deviations and the associated coefficient of variations of these parameters (*b*, *h*) for these four spread footings. The value of the standard deviation of the width for the spread footings L_1 is greater than the value of the standard deviation of L_3, showing the difficulty to respect the width of a trench in sandy soil.
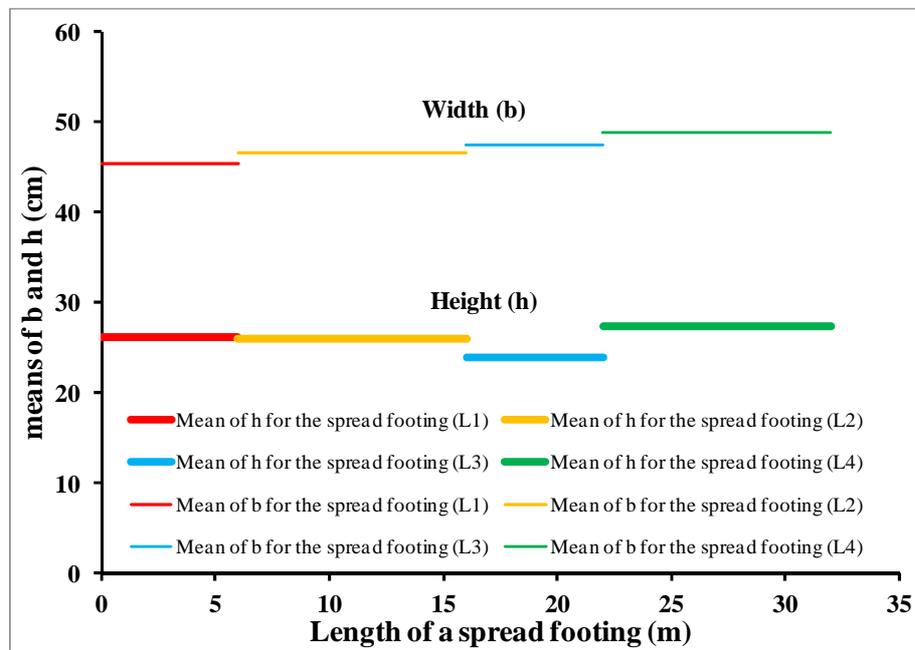
a)
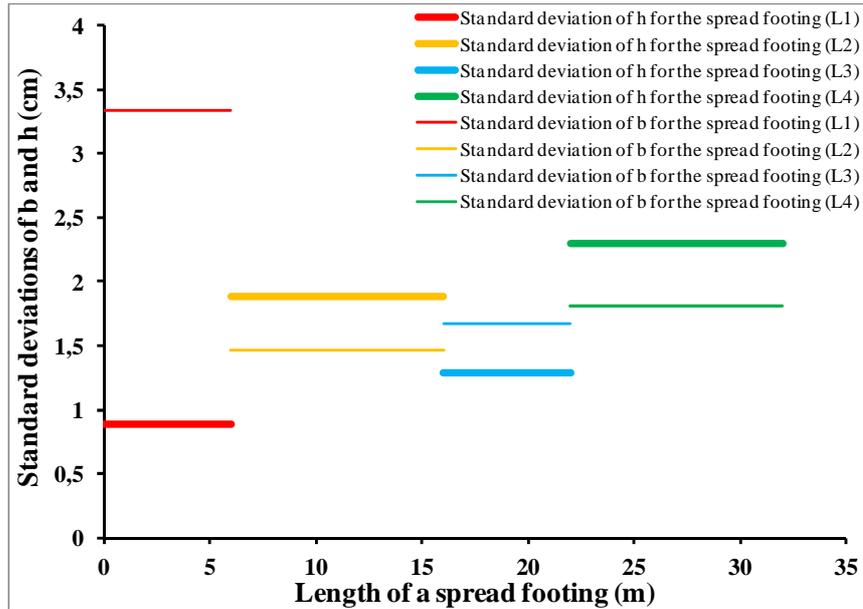
b)
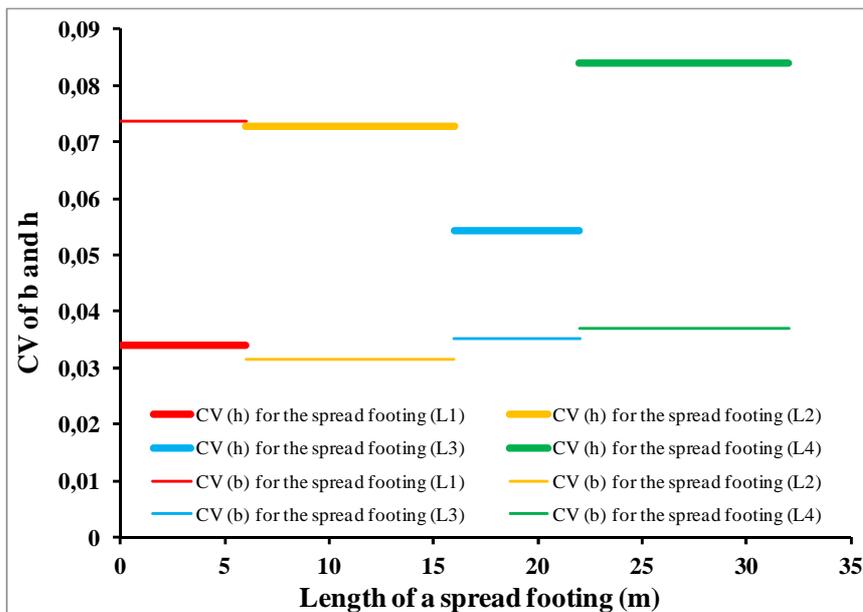
c)

Figure 2-4: a)Mean values of width (b) and height (h) along each spread footing, b) Standard deviations of these values for each spread footing and c) Associated coefficient of variations of these values for each spread footing

The maximum of inter assay *CV* for the width and height are respectively 0.074 and 0.084. The inter assay of the coefficient of variations of the width and height between the four spread

footings are respectively equal to 2.7% and 5% showing the inter variability between these spread footings. All these statistical results are resumed in Table 2-2.

Table 2-2: Intra and inter assay coefficient of variability

Spread footing	L (m)	$\bar{b}$ (m)	$\bar{h}$ (m)	σ_b (m)	σ_h (m)	CV_b	CV_h
L_1	6	45.37	26.23	3.34	0.89	0.074	0.034
L_2	10	46.52	25.95	1.47	1.89	0.031	0.073
L_3	6	47.35	23.85	1.67	1.29	0.035	0.054
L_4	10	48.83	27.38	1.81	2.30	0.037	0.084
$L_1 + L_2 + L_3 + L_4$	36	47.08	26.77	2.47	2.15	0.05	0.08
L_1, L_2, L_3, L_4 (inter assay)	-	47.01	25.85	1.26	1.27	0.027	0.049

L: length of a spread footing, $\bar{b}$: mean width, $\bar{h}$: mean height, σ_b and σ_h respectively standard deviations of b and h, CV_b and CV_h respectively coefficient of variation of b and h

Of course, these results are for the constructed individual house with only four spread footings on the experimental site of Pessac, but they give a first estimation of the coefficient of variations for these parameters in case of similar projects.

A synthesis of the origin of the soil and the structure parameters' uncertainties is presented in Table 2-3.

Table 2-3: Origin of uncertainties in the soil and structure parameters and possible range of the coefficient of variation for each parameter (in the case of spread footing and buried pipe)

Parameter	Aleatory uncertainty	Epistemic uncertainty		Possible range of the coefficient of variation %
	Natural variability	Measurement uncertainty	Construction uncertainty	
E_s	*	*		[5-50]
v_s	*	*		[2-10]
L	*			[5-50]
b			*	[2-10]
h			*	[2-10]
d			*	[2-5]
E_C			*	[2-10]

E_s: Young's soil modulus, v_s: Poisson's ratio of soil, L: length of low stiffness zone of soil beneath the pipe, b and h are respectively width and height of the spread footing, d: external diameter of the pipe, E_c: Young's modulus of buried pipe or spread footing

2.4. FOSM and SOSM methods

The calculation methods of variance used in this study are based on the first order (FOSM) and the second order (SOSM) of the Taylor series with the assumption that the input parameters act independently of each other.

Equation 1-38 and Equation 1-40, expressed in terms of variance, are rewritten in terms of the coefficient of variation CV (standard deviation divided by the mean), Equation 2-1 for the FOSM method and Equation 2-2 for the SOSM method (Imanzadeh et al., 2011):

$$CV^2_{f(x)}(x_i) = \sum_i^n \left(\frac{\partial f(x)}{\partial x_i} \cdot \frac{\overline{x_i}}{\overline{f(x)}} \right)^2 \cdot CV^2_{x_i} \qquad \text{Equation 2-1}$$

$$CV^2_{f(x)}(x_i) = \sum_i^n \left(\frac{\partial f(x)}{\partial x_i} \cdot \frac{\overline{x_i}}{\overline{f(x)}} \right)^2 \cdot CV^2_{x_i} + A_{x_i} \cdot CV^4_{x_i} \qquad \text{Equation 2-2}$$

with

$$A_{x_i} = \sum_i^n \left(\frac{1}{2} \cdot \frac{\partial^2 f(x)}{\partial x_i^2} \cdot \frac{(\overline{x_i})^2}{\overline{f(x)}} \right)^2 \cdot \lambda \qquad \text{Equation 2-3}$$

where $CV_{f(x)}(x_i)$ is the coefficient of variation of $f(x)$ for the i input variables (x_i), CV_{x_i} the coefficient of variation for the input variable i, $\overline{x_i}$ the mean of the input variables i, $\overline{f(x)}$ the mean of the function $f(x)$ and n the number of variables.

The greatest advantage of the FOSM method is its simplicity; no higher moments or distributional information on the system's basic variables are necessary. When applied to engineering design problems, one issue can be pointed out:

- The relative non-accuracy of the first order Taylor series approximation for strong non-linear problems. The SOSM method is often used to quantify the non-linear level of the studied function.

However, one of the strengthest of the FOSM method is that, it allows the assessment of the absolute contribution of the individual basic variable uncertainties to the uncertainties of the overall system (sensibility analysis).

2.5. Estimation of the influence of soil and structure parameters on the coefficient of variation of k_s

The influence of the variability of the soil parameters, the geometry and the mechanical properties of the structure (spread footing and buried pipe) on the reaction coefficient (k_s) will be successively studied for each semi-empirical model using the FOSM and SOSM methods (Equation 2-1 and Equation 2-2) in the following. All calculations are performed using MAPLE© software.

2.5.1. Common semi-empirical models for calculating the modulus of soil reaction for spread footings

Four semi-empirical models (Biot (1937), Vlassov (1960, 1966), Vesic (1961) and Ménard (Cassan, 1978)), commonly used in the design of spread footings, are considered in this study in order to obtain a value of the soil reaction modulus. These semi-empirical models are represented in Table 2-4. The calculation of k_s is a function of soil parameters (modulus of the soil E_s and Poisson's ratio of soil v_s), the parameters related to the geometry of the foundation (width b and height h) and a mechanical property of the foundation (the Young's modulus of the concrete E_c) (Table 2-4).

Table 2-4: Semi-empirical models proposed for the modulus of soil reaction (k_s) for spread footings

Author	Semi-empirical model
Biot (1937)	$k_s = \dfrac{0.95}{b} \cdot \left(\dfrac{12 E_s b^3}{E_c h^3} \right)^{0.108} \cdot \dfrac{E_s}{1 - v_s^2}$
Vlassov (1960, 1966)	$k_s = \dfrac{E_s(1 - v_s)}{(1 + v_s)(1 - 2v_s)} \cdot \left(\dfrac{\mu}{2b} \right)$
Vesic (1961)	$k_s = \dfrac{0.65}{b} \cdot \sqrt[12]{\dfrac{12 E_s b^3}{E_c h^3}} \cdot \dfrac{E_s}{1 - v_s^2}$
Ménard (Cassan, 1978)	$\dfrac{1}{k_s} = \dfrac{b}{9 E_s} \cdot \lambda_c + \dfrac{2 B_0}{9 \alpha E_s} \cdot \left(\lambda_d \dfrac{b}{B_0} \right)^{\alpha}$

E_s and v_s: Young's soil modulus and Poisson's ratio of soil, μ: non-dimensional parameter, b, h and E_c: width, height and Young's modulus of the foundation, B_0: reference width of the foundation, α: structural or rheological coefficient, E_{PMT}: Ménard's pressuremeter modulus, λ_c and λ_d: form factors of the foundation geometry

In order to compare these models between each other, we take the common dimensions of a wall footing for a residential construction: width of 0.5 m, height of 0.3 m and length of 10 m. Young's modulus of the foundation E_c is equal to 20 GPa and the parameter μ=1. In the case of the pressuremeter α=0.5, the reference width of the foundation *(B_0)* equal to 0.60 m and the form factors of the foundation geometry λ_c and λ_d are all determined as a function of the ratio between the length and the width of the foundation.

The coefficient of reaction for the modulus E_s between 1 and 30 MPa and Poisson's ratio of 0.3, presents values between 0.875 and 63 MN.m^{-3} (Figure 2-5). Ménard's model gives the greatest values of k_s and Vesic's model gives the lowest values; for the considered values in this example, a factor of two exist between these two models. The multitude of models underlines the difficulty for the practitioner to choose a value of subgrade reaction modulus for a given value of E_s.
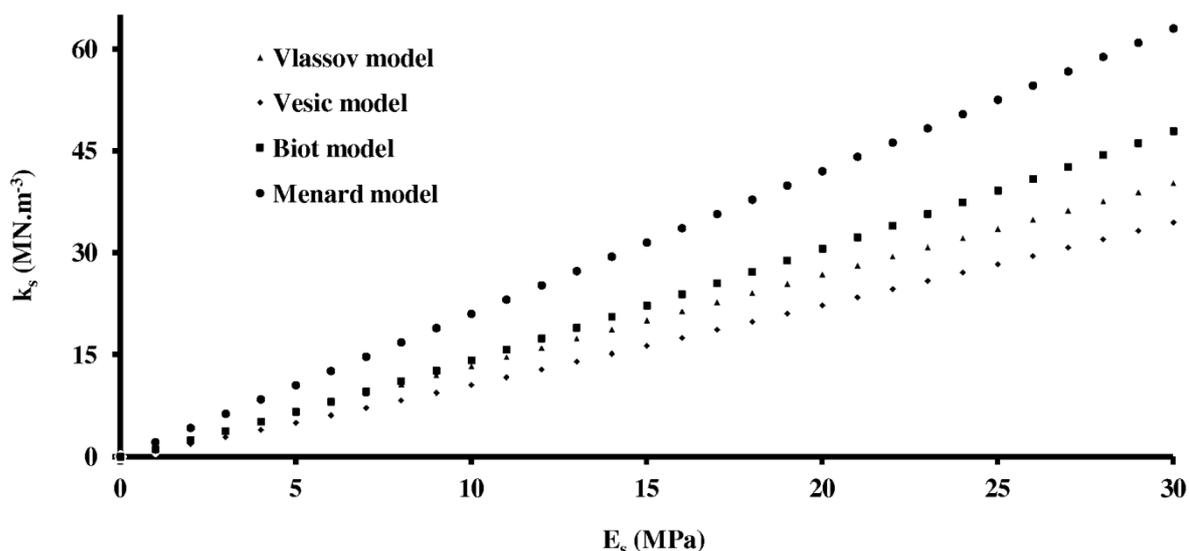
Figure 2-5: Evolution of the coefficient of soil reaction (k_s) as a function of Young's soil modulus (E_s) for studied semi-empirical models.

2.5.1.1. Estimation of the influence of soil and spread footing parameters on the coefficient of variation of k_s (FOSM method)

Soil subgrade reaction coefficient (k_s) is a function of the soil parameters (E_s, v_s) and the spread footing (b, h, E_c) (Table 2-4). The origin of uncertainties differs in the function of these parameters (Table 2-3).

Using the FOSM method, the coefficient of variation of k_s can be obtained, for the four semi-empirical models, by a unique expression including coefficients of variation of the soil and the structure parameters with different weights (Equation 2-4). The values of η_{xi} depend on each semi-empirical model and give the absolute contribution of the individual basic variable uncertainties to the uncertainty of k_s.

$$CV_{k_s} = \left((\eta_{E_s} CV_{E_s})^2 + (\eta_b CV_b)^2 + (\eta_{v_s} CV_{v_s})^2 + (\eta_h CV_h)^2 + (\eta_{E_c} CV_{E_c})^2 \right)^{0.5}$$

Equation 2-4

2.5.1.2. Estimation of the influence of the soil parameters

The relationship between the modulus of the soil (E_s) and the reaction modulus (k_s) is linear for the Ménard and Vlassov models, and non-linear for the Vesic and Biot models (Table 2-4). This leads to coefficients $\eta_{Es}=1$ for the Ménard and Vlassov models and $\eta_{Es}=1.1$ for the Vesic and Biot models.

The uncertainty of Poisson's ratio of soil is not generally taken into account and a deterministic value, from expert judgment, is often considered. However, the uncertainty of this parameter cannot be neglected in the three models with the presence of this parameter, especially in the case of the Vlassov model; its expression for η_{vs} is given by the following formula (Equation 2-5):

$$\eta_{v_s} = \frac{2v_s^2(2-v_s)}{(1-v_s^2)(1-2v_s)} \qquad \qquad Equation\ 2\text{-}5$$

For the interval between 0.15 and 0.35 for Poisson's ratio, the coefficient η_{vs} varies from 0.12 to 1.5 (Figure 2-6).

In the case of the Vesic and Biot models we obtain the same expression for the coefficient η_{vs} (Equation 2-6):

$$\eta_{v_s} = \frac{2v_s^2}{1-v_s^2} \qquad \qquad Equation\ 2\text{-}6$$

The coefficient η_{vs} for the same interval 0.15 to 0.35 for Poisson's ratio varies from 0.05 to 0.28. For these two models, the influence of the uncertainty of Poisson's ratio is less important than for Vlassov's model (Figure 2-6).
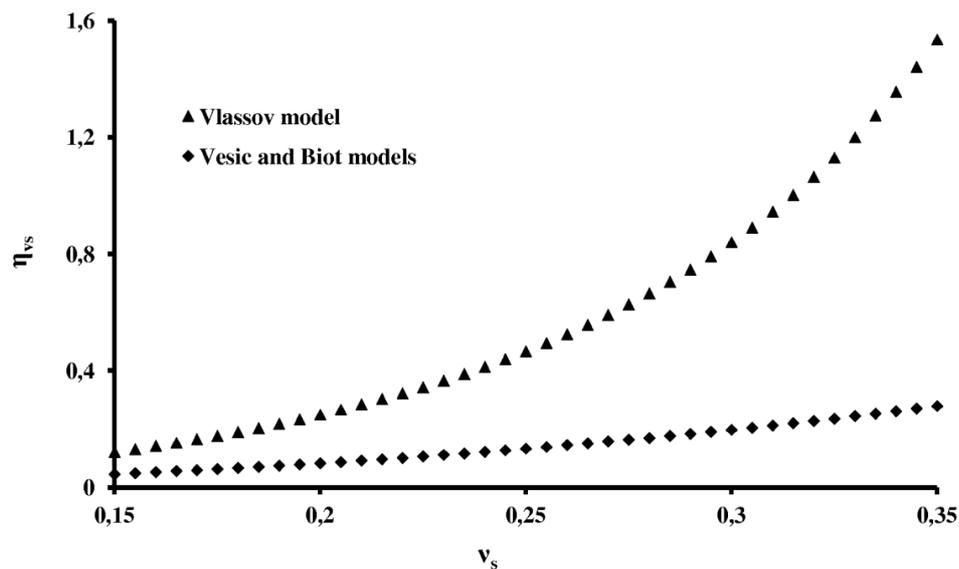
Figure 2-6 : Evolution of coefficient η_{vs} as a function of the Poisson's ratio of soil (v_s) for studied semi-empirical models (FOSM method)

2.5.1.3. Estimation of the influence of the spread footing parameters

The width of the spread footing *(b)* comes in four models, its height *(h)* and Young's modulus of concrete only in the Vesic and Biot models. For the parameter *(b)*, we obtain a coefficient η_b= 0.75, 0.675 and 1 respectively for the Vesic, Biot and Vlassov models. The coefficient η_b for the Ménard model is a function of *b*:

$$\eta_b = 0.5 \cdot \frac{830\sqrt{b} + 1401}{415\sqrt{b} + 1401} \qquad\qquad Equation\ 2\text{-}7$$

The influence of the variability of this parameter on the variability of k_s is more important for the Vlassov model, then the Vesic and Biot, and finally for the Ménard where η_b= 0.59 for the foundation width equal to 0.5 m. When the foundation width is between 1.5m and 3m (for the Ménard model), its value becomes almost constant and close to the value of the Biot model (Figure 2-7).
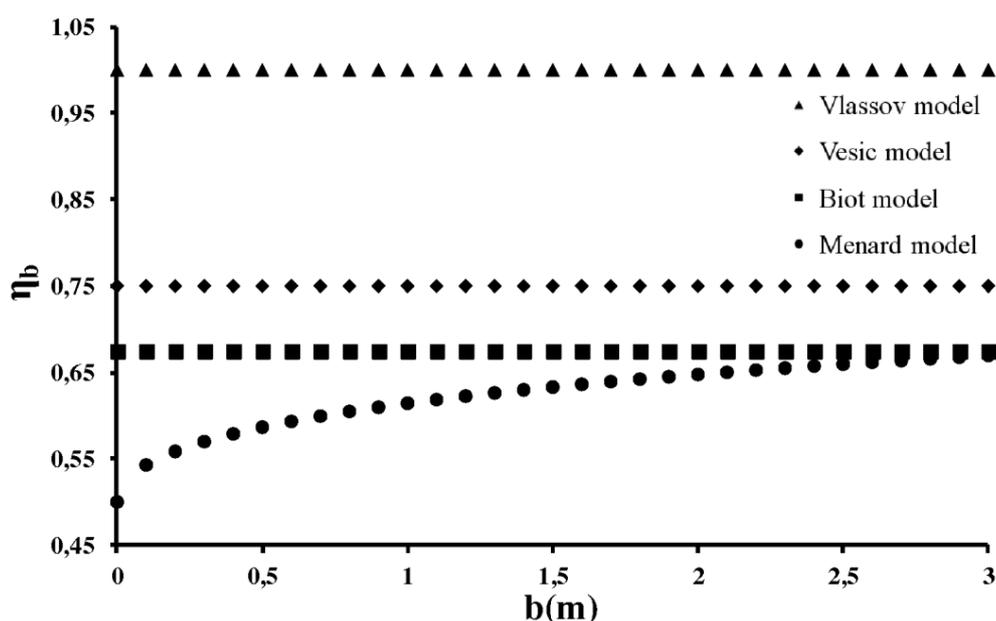
Figure 2-7: Evolution of coefficient η_b as a function of the foundation width (b) for studied semi-empirical models (FOSM method)

Concerning the height of the foundation *(h)*, we obtain the coefficients η_h=0.25 and 0.324 respectively for the Vesic and Biot models. The influence of the variability of the parameter *(h)* on the reaction coefficient *(k_s)* for the Biot model is more important than Vesic's model but remains two to three times smaller than the influence of the parameter *(b)*.

For Young's modulus of concrete, Vesic's and Biot's models give a coefficient η_{Ec}, also very similar, it is possible to give an average coefficient $\eta_{Ec}=0.1$. The value of CV_{Ec} depends on the quality of concrete. Even for concretes which their properties will be very different from a spread footing to another spread footing ($CV_{Ec}=20\%$), uncertainty on the coefficient of reaction due to this parameter remain low (2%). The uncertainty of this parameter in the estimation of the coefficient of variation of k_s can be neglected.

The synthesis table (Table 2-5) shows all the relations obtained by the FOSM method and gives, for the same value of CV_{xi}, the most influential parameters on the estimation of the variability of k_s.

Table 2-5: Coefficient η_{xi} obtained for each parameter of semi-empirical models (FOSM method)

η_{xi}	Semi-empirical models			
	Ménard	**Vlassov**	**Vesic**	**Biot**
η_{E_s}	1 ***	1 ***	1.083 ***	1.108 ***
η_b	$0.5 \cdot \dfrac{830\sqrt{b}+1401}{415\sqrt{b}+1401}$ **	1 ***	0.75 **	0.6750 **
η_{v_s}	-	$\dfrac{2v_s^2(2-v_s)}{(1-v_s^2)(1-2v_s)}$ ***	$\dfrac{2v_s^2}{1-v_s^2}$ **	$\dfrac{2v_s^2}{1-v_s^2}$ **
η_h	-	-	0.25 **	0.324 **
η_{Ec}	-	-	0.0833 *	0.108 *

*: low influence, **: moderate influence, ***: high influence

2.5.1.4. Quantification of non-linearities in the estimation of coefficient of variation of k_s (SOSM method for spread footing)

Equation 2-3 allows us to obtain the coefficient A_{xi} for each parameter of semi-empirical models using the SOSM method. All the obtained expressions are presented in Table 2-6.

The calculated coefficient values in this Table give the importance of non-linearity attached to each of the parameters.

Table 2-6: Coefficient A_{xi} obtained for each parameter of semi-empirical models (SOSM method).

The parameter of λ depends on the probability distribution

A_{x_i}	Semi-empirical models			
	Ménard	**Vlassov**	**Vesic**	**Biot**
A_{E_s}	-	-	$0.002\,\lambda$	$0.0036\,\lambda$
A_b	$0.016 \cdot \dfrac{(1377800b + 5232735\sqrt{b} + 5888403)^2\,\lambda}{(415\sqrt{b}+1401)^4}$	λ	$0.431\,\lambda$	$0.321\ \lambda$
A_{v_s}	-	$\dfrac{4\,(1-2v_s{}^3+6v_s{}^2)^2\,v_s{}^4}{(1-v_s)^2(1-2v_s)^4(1+v_s)^4}\cdot\lambda$	$\dfrac{(1+3v_s{}^2)^2\,v_s{}^4}{(1-v_s{}^2)^4}\cdot\lambda$	$\dfrac{(1+3v_s{}^2)^2\,v_s{}^4}{(1-v_s{}^2)^4}\cdot\lambda$
A_h	-	-	$0.024\,\lambda$	$0.046\,\lambda$
A_{E_c}	-	-	$0.002\,\lambda$	$0.0036\,\lambda$

The values of the coefficients A_{Es}, A_h , A_{Ec} for all these semi-empirical models and with $\lambda=2$ (for a preliminary evaluation, all random variables are assumed to follow a normal distribution) are between 4×10^{-3} and 92×10^{-3} showing insignificant effects on the second order terms of Taylor series (Equation 2-2).

The coefficient A_b for the Ménard model is a function of b (Table 2-6). Evolution of coefficient A_b as a function of the foundation width (b), for studied semi-empirical models using the SOSM method, is shown in Figure 2-8. As in the case of calculation the coefficient η_b, the value of the coefficient A_b is the greatest for the Vlassov model and the smallest for the Ménard model. When the foundation width increases the value of Ménard model is close to the value of the Biot model.
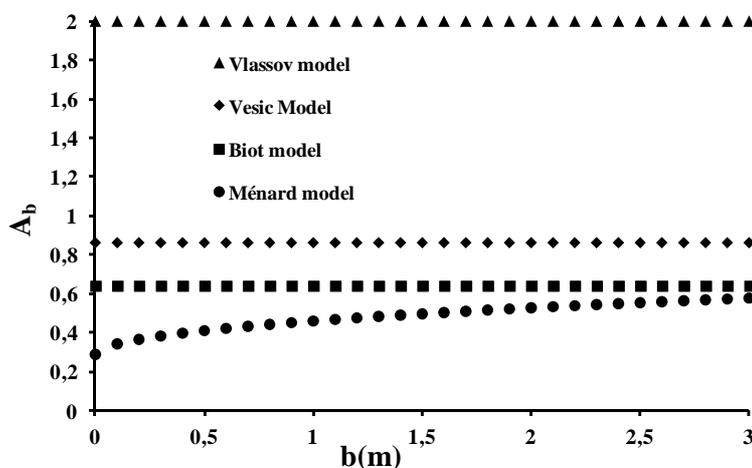
Figure 2-8: Evolution of coefficient A_b as a function of the foundation width (b) for studied semi-empirical models (SOSM method)

Concerning the Poisson's ratio of soil, the coefficient A_{vs} for these models is a function of v_s (Table 2-6). For the value of v_s between 0.25 and 0.35, the coefficient A_{vs} for the Vlassov model varies from 0.66 to 28.73 while for the Biot and Vesic models (with the same expression) it varies only in a range from 0.014 to 0.095 (Table 2-6, Figure 2-9).
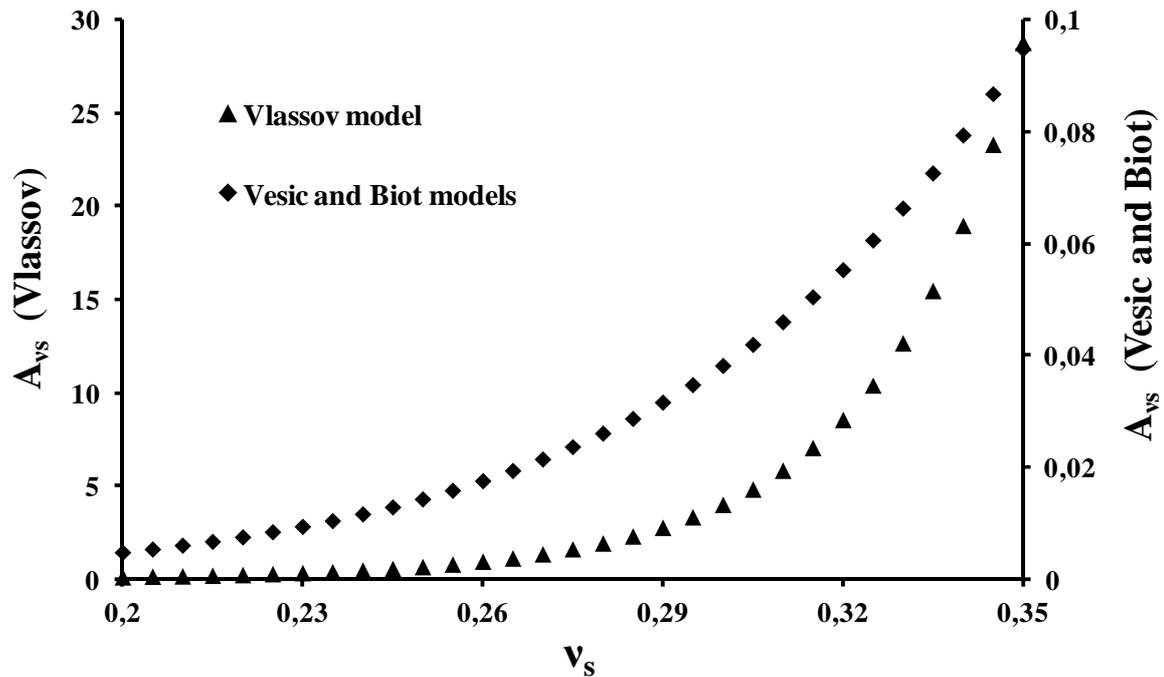
Figure 2-9: Evolution of coefficient A_{vs} *as a function of the Poisson's ratio of soil (v_s) for studied semi-empirical models (SOSM method)*

These coefficients (A_h, A_{Ec}, A_{vs}, A_b), will be multiplied by coefficients of variation below 10% with the power of four (Table 2-3, Equation 2-2), then the second order terms calculated by the SOSM method ($A_{xi} \cdot CV_{xi}^4$, Equation 2-2) can be neglected. The FOSM method alone is sufficient to correctly estimate the coefficients of variation of k_s. The improvement in accuracy is not always worth the extra computational effort, and these results confirm why SOSM method has not often found wide use in geotechnical applications.

2.5.1.5. Simplified formulas for the calculation of the coefficents of variation of k_s in the case of spread footing

The evolution of CV_{ks} (Coefficient of Variation of k_s obtained from Equation 2-4) as a function of CV_{Es} (Coefficient of Variation of E_s) for these semi-empirical models is shown in Figure 2-10. For this and as an example, different parameters have to be fixed: $b=0.5$ m, $v_s = 0.3$ and the coefficients of variation for each parameter equal to 10%.

When CV_{Es} is close to zero, the coefficient of variation of k_s is greater for the Vlassov model and then for Vesic's and Biot's models. The coefficient of variation of k_s varies between 0.06 and 0.13 (Figure 2-10). Ménard's model which only takes into account the uncertainty of the parameters b and E_s gives, as expected, the lowest value of the coefficient of variation of k_s whatever the value of CV_{Es}. For the value of CV_{Es} greater than 0.2 (Figure 2-10), we observe a linear behavior between CV_{ks} and CV_{Es}, which shows that the influence of the variability of structure parameters and Poisson's ratio is less important when the coefficient of variation of E_s is high. In this case, the coefficient of variation of k_s for the Biot model is greater than those from other expressions while the Vlassov model tends to the Ménard model. Then the coefficient of variation of k_s is directly proportional to the coefficient of variation of E_s, it can take a unique expression as (Equation 2-8):

$$CV_{k_s} = \eta_{E_s} CV_{E_s}$$

Equation 2-8

where $\eta_{Es}=1$ for the Ménard and Vlassov models and $\eta_{Es}=1.1$ for the Vesic and Biot models.

The Equation 2-8, allows us to obtain a first estimate of the coefficient of variation of k_s when the coefficient of variation of E_s is 2 to 3 times greater than the values of the coefficients of variation of the parameters b, v_s and h.
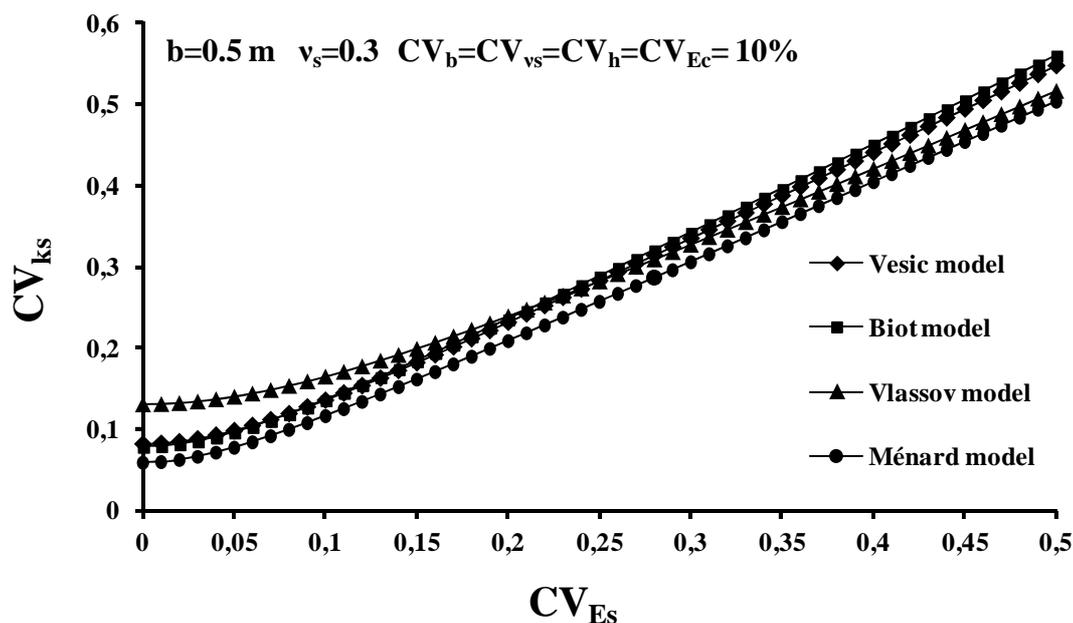
Figure 2-10: Evolution of CV_{ks} (Coefficient of Variation of k_s), as a function of CV_{Es} (Coefficient of Variation of E_s) for studied semi-empirical models (FOSM method)

The coefficient η_{xi} (Table 2-5) was simplified for the values of foundation width (*b*) and the Poisson's ratio of soil (v_s) for these semi-empirical models (Table 2-7). From Equation 2-4, simplified expressions are obtained for the values of *b* between 0.3 and 1.5 m for the Ménard model (Equation 2-9) and the values of v_s between 0.25 and 0.35 for the Vlassov (Equation 2-10), Vesic (Equation 2-11) and Biot (Equation 2-12) models:

Table 2-7: simplified coefficient η_{xi} obtained for each parameter of semi-empirical models (FOSM method)

η_{x_i}	Semi-empirical models			
	Ménard	**Vlassov**	**Vesic**	**Biot**
η_{E_s}	1 ***	1 ***	1.083 ***	1.108 ***
η_b	$(0.05b + 0.56)$ for $b = [0.3m\,;\,1.5m]$ ** 0.65 for $b = [1.5m\,;\,3m]$ **	1 ***	0.75 **	0.675 **
η_{v_s}	-	$(10.4v_s - 2.22)$ for $v_s = [0.25\ 0.35]$ ***	0.2 **	0.2 **
η_h	-	-	0.25 **	0.324 **

*: low influence, **: moderate influence, ***: high influence

$$CV_{k_s} = \left(CV_{E_s}{}^2 + ((0.05b + 0.56) . CV_b)^2 \right)^{0.5}$$

Equation 2-9

$$CV_{k_s} = \left(CV_{E_s}{}^2 + CV_b{}^2 + ((10.4\, v_s - 2.22) . CV_{v_s})^2 \right)^{0.5}$$

Equation 2-10

$$CV_{k_s} = \left((1.083 . CV_{E_s})^2 + (0.75 . CV_b)^2 + (0.2 . CV_{v_s})^2 + (0.25 . CV_h)^2 \right)^{0.5}$$

Equation 2-11

$$CV_{k_s} = \left((1.108 . CV_{E_s})^2 + (0.675 . CV_b)^2 + (0.2 . CV_{v_s})^2 + (0.324 . CV_h)^2 \right)^{0.5}$$

Equation 2-12

The error between the coefficients of variation of k_s from the simplified models and those from the full models is on average less than 2%. Simplification is acceptable and provides simplified expressions when taking into account the minimum parameters for an easier determination of the coefficient of variation of the soil reaction modulus in the case of spread footing.

2.5.2. Common semi-empirical models for calculating the modulus of soil reaction for buried pipes

Six semi-empirical models (Biot (1937), Vesic (1961), Meyerhof & Baikie (1963), Kloppel & Glock (1979), Matsubara (2000) and Selvadurai (1985)), commonly used in the design of buried pipes, are considered in this study in order to obtain a value of the soil reaction modulus (k_s) (Table 2-8). The calculation of k_s is a function of soil parameters such as the soil modulus (E_s) and soil Poisson's ratio (v_s), the parameters related to the geometry of the pipe (external diameter (d) and thickness (e)) and a mechanical property of the pipe (the Young's modulus of the concrete (E_c) or steel (E_P)) (Table 2-8).

Table 2-8: Semi-empirical models proposed for the modulus of soil reaction (k_s) for buried pipes

Authors	Semi-empirical models
Biot (1937)	$k_s = \dfrac{0.95}{d} \cdot \left(\dfrac{64.E_s d^4}{E_c \pi (d^4 - (d - 2e)^4)} \right)^{0.108} \cdot \dfrac{E_s}{1 - v_s^2}$
Vesic (1961)	$k_s = \dfrac{0.65}{d} \cdot \left(\dfrac{64.E_s d^4}{E_c \pi (d^4 - (d - 2e)^4)} \right)^{0.083} \cdot \dfrac{E_s}{1 - v_s^2}$
Meyerhof & Baikie (1963)	$k_s = \dfrac{E_s}{(1 - v_s^2)d}$
Kloppel & Glock (1979)	$k_s = \dfrac{2 E_s}{(1 + v_s)d}$
Matsubara (2000)	$k_s = \dfrac{2\pi}{\log \lambda} \cdot \dfrac{E_s}{2(1 + v_s)} \cdot \dfrac{1}{d}$
Selvadurai (1985)	$k_s = \dfrac{0.65}{d} \cdot \dfrac{E_s}{(1 - v_s^2)}$

E_s: Young's soil modulus, v_s: Poisson's ratio of soil, d: external diameter of the pipe, E_c: Young's modulus of the pipe, e: thickness of the pipe and λ: the ratio between the distance to the point at which the displacement is regarded as null and the radius of pipe.

In order to compare these models with each other, we take the common dimensions of a buried pipe: external diameter of 1.5 m and thickness of 0.15 m. Young's modulus of the concrete pipe (E_c) is equal to 20 GPa (Young's modulus of the pipe for a continuous buried steel pipe is equal to 210 GPa), Poisson's ratio of 0.3 and the magnitude of parameter λ being non-defined, it was taken to be equal to 10. The coefficient of reaction for the modulus E_s between 1 and 30 MPa, presents values between 0.293 and 48,3 MN.m^{-3} (Figure 2-11). Matsubara's model gives the greatest value of k_s and Vesic's model gives the lowest value of k_s. The value of k_s for Kloppel's model is almost the average of the values of these two models. Biot's and Selvadurai's models give almost the same value of k_s and the value of k_s for the Meyerhof model is nearly twice that of the value of the Vesic model for the considered values in this example. The multitude of models giving very different results, it underlines again the difficulty for the practitioner to choose a value of the subgrade reaction modulus for a given value of E_s.
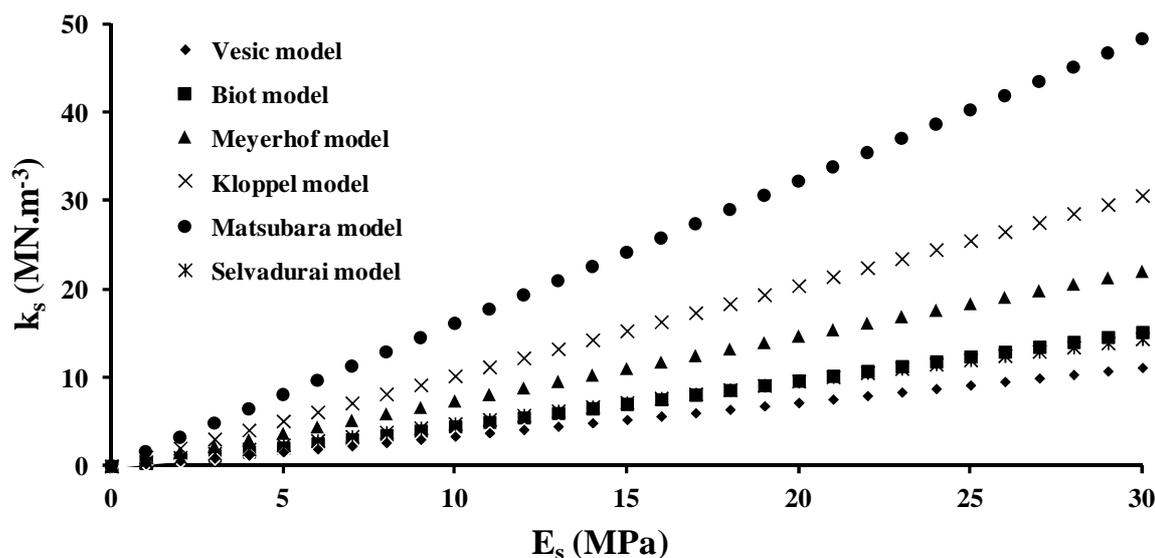
Figure 2-11: Evolution of the coefficient of soil reaction (k_s) as a function of Young's soil modulus (E_s) for studied semi-empirical models.

2.5.2.1. Uncertainty estimation of the coefficient of subgrade reaction k_s (FOSM method) for the buried pipe parameters

2.5.2.1.1. Effect of the soil parameters

Soil subgrade reaction coefficient (k_s) is a function of the soil parameters (E_s, v_s) and buried pipe parameters (d, E_c). The unwanted variation of thickness in a pipe is not taken into account and the deterministic value equal to 0.15 m is considered for a pipe thickness. As it was mentioned earlier in chapter 1 (section 1.5.2), a concrete buried pipe with the quasi rigid joints is considered in this study with the simplication of the same rigidity all along the pipeline.

The relationship between the soil modulus (E_s) and the reaction modulus (k_s) is linear for the Meyerhof, Kloppel, Matsubara and Selvadurai models, and non-linear for Vesic and Biot's models (Table 2-8). This leads to coefficients $\eta_{Es}=1$ for the Meyerhof, Kloppel, Matsubara and Selvadurai models and $\eta_{Es}=1.1$ for the Vesic and Biot models (The value of η_{xi} obtains from Equation 2-4).

In the case of the Vesic, Biot, Meyerhof and Selvadurai models we obtain the same expression for the coefficient η_{vs} (Equation 2-13):

$$\eta_{v_s} = \frac{2v_s^2}{1-v_s^2}$$

Equation 2-13

For the interval between 0.15 and 0.35 for Poisson's ratio, the coefficient η_{vs} varies from 0.05 to 0.28 (Figure 2-12).

In the case of Matsubara and Kloppel's models we obtain the same expression for the coefficient η_{vs} (Equation 2-14):

$$\eta_{v_s} = \frac{v_s}{1+v_s}$$

Equation 2-14

For the same interval 0.15 to 0.35 for Poisson's ratio, the coefficient η_{vs} varies from 0.13 to 0.26 (Figure 2-12).

For these six models, the influence of the uncertainty of Poisson's ratio on the uncertainty of k_s remains less important than the uncertainty of E_s.
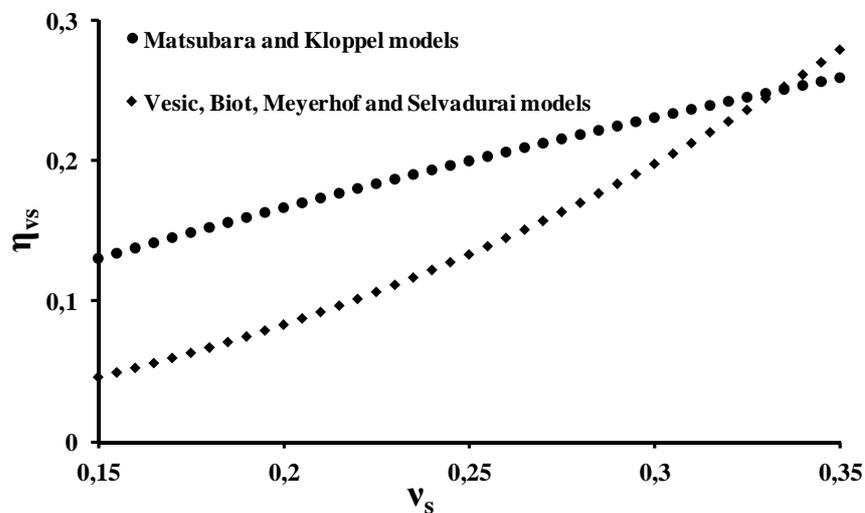

Figure 2-12: Evolution of coefficient η_{vs} as a function of the Poisson's ratio of soil (v_s) for studied semi-empirical models (FOSM method)

2.5.2.1.2. Effect of the buried pipe parameters

The external diameter of the pipe *(d)* appears in each model and Young's modulus of concrete only in Vesic and Biot's models. For the parameter *d*, we obtain a coefficient $\eta_d=1$

for the Meyerhof, Kloppel, Matsubara and Selvadurai models. The coefficient η_d for Vesic and Biot's models is a function of external diameter *(d)* and thickness *(e)* of the pipe ($\eta_d = f$ *(d³, d², d, e³, e², e))*. Evolution of coefficient η_d as a function of the external diameter of pipe *(d)* for these semi-empirical models is shown in Figure 2-13. The influence of the uncertainty of this parameter *d* on the uncertainty of k_s is more important for the Meyerhof, Kloppel, Matsubara and Selvadurai models *(η_d=1)* than for Vesic and Biot's models (for example, if *e*=0.15m and *d*>1m, the value of *η_d=0.93* for Vesic's and *η_d=0.91* for Biot's model). The influence of *d* is almost as important as that of E_s.
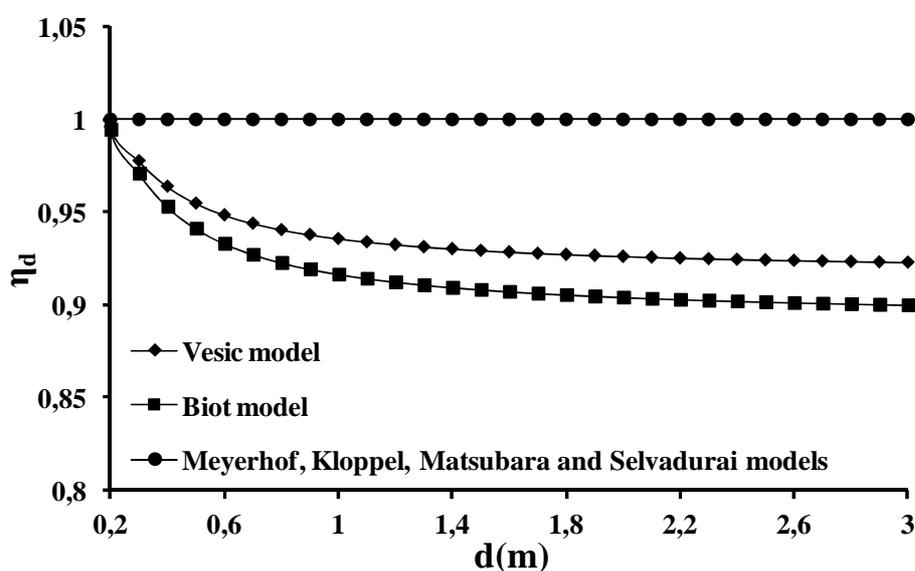
Figure 2-13: Evolution of coefficient η_d as a function of the external diameter of pipe (d) for studied semi-empirical models (FOSM method, e=0.15 m).

For Young's modulus of concrete, Vesic and Biot's models give a coefficient η_{Ec} also very similar; it is possible to give an average coefficient η_{Ec}= 0.1. As in the case of the spread footings, the uncertainty of this parameter in the estimation of the coefficient of variation of k_s can be neglected.

Table 2-9 shows all the relations obtained by the FOSM method and gives, for the same value of CV_{xi}, the most influential parameters on the estimation of the uncertainty of k_s.

Table 2-9: Coefficient η_{xi} obtained for each parameter of semi-empirical models (FOSM method)

η_{x_i}	Semi-empirical models					
	Vesic	Biot	Meyerhof	Kloppel	Matsubara	Selvadurai
η_{E_s}	1.0833 ***	1.108 ***	1 ***	1 ***	1 ***	1 ***
η_d	$f(d^3, d^2, d, e^3, e^2, e)$ ***	$f(d^3, d^2, d, e^3, e^2, e)$ ***	1 ***	1 ***	1 ***	1 ***
η_{v_s}	$\dfrac{2v_s^2}{1-v_s^2}$ **	$\dfrac{2v_s^2}{1-v_s^2}$ **	$\dfrac{2v_s^2}{1-v_s^2}$ **	$\dfrac{v_s}{1+v_s}$ **	$\dfrac{v_s}{1+v_s}$ **	$\dfrac{2v_s^2}{1-v_s^2}$ **
η_{E_c}	0.0833 *	0.108 *	-	-	-	-

*: low influence, **: moderate influence, ***: high influence

$$Vesic: \eta_d = \frac{0.5\times10^{-9}}{4d^3-6ed^2+4e^2d-e^3}\times(0.7659512690\times10^{10}\times d^3 - 0.1044524579\times10^{11}\times ed^2 + 0.6267481694\times10^{10}\times e^2 d - 0.1392866549\times10^{10}\times e^3)$$

$$Biot: \eta_d = \frac{0.15\times10^{-9}}{4d^3-6ed^2+4e^2d-e^3}\times(0.2347023783\times10^{11}\times d^3 - 0.3094282477\times10^{11}\times ed^2 + 0.1778686186\times10^{11}\times e^2 d - 0.3736293467\times10^{10}\times e^3)$$

2.5.2.2. Quantification of non-linearities in the estimation of coefficient of variation of k_s (SOSM method for buried pipe)

The coefficient A_{xi} for each parameter of semi-empirical models, using the SOSM method, is obtained from Equation 2-3. All the obtained expressions are shown in Table 2-10. As it was mentioned earlier, the calculated coefficient values in this Table give the importance of non-linearity attached to each of the parameters (Imanzadeh et al., 2013a).

Table 2-10: Coefficient A_{xi} obtained for each parameter of semi-empirical models (SOSM method)

A_{x_i}	Semi-empirical models					
	Vesic	Biot	Meyerhof	Kloppel	Matsubara	Selvadurai
A_{E_s}	$0.002\,\lambda$	$0.0036\,\lambda$	-	-	-	-
A_d	$A\,.\,\lambda$	$B\,.\,\lambda$	λ	λ	λ	λ
A_{v_s}	$\dfrac{\lambda\,.\,v_s^4\,.\,(1+3v_s^2)^2}{(1-v_s^2)^4}$	$\dfrac{\lambda\,.\,v_s^4\,.\,(1+3v_s^2)^2}{(1-v_s^2)^4}$	$\dfrac{\lambda\,.\,v_s^4\,.\,(1+3v_s^2)^2}{(1-v_s^2)^4}$	$\dfrac{\lambda\,.\,v_s^4}{(1+v_s)^4}$	$\dfrac{\lambda\,.\,v_s^4}{(1+v_s)^4}$	$\dfrac{\lambda\,.\,v_s^4\,.\,(1+3v_s^2)^2}{(1-v_s^2)^4}$

The parameter of λ depends on the probability distribution

$$A = \frac{0.2\times10^{-19}}{(d^3-3ed^2+4e^2d-2e^3)^4}\times(0.6173022949\times10^{10}\times d^6 - 0.3367250350\times10^{11}\times ed^5 + 0.8638152803\times10^{11}\times e^2 d^4 - 0.1304078356\times10^{12}\times e^3 d^3 + 0.1218223984\times10^{12}\times e^4 d^2 - 0.6559865819\times10^{11}\times e^5 d + 0.1561908512\times10^{11}\times e^6)^2$$

$$B = \frac{0.2\times10^{-18}}{(d^3-3ed^2+4e^2d-2e^3)^4}\times(0.1773678527\times10^{10}\times d^6 - 0.9353569275\times10^{10}\times ed^5 + 02307485493\times10^{11}\times e^2 d^4 - 0.3357443184\times10^{11}\times e^3 d^3 + 3046895160\times10^{11}\times e^4 d^2 - 0.1600778545\times10^{11}\times e^5 d + 0.3744064378\times10^{10}\times e^6)^2$$

The values of the coefficient A_{Es} for the Vesic and Biot models are respectively equal to 4×10^{-3} and 7.3×10^{-3} (assuming that $\lambda=2$ for a normal distribution) that can be insignificant effects on the second order terms of Taylor series (Equation 2-2).

The coefficient A_d for the Vesic and Biot models is a function of external diameter (d) and thickness (e) of the pipe where for the Meyerhof, Kloppel, Matsubara and Selvadurai models is equal to 2 (Table 2-10). Figure 2-14 shows evolution of coefficient A_d as a function of the external diameter of pipe (d) for studied semi-empirical models. As in the case of FOSM method for buried pipe, the influence of the uncertainty of this parameter d on the uncertainty of k_s is more important for the Meyerhof, Kloppel, Matsubara and Selvadurai models ($A_d =2$) than for Vesic and Biot's models (for example, if $e=0.15$m and $d >2.5$ m, the value of $A_d=1.63$ for Vesic's and $A_d=1.53$ for Biot's model).
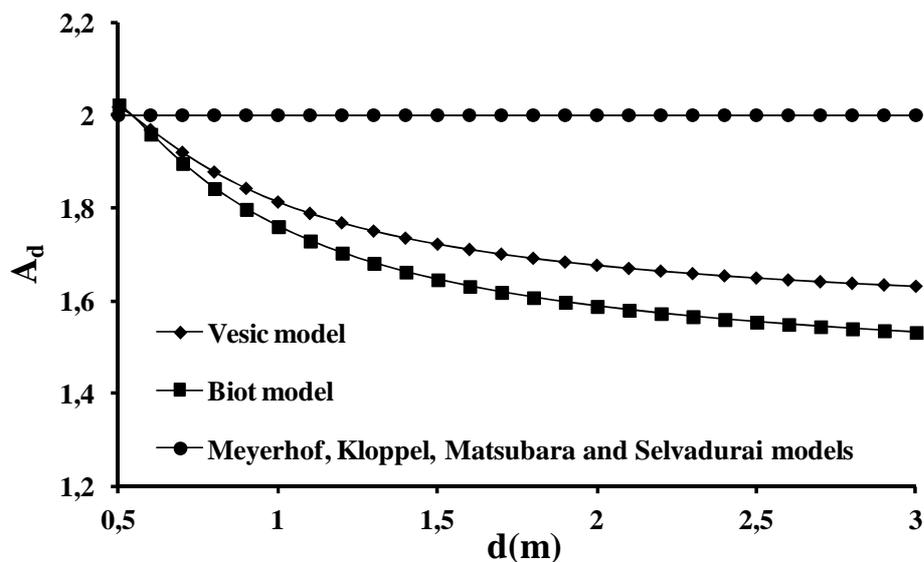
Figure 2-14: Evolution of coefficient A_d as a function of the external diameter of pipe (d) for studied semi-empirical models (SOSM method, λ=2 and e=0.15 m)

Concerning the Poisson's ratio of soil, the coefficient A_{vs} for these semi-empirical models is a function of v_s (Table 2-10). For the value of v_s ranging from 0.15 to 0.35, the coefficient A_{vs} for the Vesic, Biot, Meyerhof, and Selvadurai models (with the same expressions) varies from 1.3×10^{-3} to 95×10^{-3} while for the Matsubara and Kloppel models (with the same expressions) it varies only in a range from 0.6×10^{-3} to 9×10^{-3} (Figure 2-15). The influence of the uncertainty of the Poisson's ratio of soil for $v_s \geq 0.18$ on the uncertainty of k_s for the Vesic,

Biot, Meyerhof, and Selvadurai models is more important than the Matsubara and Kloppel models.

The obtained coefficients in Table 2-10 (A_d, A_{vs}), will be multiplied by coefficients of variation below 5% with the power of four (Table 2-3, Equation 2-2), then the second order terms calculated by the SOSM method can be neglected. Again, the FOSM method alone is sufficient to correctly estimate the coefficients of variation of subgrade reaction in case of buried pipes.
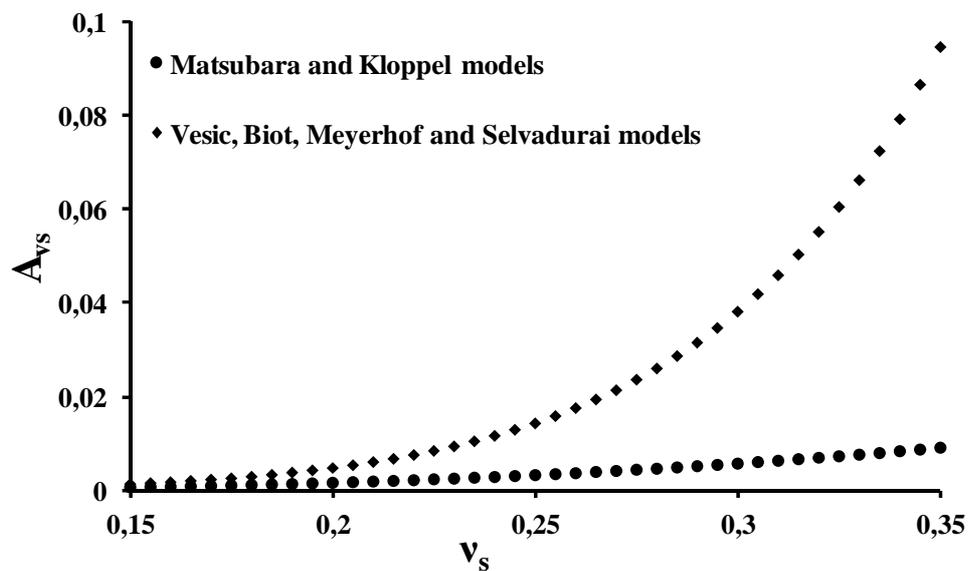
Figure 2-15: Evolution of coefficient A_{vs} as a function of the Poisson's ratio of soil (v_s) for studied semi-empirical models (SOSM method, buried pipe, $\lambda=2$)

2.5.2.3. Simplified formulas for the calculation of the coefficients of variation of k_s in the case of buried pipe

The evolution of CV_{ks} (Coefficient of Variation of k_s obtained from Equation 2-4) as a function of CV_{Es} for these six semi-empirical models is presented in Figure 2-16. For this and as an example, different parameters have to be fixed: $v_s = 0.3$, e=0.15 m, d=1.5 m and the coefficients of variation for each parameter equal to 5%.
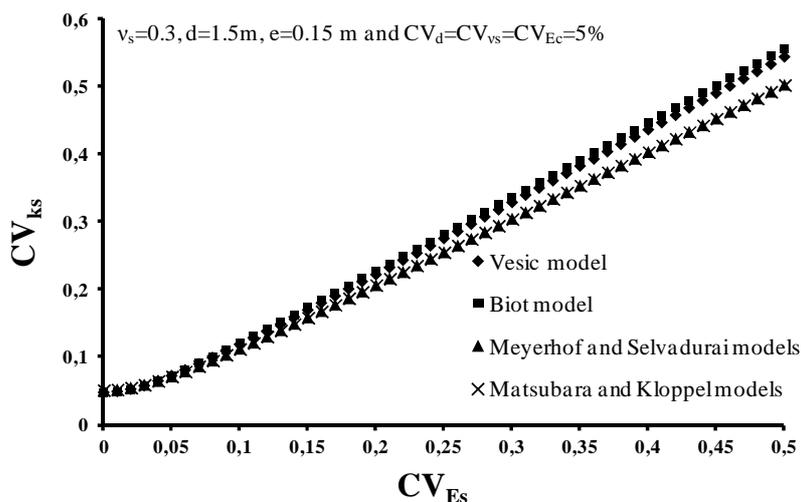
Figure 2-16: Evolution of CV_{ks} (Coefficient of Variation of k_s) as a function of CV_{Es} (Coefficient of Variation of E_s) for studied semi-empirical models (FOSM method for a buried pipe)

When CV_{Es} is less than 0.1, the value of the coefficient of variation of k_s is almost the same for all the semi-empirical models. For a value of CV_{Es} greater than 0.1, we observe a linear behavior between CV_{ks} and CV_{Es}, which shows that the influence of the uncertainties of structure parameters (d and E_c) and Poisson's ratio are less important when the coefficient of variation of E_s is high. In this case, the coefficient of variation of k_s for the Biot and Vesic models is larger than those from other expressions. On the contrary, Meyerhof's and Selvadurai's models give the lowest value of the coefficient of variation of k_s. Accordingly, the coefficient of variation of k_s is directly proportional to the coefficient of variation of E_s and can take a unique expression as we obtained in the case of the spread footing (Equation 2-8) where $\eta_{Es}=1$ for the Meyerhof, Kloppel, Matsubara and Selvadurai models, and $\eta_{Es}=1.1$ for the Vesic and Biot models.

Although the six semi-empirical models give six different values of k_s, their associated coefficients of variation of k_s are close to each other (Figure 2-16).

The coefficient η_{xi} (Table 2-9) was simplified for the external diameter of pipe (d) and the Poisson's ratio of soil (v_s) for these semi-empirical models (Table 2-11). From Equation 2-4, simplified expressions are obtained for the values of d between 1 and 3 m and v_s between 0.2 and 0.35 for the Vesic (Equation 2-15) and Biot (Equation 2-16) models and the values of v_s between 0.2 and 0.35 for the Meyerhof and Selvadurai models (Equation 2-17), Matsubara and Kloppel models (Equation 2-18):

Table 2-11: Simplified coefficient η_{xi} obtained for each parameter of semi-empirical models for $d=[1\ m;\ 3\ m]$, $v_s=[0.2;\ 0.35]$ (FOSM method)

η_{x_i}	Semi-empirical models					
	Vesic	Biot	Meyerhof	Kloppel	Matsubara	Selvadurai
η_{E_s}	1.0833 ***	1.108 ***	1 ***	1 ***	1 ***	1 ***
η_d	0.93 ***	0.91 ***	1 ***	1 ***	1 ***	1 ***
η_{v_s}	$(1.3v_s - 0.19)$ **	$(1.3v_s - 0.19)$ **	$(1.3v_s - 0.19)$ **	$(0.62v_s - 0.045)$ **	$(0.62v_s - 0.045)$ **	$(1.3v_s - 0.19)$ **

*: low influence, **: moderate influence, ***: high influence

$$CV_{k_s} = \left(\left(1.083 \cdot CV_{E_s}\right)^2 + \left(0.93 \cdot CV_d\right)^2 + \left((1.3v_s - 0.19) \cdot CV_{v_s}\right)^2\right)^{0.5}$$

Equation 2-15

$$CV_{k_s} = \left(\left(1.108 \cdot CV_{E_s}\right)^2 + \left(0.91 \cdot CV_d\right)^2 + \left((1.3v_s - 0.19) \cdot CV_{v_s}\right)^2\right)^{0.5}$$

Equation 2-16

$$CV_{k_s} = \left(CV_{E_s}^2 + CV_d^2 + \left((1.3v_s - 0.19) \cdot CV_{v_s}\right)^2\right)^{0.5}$$

Equation 2-17

$$CV_{k_s} = \left(CV_{E_s}^2 + CV_d^2 + \left((0.62v_s - 0.045) \cdot CV_{v_s}\right)^2\right)^{0.5}$$

Equation 2-18

The error between the coefficients of variation of k_s from the simplified models and those from the full models is on average less than 2%.

2.6. Summary and conclusions

In this chapter, the main concept of the modulus of soil reaction and some of the most important relationships for obtaining its value were introduced in detail. We explained the reasons and the methodology for obtaining the uncertainty on the soil reaction modulus. Soil and its structural's properties as well as their uncertainties were considered in order to reveal their effects on the uncertainty of the coefficient of soil reaction (k_s).

Eight semi-empirical models which give the coefficient of subgrade reaction were studied by considering the natural variability and measurement uncertainty of soil properties and the construction uncertainty of the structural elements.

The FOSM and SOSM methods were successively used on these semi-empirical models to determine the coefficient of variation of soil reaction modulus and to evaluate the influence of the soil and structure parameters. Results obtained using the FOSM method for the spread footings show the major effects of the uncertainties of soil modulus, Poisson's ratio and the width of the continuous wall footing on the uncertainty of the coefficient of subgrade reaction. For the latter, results in the case of buried pipes show the major effects of the uncertainties of soil modulus, the external diameter of buried pipe and Poisson's ratio of soil, on the uncertainty of the coefficient of subgrade reaction. We showed that if the additional amount of accuracy resulting from the SOSM method was insignificant then the FOSM method alone would be sufficient to correctly estimate the coefficients of variation of k_s.

Finally, simplified expressions for each semi-empirical model were proposed, taking into account the minimum parameters for determining the coefficient of variation of soil reaction modulus. For these semi-empirical models, the values of the coefficient of variation of k_s were very close if the coefficient of variation of E_s were 2 to 3 times greater than the coefficients of variation of parameters b, v_s, h and d.

The expressions obtained for the spread footings and the buried pipes could then be introduced in different analytical models such as Winkler's model with one parameter, Vlassov & Pasternak models with two parameters and the Kerr model with three parameters in order to determine the uncertainty of k_s on the settlements and bending moments of spread footings and buried pipes resting on an elastic soil. This will be discussed in detail in the following chapter.

Chapter 3

Effects of uncertainties of the subgrade reaction modulus and a low stiffness zone on the behavior of the superficial geotechnical works

(continuous spread footings and buried pipes)

3. Effect of uncertainty of the subgrade reaction modulus and a low stiffness zone on the behavior of the superficial geotechnical works

3.1. Introduction

In this chapter obtained uncertainty of k_s from the uncertainties on the soil and the structure parameters for each semi-empirical model, is introduced to the analytical solution of a beam from Winkler hypothesis and with different boundary conditions. FOSM method is used on this analytical solution in order to determine the uncertainty on the differential settlements, bending moments of the superficial geotechnical designs respectively in the specific case of continuous spread footing for residential construction and the buried pipes (buried steel pipe and buried concrete pipe) resting on an elastic soil. The obtained results then can be translated in terms of probability of ruin according to the allowable thresholds for the differential settlement and bending moment in order to assess the probability of the design not reaching the required performance.

Finally, the calculation methodology, to obtain the confidence bounds of the differential settlement and the bending moment of the superficial geotechnical designs, for each semi-empirical model, is presented. For the cases where the choice of a suitable semi-empirical model for the estimation of uncertainties (on k_s, on the differential settlement and on the bending moment of a spread footing or buried pipe) is not straightforward, a global uncertainty approach is proposed. This approach includes the uncertainties from each semi-empirical model and it can be used to verify if maximum values exceed the values for the limit state designs.

3.2. Effect of uncertainty of k_s on the behavior of a continuous spread footing

In this part, the longitudinal direction of a continuous spread footing is considered, in order to investigate the influence of longitudinal soil variability and structure uncertainty on differential settlement and the bending moment of this structural element, for the case of residential constructions with relatively lightly loaded walls.

Using the FOSM method applied on the deflection equation (Equation 1-51) and the equation of bending moment allows us to study the influence of the uncertainty of k_s on the uncertainty of the settlement and bending moment with different boundary conditions. Uncertainties on the differential settlement and bending moment, which are function of the

variation of k_s, are translated in terms of coefficients of variation (Equation 3-1 and Equation 3-2 respectively for the differential settlement and bending moment):

$$CV_w^2 = \left(\frac{\partial(w)}{\partial k_s} \cdot \frac{\overline{k_s}}{w} \right)^2 \cdot CV_{k_s}^2$$

Equation 3-1

with CV_w the coefficient of variation of the maximum deflection, w is the maximum deflection as a function of k_s, $\overline{k_s}$ the mean of k_s, the value of the maximum deflection is calculated for a given value of k_s and corresponding to an abscissa x_w considered as constant over the range of variation of k_s. The partial derivative of w with respect to k_s is calculated for this abscissa x_w.

$$CV_M^2 = \left(\frac{\partial(M)}{\partial k_s} \cdot \frac{\overline{k_s}}{M} \right)^2 \cdot CV_{k_s}^2$$

Equation 3-2

with CV_M the coefficient of variation of the maximum bending moment of the foundation, M is the maximum bending moment as a function of k_s, the value of the maximum bending moment is calculated for a given value of k_s and corresponding to an abscissa x_M considered as constant over the range of variation of k_s. The partial derivative of M with respect to k_s is calculated for this abscissa x_M.

It should be noted that the uncertainties of the geometrical parameters b and h are only taken into account in the estimation of the coefficient of variation of k_s. These uncertainties are not considered in the calculation of the moment of inertia of the cross section of continuous spread footing (*I* in Equation 1-51).

3.2.1. Hypotheses for the boundary conditions

Generally, the structure is designed to support vertical movements, but damage can appear when a differential settlement occurs on a portion or all of the structure. The damages suffered by the foundations and after by the walls that they support, have four main sources (Andrieux et al., 2011):

- Errors in the construction or design,
- Shrinkage-swelling phenomenon,

- Low stiffness zone of soft clayey soil / Rapid spatial variation of soil.
- Soil spatial variability inside the same lithological formation.

We focus on this section on the low stiffness zone. These cases can be encountered when the residential construction is built on soil with different nature and mechanical properties such as a sand and clay and when rapid spatial variation of soil is detected (Marache et al., 2009a, 2009b; Denis et al., 2011).

Four cases where an absolute settlement or a differential settlement may appear can be considered (Figure 3-1). Figure 3-1a shows two parallele spread footings of the individual house, one resting on a clayey soil of low coefficient reaction modulus (k_C), the other on a sandy soil with no settlement. The spread footing resting on a clayey soil can be modelled by considering it as a beam resting on an elastic soil with free ends as boundary conditions ($w_0(x)=0$, Equation 1-52) with only an absolute settlement and no bending moment. Figure 3-1b presents a foundation with the greatest length (spread footing with length L) resting on lenses or a layer of clayey soil with reaction coefficient k_C, while the orthogonal spread footings of previous spread footing rest on a sandy soil with coefficient k_A largely bigger than k_C ($k_A >> k_C$). In this case, the most part of the house rests on sand without settlement and differential settlement appears only for the spread footing with length L on clayey soil. Figure 3-1c shows the case where half of the house rests on a clayey soil while the other half rests on the sand. In this case (Figure 3-1c), the spread footing with length L can be modeled as resting on an elastic soil with a simple support at one of its ends and the other end being free as boundary conditions. In the case that only one of the four corners of the construction rests on clayey soil (Figure 3-1d), we can consider that this case is like the previous case (Figure 3-1c) but with a zone of low stiffness (k_c) on a part L' of the total length L. Only three first cases are dealt within the present chapter.

The shrinkage of clayey soil beneath a foundation can be simulated, in an initial approach, by taking into account a small value of k_s. The extreme case is when we observe a loss of the contact between the base of footing and the ground, which can be modeled with a value of k_s equal to zero.
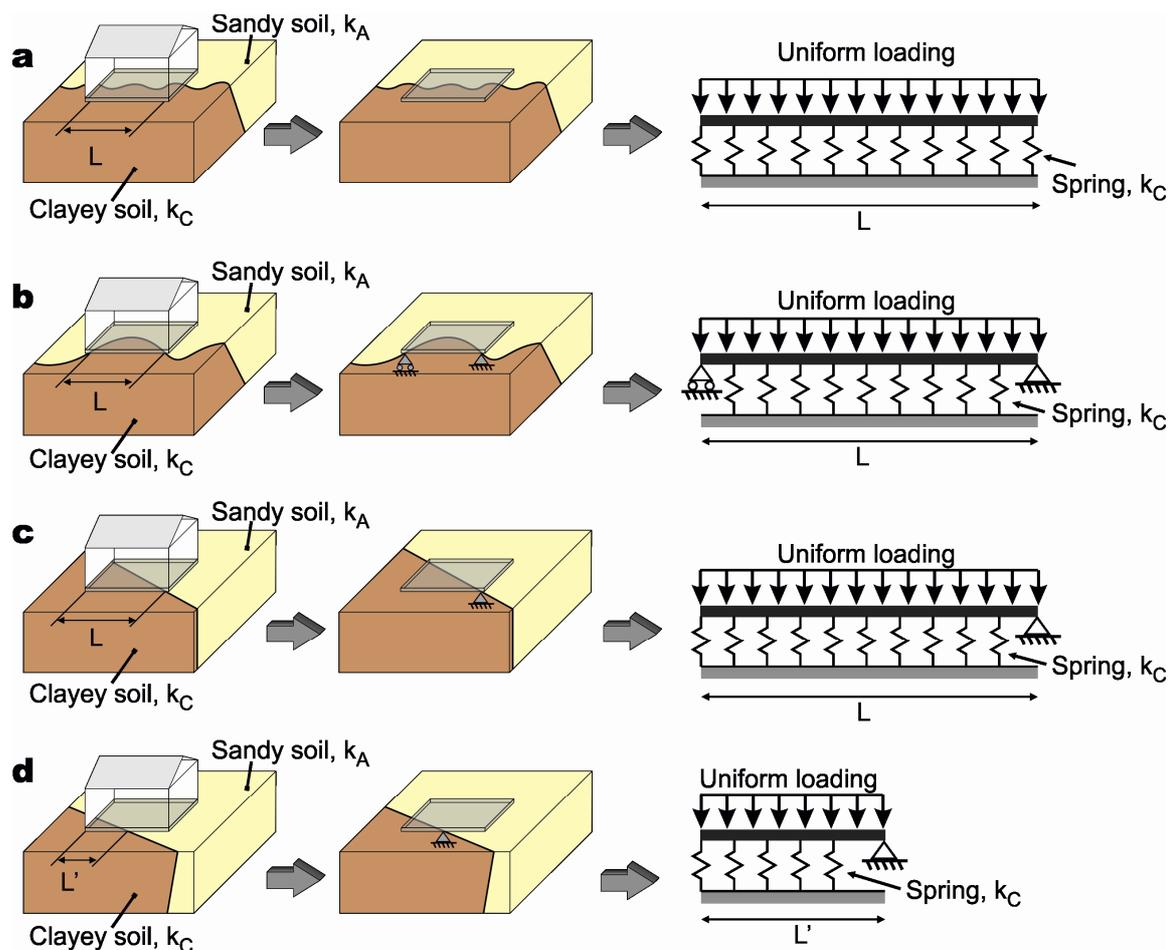
Figure 3-1: Different hypotheses for the boundary conditions: a) Two parallele spread footings of the individual house, one resting on a clayey soil of low coefficient reaction modulus (k_C), the other on a sandy soil with no settlement.b) A spread footing with the length L rests on lenses or a layer of clayey soil while the rest of the foundations remain on sand; c) half of the house rests on lenses or a layer of clayey soil and the other half rests on the sand; d) one of the four corners of the house rests on lenses or a layer of clayey soil and the rest of the house remains on a sandy soil.(all of these cases correspond to a rapid spatial variation of soil, k_A: coefficient of reaction for sandy soil, k_C: coefficient of reaction for clayey soil; $k_A >> k_C$).

3.2.2. Boundary conditions verification

We present in this section results from two different approaches to verify the considered boundary conditions for a spread footing in the cases of Figure 3-1b and Figure 3-1c: one dimensional model (analytical model, 1D) using MAPLE© software and a two dimensional model (2D) using the finite element method (CASTEM© software). It should be noted that in our models, we considered the same values of the subgrade reaction modulus of the clayey soil (k_C) or sandy soil (k_A) at each given location along a spread footing axis.

Figure 3-2 shows schematically the finite element modelling of the four spread footings (2D) in the case of Figure 3-1b. The computations are performed with the CASTEM© software (Verpaux et al., 1988) using the Winkler model.
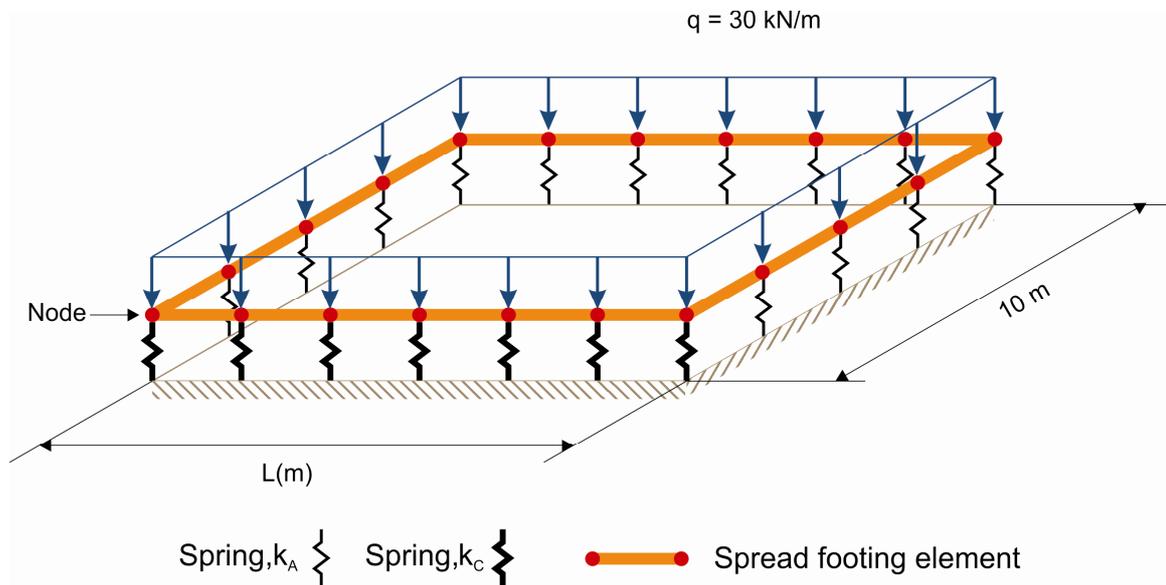
Figure 3-2: Finite element modelling of the four spread footings in the case of Figure 3-1b with the CASTEM© software using the Winkler model (two dimensional model, 2D)

Figure 3-3 and Figure 3-4 show, respectively, evolutions of the maximum differential settlement and the maximum bending moment as a function of the length of a spread footing (L) resting on a clayey soil of low coefficient reaction modulus (k_C) for different ratios of $J= k_A/ k_C$. The obtained results are compared to that one obtained from analytical model with simply supported at two ends (one dimensional model, 1D) using MAPLE© software, Figure 3-1b). We observe that the higher the ratio of J and the length of the spread footing, the higher the values of the maximum differential settlements and the bending moments. For the very high value of coefficient k_A ($J= k_A/ k_C \geq 200$, $k_C=5$ MN.m^{-3}), we obtained the same values for the maximum differential settlements and the bending moments. Then this case (Figure 3-1b) can be modeled by considering simply supported at two ends for large ratio J. For lower values J, the maximum differential settlements and the bending moments are overestimated compare to those obtained from the finite element method.
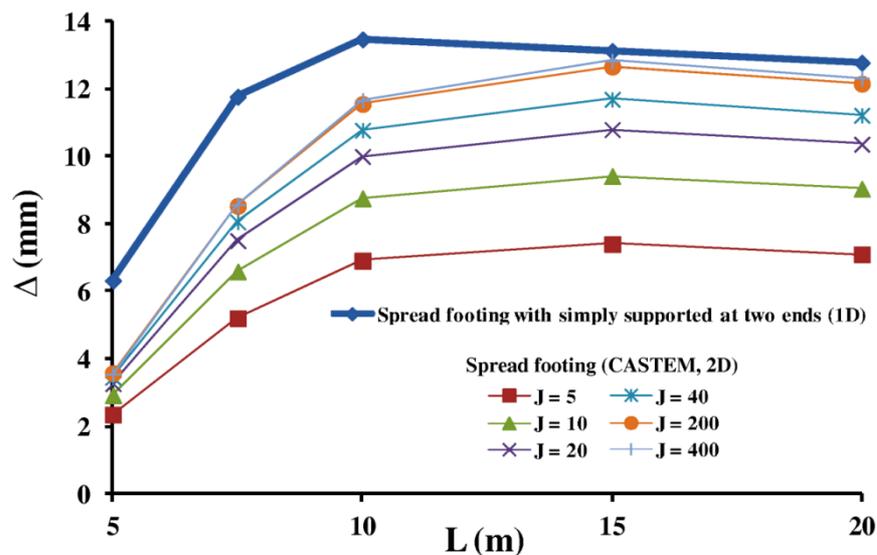
Figure 3-3: Evolution of the maximum differential settlement (Δ) as a function of the length of a spread footing (L) resting on a clayey soil of low coefficient reaction modulus (k_C) for different ratios of J= k_A/ k_C using the finite element method (CASTEM©, 2D) and compare to that one with simply supported at two ends (MAPLE©, 1D) in the case of Figure 3-1b (k_C=5 MN.m^{-3}).
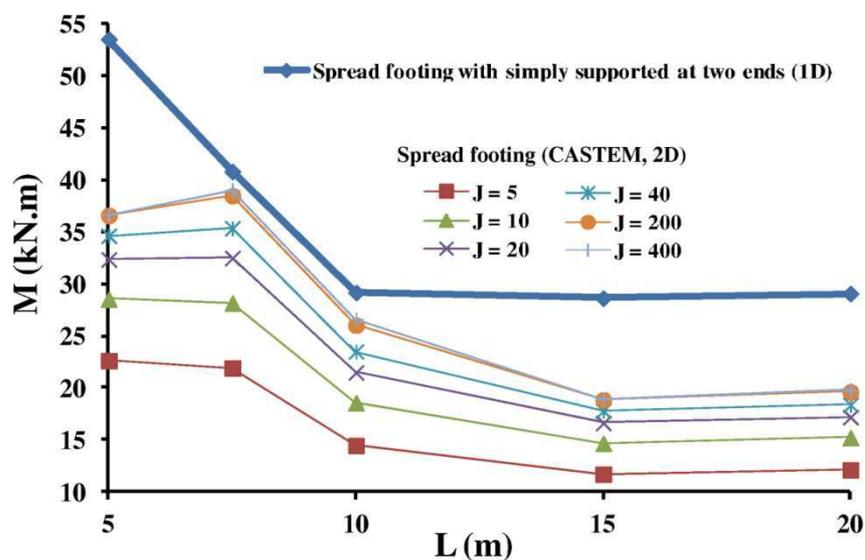
Figure 3-4: Evolution of the maximum bending moment (M) as a function of the length of a spread footing (L) resting on a clayey soil of low coefficient reaction modulus (k_C) for different ratios of J= k_A/ k_C using the finite element method (CASTEM©, 2D) and compare to that one with simply supported at two ends (one dimensional model (MAPLE©, 1D) in the case of Figure 3-1b (k_C=5 MN.m^{-3}).

Figure 3-5 depicts schematically the finite element modelling of the four spread footings (2D) in the case of Figure 3-1c.
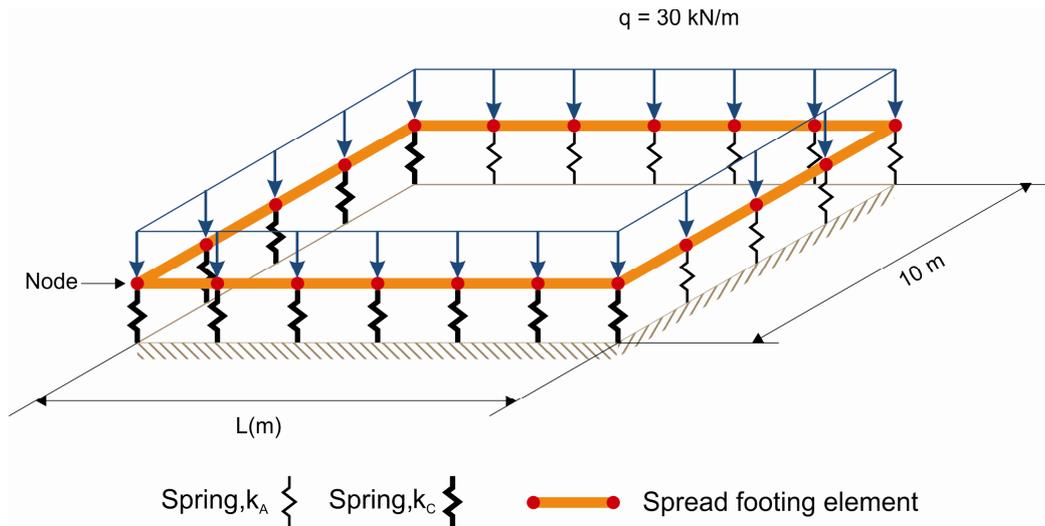
Figure 3-5: Finite element modelling of the four spread footings in the case of Figure 3-1c with the CASTEM© software using the Winkler model (two dimensional model, 2D)

Evolutions of the maximum differential settlement and the maximum bending moment as a function of the length of a spread footing (*L*) resting on a clayey soil of low coefficient reaction modulus for different ratios of *J*, using the finite element method (2D), are shown in Figure 3-6 and Figure 3-7. As in the previous case, these values are always inferior to those obtained from analytical model by considering the spread footing with a simple support at one end (1D). Then this case (Figure 3-1c) can be modeled by considering simply supported at one end for large values of J.
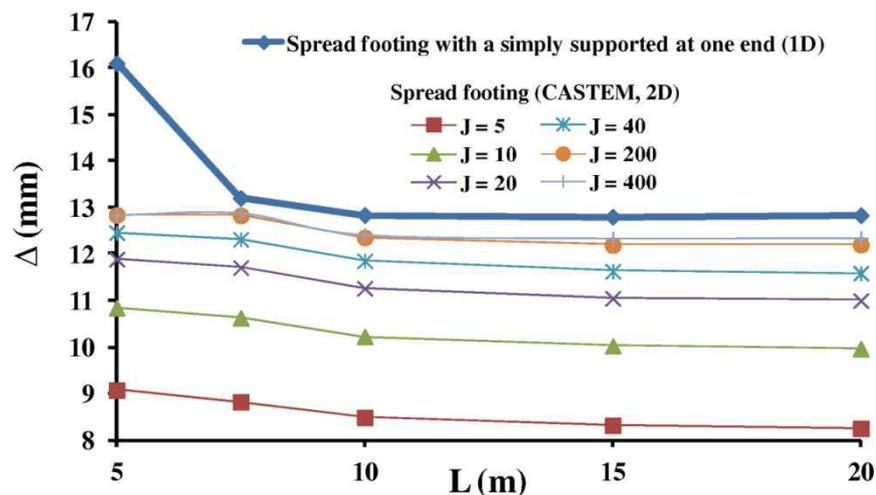
Figure 3-6: Evolution of the maximum differential settlement (Δ) as a function of the length of a spread footing (L) resting on a clayey soil of low coefficient reaction modulus for different ratios of J= k_A/ k_C using the finite element method (CASTEM©, 2D) and compare to that one with simply supported at one end (MAPLE©, 1D) in the case of Figure 3-1c (k_C=5 MN.m^{-3}).
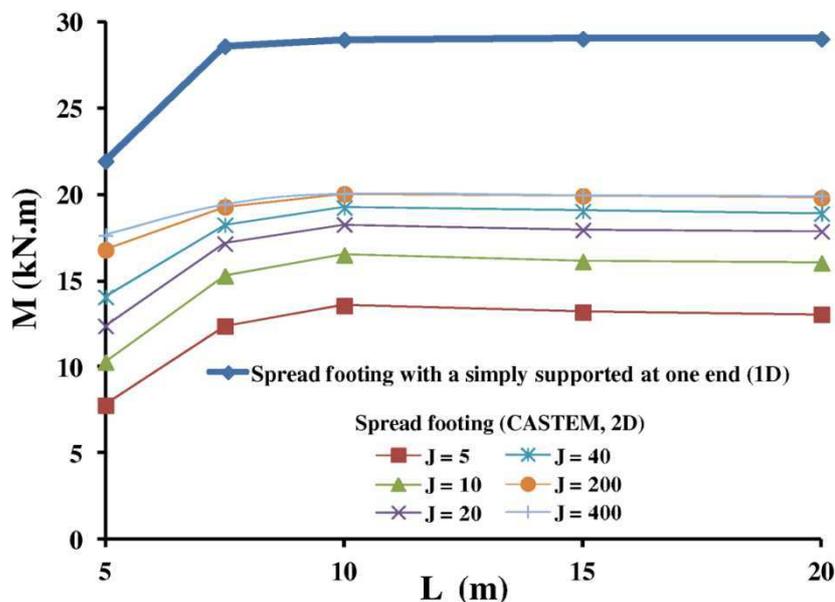
Figure 3-7: Evolution of the maximum bending moment (M) as a function of the length of a spread footing (L) for different ratios of J= k_A/ k_C using the finite element method (CASTEM©, 2D) and compare to that one with simply supported at one end (one dimensional model (1D)) in the case of Figure 3-1c (k_C=5 MN.m^{-3}).

If the hypotheses on the boundary conditions are simplified, they allow us to estimate a maximum value of the deflection with a one-dimensional analytical modeling. Boundary conditions for the spread footing with fixed ends with bending moments (torsional moment for orthogonal foundations) lead to lower values of deflection and bending moment.

The maximum deflection is considered as a differential settlement Δ in the following.

3.2.3. Influence of the uncertainty of k_s on the uncertainty of differential settlement

The uncertainty on the maximum deflection of spread footing or the maximum differential settlement of the soil (Δ) is directly related to the uncertainty of the coefficient of subgrade reaction (CV_{ks}) and boundary conditions. According to the different boundary conditions, considered in this study, and for a spread footings (*b=0.5 m, h=0.3 m, E_c= 20 GPa*) with different lengths subjected to an uniform load equal to 30 kN per running meter, we can calculate, from Equation 3-1, the ratio between the coefficient of variation of the maximum differential settlement (CV_Δ) and the coefficient of variation of subgrade reaction modulus (CV_{ks}).

Figure 3-8 and Figure 3-9 show the evolution of the ratio CV_Δ / CV_{k_s} as function of the subgrade reaction modulus of soil (k_s), respectively for the spread footing with simply supported at two ends and one end. All the results presented in these two figures are obtained from the Equation 3-3 that we can also write it in the form of a differential equation as:

$$\left(\frac{\partial(\Delta)}{\partial k_s} \cdot \frac{\overline{k_s}}{\Delta} \right)^2 = \left(\frac{CV_\Delta}{CV_{k_s}} \right)^2 = \alpha^2 \qquad\qquad \textit{Equation 3-3}$$

With α constant and where one of the solutions of this differential equation is in the following form:

$$\Delta = \frac{\varphi}{\overline{k_s}^a} \qquad\qquad \textit{Equation 3-4}$$

with φ constant that it is determined by the boundary conditions of the Equation 3-3.

Also, when α=1, we obtain $\Delta = \dfrac{\varphi}{\overline{k}_s}$, that means that the "differential settlement" is equivalent to an absolute settlement obtained by considering a foundation with free ends (case (a) in Figure 3-1, $CV_\Delta = CV_{k_s}$). In the case of α < 1, uncertainty on the differential settlement is less, for the same value of k_s, than for α=1. Equation 3-4 shows in this case that the differential settlement (Δ) as function of k_s decreases more slowly than in the case of α=1. In the case of α > 1, we obtain an inverse behavior.
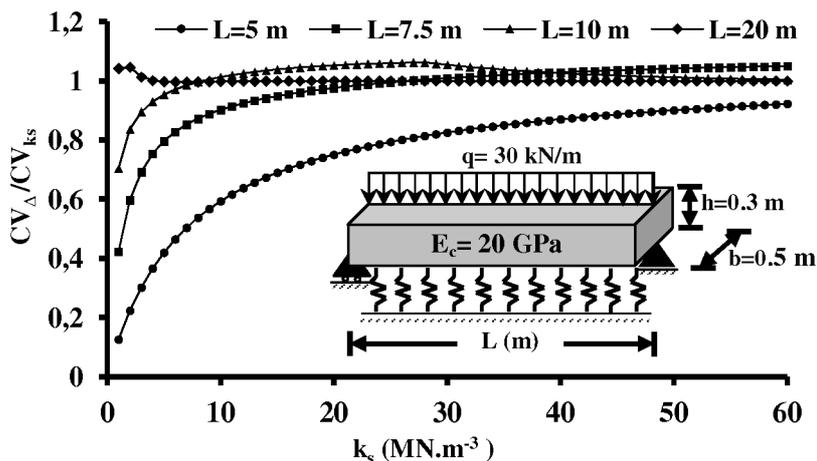
Figure 3-8: Influence of the uncertainty of k_s on the uncertainty of the maximum differential settlement for a spread footing with different lengths with simply supported at two ends as boundary conditions (CV_Δ : coefficient of variation of the differential settlement CV_{ks}: coefficient of variation of k_s)
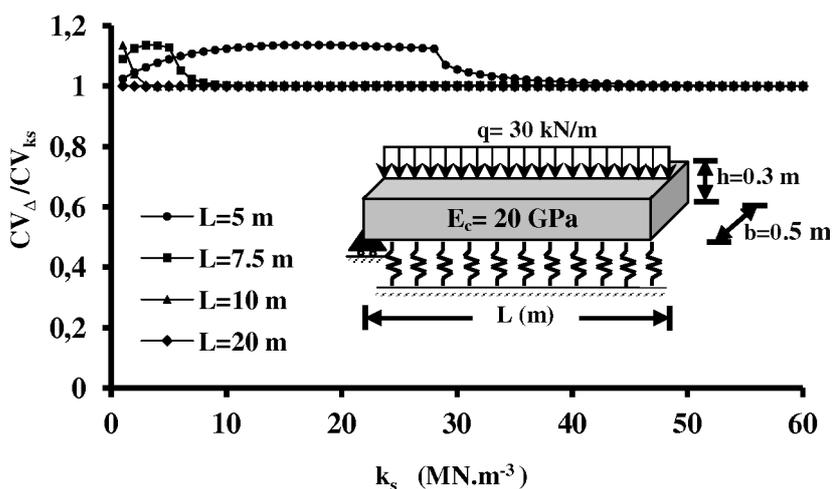
Figure 3-9: Influence of the uncertainty of k_s on the uncertainty of the maximum differential settlement for a spread footing with different lengths with simply supported at one end as boundary conditions.

Figure 3-8, in the case of a foundation with support at two ends shows that for the spread footing with lengths more than or equal to 20 m and whatever the value of k_s, the coefficient of variation of settlement is equal to the coefficient of variation of k_s. The influence of the support is negligible and the value of the differential settlement is equal to the value of the absolute settlement calculated in the case of the spread footing with free ends resting on an elastic soil. This is equal to the value of the absolute settlement that it would be calculated by considering only the transverse behavior of the spread footing.

For the spread footings of lengths less than 20 m, we observe that the lesser the values of k_s and the length of the foundation, the lesser the value of the ration CV_Δ / CV_{ks} is. This shows the influence of the support on the value of the coefficient of variation of differential settlement. Nevertheless, when k_s increases, whatever the length of the foundation, it tends to approach the behavior of spread footing with lengths greater than or equal to 20 m where the influence of the support is negligible.

In the case of spread footing with simply supported at one end (Figure 3-9) we obtain the same behavior that we had previously for the spread footing with a length of 20 m, the influence of the support is negligible on the value of the ratio CV_Δ / CV_{ks}, whatever the value of k_s, $CV_\Delta = CV_{ks}$. This behavior is also observed for a spread footing with a length of 10 m when the value of the coefficient k_s is greater than 3 MN.m^{-3}.

For the length of spread footings less than 10 m, we observe firstly an increase in the value of the ratio CV_Δ / CV_{ks} then beyond a certain value of k_s (5 MN.m^{-3} for L=7.5 m, 28 MN.m^{-3} for L=5 m) a decrease in the ratio CV_Δ / CV_{ks} until it tends to the value of 1.

In the case of a spread footing with a length of 5 m, Figure 3-8 and Figure 3-9 show very different results. For example, for the value of k_s=10 MN.m^{-3}, the ratio CV_Δ / CV_{ks} is equal to 0.5 in the case of support at two ends (Figure 3-8) whilst it is equal to 1.15 in the case of support at one end only (Figure 3-9).

These results show that for a length of spread footing less than 10 m, the considered hypothesis (simply supported at one or two ends) has a significant influence on the value of the coefficient of variation of differential settlement.

Whatever the value of k_s and the length of the foundation, we obtained $CV_\Delta \leq CV_{ks}$ for spread footings with simply supported at two ends while with simply supported at one end, it was $CV_\Delta \leq 1.2CV_{ks}$.

3.2.4. Influence of the uncertainty of k_s on the uncertainty of the bending moment

The uncertainty on the maximum bending moment of spread footing (Equation 3-2) is directly related to the uncertainty of the modulus of the subgrade reaction (CV_{ks}) and the value of the maximum bending moment that depends on the value of the coefficient of the subgrade reaction and boundary conditions.

Figure 3-10 and Figure 3-11 present for different lengths of the spread footing which are identical to those previously studied, the evolution of the ratio of the coefficient of variation of the maximum bending moment over the coefficient of variation of the subgrade reaction modulus as a function of k_s, respectively, for the spread footing supported at two ends and one end.

These figures show that for the spread footing with lengths more than or equal to 20 m, whatever the value of k_s, the value of the ratio CV_M / CV_{ks} tends to 0.5. This corresponds to a shift of the position of the maximum bending moment towards the supports. In this case, the maximum bending moment is obtained from the following formula:

$$M = \frac{\varphi'}{\overline{k}_s^{0.5}}$$

Equation 3-5

where φ' is constant.
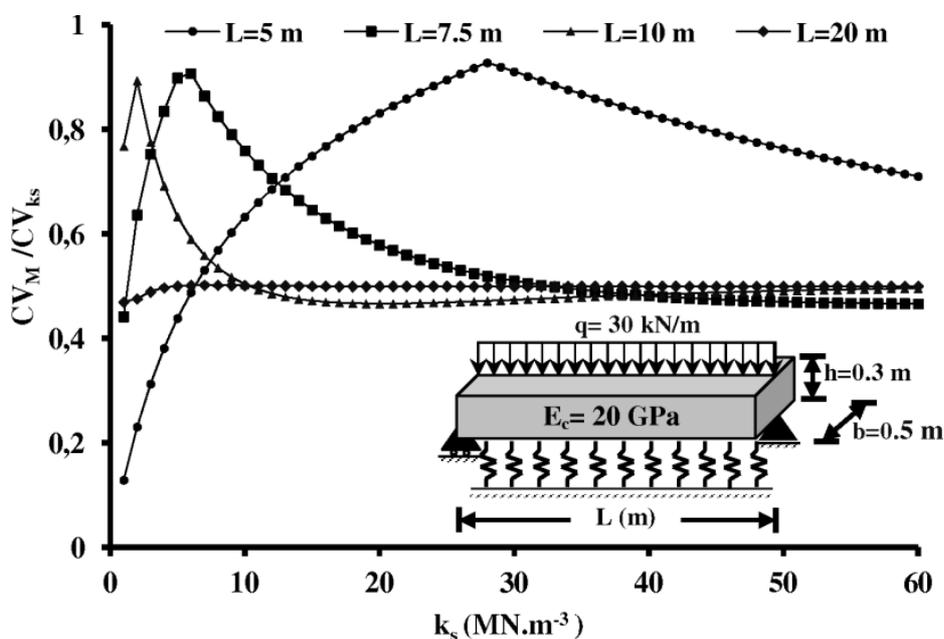
Figure 3-10: Influence of the uncertainty of k_s on the uncertainty of the maximum elastic bending moment for a spread footing with different lengths with simply supported at two ends as boundary conditions (CV_M : coefficient of variation of bending moment).
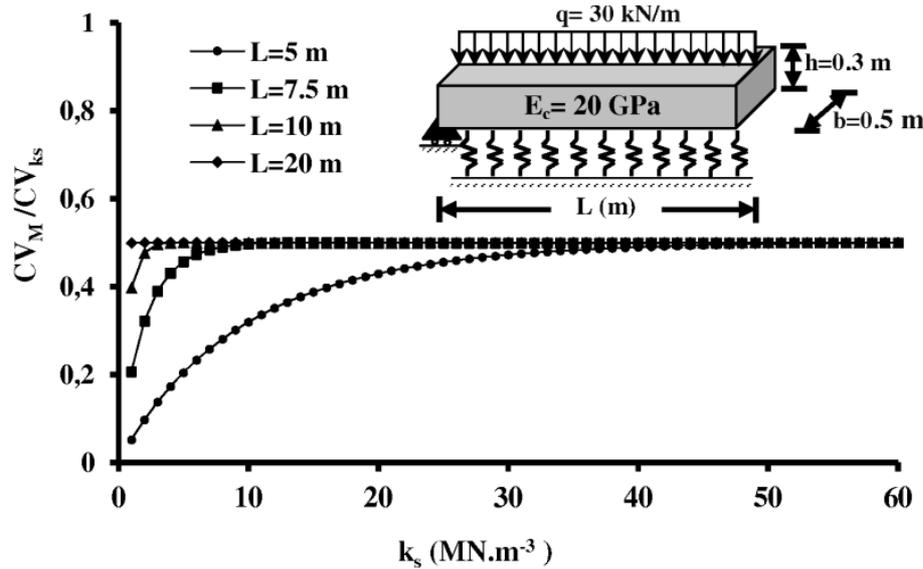
Figure 3-11: Influence of the uncertainty of k_s on the uncertainty of the maximum elastic bending moment for a spread footing with different lengths with simply supported at one end as boundary conditions.

Figure 3-10 shows, in the case of the foundation with a length of 5 m, an increase in the value of the ratio CV_M / CV_{ks} until the value of k_s equal to 28 MN.m^{-3}, then a decrease in this ratio where for the very large values of the k_s the ratio CV_M / CV_{ks} tends to 0.5. This value of k_s, equal to 28 MN.m^{-3}, corresponds to the value of k_s where the maximum bending moment is no longer in the middle of the foundation. When the position of the maximum bending moment shifts towards the supports, we observe a decrease in the uncertainty of the maximum bending moment.

We observe the same behavior for spread footings with lengths of 7.5 m and 10 m, but when the foundations are long, the displacement of the maximum bending moment towards the supports leads to the lower values of k_s respectively 6 and 2 MN.m^{-3} for the lengths of 7.5 m and 10 m.

For spread footings with simply supported at one end (Figure 3-11) and with lengths less than 20 m, we observe that the lesser the length of the foundation and the subgrade reaction modulus, the lesser the ratio CV_M / CV_{ks} is. However, whatever the length of the foundation, when k_s increases, there is a tendency towards the behavior of a spread footing with a length more than or equal to 20 m. The lesser the values of k_s, the longer the foundation, and the higher this tendency is.

As in the case of calculation the coefficient of variation of differential settlement, the value of the coefficient of variation of the bending moment is very different, for lengths of spread footings less than 10 m, depending on the considered boundary conditions (Figure 3-10 and Figure 3-11). The coefficient of variation of the bending moment can be 10 to 50% greater in the case of support at two ends.

Whatever the value of k_s and the length of the foundation we obtained $CV_M \leq CV_{ks}$ for spread footings with simply supported at two ends while with simply supported at one end, it was $CV_M \leq 0.5CV_{ks}$. The considered hypothesis (simply supported at one and two ends) has also a significant influence on the value of the coefficient of variation of the bending moment.

Hence, having evaluated the uncertainty of the differential settlement and the bending moment, these obtained results will be translated in terms of probability of failure according to the allowable thresholds for the differential settlement and bending moment. Thereafter we will obtain the confidence bounds for each semi-empirical model in order to calculate a global uncertainty by the hypothesis of a log-normal distribution.

3.2.5. Reliability analysis for a continuous spread footing

In the probabilistic analysis, considering uncertainty in the input soil and structure parameters, the response of the structure and the assessment of safety are provided in terms of a safety index β known as the reliability index or in terms of probability of failure. In this study we will focus on the serviceability limit state (SLS).

From the design considerations, a spread footing for a residential construction satisfies the serviceability limit state (SLS) if the maximum differential settlement (Δ) and the maximum bending moment (M) are less or equal to the allowable differential settlement (Δ_{all}) and maximum elastic bending moment (M_e) respectively. That means the spread footing does not lead to a violation of serviceability limit state if,

$$\Delta \leq \Delta_{all} \quad or \quad M \leq M_e$$

Equation 3-6

where Δ and M are considered as random variables. Δ_{all} and M_e are the deterministic values. Δ_{all} is calculated from the angular distortion equal to 1/750 for the residential

construction (Bjerrum, 1963). The value of M_e is calculated from ($\frac{bh^2}{6} \cdot \sigma_e$) where σ_e is the maximum elastic stress of concrete. Considering Δ as Normal variable, the probability that the computed maximum differential settlement is more than the allowable differential settlement of foundation can be stated as

$$P_f\left(\Delta \ge \Delta_{all}\right) = 1 - \phi\left(\beta_\Delta\right) \qquad with \quad \beta_\Delta = \frac{\Delta_{all} - \mu_\Delta}{\sigma_\Delta}$$

<div align="right">*Equation 3-7*</div>

where ϕ is the cumulative normal distribution, μ_Δ and σ_Δ are the mean and standard deviation of the maximum differential settlement of foundation.

Considering M as Normal variable, the probability of serviceability limit state (P_{SLS}) is also computed for the case of maximum bending moment (M) greater than the maximum elastic bending moment of the foundation that can be stated as

$$P_f\left(M \ge M_e\right) = 1 - \phi\left(\beta_M\right) \qquad with \quad \beta_M = \frac{M_e - \mu_M}{\sigma_M}$$

<div align="right">*Equation 3-8*</div>

where μ_M and σ_M are the mean and standard deviation of the maximum elastic bending moment of the foundation.

The target value of the reliability index β to be reached in the Eurocode 1 is equal to 1.5 for the SLS (Eurocode 1, 1991). The probability of failure (P_f) should be less than 0.067 to avoid exceed the serviceability limit state.

The obtained results in the previous sections can now be translated in term of probability of failure according to the allowable thresholds for differential settlement and bending moment. We will consider only one length of spread footing (L= 7.5 m) in order to illustrate this part. Poisson's ratio is fixed at 0.3, the coefficients of variation of v_s, h and b are 10% and E_s equal to 15%. The geometry of the spread footing and the load remain unchanged. Maximum allowable differential settlement (Δ_{all}) for the spread footing with simply supported at two ends and one end for the angular distortion equal to 1/750 are respectively 5 and 10 mm.

The calculation methodology to estimate and compare the probability of failure with the probability of serviceability limit state for the maximum differential settlement and the maximum bending moment of a spread footing is presented in Figure 3-12. This flowchart is illustrated for a single value of E_s. The same calculation is repeated in order to obtain the probability of failure for different values of E_s. The deterministic values of the maximum differential settlements and the maximum bending moments for a single value of E_s are obtained through the traditional use of the Winkler model for the four semi-emprical models. For this purpose, the value of k_s for each semi-emprical model is introduced in the Winkler model with different boundary conditions and lengths of spread footings (Figure 3-12). Through the uncertainty approach, the FOSM method is applied on four semi-empirical models to determine the coefficient of variation of k_s for each model. Thereafter, the Winkler model with different boundary conditions and lengths of spread footings is used to model the behavior of spread footings on a construction site. The FOSM method is applied again on the analytical equations of the deflection and bending moment from the Winkler model to determine the coefficient of variation of differential settlement and the bending moment for each model. Finally, by choosing values of Δ_{all} and M_e and considering the hypothesis on the distribution probability for the differential settlement and bending moment, these two approaches (the traditional approach and the uncertainty approach) are combined to calculate the probability of failure for each of the four models. At the end, the obtained results from the probability of failure are compared with the probability of serviceability limit state to test the validity of design. If the probability of failure is smaller than the probability of serviceability limit state then the design is acceptable. Otherwise, the design should be reviewed. The following results are obtained using this methodology.
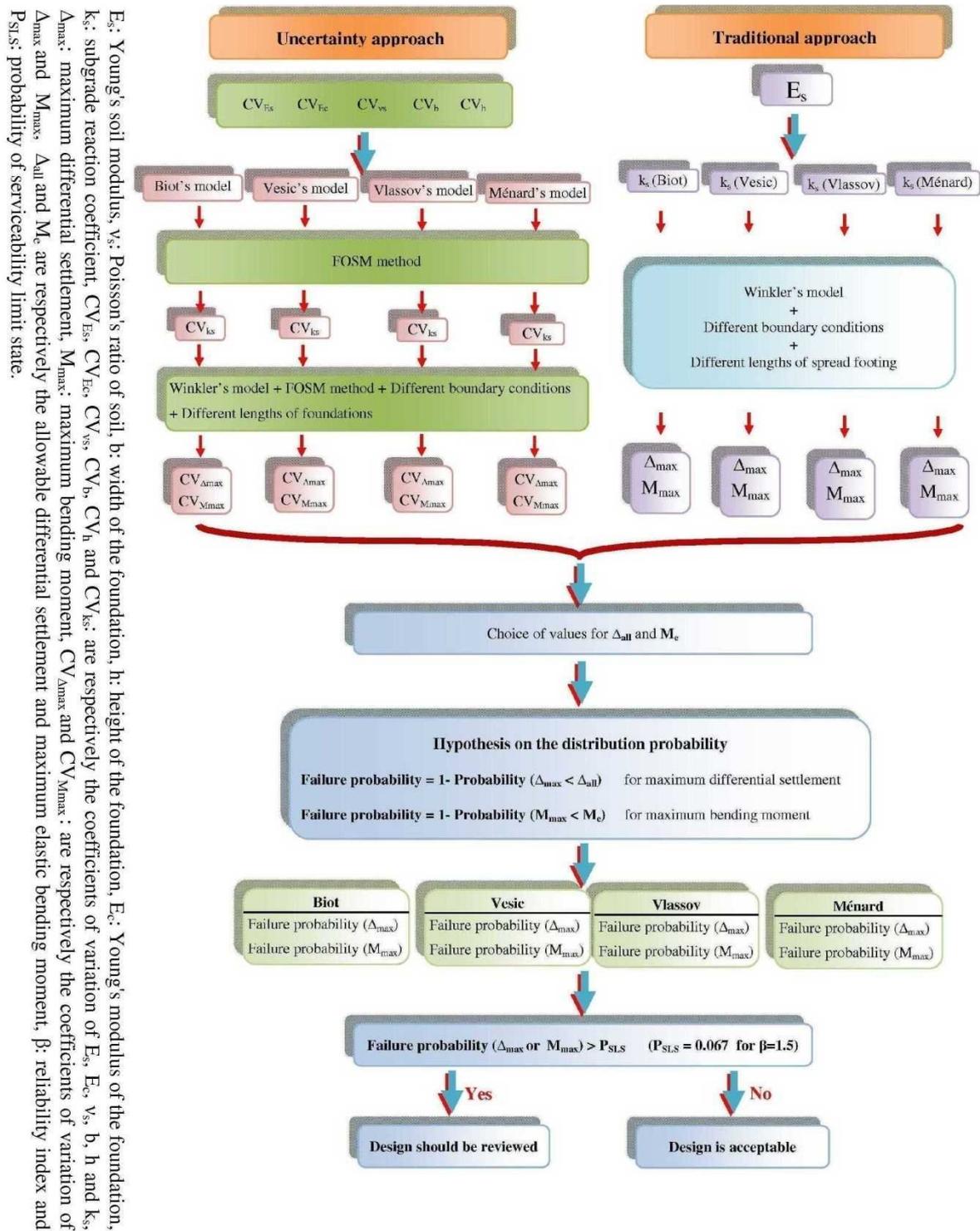
Figure 3-12: Flow chart of the methodology to estimate and compare the probability of failure with the probability of serviceability limit state for a maximum differential settlement and a maximum bending moment of a spread footing, resting on an elastic soil for a single value of E_s

Figure 3-13 and Figure 3-14 show the results obtained for the probability of failure versus E_s for the four semi empirical models, respectively for the spread footing with simply supported at two ends and one end.
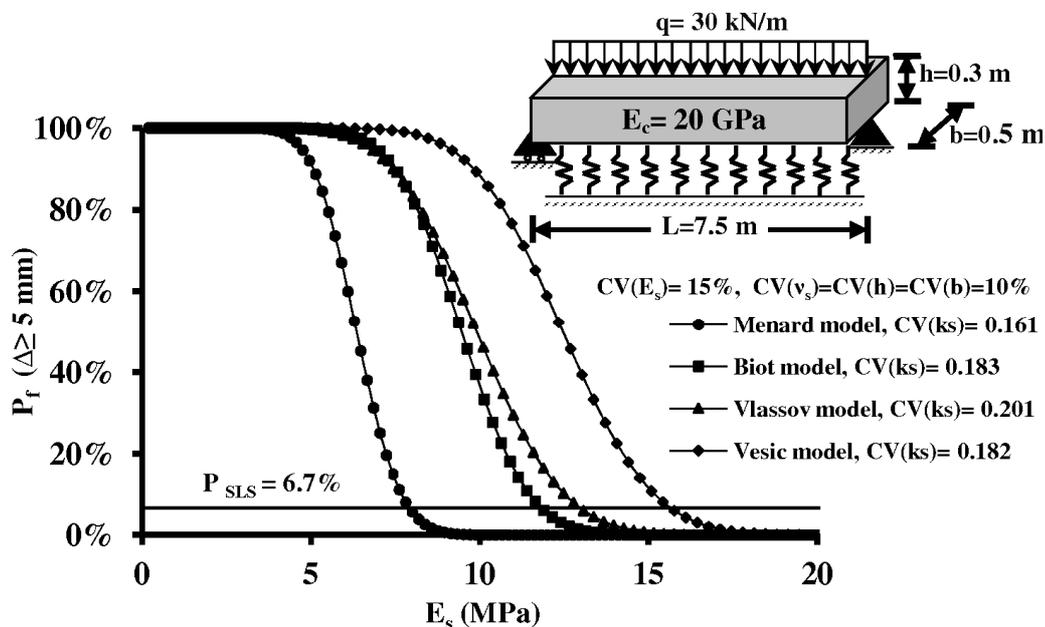
Figure 3-13: Estimation of the probability of failure (P_f) as function of E_s for a maximum differential settlement of a spread footing with simply supported at two ends as boundary conditions (for the four semi empirical models).
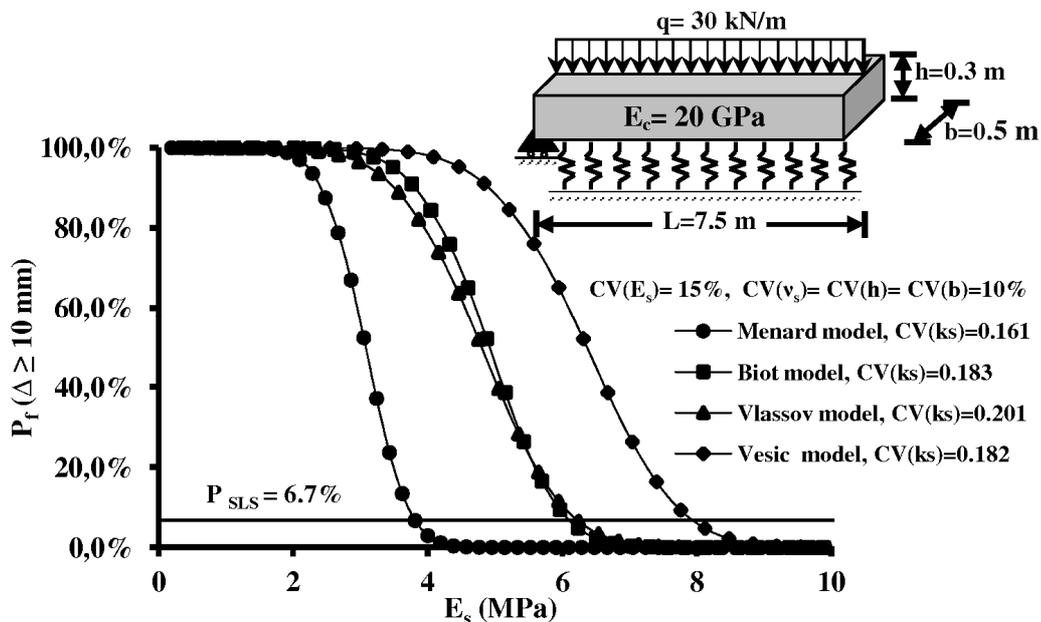
Figure 3-14: Estimation of the probability of failure (P_f) as function of E_s for a maximum differential settlement of a spread footing with simply supported at one end as boundary conditions (for the four semi empirical models).

118

If for the four semi-empirical models, the values of the coefficient of variation of k_s are close, the values of E_s in order to $P_f \geq 0.067$ are very different. Also, whatever the considered boundary conditions (Figure 3-13 and Figure 3-14) the value of E_s will always be greatest with the Vesic model, always lowest with the Ménard model and with intermediate values with the models of Biot and Vlassov. For the same semi-empirical model to calculate k_s, the value of E_s in order to $P_f \geq 0.067$ is almost twice greater with two simply supported (Figure 3-13) than with one simply supported (Figure 3-14). For example, for the spread footing rests on elastic soil with $E_s = 10$ MPa, the probability of failure is less than 0.067 for the four models of calculate k_s in the case of simply supported at one end, while for the same value of E_s the probability of failure is largely greater than P_{SLS} in the hypothesis of simply supported at two ends for the models of Biot, Vlassov and Vesic. This shows that considered hypothesis (simply supported at two ends and one end, which depend on soil investigation) and the selected semi-empirical model have a great importance on the conclusion about the reliability analysis.

We will consider, by hypothesis, that the maximum bending moment (M) is equal to 37.5 kN.m that it corresponds to a σ_e equal to 5 MPa. Figure 3-15 and Figure 3-16 show the results obtained for the probability of failure as function of E_s, for the four semi-empirical models, respectively for a spread footing with simply supported at two ends and one end. The interpretation of these results is identical to the analysis presented for the Figure 3-13 and Figure 3-14 concerning the differential settlement but with values of E_s lower than in the case of differential settlements in the case presented in this section. These results show again the importance of boundary conditions and the choice of semi-empirical model.
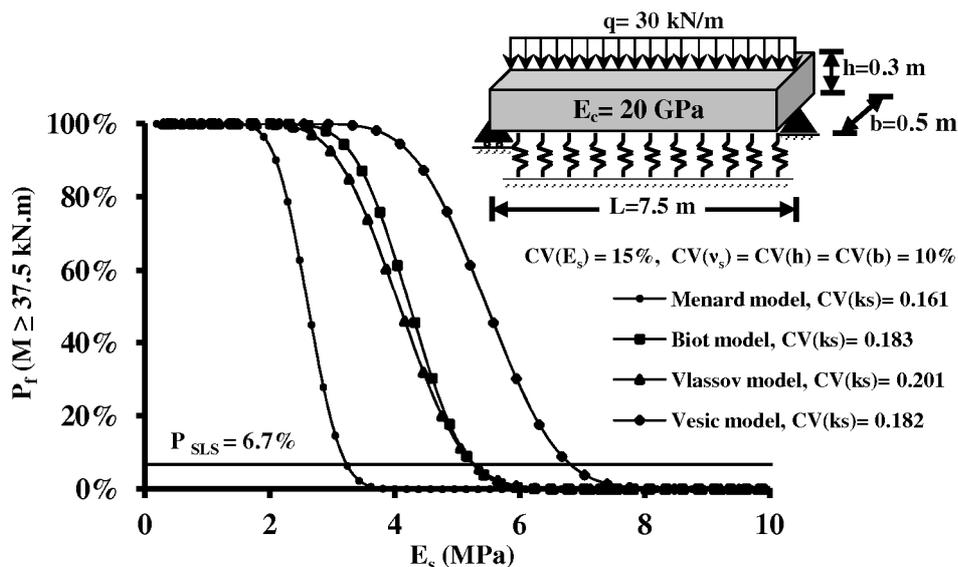
Figure 3-15: Estimation of the probability of failure (P_f) as function of E_s for a maximum elastic bending moment of a spread footing with simply supported at two ends as boundary conditions (for the four semi empirical models).
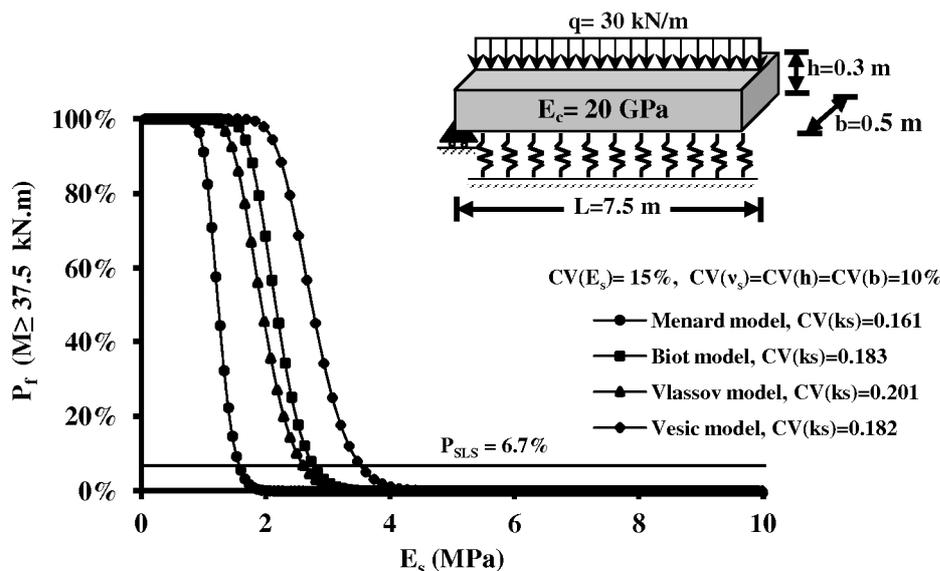
Figure 3-16: Estimation of the probability of failure (P_f) as function of E_s for a maximum elastic bending moment of a spread footing with simply supported at one end as boundary conditions (for the four semi empirical models).

In order to complete the previous analysis, we can study the influence of the value of the coefficient of variation of k_s on the probability of failure in the case of differential settlement from the semi-empirical model of Ménard.

Figure 3-17 and Figure 3-18 show the obtained results for the probability of failure with different values of CV_{ks}, respectively in the hypothesis of simply supported at two and one

end. If these results show, again the important difference between the hypothesis the simply supported at one and two ends, they also show, as expected, the importance of the value of the coefficient of variation of k_s and then the values of the coefficients of variation of E_s and b in the case of the semi-empirical model of Ménard. For example, in the case shown in Figure 3-17, the soil of the foundation with $E_s= 7$ MPa, should have a coefficient of variation of k_s less than 5% in order to not exceed the value of $P_{SLS}=0.067$; the soil of the foundation with $E_s= 9$ MPa, a coefficient of variation of k_s less than 30%.
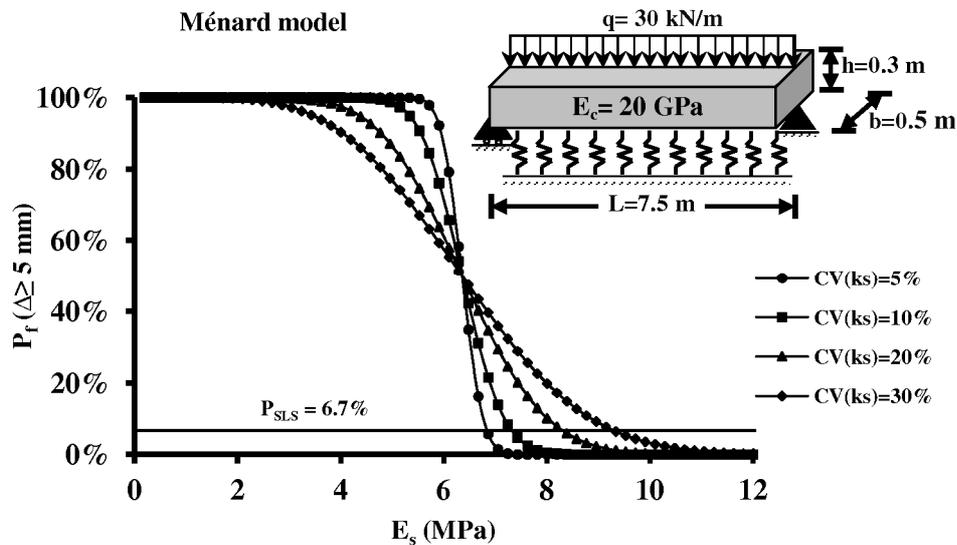
Figure 3-17: Probability of failure (P_f) for a maximum differential settlement of a spread footing with simply supported at two ends as boundary conditions for different values of CV_{ks} (Ménard's model).
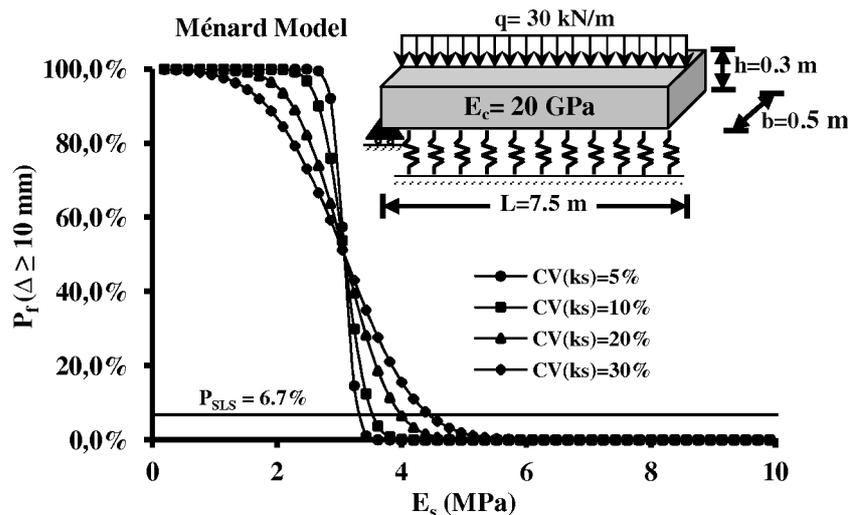
Figure 3-18: Probability of failure (P_f) for a maximum differential settlement of a spread footing with simply supported at one end as boundary conditions for different values of CV_{ks} (Ménard's model)

The same figures could, naturally, be obtained for the three other semi-empirical models, bending moment and for different foundation geometries and loading (q) in order to obtain different charts to help a better design of spread footing for the residential construction when rapid spatial variation of soil's properties are present on the construction site.

All of the presented results for the reliability analysis are based on the hypothesis of a normal distribution for the values of the maximum differential settlement and the maximum bending moment. The obtained results by the hypothesis of a log-normal distribution for these values are nearly identical to those ones obtained for a normal distribution and are presented in appendix 1.

3.2.6. Application to global uncertainty analysis (for a continuous spread footing)

We propose in this part a basic uncertainty analysis based on the determination of confidence bound. The calculation methodology, to obtain the confidence bounds of the differential settlement and the bending moment of a spread footing, resting on an elastic soil, for each semi-empirical model, is presented in Figure 3-19. The deterministic values of maximum differential settlement and the bending moment are obtained through the traditional use of the Winkler model. For this purpose, the different values of subgrade reaction modulus for each semi-empirical model are introduced in the Winkler model with different boundary conditions and lengths of spread footings (Figure 3-19). Through the uncertainty approach, the FOSM method is applied on four semi-empirical models to determine the coefficient of variation of k_s for each model. Thereafter, the Winkler model with different boundary conditions and lengths of spread footings, is used to model the behavior of spread footings on a construction site. The FOSM method is applied again on the analytical equations of the deflection and bending moment from the Winkler model to determine the coefficient of variation of differential settlement and the bending moment for each model. Finally, by considering the hypothesis on the distribution probability for the differential settlement and bending moment, these two approaches (the traditional approach and the uncertainty approach) are combined to calculate the confidence intervals for each of the four models. At the end, a global uncertainty is proposed which corresponds to the range between the maximum of the four upper bounds and the minimum of the four lower bounds.

Figure 3-19: Flow chart of the methodology to estimate the global uncertainties of the differential settlement and bending moment of a spread footing, resting on an elastic soil.

To illustrate some steps of the methodology, Figure 3-20 presents for the Ménard model, the evolutions of the maximum differential settlement (Figure 3-20a), the bending moment (Figure 3-20c) and their standard deviations (Figure 3-20b and Figure 3-20d) as functions of k_s and the length of the spread footing. All of these results are obtained for the following values: b=0.5 m, h=0.3 m, v_s=0.3, E_c=20 GPa, CV_{Es}=15% and CV_b=CV_h=CV_{vs}=10%.
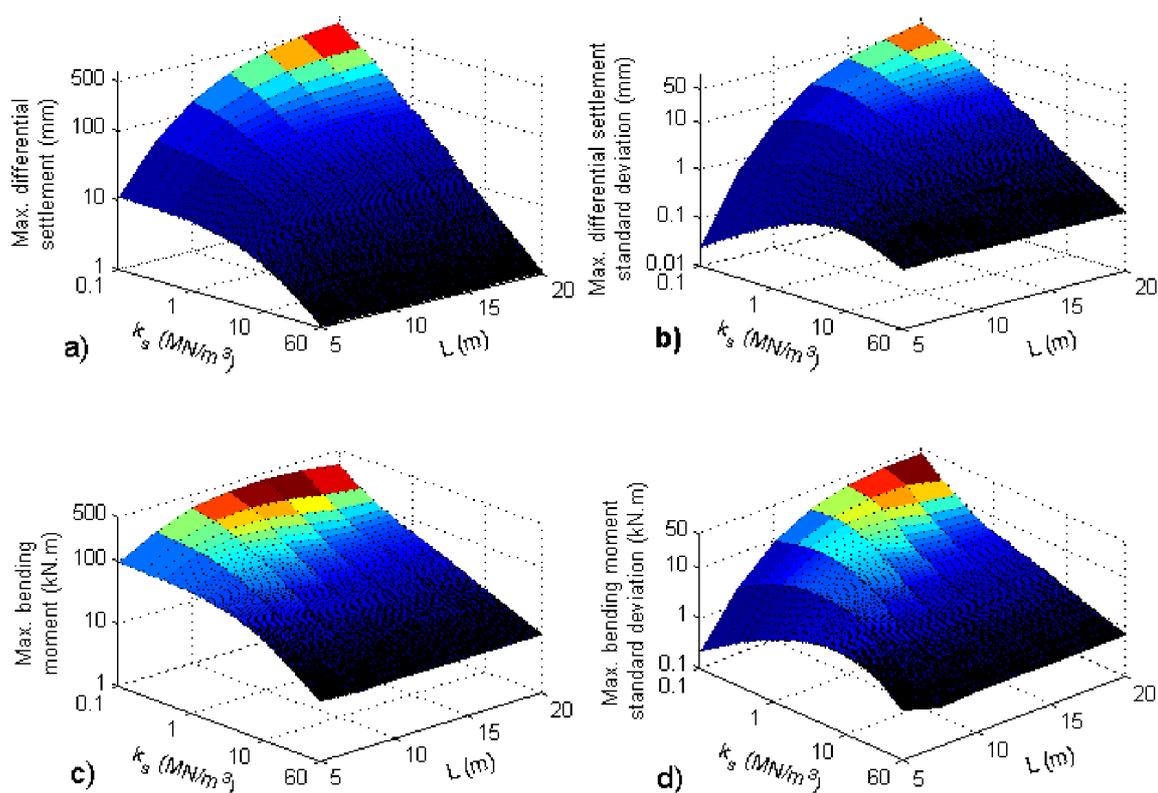
Figure 3-20: Evolutions of the maximum differential settlement (a), bending moment (c) and associated standard deviations (b and d) as function of the k_s and length of the spread footing for the values of b=0.5 m, h=0.3 m, v_s=0.3, E_c=20 GPa, CV_{Es}=15% and CV_b=CV_h=CVv_s=10% for the Ménard model.

Figure 3-20b and Figure 3-20d show that for a small length of the spread footing, the maximum values of the standard deviations of the differential settlement and the bending moment do not correspond to the smallest values of the subgrade reaction modulus (for example for a length equal to 5 m, the value of k_s for the maximum value of these standard deviations is equal to 8 MN.m^{-3}). However, increasing the spread footing length leads to the maximum of these standard deviations in accordance with very low values of k_s (for example for a length of 20 m the value of k_s for the maximum value of these standard

deviations is equal to 0.1 MN.m^{-3}). Thus, the confidence bound which depends on the standard deviation is a complex function of k_s and L.

In order to illustrate the complete use of this methodology, we take as an example a residential construction where one of its spread footings of 10 m is built on weak soil (Figure 3-1b) with a Young's modulus E_s of 6 MPa (soft clay) estimated from a geotechnical investigation. From published values in the literatures, the coefficient of variation of E_s is estimated to 15%. The soil parameters, the mechanical property and geometrical dimensions of this spread footing are identical to those previously studied in Figure 3-20. For this case, the deterministic values of the subgrade reaction modulus, the differential settlement and the bending moment are obtained for each semi-empirical model. Thereafter, using the methodology explained previously and assuming a lognormal distribution (which is a fairly common assumption) for the subgrade reaction modulus, the differential settlement and the bending moment, 95% confidence bounds are obtained for each semi-empirical model. The results for this application case are presented in Figure 3-21. As expected the deterministic values of k_s, Δ, M and their confidence intervals are different for each semi-empirical model (Figure 3-21a, Figure 3-21b and Figure 3-21c). The value of k_s and its associated confidence interval are the highest for the Ménard model and the smallest for the Vesic model. In the case of the Biot and Vlassov models, we obtain almost the same value and confidence interval (Figure 3-21a). Figure 3-21b and Figure 3-21c show that the deterministic values and confidence bounds of the differential settlement and the bending moment are the most important for the Vesic model and the least important for the Ménard model and are almost the same for the Biot and Vlassov models.

In the case where choosing a suitable semi-empirical model is difficult, a global uncertainty is introduced. This includes the uncertainties from each semi-empirical model and corresponds to the range between the maximum of the four upper bounds and the minimum of the four lower bounds. The global uncertainties for Δ, M and for the case under consideration, are respectively [3.84; 15.54] (mm), [15.12; 31.80] (kN.m) (Figure 3-21b and Figure 3-21c).

Angular distortions, which correspond to the ratio between Δ and $x_{max(\Delta)}$ (see section 3.2), can be obtained from the deterministic values of the maximum differential settlements for these semi-empirical models. For these models, except for the Vesic model with an

angular distortion of 1/445, the angular distortions are smaller than the limit angular distortion defined for a residential construction (1/750 (Bjerrum, 1963)). However, the angular distortions obtained from the global uncertainty of the maximum differential settlements range from 1/1300 to 1/300 showing it is possible to exceed the limit angular distortion. Maximum bending moment values deduced from the global uncertainties (Figure 3-21c) are less than the value of the maximum plastic bending moment equal to 56.25 MN.m that it corresponds to a σ_e equal to 5 MPa ($0.25b.h^2.\sigma_e$).

Finally, the flow chart of Figure 3-22 illustrates the methodology in the considered application case with all results.

The same results could naturally be carried out for different foundation geometries, boundary conditions, and loading (q) in order to obtain different charts to help a better design of continuous spread footing for a residential construction when zones of weak soil are present on the construction site.
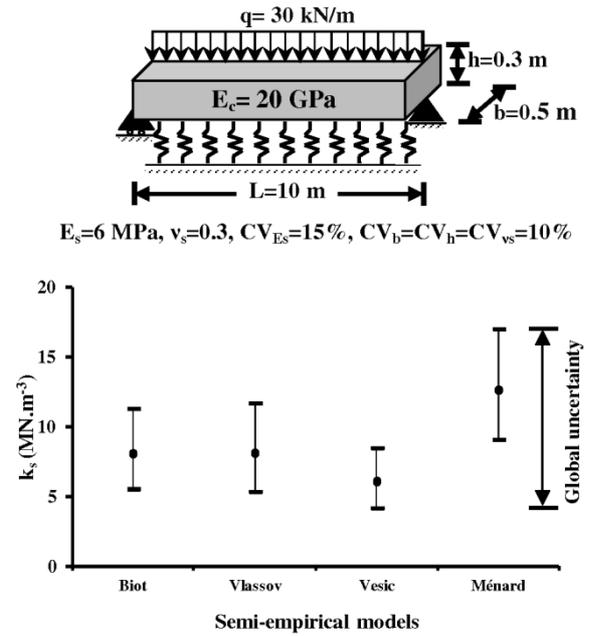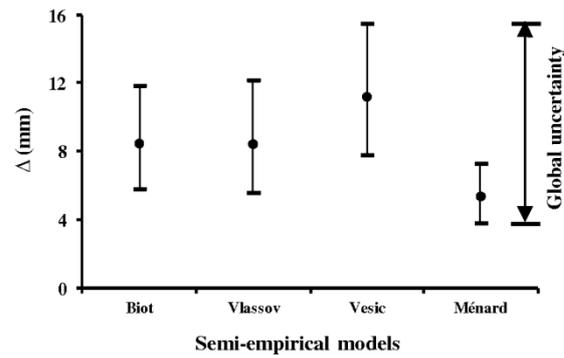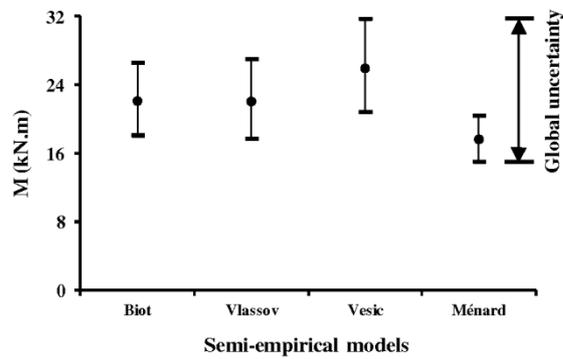
Figure 3-21: Global uncertainties for the a) Subgrade reaction modulus k_s, b) Maximum differential settlement Δ and c)Maximum bending moment M by considering 95% confidence bound for each semi-empirical model with log-normal distribution.
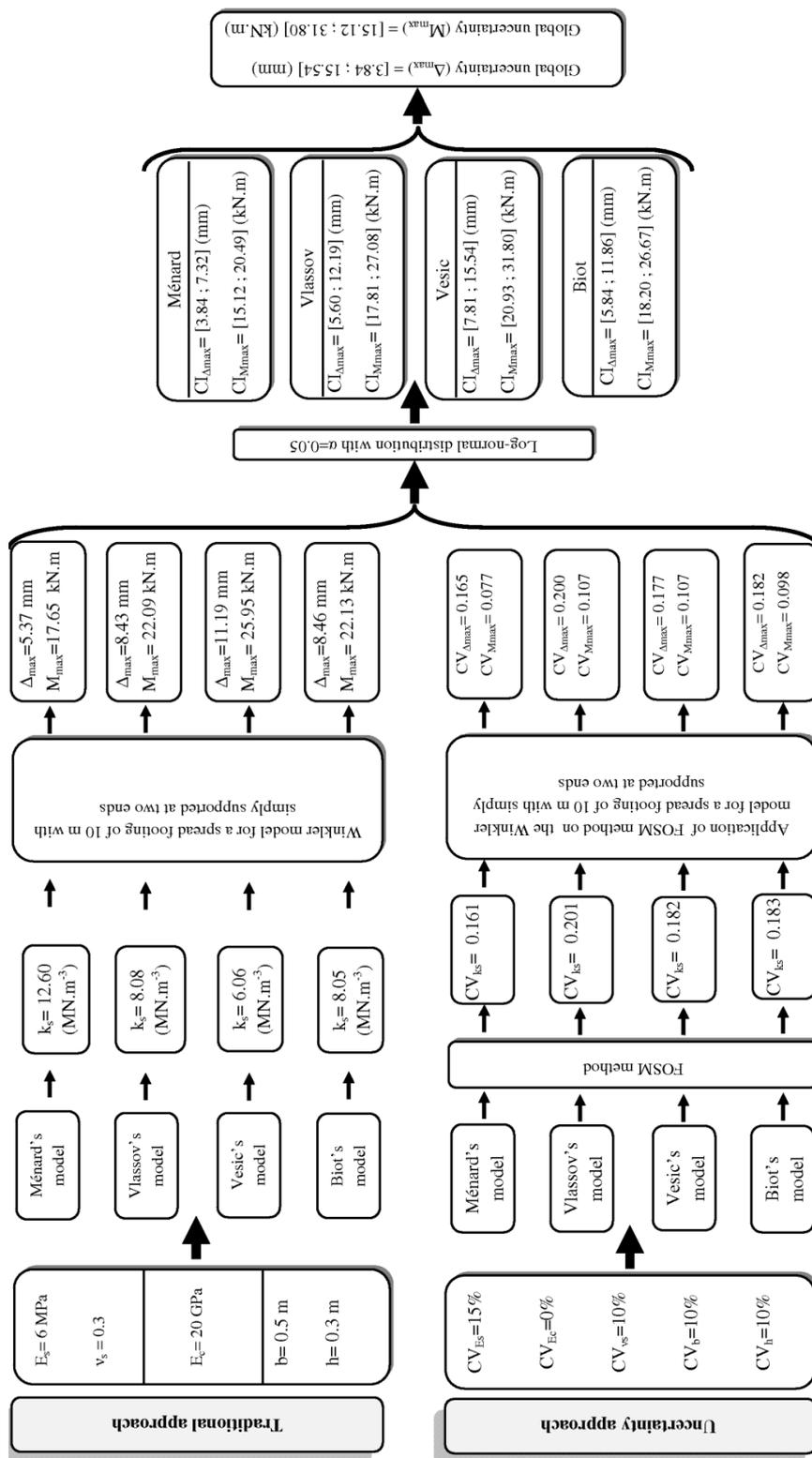
Figure 3-22: Results of the methodology applied to a spread footing with length of 10 m.

In the following, the same work is done for a buried pipe resting on elastic soil.

3.3. Effect of uncertainty of k_s and a low stiffness zone of soil on the behavior of a buried pipe

3.3.1. Hypotheses for the boundary conditions

The failure of buried pipes from differential settlements is one of the most common causes of structural failure, and a design analysis should therefore be carried out for an evaluation of permissible differential settlements. The differential settlements can be encountered when the buried pipe is installed on soil with different lithologies and mechanical properties such as clayey zones of low stiffness compared to sand. For this low stiffness zone, the values of E_s are between 0.4 MPa and 6 MPa (Cassan, 1978). For these values of E_s, the correspondence values of k_C (coefficient of reaction for clayey soil) can be calculated from the semi-empirical models. In the case of the Matsubara model with the Poisson's ratio of 0.3 and external pipe diameter of 1.5 m, the values of k_C are between 0.64 MN.m^{-3} and 9.7 MN.m^{-3}.

Different cases where an absolute settlement or a differential settlement may appear can be considered (Figure 3-23). Figure 3-23a presents a buried pipe resting on a sandy soil with a reaction coefficient k_A. This case can be modeled by considering a pipe as a beam resting on an elastic soil ($w_0(x) = 0$, Equation 1-52) with only an absolute settlement and no bending moment. Figure 3-23b shows a part of the length of the pipe resting on a low stiffness zone of clay with reaction coefficient k_C, while the remaining length of the pipe rests on a sandy soil with coefficient k_A much larger than k_C. In this case, the pipe affected by a low stiffness zone of length L can be modeled by considering a beam with fixed ends as boundary conditions. In the case that the largest part of the pipe rests on a low stiffness zone (Figure 3-23c) we can consider that this case is like the previous case but with a very large length L, where the influence of one of the fixed ends becomes insignificant.

Note that when there are manholes at both ends of a buried pipe, it can be modeled by considering a beam with fixed ends as boundary conditions. In the following, we focus on the behavior of the buried pipe in the case of the Figure 3-23b and where it is assumed that the settlement of the pipe occurs only into the zone of low coefficient of reaction.

$\overline{-}\ \overline{-}$: Deformation of buried pipe

Figure 3-23: Different hypotheses for the boundary conditions: a) Buried pipe resting on a sandy soil with only an absolute settlement and no bending moment. b) A part of the length of the pipe resting on low stiffness zone of clay (L), while the remaining length of the pipe rests on a sandy soil. c) The largest part of the pipe rests on a low stiffness zone (length L being very large). (L: is a part of the pipe length affected by a low stiffness zone, k_A: coefficient of reaction for sandy soil, k_C: coefficient of reaction for clayey soil; $k_C \ll k_A$).

3.3.2. Boundary conditions verification

We present in this section results from two different approaches to verify the considered boundary conditions for a buried pipe in the case of Figure 3-23b: one dimensional models using MAPLE© software (analytical model) and a finite element method (CASTEM© software). It should be noted that in our models, we considered the same values of the subgrade reaction modulus of the clayey soil (k_C) or sandy soil (k_A) at each given location along a buried pipe axis.

Figure 3-24 shows schematically the finite element modelling of a buried pipe (1D) in the case of Figure 3-23b. The computations are done with the CASTEM© software using the Winkler model.
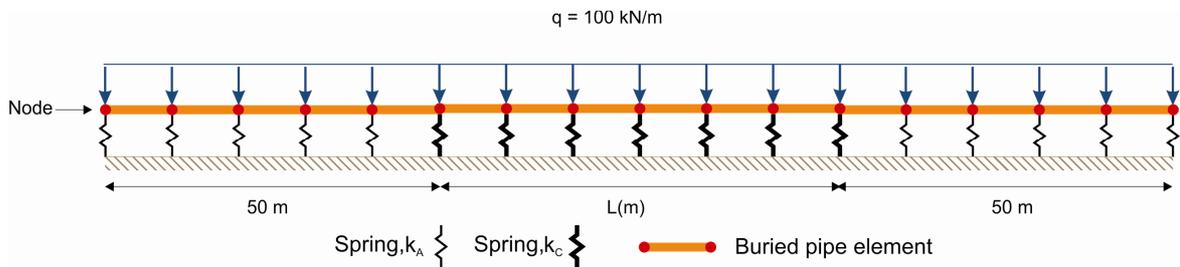
Figure 3-24: Finite element modelling of a buried pipe in the case of Figure 3-23b with the CASTEM© software using the Winkler model (one dimensional model, 1D)

Figure 3-25 and Figure 3-26 show, respectively, evolutions of the maximum differential settlement and the maximum bending moment as a function of the length of a low stiffness zone beneath the buried pipe (*L*) for different ratios of $J= k_A/ k_C$ using the finite element method (1D) and compare to that one with fixed ends (analytical model, 1D). These figures show that for the very high value of coefficient k_A ($J= k_A/ k_C \geq 400$, $k_C=5$ MN.m^{-3}), the values of the maximum differential settlements and the bending moments are almost the same as those of with fixed ends. Then in this case, the pipe affected by a low stiffness zone of length *L* can be modeled by considering a beam with fixed ends as boundary conditions.

131
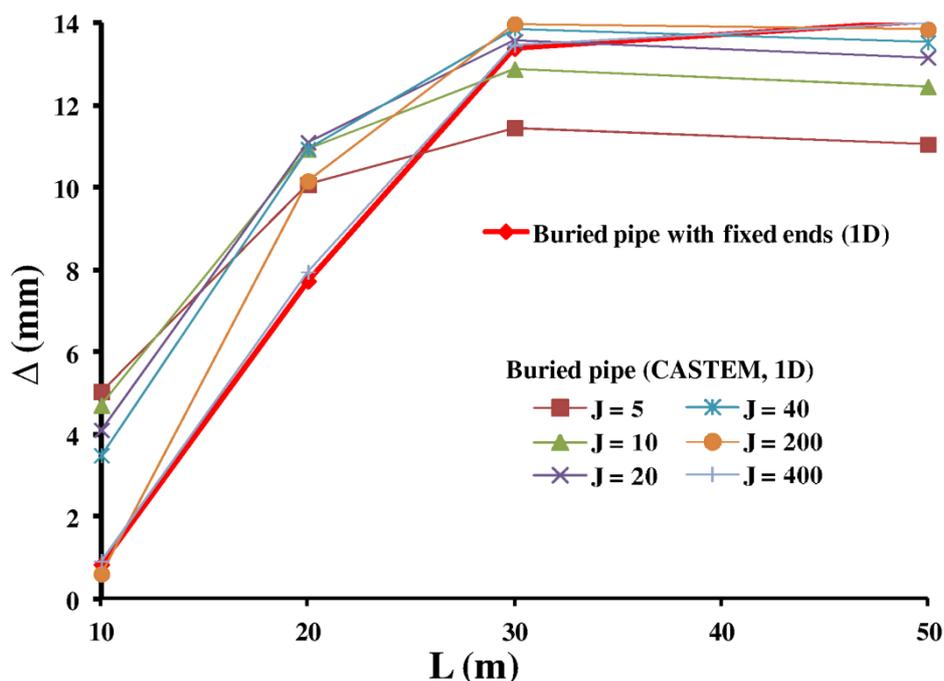
Figure 3-25: Evolution of the maximum differential settlement (Δ) as a function of the length of a low stiffness zone beneath the buried pipe (L) for different ratios of J= k_A/ k_C using the finite element method (CASTEM©, 1D) and compare to that one with fixed ends (MAPLE©, 1D) in the case of Figure 3-23b (k_C=5 MN.m^{-3}).
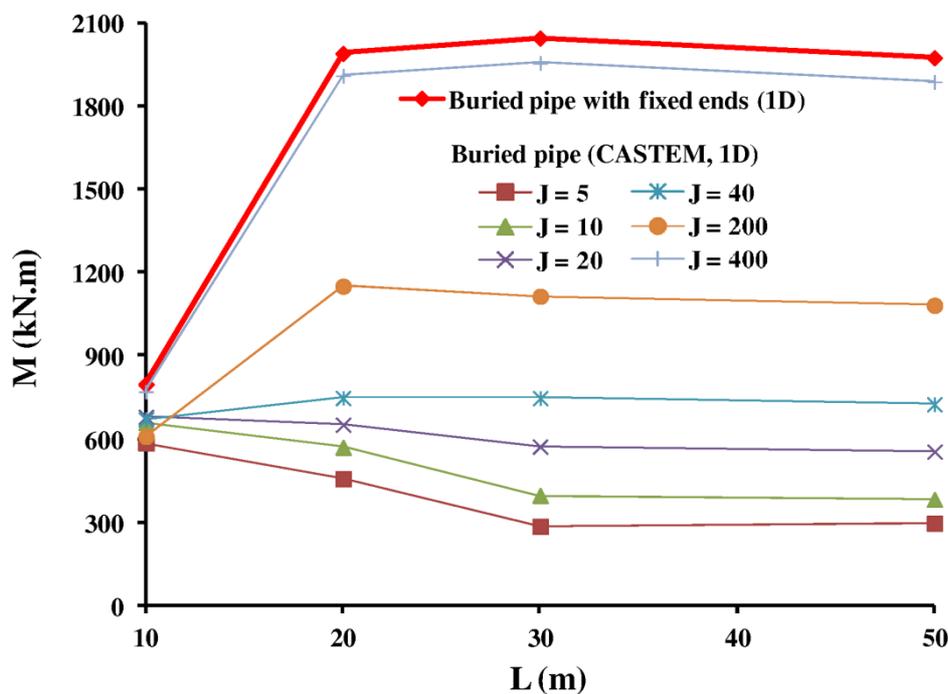
Figure 3-26: Evolution of the maximum bending moment (M) as a function of the length of a low stiffness zone beneath the buried pipe (L) for different ratios of J= k_A/ k_C using the finite element method (CASTEM©, 1D) and compare to that one with fixed ends (MAPLE©, 1D) in the case of Figure 3-23b (k_C=5 MN.m^{-3}).

If the hypotheses on the boundary conditions are simplified, they allow us to estimate a maximum value of the deflection with a one-dimensional analytical modeling, which depends on only two parameters, the coefficient of reaction and the length of the low stiffness zone.

3.3.3. Estimation of the uncertainty of the differential settlement and bending moment

Using the FOSM method applied on the deflection equation (Equation 1-51) and on the equation of the bending moment allows us to study the influence of the uncertainties of k_s and L on the uncertainties of the differential settlement and the bending moment. The uncertainties of the differential settlement and the bending moment can be decomposed into two parts, one part is a function of the uncertainty of k_s and the other part is a function of the uncertainty of the length of the low stiffness zone. These uncertainties, translated in terms of the coefficients of variation, are obtained from the following equations (Equation 3-9 and Equation 3-10 respectively for the coefficients of variation of the differential settlement (CV_w) and the bending moment (CV_M) (Imanzadeh et al., 2013b) :

$$CV_w^2 = CV_{w/k_s}^2 + CV_{w/L}^2 \qquad\qquad \textit{Equation 3-9}$$

$$CV_M^2 = CV_{M/k_s}^2 + CV_{M/L}^2 \qquad\qquad \textit{Equation 3-10}$$

where

$$CV_{w/k_s}^2 = \left(\frac{\partial(w)}{\partial k_s} \cdot \frac{\overline{k_s}}{w} \right)^2 . CV_{k_s}^2 \qquad\qquad \textit{Equation 3-11}$$

$$CV_{w/L}^2 = \left(\frac{\partial(w)}{\partial L} \cdot \frac{\overline{L}}{w} \right)^2 . CV_L^2 \qquad\qquad \textit{Equation 3-12}$$

$$CV^2_{M/k_s} = \left(\frac{\partial (M)}{\partial k_s} \cdot \frac{\overline{k_s}}{M} \right)^2 \cdot CV^2_{k_s}$$

Equation 3-13

$$CV^2_{M/L} = \left(\frac{\partial (M)}{\partial L} \cdot \frac{\overline{L}}{M} \right)^2 \cdot CV^2_L$$

Equation 3-14

where in Equation 3-11, $CV_{w/ks}$ is the coefficient of variation of the maximum deflection with respect to k_s, CV_{ks} the coefficient of variation of k_s, w is the maximum deflection as function of k_s, $\overline{k_s}$ the mean of k_s, the value of the maximum deflection is calculated for a given value of k_s corresponding to an abscissa x_w considered as constant over the range of variation of k_s. The partial derivative of w with respect to k_s is then calculated for this abscissa x_w. Equation 3-12 is defined in the same manner as Equation 3-11 except the parameters and the partial derivative are with respect to L.

For Equation 3-13, $CV_{M/ks}$ is the coefficient of variation of the maximum bending moment of the pipe with respect to k_s, M is the maximum bending moment as a function of k_s, the value of the maximum bending moment for a given value of k_s corresponding to an abscissa x_M considered as constant over the range of variation of k_s. The partial derivative of M with respect to k_s is calculated for this abscissa x_M. Again, Equation 3-14 has the same definition but in term of L.

3.3.3.1. Influence of the uncertainties of k_s and the low stiffness zone on the uncertainty of the differential settlement

Four variables have an influence on the uncertainty on the maximum deflection of buried pipe or the maximum differential settlement of the soil (Equation 3-9): the uncertainty of the coefficient of subgrade reaction *(CV$_{ks}$)*, the uncertainty of the coefficient of low stiffness zone length *(CV$_L$)*, the value of the coefficient of subgrade reaction and the part of the pipe affected by a low stiffness zone of length *L*. The maximum deflection is then considered as a differential settlement Δ in the following. According to the boundary conditions considered in this study and for the buried pipes (*e=0.15m, d=1.5m, E$_c$=20 GPa*) with different lengths of low stiffness zones subjected to an uniform load equal to

100 kN per running meter of pipe, we can calculate, from the Equation 3-11, the ratio between the coefficient of variation of the maximum differential settlement with respect to k_s ($CV_{\Delta/ks}$) and the coefficient of variation of the subgrade reaction modulus (CV_{ks}).

Figure 3-27 depicts the evolution of the ratio $CV_{\Delta/ks}/CV_{ks}$ as a function of the subgrade reaction modulus, for different low stiffness zone lengths. For a low stiffness zone length greater than or equal to 50 m and for any value of k_s, the coefficient of variation of the settlement respect to k_s is close to the coefficient of variation of k_s (Figure 3-27). For this length the influence of the supports is negligible and the value of the differential settlement is close to the value of the absolute settlement calculated in the case of the buried pipe with free ends resting on an elastic soil. This is also the maximum value of the differential settlement that it would be calculated by considering the third case in Figure 3-23. For the same mentioned length and if the value of CV_{Es} is greater than 10% we obtain $CV_{\Delta/ks}=CV_{ks}$ $\approx CV_{Es}$. At the opposite, the uncertainty on the maximum differential settlement is insignificant ($CV_{\Delta/ks} \approx 0$) for a low stiffness zone length inferior or equal to 5 m.
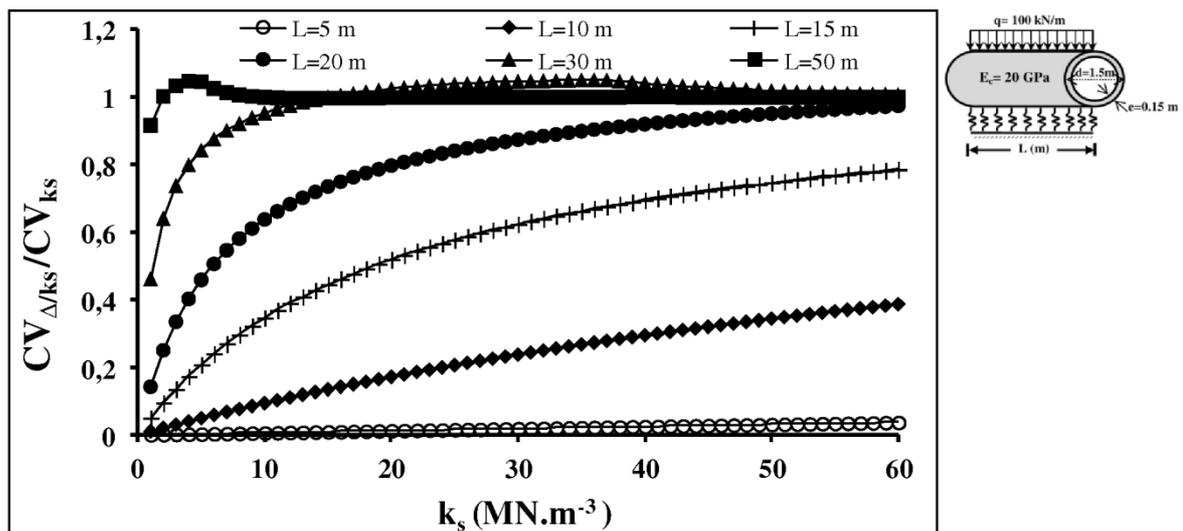
Figure 3-27: Influence of the uncertainty of k_s on the uncertainty of the maximum differential settlement for the different low stiffness zone lengths (L) ($CV_{\Delta/ks}$: coefficient of variation of the differential settlement with respect to k_s; CV_{ks}: coefficient of variation of k_s).

For the low stiffness zone lengths between 5 m and 50 m, we observe that the lower the values of k_s and the low stiffness zone lengths, the lower the values of the ratio $CV_{\Delta/ks}/CV_{ks}$ are. This shows the influence of the fixed ends on the value of the coefficient of variation of differential settlement. Nevertheless, when the value of k_s increases, whatever the length

of the low stiffness zone, the ratio tends to approach to the behavior of the low stiffness zone lengths greater than or equal to 50 m. For these lengths, the uncertainty of the differential settlement with respect to k_s is almost always less than or equal to the uncertainty of the subgrade reaction modulus ($CV_{\Delta/ks} \leq CV_{ks}$).

The ratio between the coefficient of variation of the maximum differential settlement with respect to L $(CV_{\Delta/L})$ and the coefficient of variation of the length of the low stiffness zone (CV_L) can be calculated from Equation 3-12. Figure 3-28 shows that the uncertainty of the differential settlement respect to L is the most important for a low stiffness zone less than or equal to 5m compare to the uncertainty of the other lengths of low stiffness zones. For this length of 5 m and whatever the value of k_s, the ratio $CV_{\Delta/L}/CV_L$ is close to the value of 4 showing the significant effect of boundary conditions compared to the effect of Winkler's springs. The value of 4 corresponds to the power of L in the equation of the deflection in the case of a beam with two fixed ends with uniform loading. For the low stiffness zone greater than or equal to 50 m and for any value of k_s (except for k_s=0 MN.m^{-3}), the value of $CV_{\Delta/L}$ is close to zero.
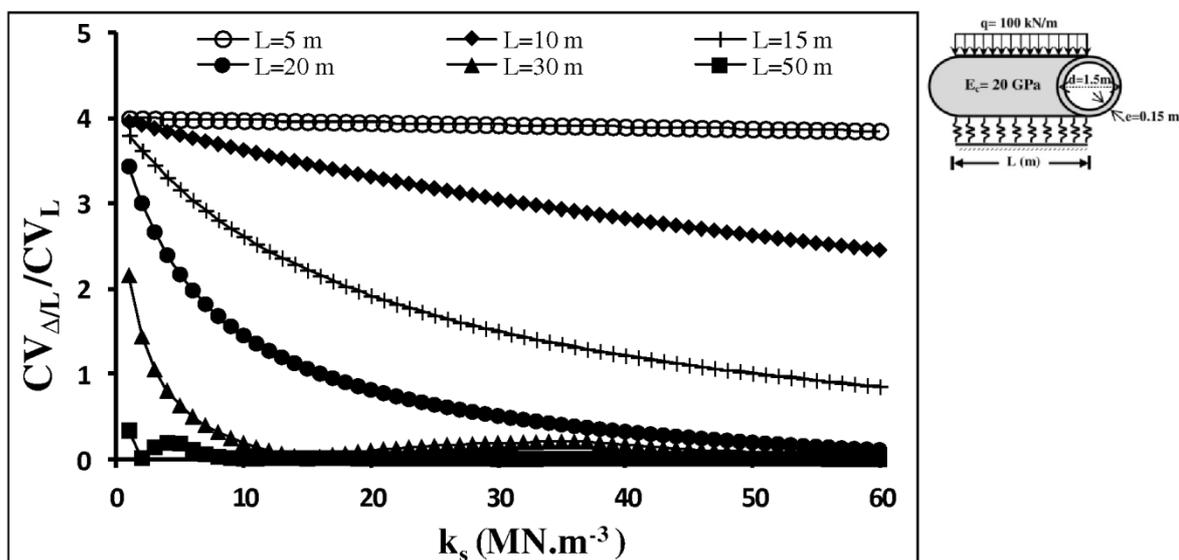
Figure 3-28: Influence of the uncertainty of L on the uncertainty of the maximum differential settlement for the different low stiffness zone lengths (L) ($CV_{\Delta/L}$: coefficient of variation of the differential settlement with respect to L, CV_L: coefficient of variation of L).

In the case of low stiffness zones between 5 m and 50 m the effect of Winkler's springs becomes significant and we observe that the lower the values of k_s and the low stiffness zone lengths, the greater the values of the ratio $CV_{\Delta/L}/CV_L$ are. For k_s values inferior or

equal to 15 MN.m^{-3}, the value of $CV_{\Delta/L}$ is between one and four times CV_L for lengths between 5 m and 20 m. For lengths between 20 m and 30 m, the previous remark is valid only for very small values of k_s.

3.3.3.2. Influence of the uncertainties of k_s and the low stiffness zone on the uncertainty of the bending moment

The uncertainty on the maximum bending moment of buried pipes (Equation 3-10) depends on the same four variables as for the uncertainty on the maximal differential settlement.

Figure 3-29 shows for the different low stiffness zone lengths (identical to those previously studied for the differential settlement) the evolution of the ratio $CV_{M/ks}/CV_{ks}$ (Equation 3-13) as a function of the coefficient k_s. In the case of a low stiffness zone greater or equal to 50 m and whatever the value of k_s, the value of the ratio $CV_{M/ks}/CV_{ks}$ tends to 0.5. For a low stiffness zone less than or equal to 5 m and for any value of k_s, the value of $CV_{M/ks}$ is close to zero. For lengths between 5 m and 50 m we obtain $CV_{M/ks} < 0.5$ CV_{ks} showing that the uncertainty of the bending moment with respect to k_s is less than half of the uncertainty of the subgrade reaction modulus.
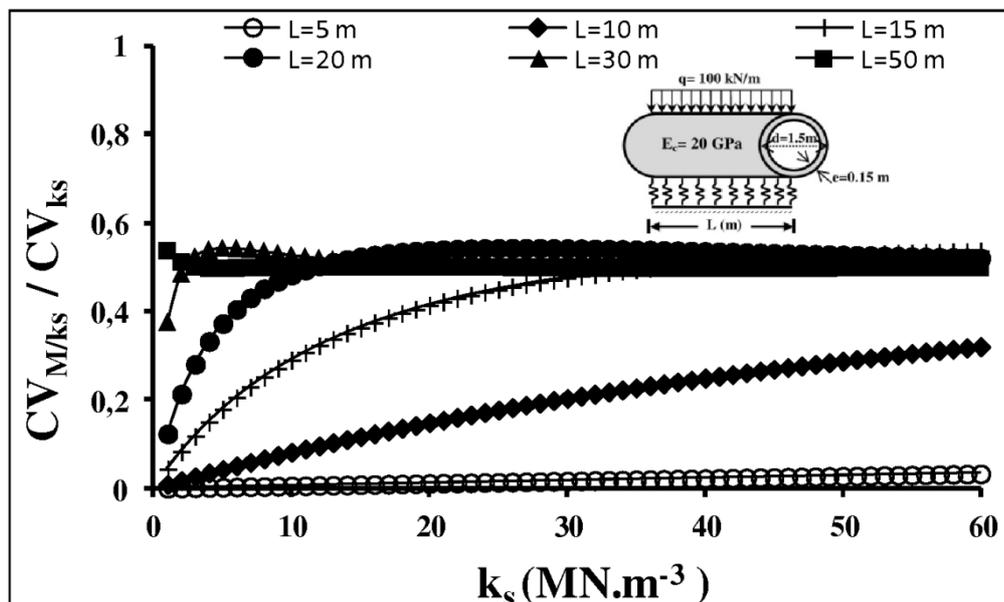
Figure 3-29: Influence of the uncertainty of k_s on the uncertainty of the maximum bending moment for the different low stiffness zone lengths (L) ($CV_{M/ks}$: coefficient of variation of the bending moment with respect to k_s).

Figure 3-30 depicts, for the different low stiffness zone lengths, the evolution of the ratio of the coefficient of variation of the maximum bending moment with respect to L over the coefficient of variation of the low stiffness zone length (Equation 3-14) as a function of the coefficient of k_s. As in the case of the calculation of the coefficient of variation of differential settlement with respect to L, the value of the coefficient of variation of bending moment with respect to L is also very different for the different values of low stiffness zone lengths. This uncertainty is the most important for a low stiffness zone inferior or equal to 5 m where the value of the ratio $CV_{M/L}/CV_L$ is nearly equal to 2 whatever the value of k_s. In fact, the value of 2 corresponds to the power of L in the equation of the bending moment in the case of a beam with two fixed ends with uniform loading. This shows, as we mentioned earlier for the length of 5 m in Figure 3-28, the insignificant effect of Winkler's springs compared to the boundary conditions.

In the case of a low stiffness zone ranging from 5 m to 50 m and for any value of k_s, the value of $CV_{M/L}$ is always less than twice the value of CV_L and tends to zero for a large value of k_s (Figure 3-30).
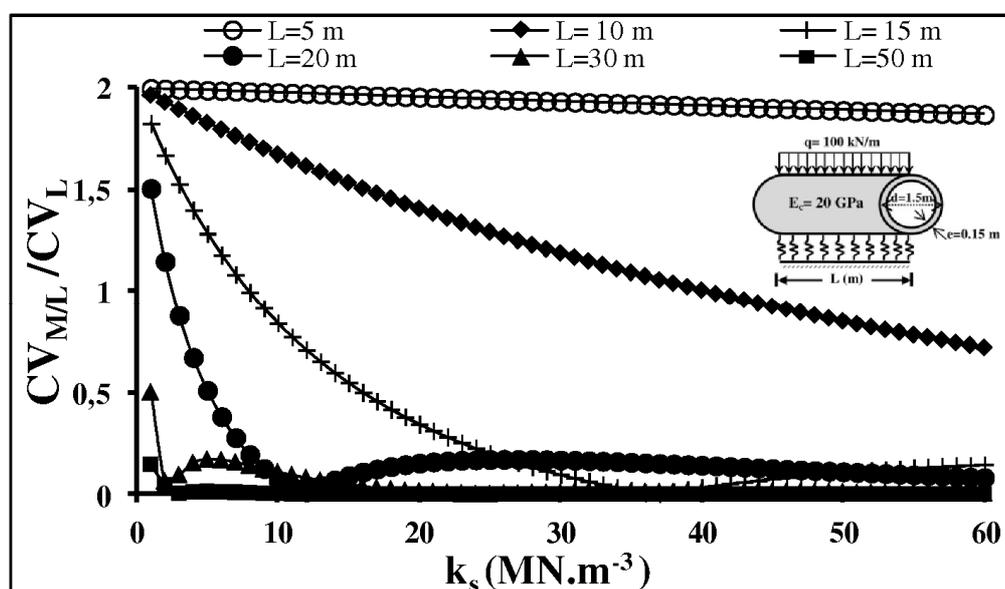
*Figure 3-30: Influence of the uncertainty of L on the uncertainty of the maximum bending moment for the different low stiffness zone lengths ($CV_{M/L}$: coefficient of variation of the bending moment with respect to L).*

For a low stiffness zone length between 5 m and 20 m and for a value of k_s inferior to 5 MN.m^{-3}, we observed that $0.5CV_L < CV_{M/L} < 2CV_L$. For lengths ranging from 20 m to 50

m the uncertainty of $CV_{M/L}$ becomes insignificant except if a void is present under the pipe ($k_s = 0$ MN.m^{-3}), in this case the value of $CV_{M/L}$ is twice the value of CV_L.

These results show that, for values of k_s inferior to 10 MN.m^{-3} and for small values of L, the major effect of the uncertainty of L (compared to the uncertainty of k_s) on the uncertainty of the differential settlement and the bending moment ($CV_{\Delta/L} > CV_{\Delta/ks}$ and $CV_{M/L} > CV_{M/ks}$ for $CV_{ks}=CV_L$). The only way to reduce the uncertainty of the differential settlement and the bending moment is then to reduce the value of the coefficient of variation of the length of the low stiffness zone, which requires a soil reconnaissance able to detect and precisely locate these zones along a buried pipe.

We have done the same work for a continuous buried steel pipe with an external diameter of 1.5 m, a thickness of 0.02 m, Young's modulus of a pipe equal to 210 GPa and the other required parameters are identical to those previously studied here. The results are nearly identical to those obtained for a concrete buried pipe. These results are presented in appendix 1.

3.3.4. Total uncertainties contributions of the maximum differential settlement and the maximum bending moment with respect to the uncertainties of soil reaction modulus and a low stiffness zone

The total uncertainties contributions of the maximum differential settlement and the maximum bending moment are decomposed into contributions from the uncertainties of soil reaction modulus (k_s) and a low stiffness zone (L) (Equation 3-9 and Equation 3-10). These total uncertainties contributions can be obtained through Equation 3-15 and Equation 3-16 respectively for the maximum differential settlement and the maximum bending moment.

$$\frac{CV_{\Delta/k_s}^2}{CV_\Delta^2} + \frac{CV_{\Delta/L}^2}{CV_\Delta^2} = 1 \qquad\qquad\qquad Equation\ 3\text{-}15$$

$$\frac{CV_{M/k_s}^2}{CV_M^2} + \frac{CV_{M/L}^2}{CV_M^2} = 1 \qquad\qquad\qquad Equation\ 3\text{-}16$$

where $\dfrac{CV_{\Delta/k_s}^2}{CV_\Delta^2}$ and $\dfrac{CV_{M/k_s}^2}{CV_M^2}$ are respectively the total uncertainties contributions of the maximum differential settlement and the maximum bending moment respect to k_s. The ratios $\dfrac{CV_{\Delta/L}^2}{CV_\Delta^2}$ and $\dfrac{CV_{M/L}^2}{CV_M^2}$ are defined in the same manner as the latter ratios except these ratios are with respect to L.

In the following, this contribution of uncertainty is explained for different lengths of low stiffness zones for the values of CV_{ks} and CV_L respectively equal 20% and 10%. Additionally, this contribution of uncertainty is discussed for the six semi-empirical models and for a low stiffness zone lengh of 15 m.

3.3.4.1. Total uncertainty contribution of the maximum differential settlement with respect to the uncertainties of soil reaction modulus and a low stiffness zone

Figure 3-31 shows, using Equation 3-15, the total uncertainty contribution of the maximum differential settlement with respect to k_s and L (respectively Figure 3-31a and Figure 3-31b) for different lengths of low stiffness zones. As it shown from Figure 3-31a, for a low stiffness zone length greater than or equal to 50 m and for any value of k_s, the total uncertainty contribution of the maximum differential settlement with respect to k_s is equal to 100%. This illustrates that the total uncertainty contribution of the maximum differential settlement with respect to L is equal to 0%. On the contrary, this uncertainty contribution with respect to k_s is insignificant for a low stiffness zone length inferior or equal to 10 m (for example: $\dfrac{CV_{\Delta/k_s}^2}{CV_\Delta^2} \approx 0$ for L=5 m). For the low stiffness zone lengths between 10 m and 50 m, we observe that the lower the values of k_s and the low stiffness zone lengths, the lower the values of the ratio $\dfrac{CV_{\Delta/k_s}^2}{CV_\Delta^2}$ are. Nevertheless, when the value of k_s increases, whatever the length of the low stiffness zone, this ratio tends to approach to the behavior of the low stiffness zone lengths greater than or equal to 50 m. For the total uncertainty contribution of the maximum differential settlement with respect to L (Figure

3-31b) we obtain, as expected, an inverse behavior compare to this total uncertainty contribution with respect to k_s (Figure 3-31a).

a)

b)
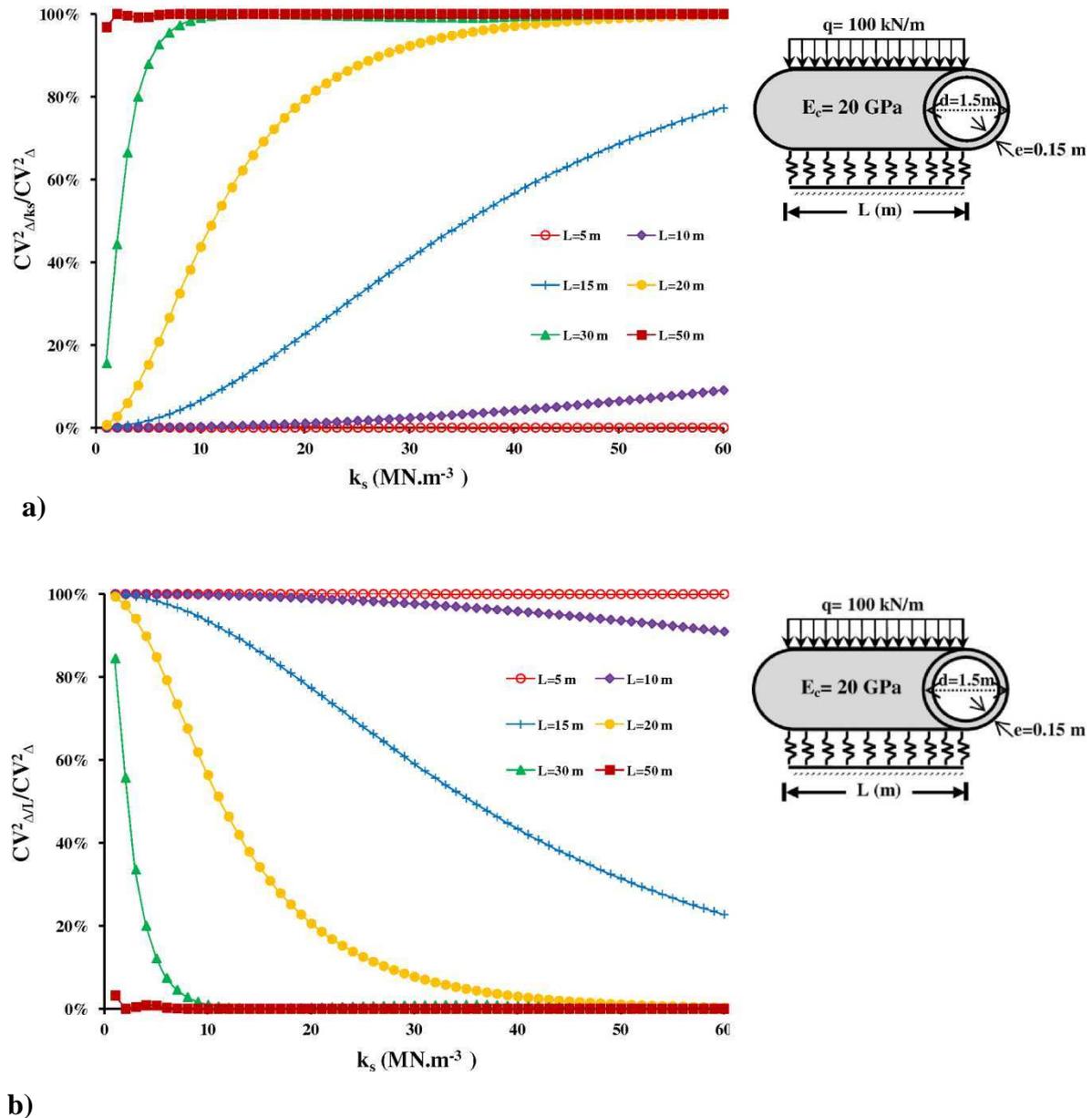
Figure 3-31: Total uncertainty contribution of the maximum differential settlement with respect to k_s *and* L *(respectively figures a and b) for different lengths of low stiffness zones.*

For example, Figure 3-32 shows the total uncertainty contribution of the maximum differential settlement with respect to k_s and L (respectively Figure 3-32a and Figure 3-32b) for the six semi-empirical models and for a low stiffness zone lengh of 15 m. As can be seen from Figure 3-32a, for small values of E_s inferior to 8 MPa for all of these

semi-empirical model except for the Matsubara model, the total uncertainty contribution of the maximum differential settlement with respect to k_s is almost insignificant. Beyond this value of E_s ($E_s \geq 8$ MPa) Matsubara's model gives the greatest value of the ratio $\dfrac{CV^2_{\Delta/k_s}}{CV^2_{\Delta}}$ and Vesic's model gives the lowest value of this ratio. The value of this ratio for the Kloppel model is almost the average of the values of the Matsubara and Meyerhof models. The value of this ratio for the Meyerhof model is nearly the mean of the values of the Kloppel and Biot models. Biot's and Selvadurai's models give nearly the same value of this ratio for the considered values in this example.

a)

b)
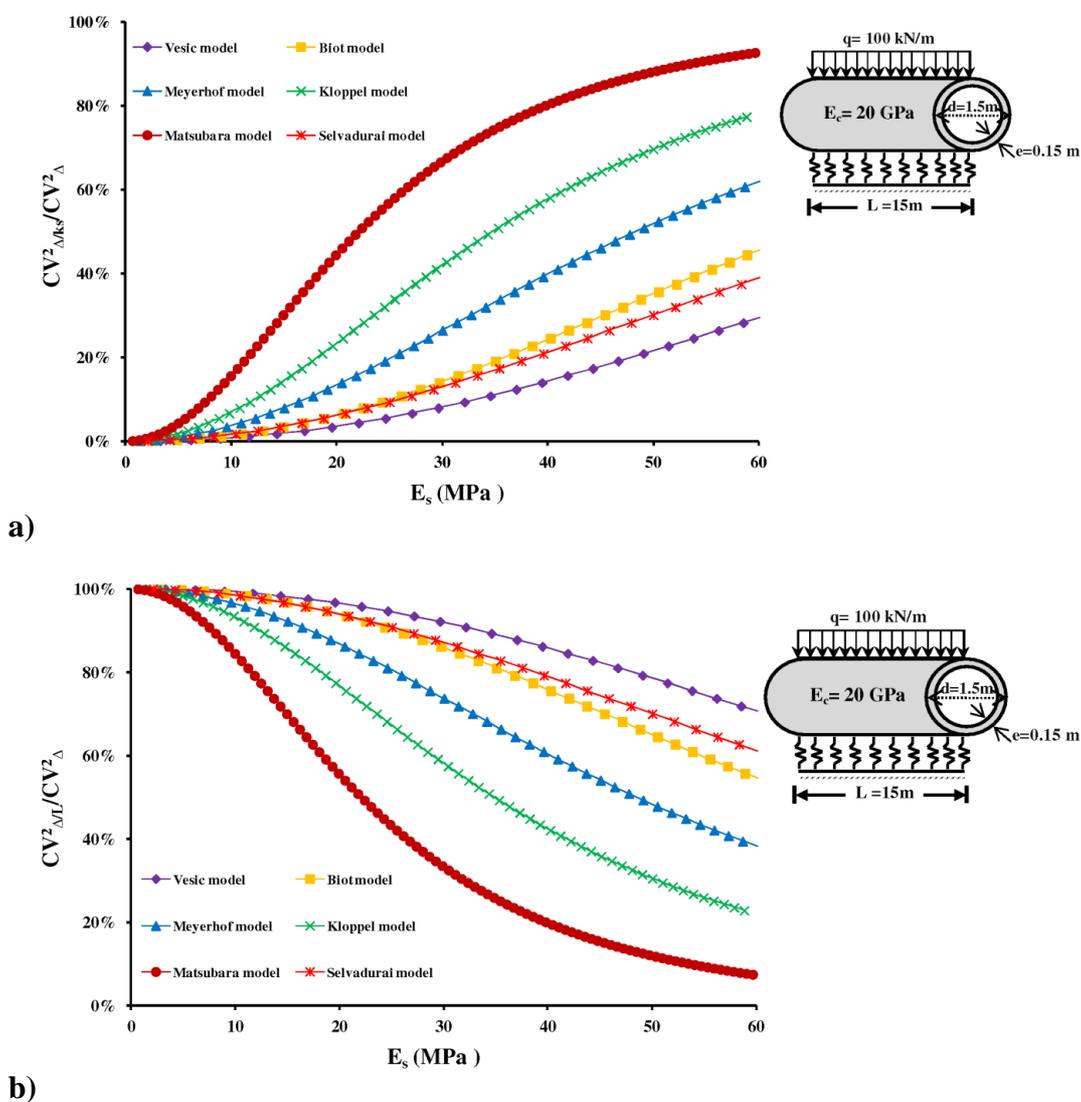
Figure 3-32: Total uncertainty contribution of the maximum differential settlement with respect to k_s *and L (respectively figures a and b) for the six semi-empirical models and for a low stiffness zone lengh of 15 m*

For the total uncertainty contribution of the maximum differential settlement respect to L (Figure 3-32b) and for the considered parameters in this example, we obtain an inverse behavior compare to those obtained with respect to k_s (Figure 3-32a).

3.3.4.2. Total uncertainty contribution of the maximum bending moment with respect to the uncertainties of soil reaction modulus and a low stiffness zone

Figure 3-33 shows, using Equation 3-16, the total uncertainty contribution of the maximum bending moment with respect to k_s and L (respectively Figure 3-33a and Figure 3-33b) for different lengths of low stiffness zones. Figure 3-33a shows for a low stiffness zone length greater than or equal to 50 m and whatever a value of k_s, the total uncertainty contribution of the maximum bending moment with respect to k_s is equal to 100%. This shows the total uncertainty contribution of the maximum bending moment with respect to L is equal to 0%. On the contrary, this uncertainty contribution with respect to k_s is insignificant for a low stiffness zone length inferior or equal to 5 m (for example:

$$\frac{CV^2_{M/k_s}}{CV^2_M} \approx 0 \text{ for } L=5 \text{ m}).$$

For the low stiffness zone lengths between 30 m and 15 m and for the small values of k_s inferior to 20 MN.m^{-3} the values of the ratio $\dfrac{CV^2_{M/k_s}}{CV^2_M}$ increase rapidly. For the low stiffness zone lengths between 10 m and 5 m the values of this ratio increase slowly. Nevertheless, when the value of k_s increases, whatever the length of the low stiffness zone, this ratio tends to approach to the behavior of the low stiffness zone lengths greater than or equal to 50 m. For the total uncertainty contribution of the maximum bending moment with respect to L (Figure 3-33b) we obtain, as expected, an inverse behavior compare to the total uncertainty contribution with respect to k_s (Figure 3-33a).
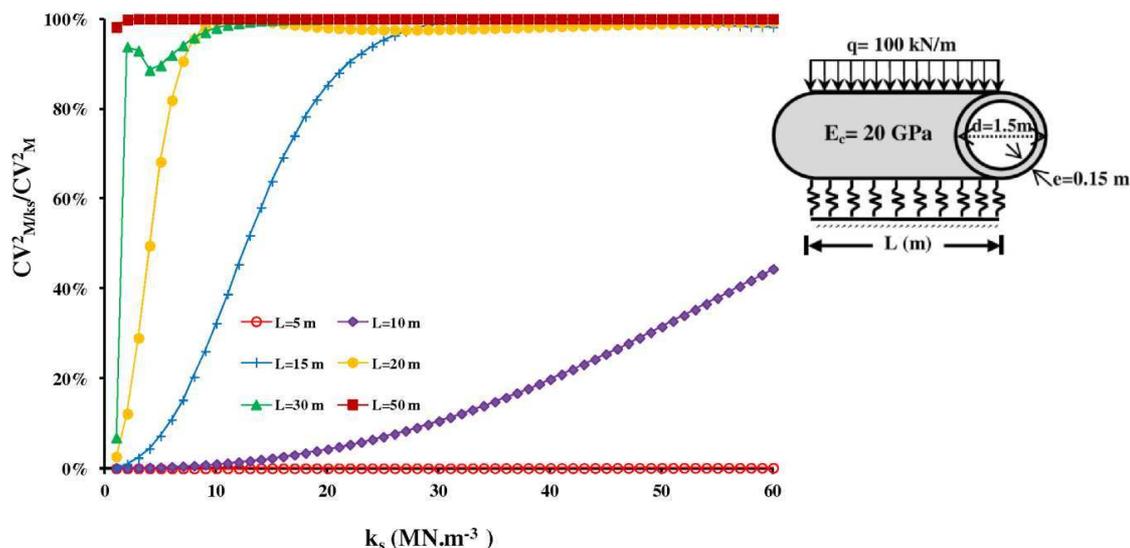
a)
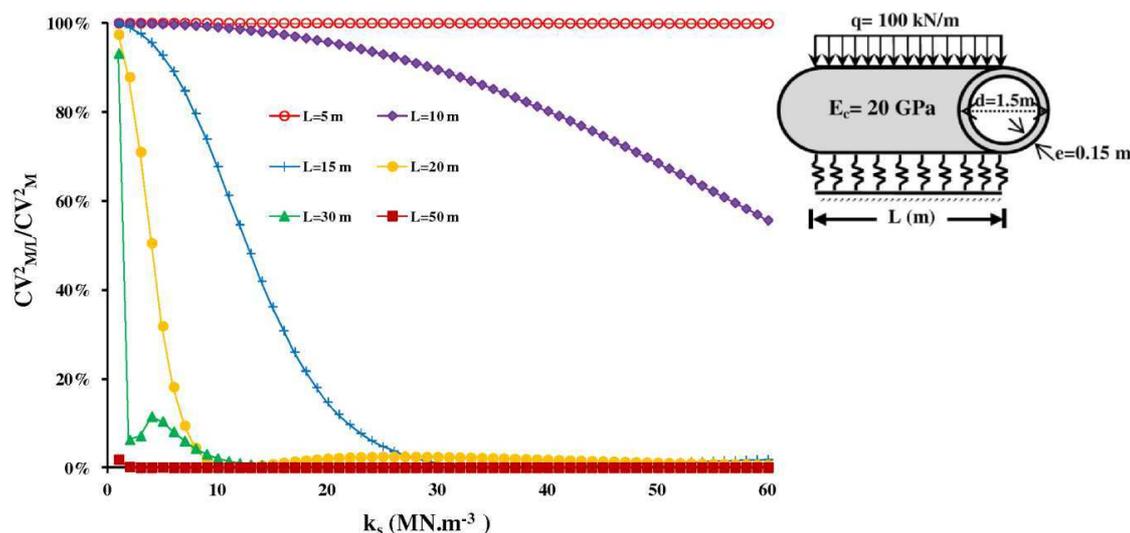
b)

Figure 3-33: Total uncertainty contribution of the maximum bending moment with respect to k_s and L (respectively figures a and b) for different lengths of low stiffness zones

Finally, as in the case of maximum differential settlement, Figure 3-34 illustrates the total uncertainty contribution of the maximum bending moment with respect to k_s and L (respectively Figure 3-34a and Figure 3-34b) for the six semi-empirical models and for a low stiffness zone lengh of 15 m.

As shown in Figure 3-34a, for the values of $E_s \leq 10$ MPa the values of the ratio $\dfrac{CV_{M/k_s}^2}{CV_M^2}$ increases very rapidly for the Matsubara and Kloppel models. This shows the importance

of the uncertainty of k_s on the total uncertainty contribution for these two models. On the contrary it is very slowly in the case of the Vesic model compare to the five other models. Nevertheless, when the value of E_s increases, this ratio tends to a value of 100% illustrating the uncertainty of L on the total uncertainty contribution is insignificant ($\frac{CV^2_{M/L}}{CV^2_M} \approx 0$).

For the total uncertainty contribution of the maximum bending moment with respect to L (Figure 3-34b) an inverse behavior is obtained compare to the total uncertainty contribution with respect to k_s (Figure 3-34a).


a)

b)
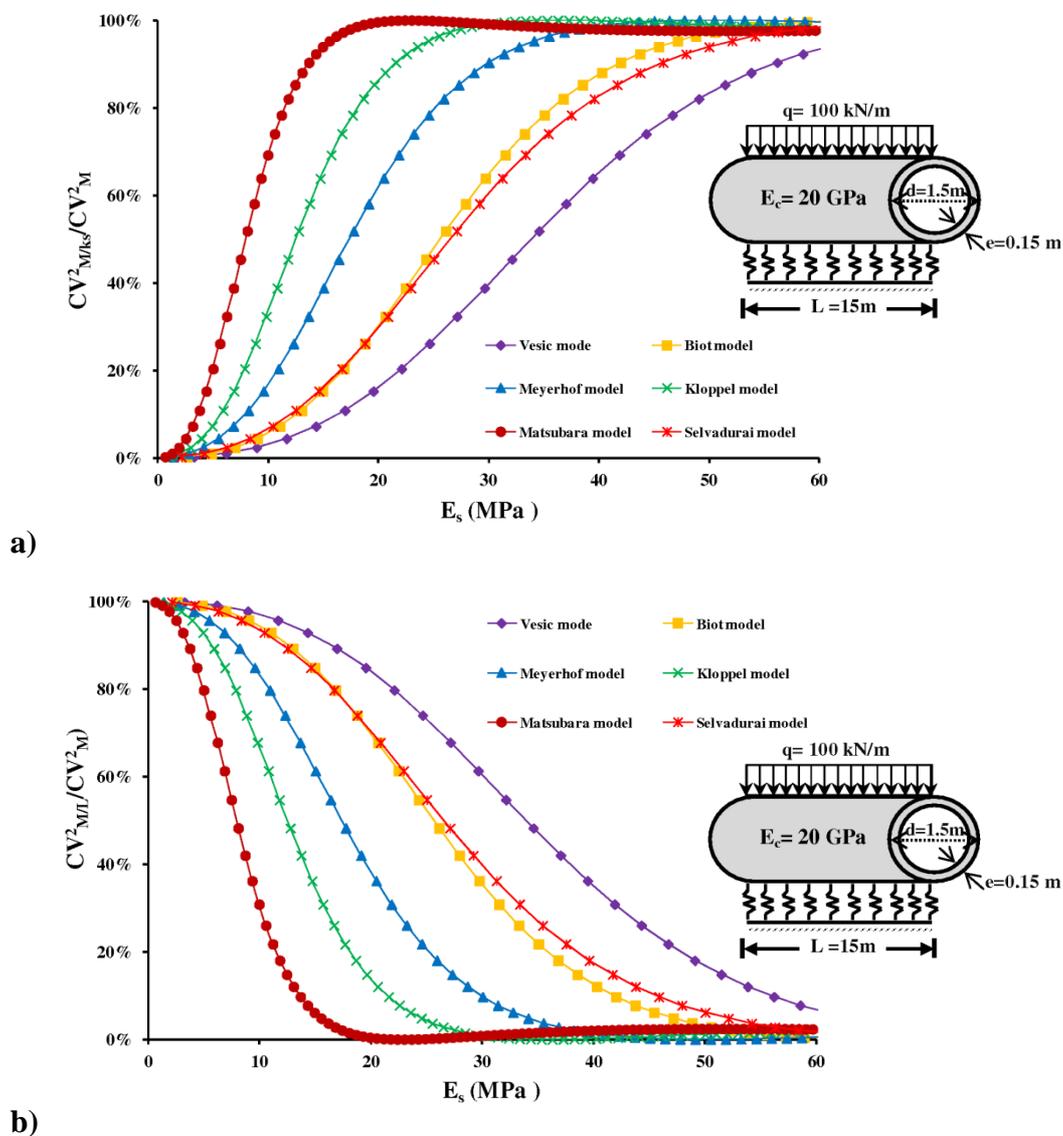
Figure 3-34: Total uncertainty contribution of the maximum bending moment with respect to k_s and L (respectively figures a and b) for the six semi-empirical models and for a low stiffness zone lengh of 15 m

Results presented in this section show the major contribution of a small length of low stiffness zone in the uncertainty of the differential settlement and bending moment. The choice of semi-empirical model appears important. Results of the different contributions can be very different between these six semi-empirical models.

These previous results then can be translated in terms of probability of failure according to the allowable thresholds for the differential settlement and bending moment of a buried pipeline. Thereafter, the confidence bounds for each semi-empirical model are obtained in order to calculate a global uncertainty by the hypothesis of a lognormal distribution.

3.3.5. Reliability analysis for a buried concrete pipe

The obtained results in the previous sections can now be translated in term of probability of failure according to the allowable thresholds for differential settlement and bending moment by the hypothesis of normal distribution. We will consider only one length of buried pipe (L=30 m) in order to illustrate this part. Poisson's ratio is fixed at 0.3, the same coefficients of variation of v_s and d equal to 5% and the coefficients of variation of E_s and L respectively equal to 15% and 10%. The geometry of the buried pipe and the load remain unchanged. Maximum allowable differential settlement (Δ_{all}) for the buried pipe for a value of angular distortion of 1/500 is equal to 30 mm.

Figure 3-35 shows the results obtained for the probability of failure as function of E_s for the six semi empirical models for a buried pipe of 30 m. If for the six semi-empirical models, the values of the coefficient of variation of k_s are close to each other, the values of E_s in order to $P_f \geq 0.067$ are very different. Also, the value of E_s will always be greatest with the Vesic model, always lowest with the Matsubara model and with intermediate values with the models of Kloppel, Meyerhof, Selvadurai and Biot. For example, the soil modulus with E_s=7MPa for the Vesic model does not exceed the value of P_{SLS}=0.067 while this value of E_s for the Matsubara model is equal to 1.5 MPa in order to not exceed the value of the probability of SLS.
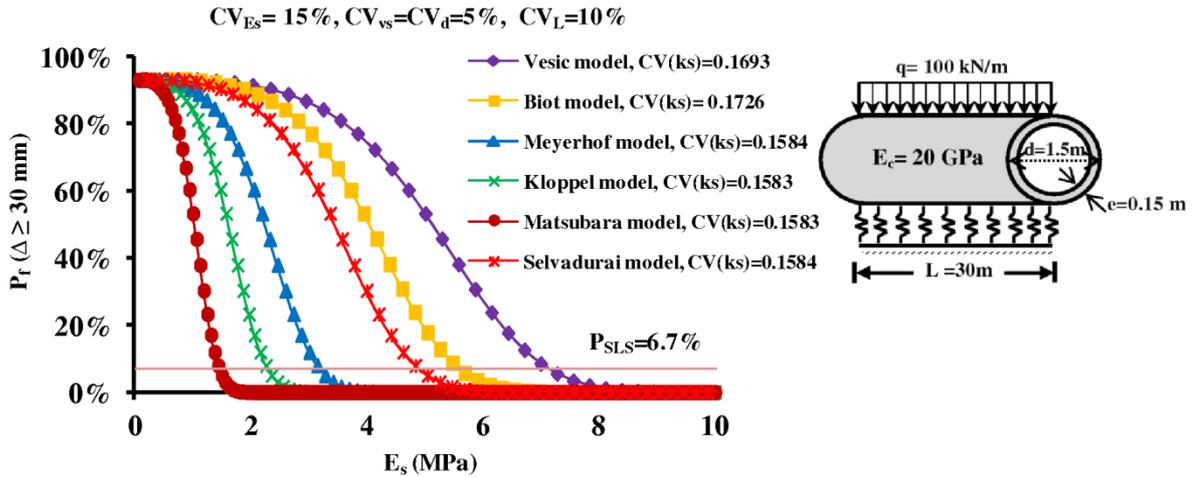
Figure 3-35: Estimation of the probability of failure (P_f) as function of E_s for the maximum differential settlement of a buried pipe (for the six semi-empirical models).

We will consider, by hypothesis, that the maximum bending moment (M) is equal to 2880 kN.m that it corresponds to a σ_e equal to 10 MPa (σ_e: maximum elastic stress of concrete). Figure 3-36 shows the results obtained for the probability of failure as function of E_s, for the six semi-empirical models. The interpretation of these results is identical to the analysis presented for Figure 3-35 concerning the differential settlement but with values of E_s greater than in the case of differential settlements in the case presented in this section. These results show again the importance of the choice of a semi-empirical model.
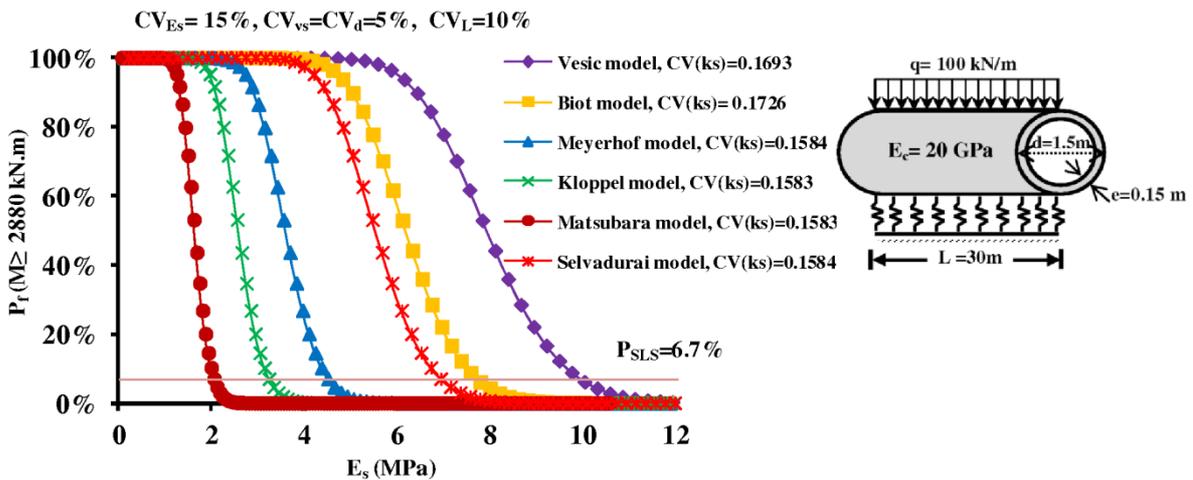
Figure 3-36: Estimation of the probability of failure (P_f) as function of E_s for the maximum elastic bending moment of a buried pipe (for the six semi-empirical models and for a maximum elastic stress of concrete equal to 10 MPa).

The probability of failure for the maximum bending moment (M) of 1440 kN.m (corresponds to a σ_e equal to 5 MPa) is presented in appendix 1.

In order to complete the previous analysis, we can study the influence of the values of the coefficient of variation of k_s and L on the probability of failure in the case of differential settlement and the semi-empirical model of Vesic.

Figure 3-37 and Figure 3-38 show the obtained results for the probability of failure respectively for the different values of CV_{ks} and CV_L. Figure 3-37 depicts nearly the same values of the probability of failure for the different values of CV_{ks} illustrating the unimportance of the value of the coefficient of variation of k_s. On the contrary, Figure 3-38 shows the importance of the value of the coefficient of variation of L in the case of the semi-imprical model of Vesic. For example, in the case shown in Figure 3-38, the soil of the foundation with E_s= 7 MPa, should have a coefficient of variation of L less than 5% in order to not exceed the value of P_{SLS}=0.067; the soil of the foundation with E_s= 9 MPa, a coefficient of variation of L less than 30%.
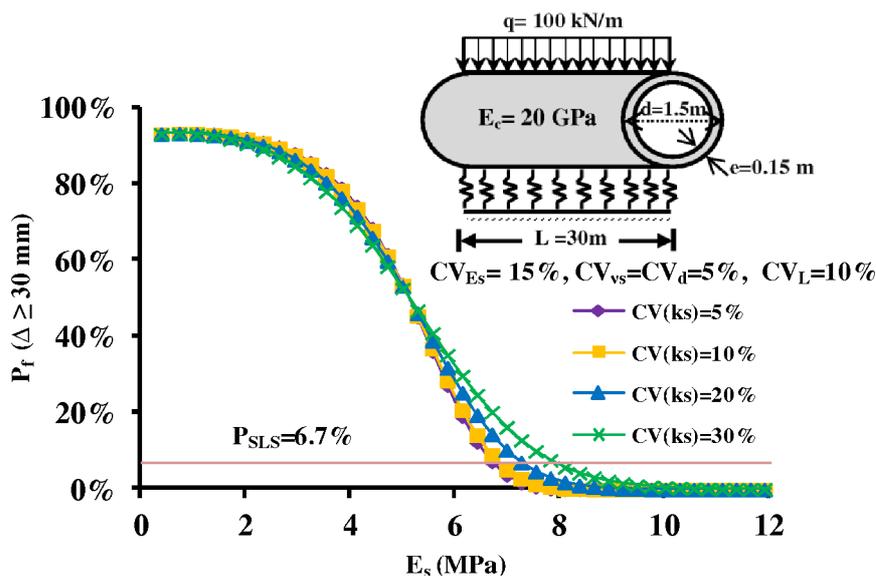
Figure 3-37: Comparing the probability of failure (P_f) for the maximum differential settlement of a buried pipe for different values of CV_{ks} (Vesic's model)
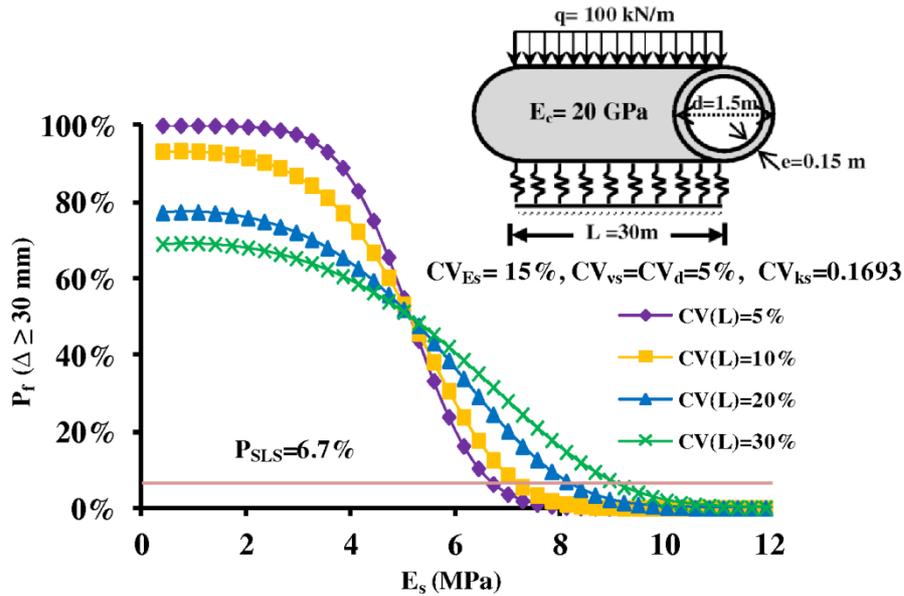
Figure 3-38: Comparing the probability of failure (P_f) for the maximum differential settlement of a buried pipe for different values of CV_L (Vesic's model)

Figure 3-39 show the obtained results for the probability of failure for the different values of CV_{ks} and CV_L. The probability of failure for the differential settlement is almost close to those obtained from Figure 3-38 showing again the importance of the value of CV_L compare to CV_{ks}.
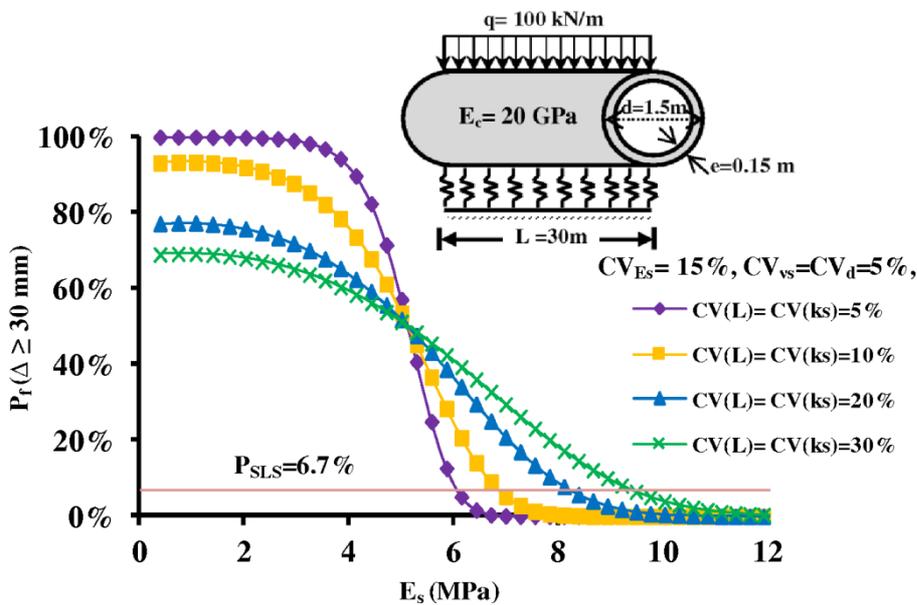
Figure 3-39: Comparing the probability of failure (P_f) for the maximum differential settlement of a buried pipe for different values of CV_{ks} and CV_L (Vesic's model)

The same figures could be obtained for the five other semi-empirical models, bending moment and for different buried pipes geometries and loading (q) in order to obtain different charts to help a better design of buried pipe when the soil modulus and the geometrical dimensions of pipe are uncertain and where weak soil zones are present on the construction site.

All of the presented results in this section for the reliability analysis are based on the hypothesis of a normal distribution for the values of the maximum differential settlement and the maximum elastic bending moment. The obtained results by the hypothesis of a log-normal distribution for these values are almost identical to those ones obtained for a normal distribution as presented in appendix 1.

3.3.6. Application to global uncertainty analysis (for a buried concrete pipe)

In this section, for each semi-empirical model, we use the presented methodology (Figure 3-19) for the calculation of the confidence bounds of the differential settlement and the bending moment of a buried pipe resting on an elastic soil and in the presence of a low stiffness zone in order to verify that values of limit states design are not included into confidence bounds.

Firstly, the deterministic values of the maximum differential settlement and the bending moment are obtained through the traditional use of the Winkler model. For this purpose, starting from values of E_s, v_s, d, E_c, we obtain from each semi-empirical model different values of the subgrade reaction modulus which are introduced in the Winkler model for a given length of low stiffness zone. In a second step, through the uncertainty approach, the FOSM method is applied on the six semi-empirical models knowing the coefficient of variation of each parameter (E_s, E_c, v_s, d) to determine the coefficient of variation of k_s for each model. Thereafter, the FOSM method is applied again on the analytical equations of the deflection and the bending moment (for a given CV_L) to determine the coefficient of variation of differential settlement and the bending moment for each model. Finally, by considering the hypothesis on the distribution probability for the differential settlement and bending moment, both approaches (traditional approach and uncertainty approach) are combined to calculate the confidence intervals for each of the six models. At the end, a global uncertainty is proposed which corresponds to the range between the maximum of the six upper bounds and the minimum of the six lower bounds.

In order to illustrate the complete use of this methodology, we take as an example a continuous buried steel or concrete pipe resting on soil in the presence of a low stiffness zone of 30 m (Figure 3-23b) with a Young's modulus (E_s) of 2 MPa (very soft clay) estimated from a geotechnical investigation. The coefficient of variation of E_s and L are estimated to 15% and 10% from published values in the literatures and expert judgment respectively. The soil parameters, the mechanical property and the geometrical dimensions of this buried pipe are identical to those previously studied in this paper. For this considered case, the deterministic values of the subgrade reaction modulus, the differential settlement and the bending moment are obtained for each semi-empirical model (Figure 2-11 and Equation 1-51). Thereafter, using the methodology explained previously and assuming a lognormal distribution (which is a fairly common assumption) for the subgrade reaction modulus, the differential settlement and the bending moment, their 95% confidence bounds are obtained for each semi-empirical model. The results for the application case are presented in Figure 3-40. As expected the deterministic values of k_s, Δ, M and then their confidence intervals are different for each semi-empirical model (Figure 3-40a, Figure 3-40b and Figure 3-40c). The value of k_s and its associated confidence interval are the highest for the Matsubara model and the smallest for the Vesic model (Figure 3-40a). Figure 3-40b and Figure 3-40c show that the deterministic values and confidence bounds of the differential settlement and the bending moment are the most important for the Vesic model and the least important for the Matsubara model.

In the case wherein choosing a suitable semi-empirical model is difficult, a global uncertainty is introduced. This includes the uncertainties from each semi-empirical model and corresponds to the range between the maximum of the six upper bounds and the minimum of the six lower bounds. The global uncertainties for Δ and M for the case under consideration are respectively [13.93; 78.13] (mm) and [2.190; 6.401] (MN.m) (Figure 3-40b and Figure 3-40c).

The counter slope for the buried pipe, which correspond to the ratio between Δ and $x_{max(\Delta)}$ (see section 3.2), can be obtained from the deterministic values of the maximum differential settlements for these semi-empirical models. This slope should be compared to the serviceability limit state, corresponding to a value of counter slope of 1/250 (it is taken as an average limit value), which can prevent the normal flow of fluids. For the six models the deterministic values of counter slopes are smaller than the limit value of 1/250.

151

However, the values of counter slopes obtained from the global uncertainty of the maximum differential settlements ranging from 1/1000 to 1/190 showing it is possible to exceed the limit counter slope. By considering the maximum elastic stress of concrete (σ_e) equal to 20 MPa, for the bending moment, the maximum values deduced from the global uncertainties (Figure 3-40c) are less than the value of the maximum plastic bending moment equal to 6.75 MN.m.

The same results could naturally be carried out for different buried pipes geometries, boundary conditions and loading (q) in order to obtain different charts to help a better design of buried pipes, like sewer networks, when weak soil zones are present on a construction site.
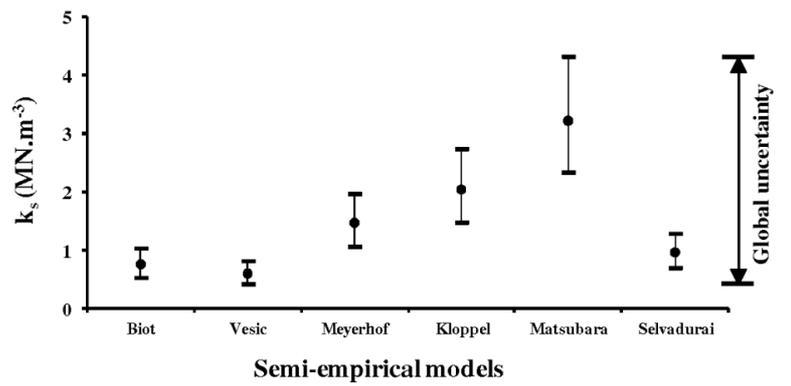
a)
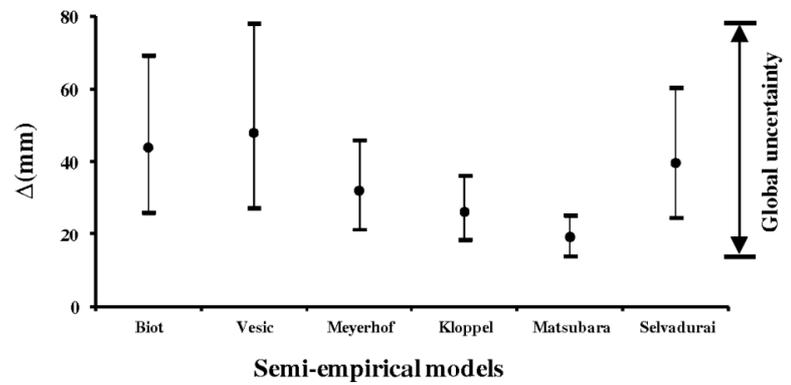
b)
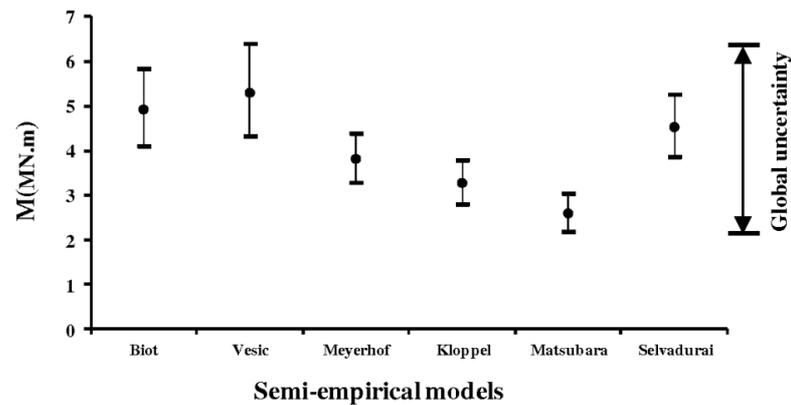
c)

Figure 3-40: Global uncertainties for the a) Subgrade reaction modulus k_s, b) Maximum differential settlement Δ and c) Maximum bending moment M by considering 95% confidence bound for each semi-empirical model with log-normal distribution (E_s=2 MPa, E_c=20 GPa, , v_s=0.3, d=1.5 m, e=0.15 m, L=30 m, q= 100 kN/m, CV_{Es}=15%, CV_L=10%, CV_d= CV_{vs}= CV_{Ec}=5%).

Results of the application to global uncertainty analysis for a continuous buried steel pipe are presented in appendix 1.

3.4. Comparison of FOSM and Monte Carlo analysis results

The Monte Carlo Method is widely used in stochastic modeling. It is a versatile method which, in principle, can always be applied. It consists of performing a large number of deterministic calculations for random realizations of the problem and a statistical analysis of results. The computational effort may become huge, however, before results converge, and the number of realizations necessary is at best only approximately known in advance.

It is common to use the Monte Carlo method to verify other approximate solutions, like FOSM and FORM. For example, Silva et al. (2008) used these two previous methods (FOSM and Monte Carlo simulation) for a reliability evaluation of reinforced concrete pipes in crack opening limit state. Quantification of uncertainty in groundwater modeling and uncertainty analysis of Lake Erie Net Basin Supplies, using these methods, were respectively studied by Kunstmann et al. (2002) and Bruxer (2011).

In the following the results of the Monte Carlo technique are compared to those from the FOSM method for the superficial geotechnical designs (continuous spread footings and buried pipes). The comparisons, for simplicity, will do for a length of spread footing and for a low stiffness zone of soil beneath the buried pipe with a lognormal distribution for each of the soil and structure parameters.

The evolutions of CV_{ks} as a function of CV_{Es} for the four semi-empirical models in the case of spread footing, using the Monte Carlo approach are shown in Figure 3-41.This figure is for the values of E_s equal to 5 MPa (Figure 3-41a) and 25 MPa (Figure 3-41b) for the generation of 1000 values of this parameter. This figure was obtained by assuming the values of v_s, b, h and E_c to have a log-normal distribution respectively with mean values of 0.3, 0.5 m, 0.3 m and 20 GPa, the coefficients of variation for each parameter equal to 10%, from the generation of 1000 values of these parameters. Statistical analysis of Monte Carlo results is performed to obtain one value of CV_{ks} for one value of CV_{Es}. As can be seen, the results of the Monte Carlo (Figure 3-41) and FOSM (Figure 2-10) methods are as expected nearly identical for all semi-empirical models.

Figure 3-42 presents for a buried pipe and for the values of E_s equal to 5 MPa (Figure 3-42a) and 25 MPa (Figure 3-42b), using the Monte Carlo approach, the evolutions of CV_{ks}

as a function of CV_{Es} for six semi-empirical models. The values of E_c equal to 20 GPa, coefficients of variation for each parameter (d, v_s and E_c) equal to 5%, and other required parameters are identical to those previously studied in Figure 2-16. This figure was obtained from the generation of 1000 values of soil and buried pipe parameters and for one value of coefficient of variation of E_s which give, after a statistical analysis, one value of CV_{ks}. As expected, there is a little difference in the results between Monte Carlo (Figure 3-42) and FOSM (Figure 2-16) approaches.

a)

b)
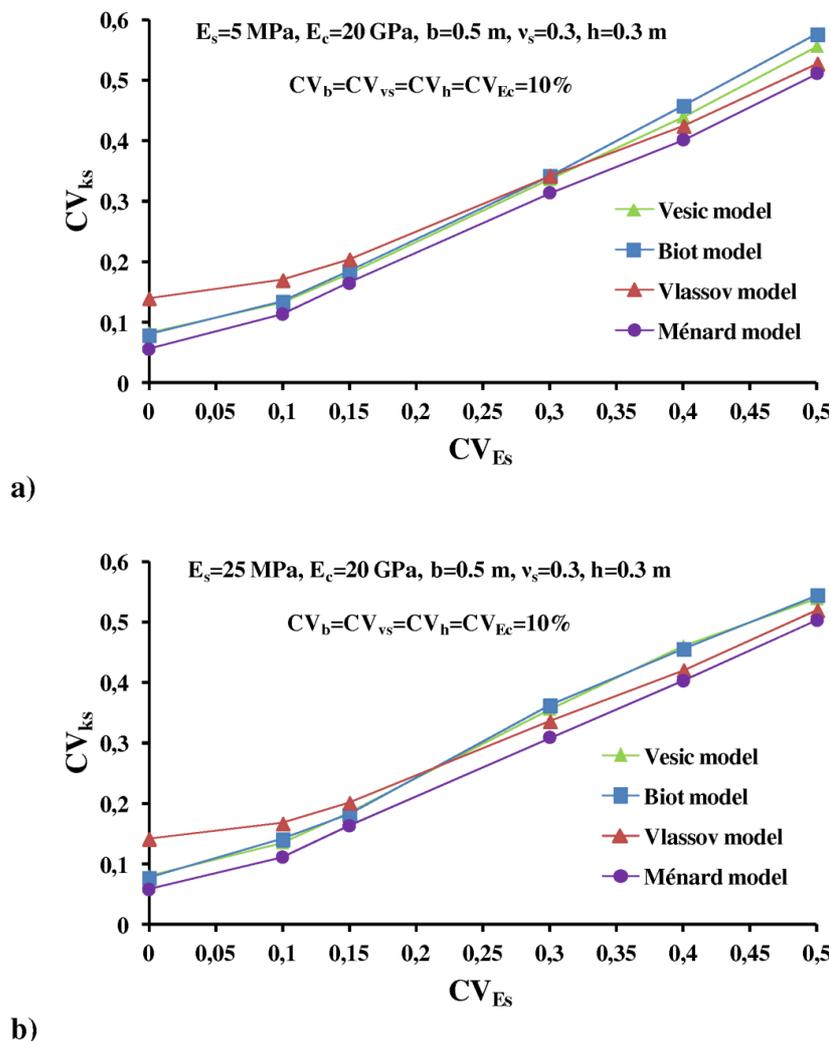
Figure 3-41: Evolution of CV_{ks} (Coefficient of Variation of k_s) as a function of CV_{Es} (Coefficient of Variation of E_s) for the values of E_s equal to 5 and 25 MPa (Figure 3-41a and Figure 3-41b) for studied semi-empirical models (Monte Carlo method for a spread footing).

155

a)

b)
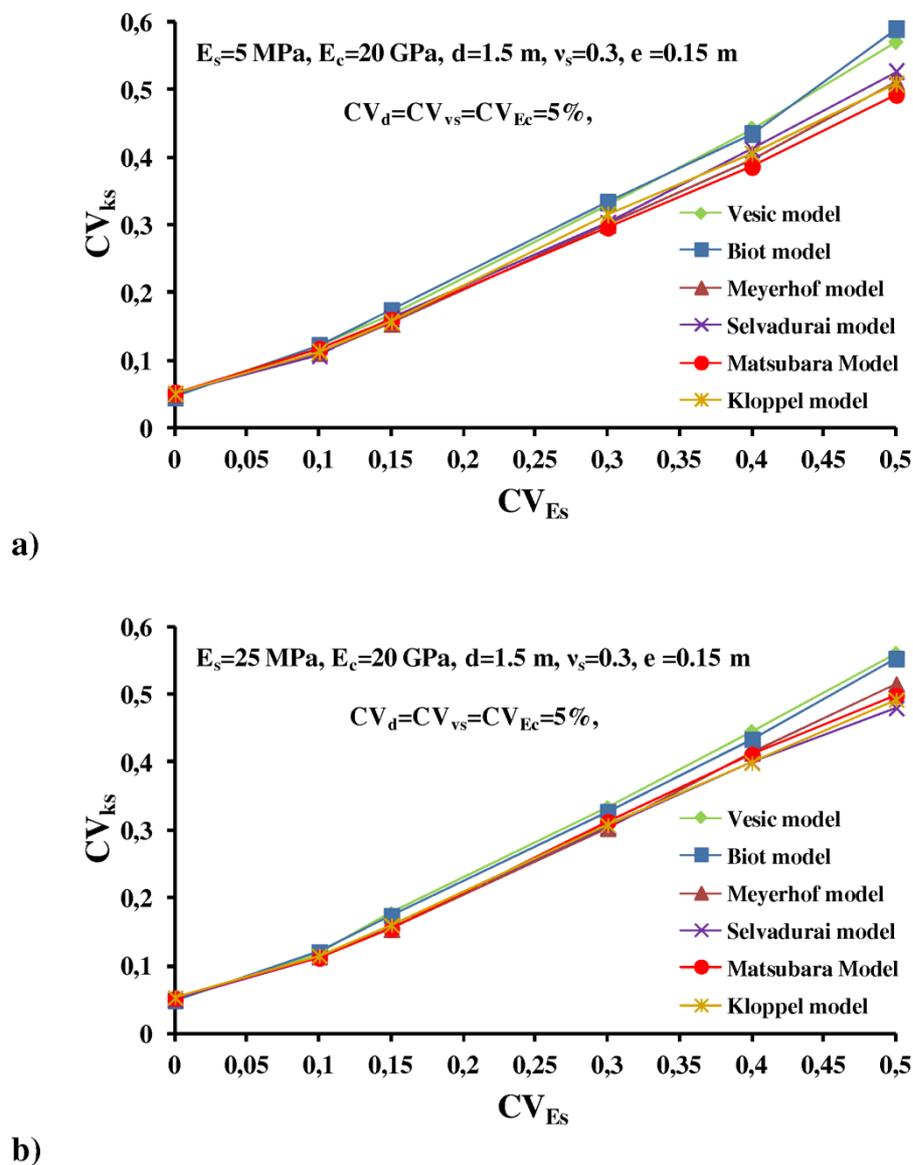
Figure 3-42: Evolution of CV_{ks} (Coefficient of Variation of k_s) as a function of CV_{Es} (Coefficient of Variation of E_s) for the values of E_s equal to 5 and 25 MPa (Figure 3-42a and Figure 3-42b) for studied semi-empirical models (Monte Carlo method for a buried pipe).

FOSM method has several advantages over Monte Carlo method, which can be resumed as follows:

- its analytical relationship,
- much less time consuming,
- no distributional information on the system's basic variables and
- determination of the important parameters between variables.

In contrast to FOSM method, Monte Carlo approach is extremely time consuming and requires a lot of computer memory.

Figure 3-43 presents for a spread footing considered in this chapter (section 3.2.1) and for the length of 5 m, using the Monte Carlo and FOSM approaches, the evolutions of a coefficient of variation of the maximum differential settlement with respect to k_s ($CV_{\Delta/ks}$, Figure 3-43) as function of soil reaction modulus. This figure is obtained from the generation of 150 values of the involved parameters and for 40 simulations of coefficient of variation of the maximum differential settlement. The value of CV_{ks} equal to 15% and other required parameters are identical to those previously studied in Figure 3-41.
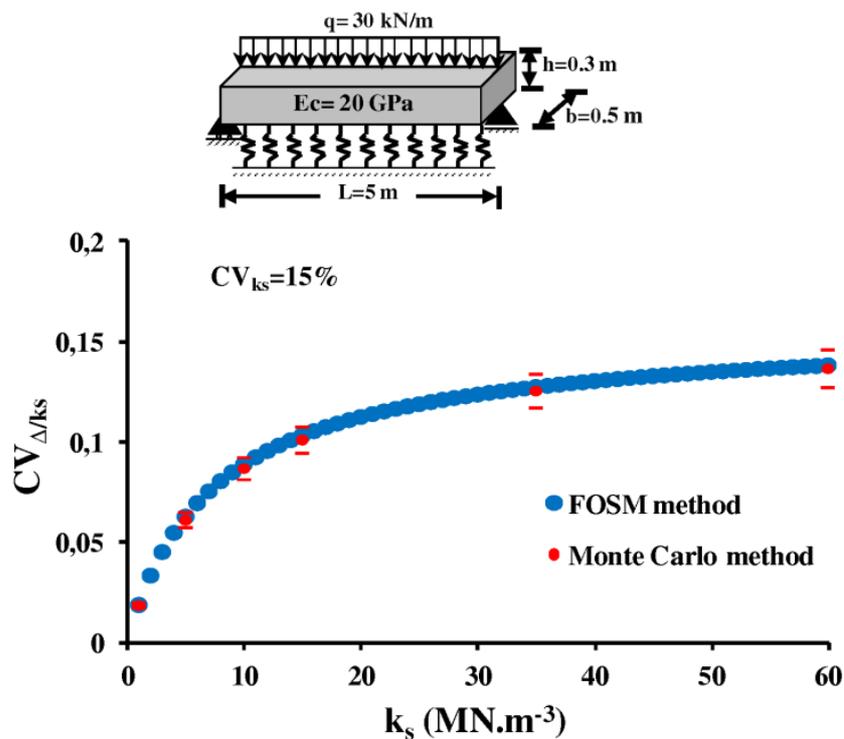
Figure 3-43: Comparison of the results of Monte Carlo simulation with those from FOSM method for the coefficient of variation of the maximum differential settlement with respect to k_s ($CV_{\Delta/ks}$)

Figure 3-44 is obtained in the same way and with the same required parameters as the previous one (Figure 3-43) for the coefficient of variation of the maximum bending moment in the case of a spread footing with simply supported at two ends as boundary conditions.
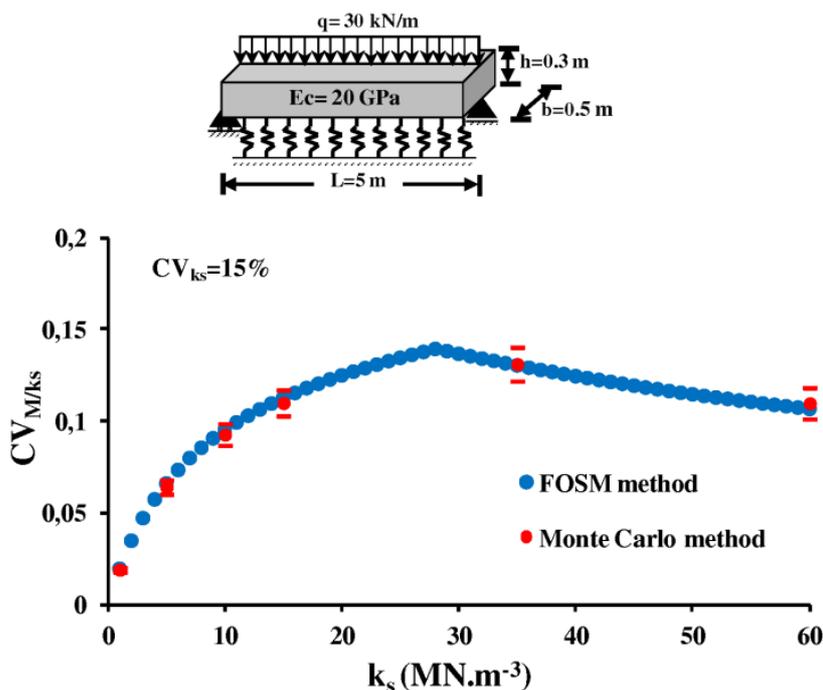
Figure 3-44: Comparison of the results of Monte Carlo simulation with those from FOSM method for the coefficient of variation of the maximum bending moment with respect to k_s ($CV_{M/ks}$)

These figures (Figure 3-43 and Figure 3-44) allow the comparison of the results of Monte Carlo simulation with those from FOSM method. The values of $CV_{\Delta/ks}$, and $CV_{M/ks}$ with associated uncertainty bounds from Monte Carlo simulation are satisfactorily similar to those from FOSM method.

Figure 3-45 depicts for a buried pipe considered in this chapter (section 3.3.1) and for a length of low stiffness zone 15 m beneath the buried pipe, using the Monte Carlo and FOSM methods, the evolutions of a coefficient of variation of the differential settlement with respect to k_s ($CV_{\Delta/ks}$, Figure 3-45a), with respect to L ($CV_{\Delta/L}$, Figure 3-45b) and with respect to k_s and L (CV_{Δ}, Figure 3-45c) as function of soil reaction modulus. As in the case of a spread footing, this figure comes from the generation of 150 values of the involved parameters and from 40 simulations of coefficient of variation of the maximum differential settlement. The values of CV_{ks} and CV_L are respectively equal to 15% and 10% and other required parameters are identical to those previously studied in Figure 3-42.

Figure 3-46 is obtained in the same way and with the same required parameters as in Figure 3-45 for the coefficient of variation of the maximum bending moment.

Figure 3-45 and Figure 3-46 show again the values of the coefficients of variation of the maximum differential settlements and the bending moments with their associated

uncertainty bounds obtained by the Monte Carlo method fit well with the results obtained by the FOSM method and this method nearly reproduced the FOSM result.

Monte Carlo techniques are suited for these analyses but imply a huge computational effort. An alternative and computationally efficient approach, however, is the FOSM method which directly propagates parameter uncertainty into the result.

Overall, as the above results show, use of the Monte Carlo approach to determine uncertainties in the maximum differential settlements and the bending moments of the spread footings and the buried pipes is likely unnecessary, given that the results from the FOSM and Monte Carlo methods are nearly identical. This is to be expected given the low non-linearity of the different models but should be demonstrated.
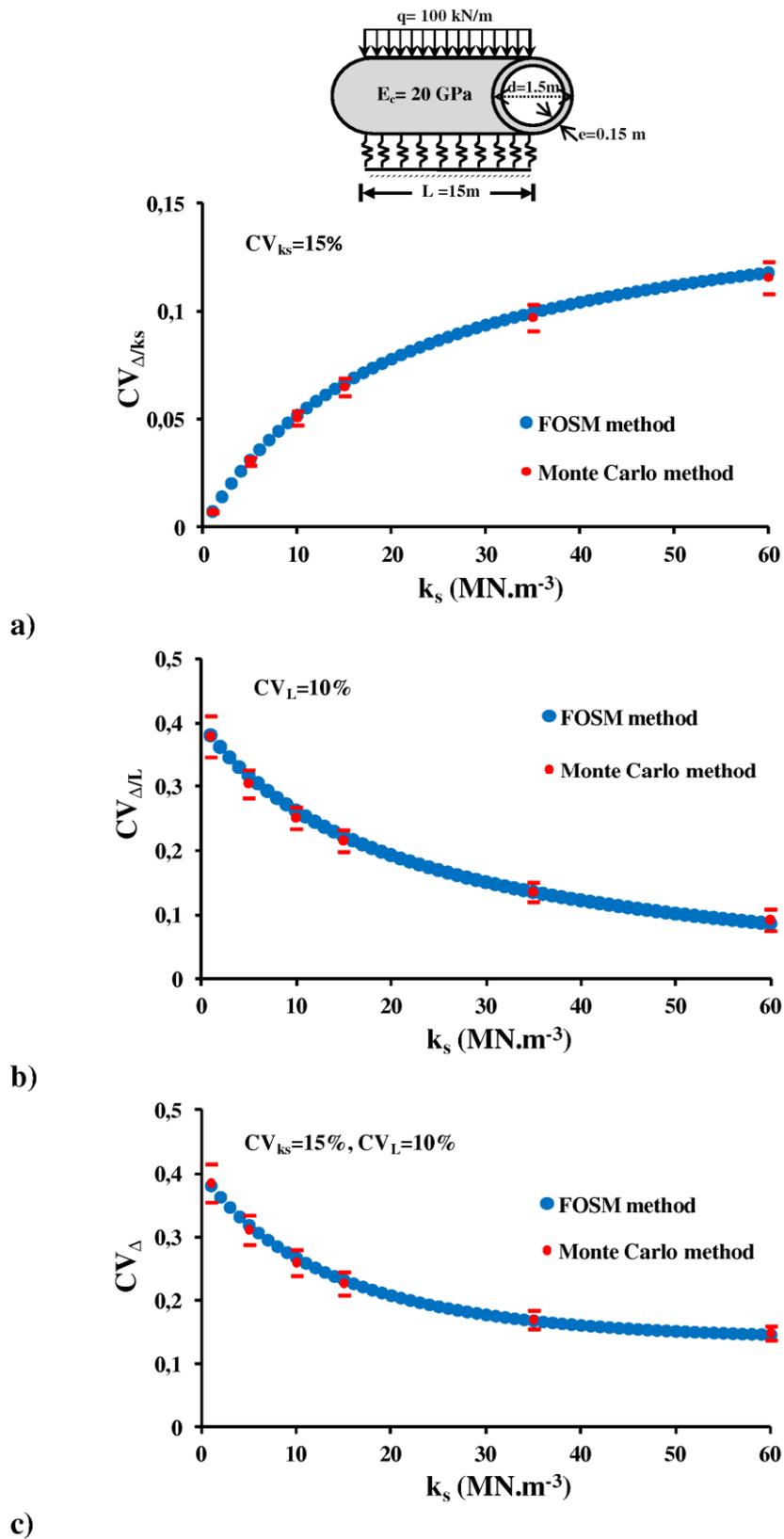
Figure 3-45: Comparison of the results of Monte Carlo simulation with those from FOSM method for the coefficient of variation of the maximum differential settlement a) with respect to k_s ($CV_{\Delta/ks}$) b) with respect to L ($CV_{\Delta/L}$) and c) with respect to k_s and L (CV_Δ) as a function of soil reaction modulus for a buried pipe.

160
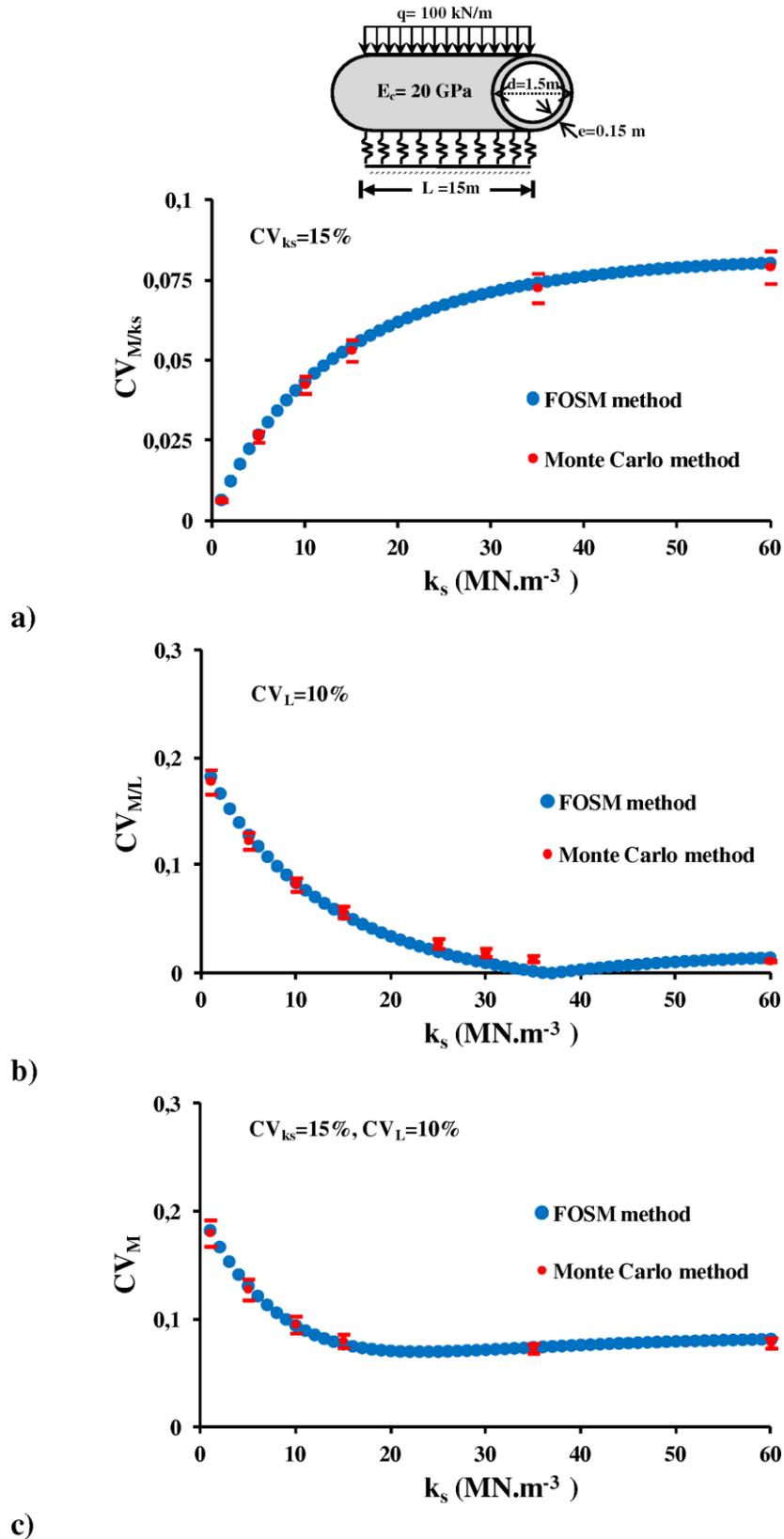
Figure 3-46: Comparison of the results of Monte Carlo simulation with those from FOSM method for the coefficient of variation of the maximum bending moment a) with respect to k_s ($CV_{M/ks}$) b) with respect to L ($CV_{M/L}$) and c) with respect to k_s and L (CV_M) as a function of soil reaction modulus for a buried pipe.

3.5. Summary and conclusions

In this chapter, the soil and structural properties and their uncertainties were considered in order to reveal their effects on the longitudinal behavior of continuous spread footings and buried pipelines resting on elastic soil.

We then studied the incorporation of the uncertainty of modulus of subgrade reaction (k_s) in an analytical model, its influence on the differential settlement and bending moment of a shallow foundation and the buried pipelines in the longitudinal direction.

The FOSM method was used again on the analytical solution of a beam on an elastic foundation from Winkler's hypothesis, with different boundary conditions.

Results from the FOSM method, for the spread footings, show that the uncertainties of the differential settlement (CV_Δ) and the bending moment (CV_M) are very different depending on the length of the spread footing and the boundary conditions considered in order to model a zone of weak soil at the construction site. For any value of k_s and the foundation length we showed that, for the spread footings with simply supported at two ends, $CV_\Delta \leq CV_{ks}$ and $CV_M \leq CV_{ks}$. For spread footings which are simply supported at one end, we showed that $CV_\Delta \leq 1.2CV_{ks}$ and $CV_M \leq 0.5CV_{ks}$. For the differential settlement or bending moment, the obtained results concerning the probability of the serviceability limit state (P_{SLS}) show the importance of the choice of the semi-empirical model and the boundary conditions. For the semi-empirical model and the boundary conditions selected, when the uncertainty on the value of k_s is high, the probability of the serviceability limit state can be exceeded even if the soil has good mechanical properties.

Results in the case of buried pipes show two things. The uncertainties of the differential settlement and the bending moment are very different depending on the length of the low stiffness zone beneath the buried pipe and its value of E_s. Additionally, these uncertainties are more influenced by the length of the low stiffness zone than the value of the subgrade reaction modulus. From a practical point of view, this indicates that an accurate knowledge of soil is more important in determining low stiffness zone lengths than soil properties in case of soil reconnaissance for buried pipes.

In cases where choosing a suitable semi-empirical model for the estimation of uncertainty on k_s - and therefore on the differential settlement and the bending moment of a spread footing or buried pipe - is difficult, we propose a global uncertainty approach. This approach includes the uncertainties from each semi-empirical model and can be used to

verify whether the maximum values exceed the serviceability values for the ultimate limit state.

The FOSM method proved simpler to apply than the Monte Carlo method which requires greater computational resources. This is to be expected given the low non-linearity of the model. However, the Monte Carlo method is feasible, due to the simplicity of the model and currently available computer software.

Finally, the results obtained here showed that, when the soil modulus and the geometrical dimensions of structure are uncertain and where a low stiffness zone or shrinkage of clayey soil is present, the longitudinal behavior of continuous spread footings or buried pipes should also be considered in their design.

Chapter 4

Soil spatial variability on a

construction site

4. Soil spatial variability on a construction site

4.1. Introduction

In this chapter the geological conditions of a studied construction site and available data from the geotechnical and geophysical investigations are presented. Thereafter the appropriated geostatistical methods are used to improve the quality of geotechnical data and bring more information to the soil spatial variability on the construction site. It is shown how the combination of the geotechnical and geophysical information can improve thanks to collocated cokriging, the knowledge of mechanical characteristics on the construction site. In a last stage, it is focused on the spatial modelling of the Young's soil modulus. The conditional simulation method enables to obtain the spatial probability of occurrence of a given soil modulus value. Coupled with other information, the analysis of these statistical and geostatistical models makes possible to develop decision support tools and to describe the behavior of the superficial geotechnical designs (continuous spread footings and buried pipes) when they are constructed on different locations on the construction site.

4.2. Presentation of the studied site and available data

The study site has a surface area of $25\,000$ m^2. In view of its large area, it was decided to implement a preliminary VLF-R type of geophysical survey campaign in order to qualify the homogeneity of the site, and ascertain those zones most suitable for construction, before proceeding with borehole and pressuremeter soundings.

4.2.1. Geological settings

The study site is located to the south of the city of Pessac in France; Pessac is about 5 km west of Bordeaux.

From a geological point of view, Pessac is located at the boundary between the large Landes moorland area (Landes sandy deposits) to the west, and the alluvial terraces of the Garonne to the east (Figure 4-1a). The study site belongs to the alluvial terraces of the Garonne, which is characterized by clayey-sandy plio-quaternary deposits (Figure 4-1a and b). More precisely, the study site rests on an alluvial terrace dating to the lower Pleistocene (Dubreuilh, 1976), covering more than 20% of the town surface area. This formation, a

witness to the ancient alluvial water tables created during the interglacial periods of the Pleistocene, is characterized by soils with high clay content with a blue-gray to dark gray appearance. The clay content can reach 80%, with a mineral distribution comprising mainly kaolinite, illite and interstratified (Dubreuilh, 1976). Its thickness varies between 4 m and 12 m.

The engineering properties of alluvium deposits vary over a wide range. In area such as Pessac, dominated by sluggish streams, very thick deposits of clayey silt occur, giving rise to lack of bearing strength for large load. In this case, pilings are extensively used for multi-story buildings. Engineering problems associated with clayey soil are due to their low shear strength, which make them very hazardous for shallow foundations. Clayey soils are also hazardous due to expansion and contraction accompanying soil moisture changes. They cause damage when they shrink upon drying or when they expand upon wetting and the resulting soil movements can disrupt houses. Poorly-built houses with inadequate shallow foundations develop damage ranging from sticking doors and hairline plaster cracks to complete destruction. Moreover, alluvial deposits are often heterogeneous and vary both vertically and horizontally over short distances.

Numerous residential constructions, recent and old, with no previous history of even minimal differential movements, have developed foundation problems over a very short period of time, due to changes in moisture content during extended periods of drought, as were experienced in this region between 1989 and 2005, 2008 and 2010. Many of these homes are resting on this alluvial terrace, even though it is classed as being a formation of moderate swelling and shrinkage potential (Figure 4-2). The corresponding maps are currently being updated.
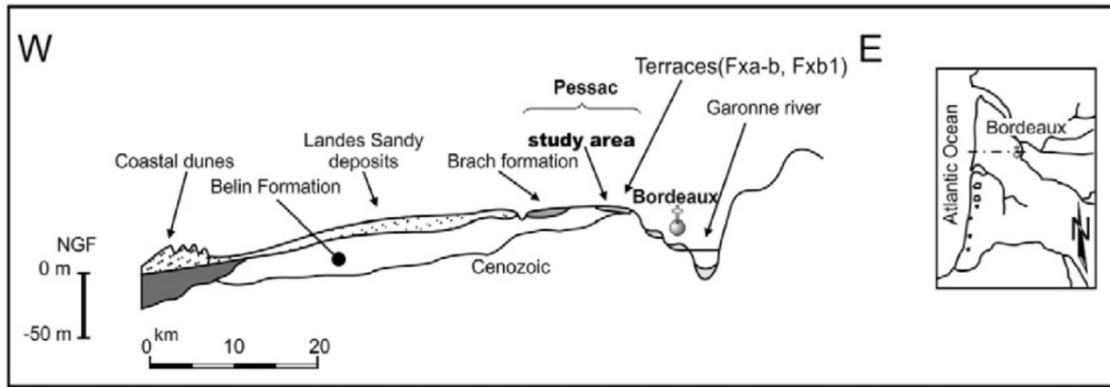
a)
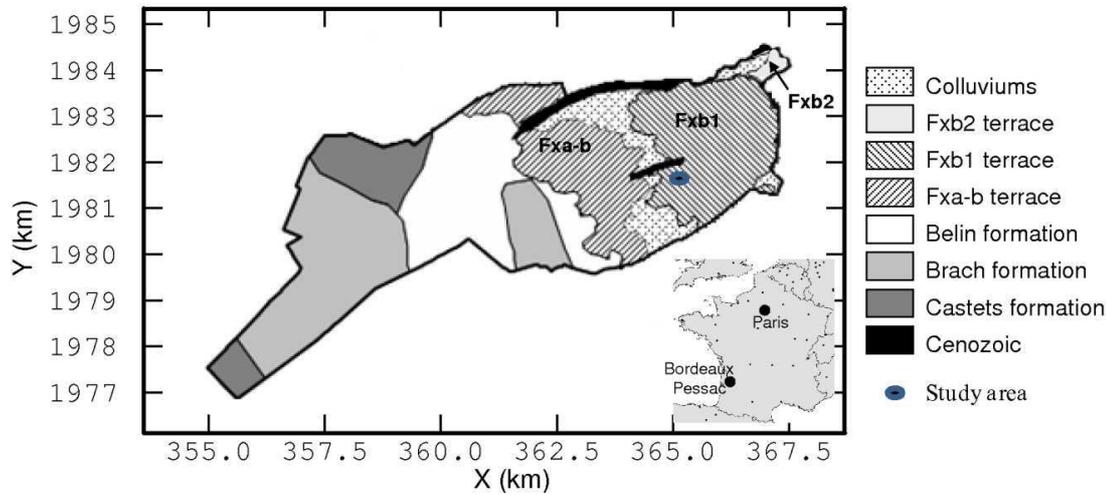
b)

Figure 4-1:a) Geological cross section from Bordeaux to Atlantic Ocean and b) Geological map of the Pessac area (Marache et al., 2009b)
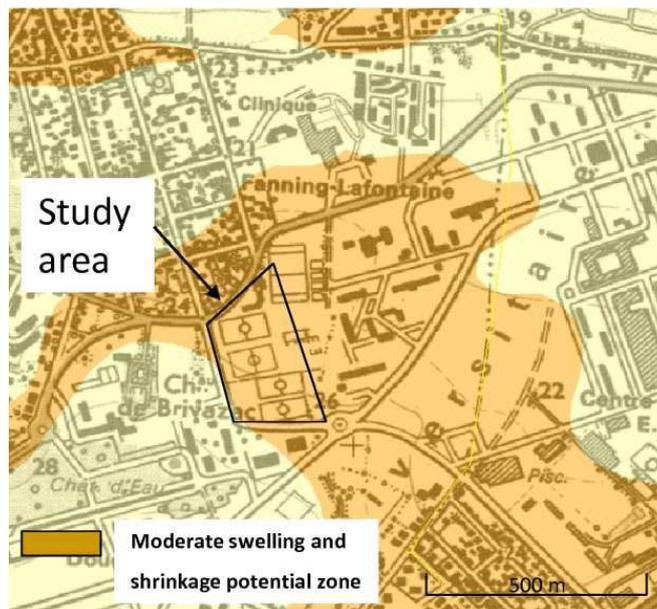
Figure 4-2: Localization of the studied area, and shrinkage-swelling clay hazard map (Denis et al., 2011)

169

4.2.2. Geophysical investigations

The reconnaissance of a site of large surface area using an R (Resistivity) mode VLF (Very Low Frequency) technique can provide an interesting alternative to conventional methods such as the direct current electrical method (Benson et al., 1997; Oskooi and Pedersen, 2005). Although the latter reveals important information pertaining to the nature and distribution of surface soils and subsoils (Spies, 1996; Denis et al., 2002), they suffer from the drawback of requiring a considerable amount of time for their implementation with such surfaces. The VLF method makes use of the power of radio frequency transmitters, which operate at frequencies ranging between 15 and 25 kHz. The transmitted waves, of high power, induce electric currents in the most conductive parts of the ground, which in turn generate a secondary magnetic field which can be detected at the surface through measurements of deviations to the normal field. The depth to which investigations can be made depends on the frequency of the transmitter used and the ground resistivity (Spies, 1989). In the case of soils with a resistivity between 8 and 50 Ω.m, the maximum studied depth is estimated to lie between 8 and 20 m. The presence of clayey soils of lower resistivity can lead to more shallow study depths. In the present study, in which the aim was rather to reveal the presence of clayey soils which are thus conductive, with thicknesses of at least 6 m, the inherent limitation of this chosen technique was not a serious limitation.

The measurement points are distributed over uniform profiles with mean spacing of 10 m between measurement points. The profiles are aligned in the east-west direction, over a length of approximately 190 m. The full reconnaissance campaign included a total of 272 soil resistivity measurement points (Figure 4-3).
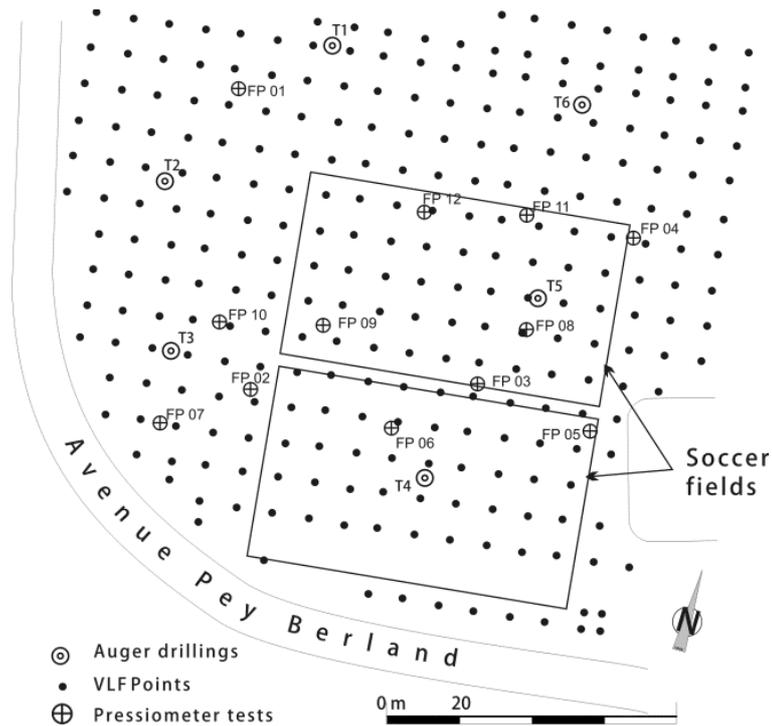
Figure 4-3: Localization of the VLF point measurements, wells and pressuremeter tests in the studied area

The frequency of the transmitted electromagnetic waves was 16 kHz. In view of the fact that we had no complementary data concerning the resistivity of the deeper layers, we made the assumption of a single layer of terrain. This hypothesis is all the more justified since the resistivity of the upper layer is low, thereby reducing the depth of analysis.

A geostatistical approach was used to identify the inherent variability of the resistivity of soil (kriging estimation) using ISATIS© software. It should be noted that in this study, we calculate the semi-variogram but the term variogram is used in place of semi-variogram. The first step was to compute the experimental variogram map of the resistivity of soil in various directions. The next step is to fit a model to the experimental variogram in both directions of anisotropy, if such anisotropy exists.

During the variographical analysis, it is important to check for the presence of potential directions of anisotropy if the target variable presents a more continuous behavior in a given direction than in another one. For this purpose directional variograms are computed. When for the same variable, variogram values for two perpendicular directions require different sills or ranges then anisotropy is present. When data are densely sampled, a variogram map can be obtained by automatically calculating directional variograms in every direction.

171

Firstly the variogram map of the soil resistivity needs to be produced with soil resistivity measurement points, allowing variogram values to be determined for all lags in all directions. This process thus enables the two principal directions of anisotropy to be defined, if such anisotropy exists. Each cell of the map, in a given direction, corresponds to the variogram value for a lag (distance between two points) which can vary from 0 m (centre of the map) up to a value of 90 m (Figure 4-4a and b) with a step of 10 m.

From this map, the variograms in the two main directions of anisotropy are computed. The resulting directions (N50 and N140) are nearly identical over the distance [0, 50 m]. Anisotropy is present beyond this interval. In this case, with increasing the distance, the difference between the variograms of these two directions increases. In the following, the interpolations will be done using a circular neighborhood of radius 50 m, so the variogram of the soil resistivity is omnidirectional up to this distance. This distance is one quarter of the study area.

a)   b)
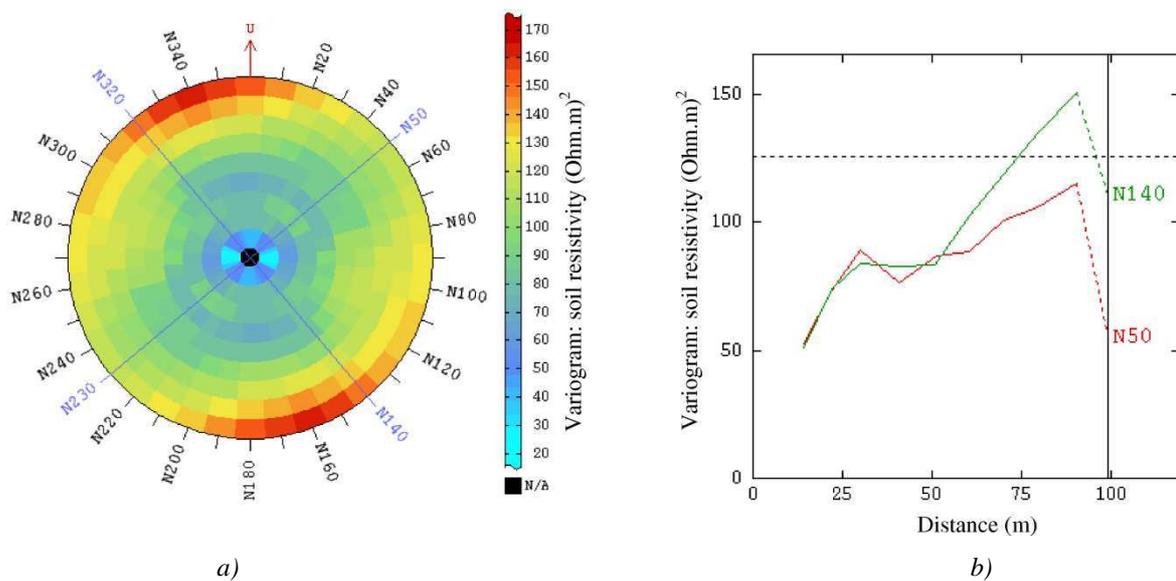
Figure 4-4: a) Variographical map of the soil resistivity (up to a value of 90 m) and b) Experimental variograms in the two main directions of anisotropy

The experimental variogram is not sufficient for a geostatistical estimation because the variogram used in estimation must satisfy some mathematical constraints. For this reason an analytical mathematical function is fitted on the experimental variogram: the variogram model.

Variographical analysis result of the resistivity of soil dataset is shown in Figure 4-5, which presents an omnidirectional experimental variogram (black line), showing a sill equal to 85 (Ohm. m)^2 associated with a range equal to 37 m. Beyond 50 m, a non-stationary behavior can be observed. If we wanted to take all these observations into account in the variogram model, it would be necessary to sum a stationary and a non stationary basic model. However, as explained previously and considering that the length of the continuous wall footing and low stiffness zones of soil beneath the buried pipes are small compared to 37 m, the model is only an exponential component with a range of 37 m (Equation 4-1), which represents the isotropic variogram for the data-set, which is also represented by a red line in Figure 4-5.

$$\gamma(h) = 85. \left[1 - exp\left(\frac{-3h}{37} \right) \right], \qquad h : lag \ (m) \qquad\qquad \textit{Equation 4-1}$$
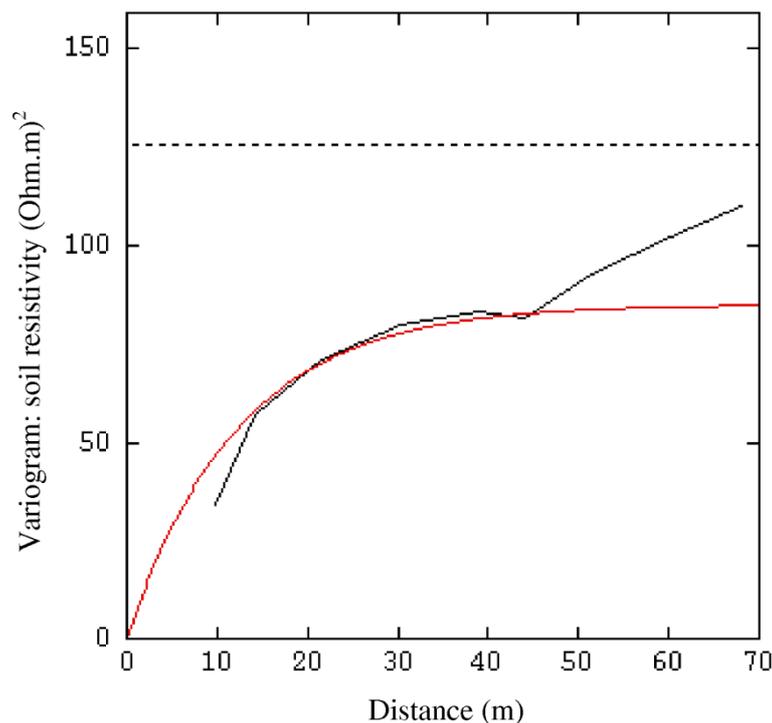
Figure 4-5: Experimental (black line) and modelled (red line) isotropic variograms of the soil resistivity

The quality of this model is quantified by cross-validation (Figure 4-6), which is achieved by iteratively eliminating each data point from the data-set and comparing the

estimated value at this point using the model with the real value. Figure 4-6a shows the spatial distribution of the soil resistivity values. The coefficient of correlation between the estimated (z^*) and measured (z) values is equal to 0.89 (Figure 4-6b). This value of coefficient is acceptable but it was reduced by the presence of two non-robust data in the soil resistivity values (shown by a green point in Figure 4-6). These points correspond to the outlier values which can not be well predicted by the model. The standardized error ((z^*-z)/s^*) has a mean close to zero and it is nearly uncorrelated with the estimated values (Figure 4-6c and Figure 4-6d), then data are unbiased. These different criteria allow us to validate the quality of variogram model fitted to the experimental variogram.
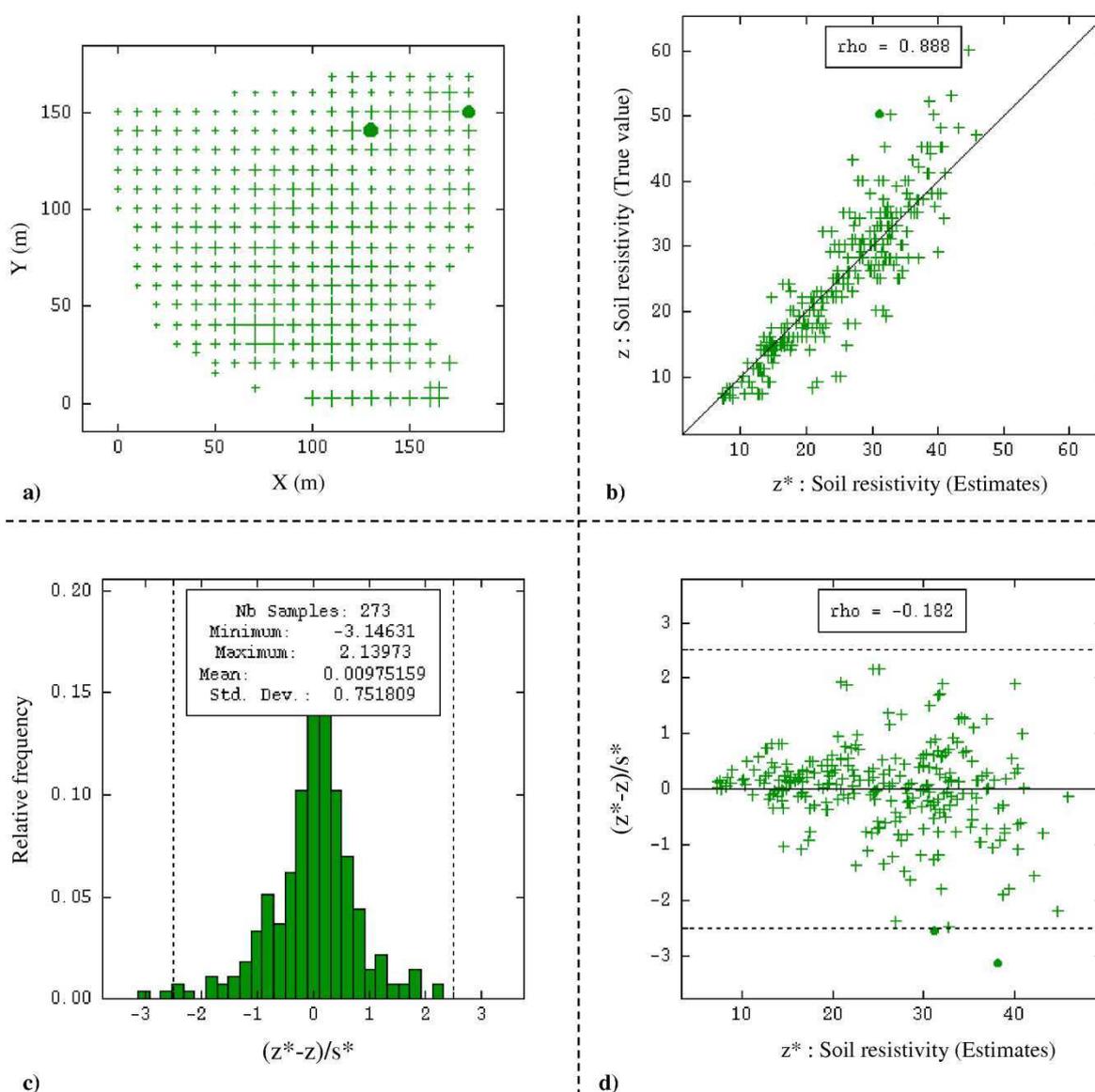
Figure 4-6: Cross-validation

174

The ground resistivity map resulting from kriging with the previous variogram model and a circular neighborhood equal to 50 m is shown in Figure 4-7a. This estimation is done over a regular grid with a mesh of 10 m × 10 m. The resistivity ranges from a clayey pole with values between 4 and 10 Ω.m to a clayey-sandy pole with resistivity values greater than 50 Ω.m. The spatial resistivity distribution (Figure 4-7a) illustrates the heterogeneity of the surface layer formations on this site, on the north part of which, over a distance of 30 m, one can observe a change from sandy-clayey soil to clay. The zones with the lowest resistivity are found mainly in the eastern and western parts and appear to outline a corridor of more resistant soil, which could correspond to the filling of a north-south aligned paleochannel.

Figure 4-7b shows the map of the kriging standard deviation of the resistivity. The value of the standard deviation is between 0.1 and 6 Ω.m except for the zones with the high values of the standard deviation of resistivity (between 6 and 8.6 Ω.m). These high values are found mainly in the southern and western parts because of very small number of soil resistivity experimental values in these parts.

a)

b)
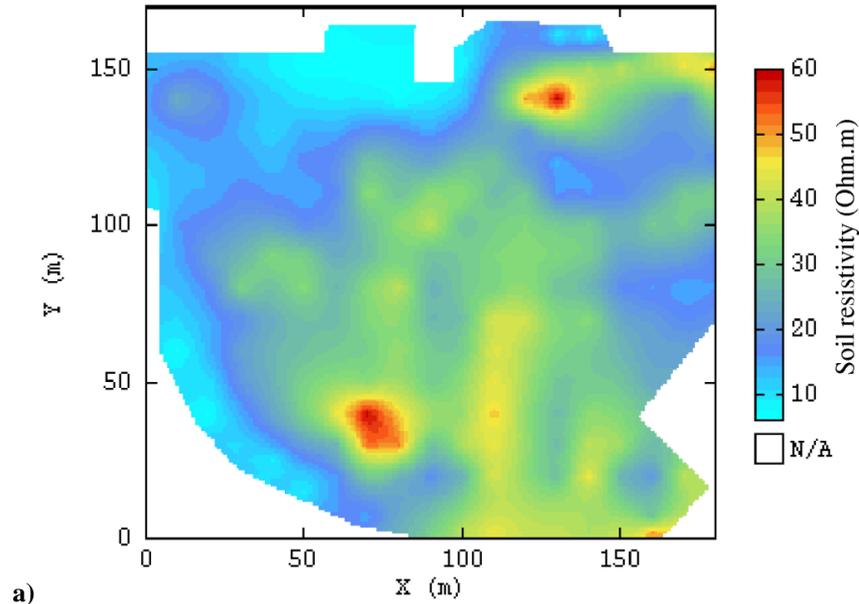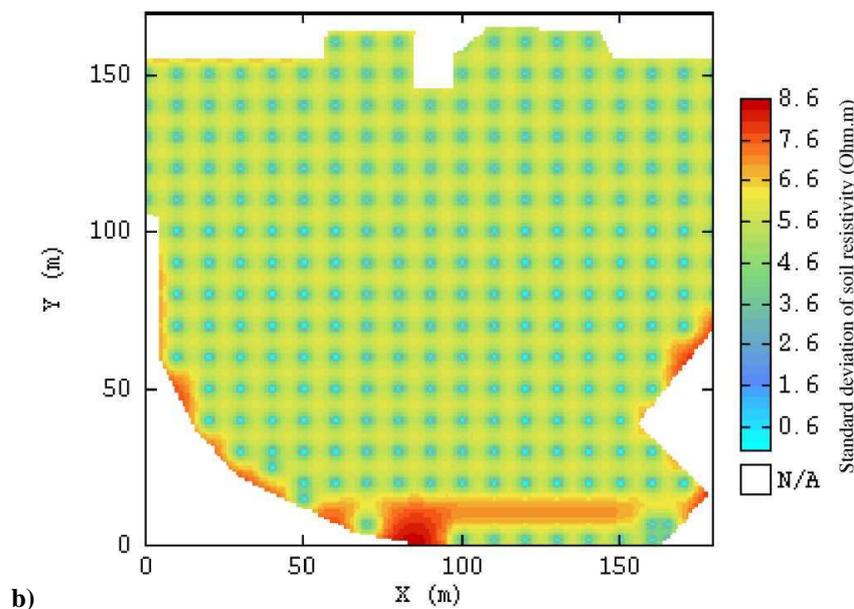
Figure 4-7: Analysis for soil resistivity data a)Kriging estimate for electrical resistivity from VLF-R (16 kHz) measurements b) Associated kriging standard deviation of soil resistivity

4.2.3. Geotechnical investigations

The reconnaissance soundings (6 auger boreholes to a depth of 8 m) and twelve pressuremeter tests (depth of boreholes ranging between 8 and 12 m) enabled the surface formations detected using the VLF-R technique to be confirmed. Boreholes T1 and T2 (Figure 4-3) drilled in the zones, with resistivities ranging between 0 and 10 Ω.m and 10–20 Ω.m respectively, revealed clayey soils down to a depth of 8 m, which was confirmed by laboratory tests carried out on these soils, for which the plasticity index ranged between 30% and 40%. Borehole T3 (zone with resistivities between 20 and 30 Ω.m) revealed sandy clay between the depths of 1.20 and 8 m, whereas borehole T5 (zone with resistivities between 30 and 40 Ω.m) revealed sandy clay containing gravel beds. For zones having a higher resistivity, boreholes T4 (40–50 Ω.m) and T6 (resistivity>50 Ω.m) revealed the presence of clayey sand and a gravely clay.

The pressuremeter soundings made to a maximum depth of 12 m, including a test measurement every meter, confirmed the sandy-clayey character of the soil with, for some soundings, the presence of sand, which occurs as embedded lenses rather than continuous seams or layers at depths greater than 7 m. In the case of shallow foundations for individual houses, the slice of ground beneath the foundation, affected by the loading, can be estimated to have a thickness of approximately 6 m (Cassan, 1978). For the full set of 12 pressuremeter soundings, and for a slice of ground for which measurements were taken

176

at depths ranging between 1 and 7 m (i.e. 6 pressure limit and deformation modulus measurements per sounding), the 72 values of pressure limit and deformation modulus were respectively comprised between 0.3 and 1.3 MPa, and 3 and 7 MPa. The average values found for the pressure limit and the deformation modulus for each sounding are provided in Table 4-1. The ratio between the mean deformation modulus and the mean pressure limit ranged between 5 and 8.1, thus confirming the sandy–clayey character of the soils encountered (Cassan, 1978).

Table 4-1: Average values for the deformation modulus E_{PMT} and pressure limit P_L

	FP1	FP2	FP3	FP4	FP5	FP6	FP7	FP8	FP9	FP10	FP11	FP12
E_M (MPa)	3.71	3.21	5.1	3.55	4.41	6.5	3.88	4.38	4.46	3.58	3.65	4.19
P_{LM} (MPa)	0.73	0.64	0.8	0.5	0.81	1.05	0.69	0.87	0.88	0.7	0.45	0.7
E_M/P_{LM}	5.08	5.02	6.38	7.1	5.44	6.19	5.62	5.03	5.06	5.11	8.11	7

4.3. Geostatistical modeling of Young's soil modulus

The aim here is to model the spatial distribution of geotechnical parameters. To illustrate the methodology, we have chosen to focus on the Young's soil modulus. This modulus can be assessed from pressuremeter modulus, using common relation: $E_{PMT}=\alpha.E_s$. As it was mentioned earlier (see section 1.2.2.2) a lot of geostatistical methods are available to perform such a model (kriging, cokring or simulations methods with many variants) using only one parameter or auxiliary parameters too (Raspa et al., 2008). This is described in the ensuing sections and the most appropriate method will be chosen to localize sensitive zones during the decision stage of the superficial geotechnical projects.

4.3.1. Young's soil modulus modeling using kriging

To model Young's soil modulus E_s, a first option is to use Young's soil modulus known at the boreholes location and interpolate between the boreholes by means of kriging. The experimental variogram resulting from the twelve value of soil modulus is shown in Figure 4-8. Because of the poor number of data, the experimental variogram is very erratic and it is not possible to fit a good variogram model to the experimental variogram. So we have decided to use the kriging with linear model to perform the estimation. Figure 4-9 shows,

using this method, the maps of soil modulus with its associated standard deviation. The soil modulus ranges from a clay soil with values between 5.5 and 9 MPa to a clayey-sandy soil with values between 9 and 14 MPa (Figure 4-9a). On the south part of which, over a distance of 50 m, one can observe a change from clayey soil to sandy-clayey soil. The zones with the lowest soil modulus are found mainly in the northeastern and western parts (Figure 4-9a). The map of the kriging standard deviation of soil modulus is shown in Figure 4-9b. The value of the standard deviation is between 0.1 and 3.4 MPa. The high values of the standard deviation of soil modulus (2.6 to 3.4 MPa) are mostly found in the northern, western and southern parts because there is no measured deformation modulus (E_{PMT}) in these parts.

Partly due to the low number of boreholes (twelve measured deformation modulus, E_{PMT}), these outcomes are really smooth and do not seem geologically consistent (Figure 4-9). More dense information can be integrated in order to improve the estimation of Young's soil modulus using a multivariate geostatistical estimation called collocated cokriging which is explained below.
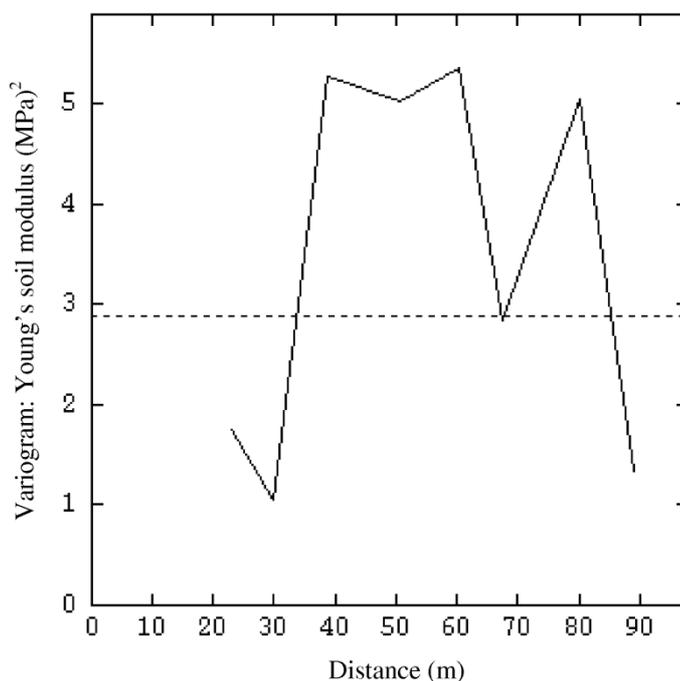
Figure 4-8: Experimental variogram of the twelve values of Young's soil modulus
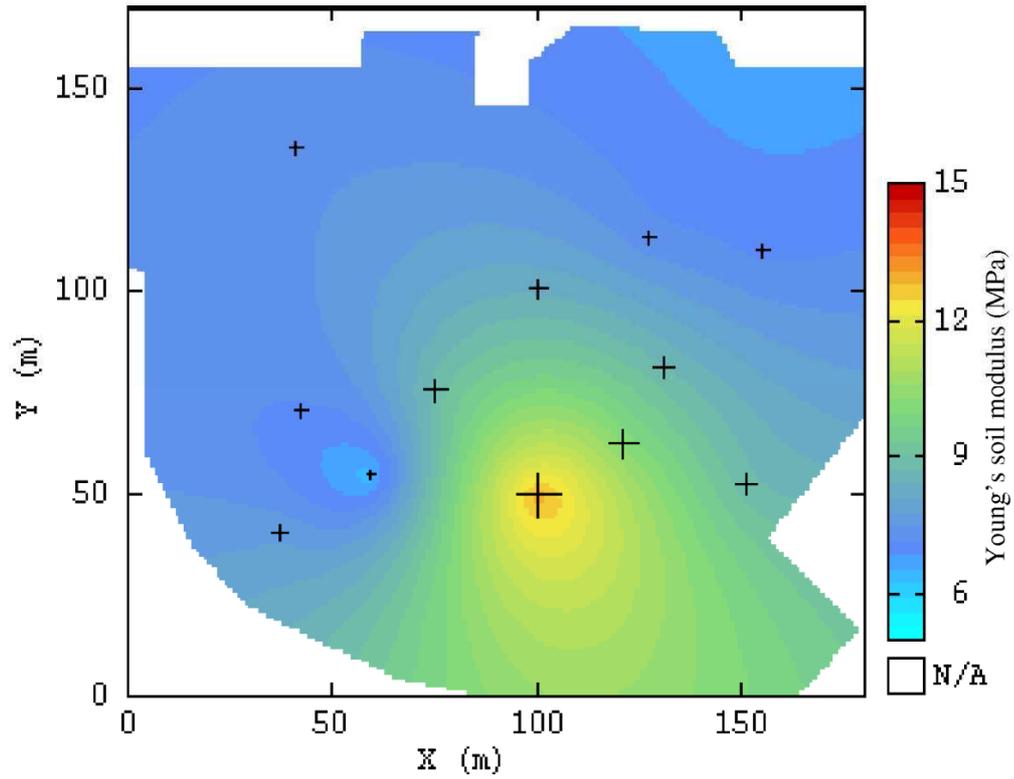
a)
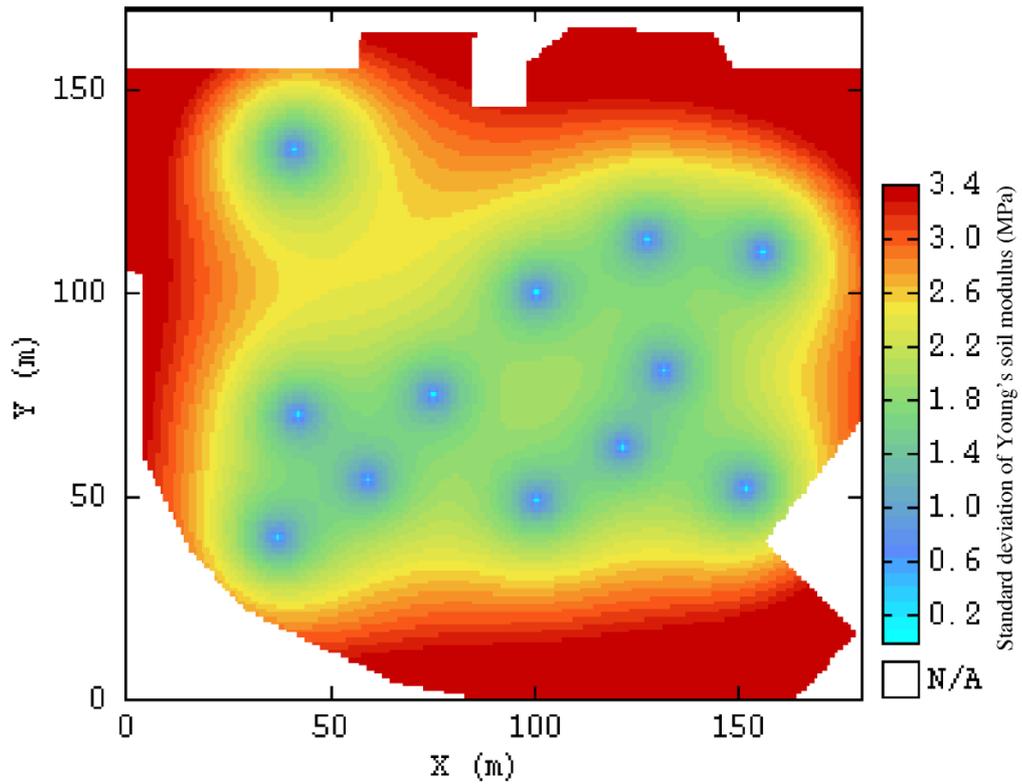
b)

Figure 4-9: a)Kriging estimate for soil modulus with data points displayed (+) b) Associated kriging standard deviation of soil modulus

4.3.2. Maps of Young's soil modulus using collocated cokriging

When several correlated variables are available, a multivariate geostatistical estimation called cokriging can be performed: the use of one (or several) correlated variable(s) allows improving the estimation of the main property.

A particular heterotopic situation encountered in practice is when we have a variable of interest known in few points and an auxiliary variable known everywhere in the domain (or at least at all nodes of a given estimation grid and at the data locations of the variable of interest). In this case, an extension of cokriging called collocated cokriging is particularly appropriate. In this method, the auxiliary variable is incorporated at each target location. It allows bringing more information to the estimation. So the estimate is expected to have a better consistency (Chilès and Delfiner 1999). This multivariate technique require the computation and fitting of a variogram model that contains simple variograms for each variable and a cross variogram measuring the spatial correlation between the variables.

Attempts to relate geotechnical properties to geophysical data are uncommon and the literature contains some contradictions. Braga et al. (1999) show that the resistivity is weakly correlated with geotechnical data from the SPT (Standard Penetration Test) and that there is no relationship between SPT blow counts N and the chargeability from induced polarization method. Cosenza et al. (2006) obtained the same result in a case study with a dynamic cone penetration test, an in situ vane shear test and a geophysical survey (Electrical Resistivity Tomography). No clear relationship between the cone resistance and the inverted resistivity values was observed. On the other hand, Endres and Clement (1998) revealed relationships between the soil types determined from the mechanical properties measured by CPT (Cone Penetration Test), and the electrical properties (resistivity and dielectric permittivity) of a site with lithologies ranging from clayey silt to coarse sand units. The authors suggest that these relationships may provide a petro-physical basis for the combination of information derived from CPT and electrical methods. Denis et al., (2011) tried to show relationship between the geotechnical parameter E_{PMT} and soil resistivity derived from geophysical investigation (VLF-R). Monnet et al. (2008) showed relationship between E_{PMT} and soil resistivity derived from a direct electrical method (electrical panel).

The data-set in this study is constituted of a few set of pressuremeter boreholes with the deformation modulus E_{PMT} values (12 data of interest) and a lot of soil resistivity values

(272 auxiliary data) (Denis et al., 2011). In a clayey-sandy soil with no important change in water content, more the sand is, more the deformation modulus and resistivity are. Thus it is assumed that deformation modulus is indirectly linked to soil resistivity derived from geophysical methods (Monnet et al., 2008, Denis et al., 2011). Note that for a same clayey-sandy soil a less the water content is, more the deformation and resistivity are. In these two cases, it will be relevant to use the dense soil resistivity information as auxiliary variable for a better estimation of Young's soil modulus. A collocated cokriging of the deformation modulus integrating the soil resistivity is particularly appropriate to bring more information to the estimation of the deformation modulus.

For a collocated cokriging, the influence of soil resistivity information will be more important if the correlation between both variables is high. A linear relationship with a correlation of 0.6 was obtained between the deformation modulus and resistivity values (Figure 4-10). This correlation value was influenced by the data from two boreholes (FP2 and FP6).
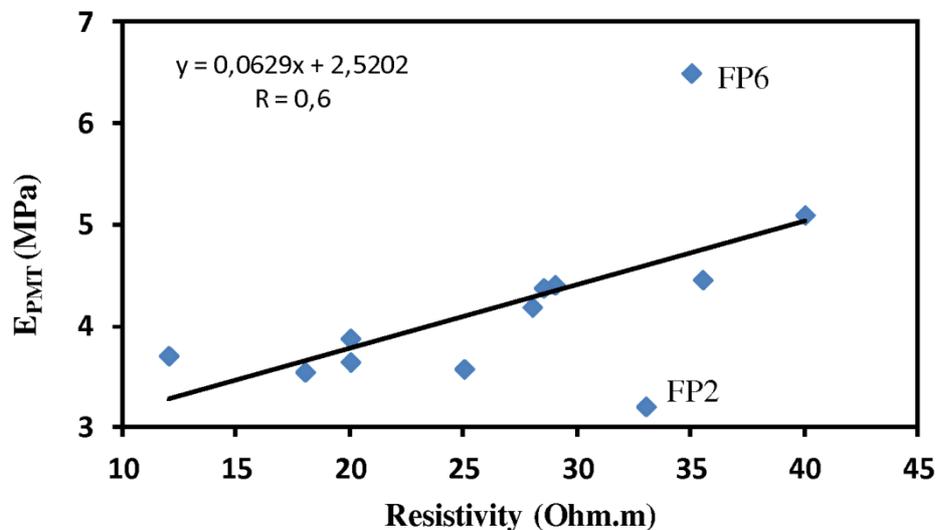
Figure 4-10: Modulus E_{PMT} derived from pressuremeter tests, versus resistivity, derived from VLF-R.

For the collocated cokriging a bivariate variogram model is required. Nevertheless, because the small number of soil modulus values, this bivariate model is tedious to establish. For this reason, a bundled version of the collocated cokriging will be used which takes into account only the spatial correlation of the auxiliary variable (soil resistivity, Figure 4-5). The bivariate model is deduced from this model and the coefficient of

correlation and variance ratio between both variables. As previously, the interpolations will be done using a circular neighborhood of radius 50 m.

The collocated cokriging of soil modulus E_s with its associated kriging standard deviation are displayed in Figure 4-11. The zones with the lowest soil modulus values are found mainly in the western parts, and appear to outline a corridor of high soil modulus values aligned south to north (Figure 4-11a). As it has been mentioned before, the collocated cokriging brings more information to the estimation of the deformation modulus than the use of the kriging alone. For example, both zones of high values of soil resistivity found in northern part at {130, 140} and southern part at {70, 40} appear, whereas no measured deformation modulus are present at these points. Using collocated cokriging gives the possibility to estimate value of deformation modulus at these points with more precision than from kriging of Young's soil modulus (Figure 4-9a and Figure 4-11a). This map presents more variability than the kriging one. This added variability comes from the soil resistivity integrated at the target location through the collocated cokriging process (Figure 4-7a)

The map of the cokriging standard deviation of E_s (Figure 4-11b) is compared to that one from kriging (Figure 4-9b). This shows that the use of collocated cokriging decreases the uncertainty in the interpolation.
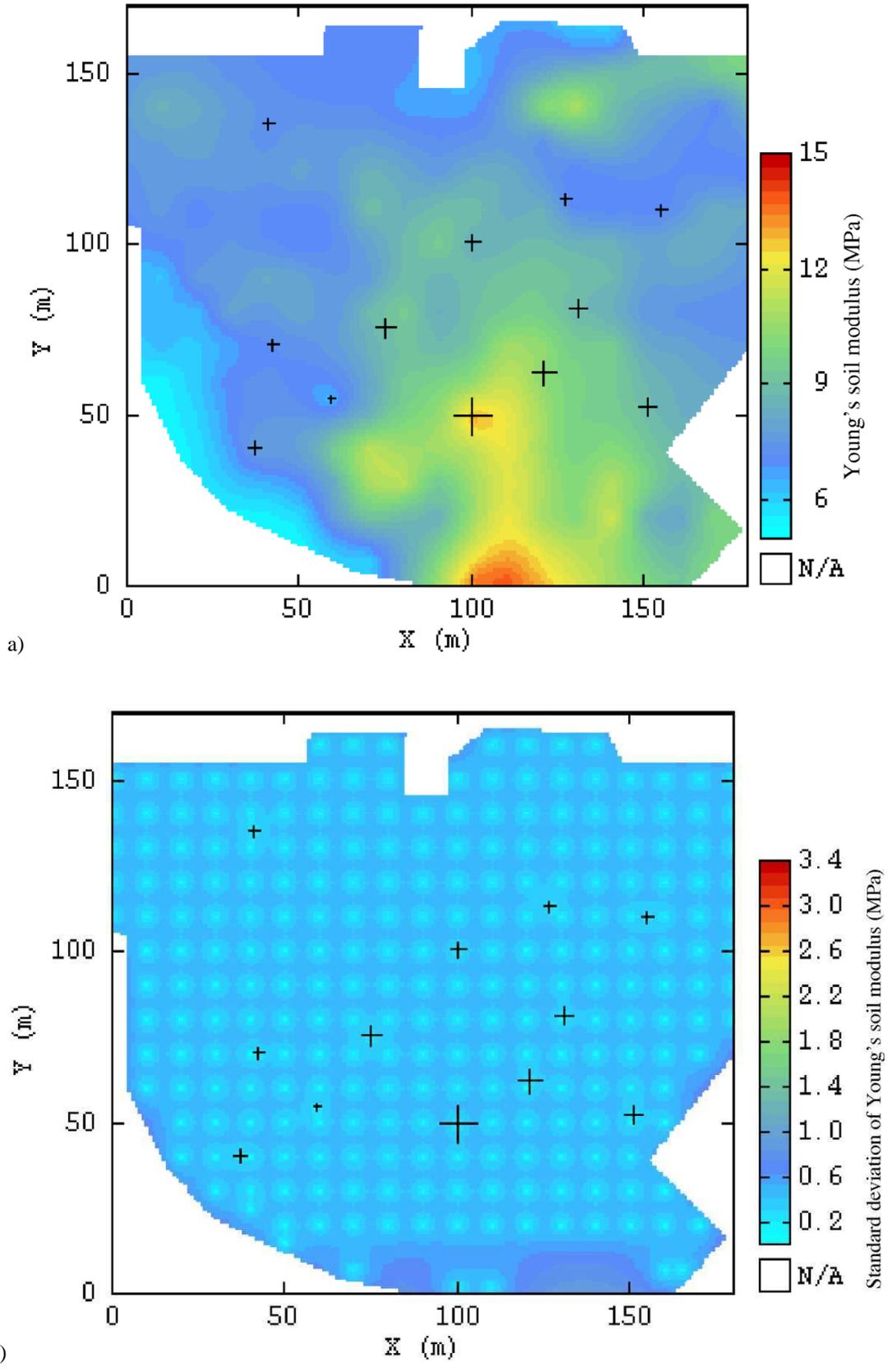
Figure 4-11: a) Map of soil modulus using soil resistivity as auxiliary variable b) Associated cokriging standard deviation

4.3.3. Young's soil modulus modeling using simulation

In order to choose the most appropriate method, first and foremost we must think to the final aim: we want to obtain a model which could be used as a decision support framework. So it is important to be able to evaluate a geotechnical parameter value at a location, but we also want to localize zones with poor geotechnical characteristics in order to assess risks, for instance due to excessive settlements.

In a first approach, estimation methods have been realized (see sections 4.3.1 and 4.3.2). However, these methods are not the most appropriate for two main reasons:

-   Estimation methods give a smoothed image of the reality, thus underestimates the proportion of extreme values. In our case, extreme low values are very important to define zones with poor geotechnical parameters for example,

-   We want to obtain results in terms of probability of occurrence of a geotechnical parameter value, which is very important for the future use of the model at the design stage of the superficial geotechnical designs.We do not want a model with a parameter value which could be considered as the "exact" value at a given location. Thus, results in terms of probability are more representative of the real state of knowledge and best fitted to engineering purposes.

In order to satisfy these two remarks, we have chosen to use the conditional simulation method. This estimation is done over a regular grid with a mesh of 0.5×0.5 m^2 to obtain more values of E_s beneath a structure to introduce in the finite element methods. This method better describes natural variability which is attenuated when using only estimation methods. Starting from estimation results on a 10×10 m^2 mesh and computing new results on a 0.5×0.5 m^2 mesh is authorized by the application of the three perpendicular theorem (Chilès and Delfiner, 1999). Finally, it provides results in terms of probability by post-processing simulations.

For this, the raw data must be transformed with an anamorphosis in order to achieve a normal statistical distribution to avoid biases in simulation results and the variogram model is also transformed into this new space. Values are simulated in this space, in accordance with the variogram model, and are then back transformed into the raw data space.

Modeling the anamorphosis function includes the following points (Dowd, 2003):

-   minimal differences between basic statistics of raw and back-transformed variable,

184

- the mean of the transformed variable is 0 and its variance is equal to 1 as close as possible,

- the average of differences between raw and back-transformed values is 0 and variance minimal,

- the shapes of the experimental histograms of raw and back-transformed variables is the same and

- correlation between raw and back-transformed variables is maximal positive.

Variographical map of the Young's soil modulus in the Gaussian space up to a distance of 70 m with a step of 10 m is illustrated in Figure 4-12a. This variographical map shows an omnidirectional behavior. The Young's soil modulus data-set have been computed from a collocated cokriging of the deformation modulus integrating the soil resistivity. Variographical analysis of the Young's soil modulus data-set in the Gaussian space is shown in Figure 4-12b which presents an omnidirectional experimental variogram (black line) in the Gaussian space with a first range (or correlation length) equal to 42.7 m. As in the case of the variographical analysis of the soil resistivity (Figure 4-5) an isotropic variogram model (red line) in the Gaussian space was fitted to this experimental variogram. This model is only a spherical component with range and sill equal to 42.7 m and 0.58 $(MPa)^2$ respectively (Equation 4-2).

a)   b)
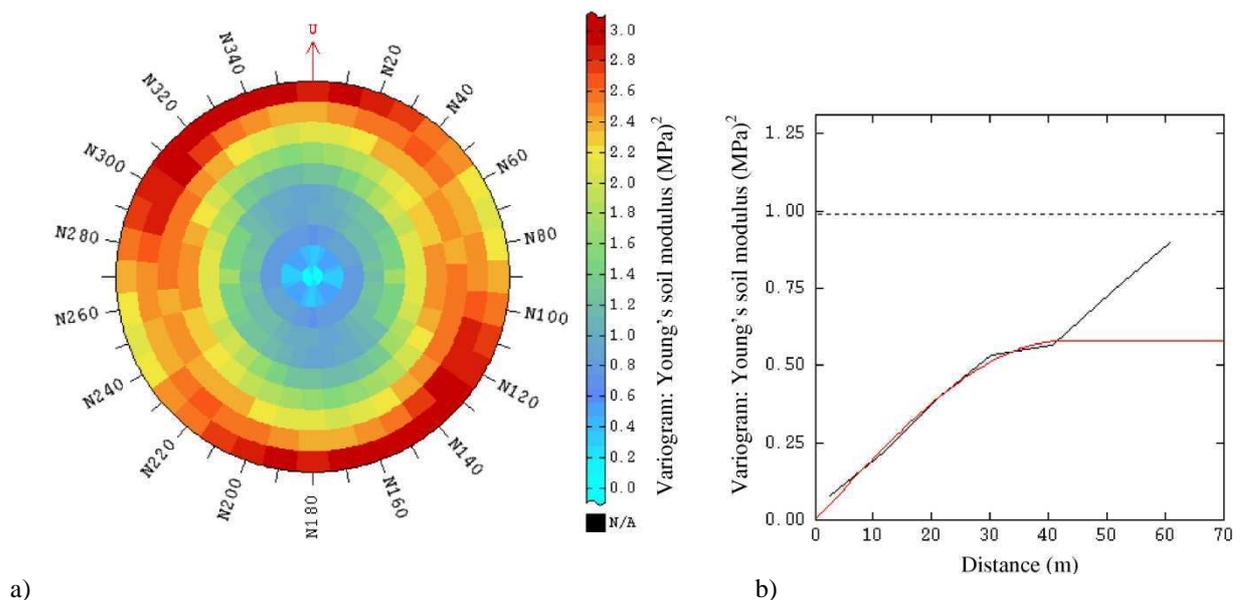
Figure 4-12: a) Variographical map of the Young's soil modulus in the Gaussian space (up to a value of 70 m) and b) Experimental (black line) and modelled (red line) isotropic variograms of the Young's soil modulus in the Gaussian space

$$\gamma(h) = 0.58 \left[\frac{3}{2}\left(\frac{h}{42.7} \right) - \frac{1}{2}\left(\frac{h}{42.7} \right)^3 \right] \qquad \text{for } h < 42.7 \text{ m}$$

Equation 4-2

$$\gamma(h) = 0.58 \, (MPa)^2 \qquad \text{for } h > 42.7 \text{ m}$$

The conditional simulation procedure can then be performed for a series of 1000 simulations using a moving neighborhood (circular neighborhood of radius 50 m) in accordance with variogram model. Two simulation results are shown in Figure 4-13. Zones of low or high values of soil modulus are located in the same area than previously. However, one can see that the simulation increases the spatial variability of the soil modulus.
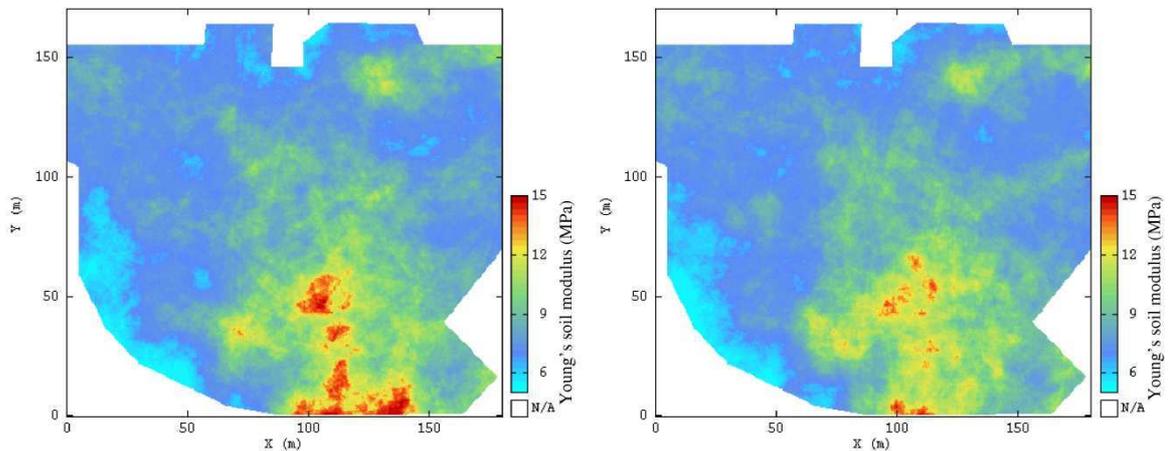
Figure 4-13: Example of spatial distribution of the Young's soil modulus on the construction site for two simulations

Young's soil modulus along a profile length of 10 m for the first 250 simulations is shown in Figure 4-14 to illustrate the variation of soil modulus along this profile.

186
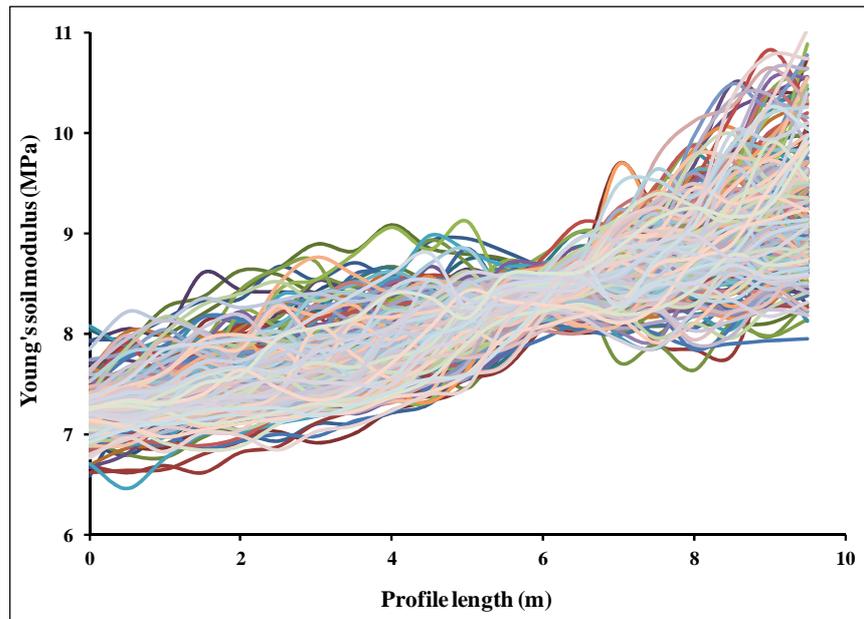
Figure 4-14: Young's soil modulus along a profile length of 10 m for the first 250 simulations

It should be noted that in the probabilistic analysis in the ensuing sections, the number of simulations influences the accuracy of the results. Since the increase in number of simulations also increases the computational efforts, a compromise between accuracy and computational time is achieved by estimating the mean of Young's soil modulus in Figure 4-15 for several numbers of simulations. In this approach, simulations are carried out for a large numbers till there is no significant change in the mean values of the Young's soil modulus. From Figure 4-15 it can be noted that between 700 and 1000 simulations the variations of the mean is almost negligible and it can be expected that a further increase in the number of simulations will not significantly affect the accuracy of the results. Therefore, in the present analysis, 1000 simulations are run for estimating the probability of soil modulus for different threshold values, the statistical parameters of the maximum differential settlement and the maximum bending moment for the spatial variablility of soil profile.

From 1000 simulation results, a local histogram of the Young's soil modulus can be built; an example is shown in Figure 4-16 for the point {18, 67} which is located inside a zone with low soil modulus values. As it shown from this figure, 10%, 50% and 90% of the soil modulus values are respectively inferior to 5.73, 6.02 and 6.44 MPa.

187
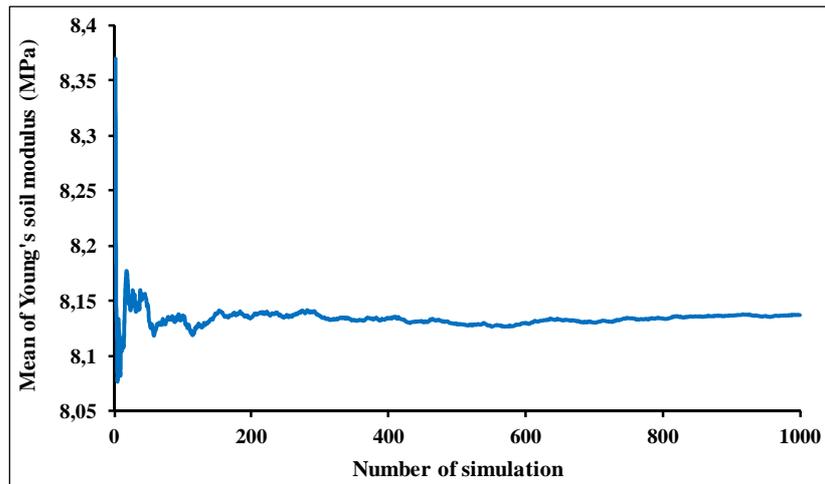
Figure 4-15: Convergence of the mean of Young's soil modulus versus the number of simulations
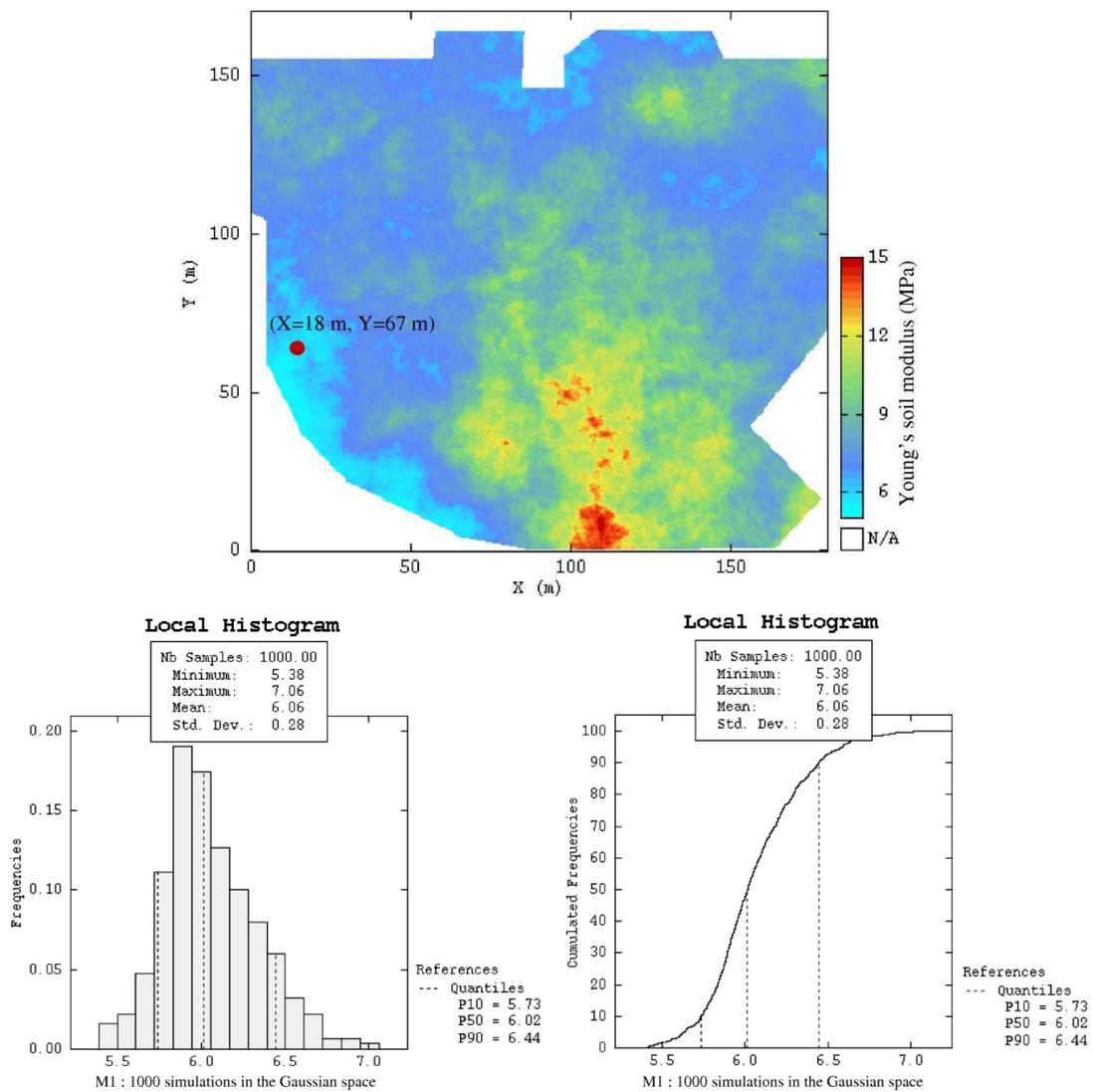
Figure 4-16: Local histogram of the Young's soil modulus at (X=18 m, Y=67 m), on the zone with low soil modulus values for 1000 simulations of soil modulus maps in the Gaussian space

Map of the soil modulus obtained from the mean of the maps resulting from 1000 simulations is shown in Figure 4-17. As expected, this figure is quite identical to the cokriging result (Figure 4-11a).
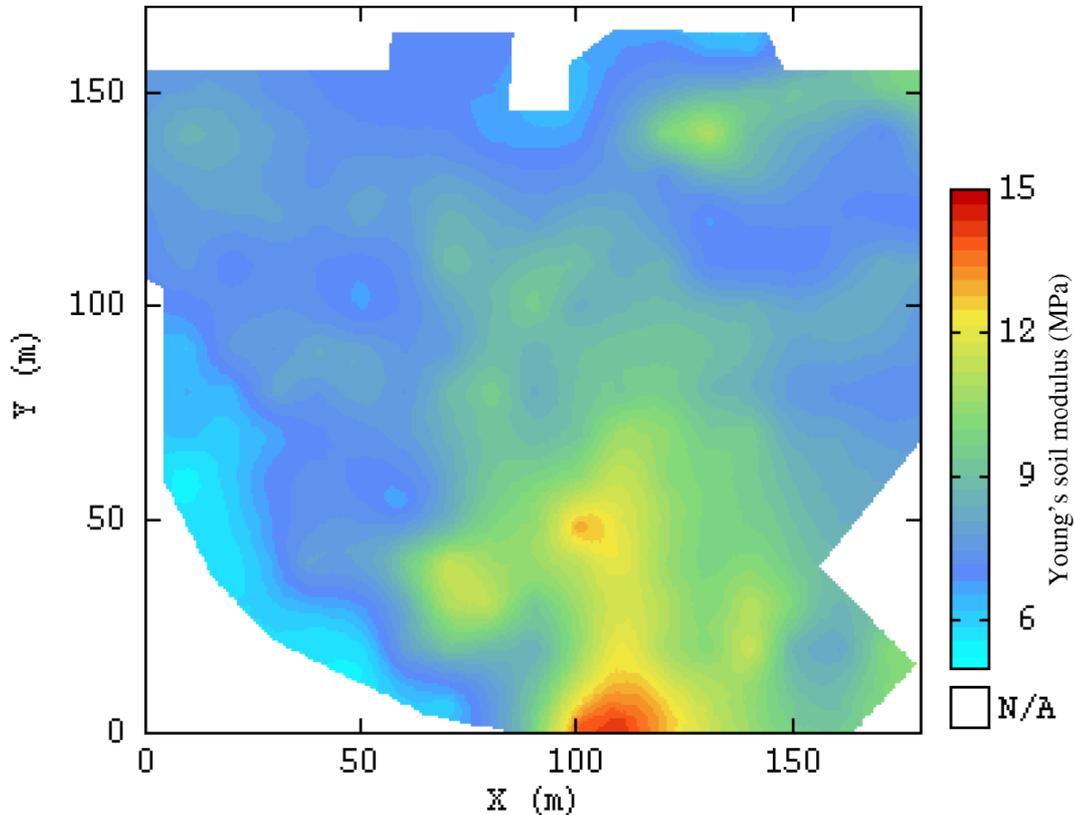
Figure 4-17: Map of the soil modulus obtained from the mean of the maps resulting from 1000 simulations

After a series of 1000 simulations, these results can be translated in terms of probability, by post-processing the simulation results to obtain 2D map of probabilities, which is useful in terms of support decision framework. As an illustration, Figure 4-18 shows the probability of soil modulus for the different threshold values of E_s in order to show the location of areas with a high probability to encounter low soil modulus values. For instance, a zone with a high probability of a soil modulus smaller than 7 MPa is located on the northern and west southern parts of the construction site (Figure 4-18b). A high probability of a soil modulus less than 12 MPa can be found in all parts of the construction site except small southern part of site (Figure 4-18g). The area of zones where the probability to obtain a soil modulus lower than 8 and 10 MPa are respectively larger than 50% and 85% of the total area (Figure 4-18c and Figure 4-18e).

Probability ($E_s \leq 6$ MPa)

a)

Probability ($E_s \leq 7$ MPa)

b)

Probability ($E_s \leq 8$ MPa)

c)

Probability ($E_s \leq 9$ MPa)

d)

Probability ($E_s \leq 10$ MPa)

e)

Probability ($E_s \leq 11$ MPa)
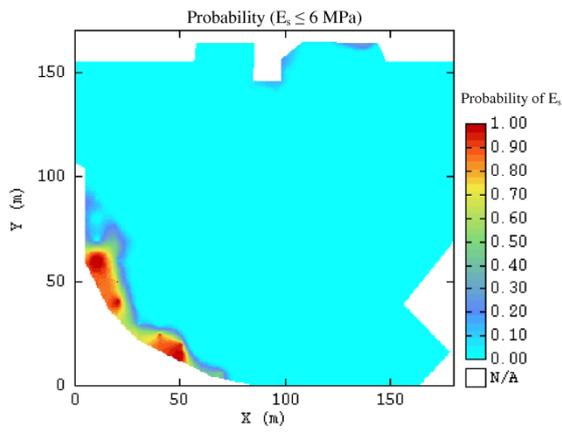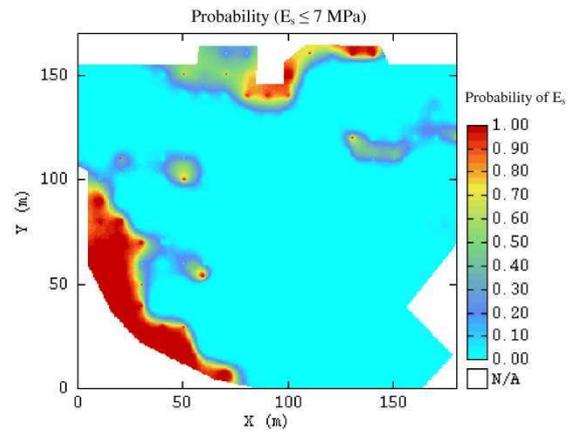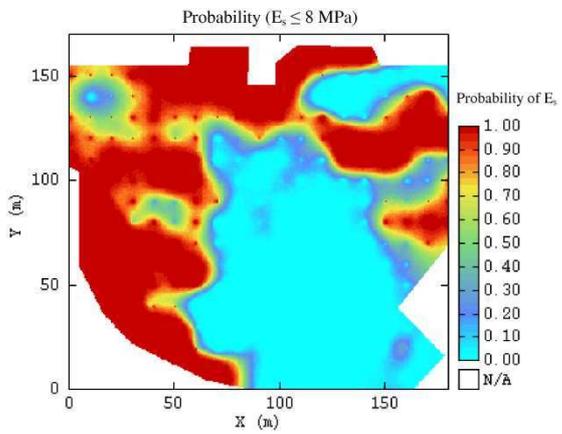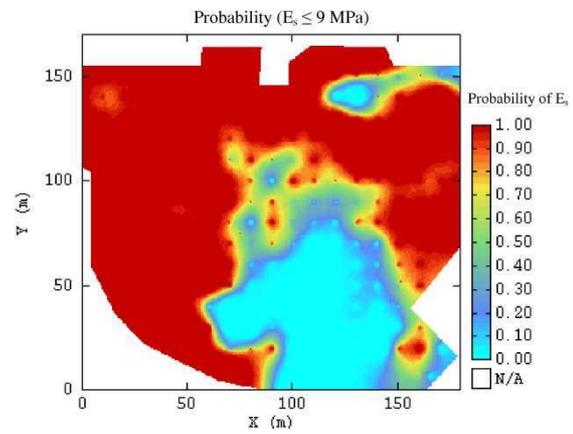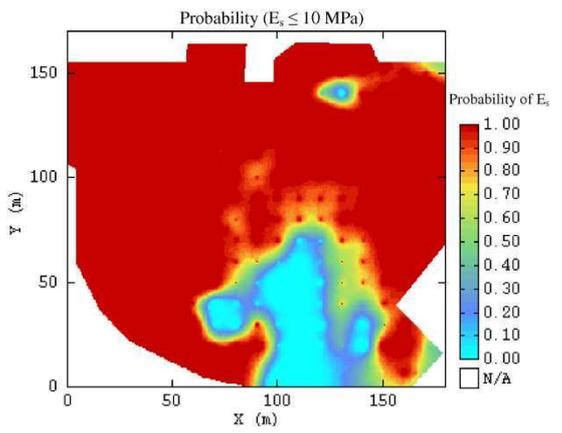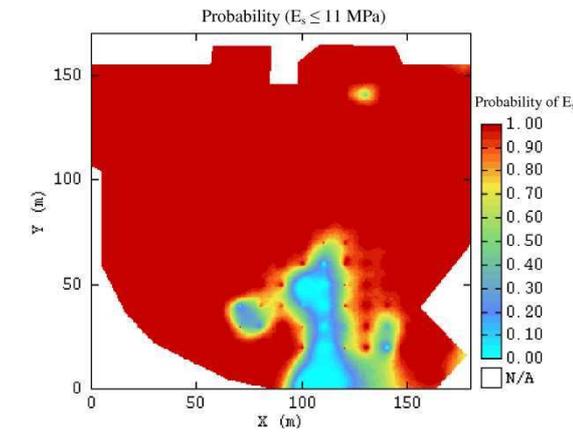
f)
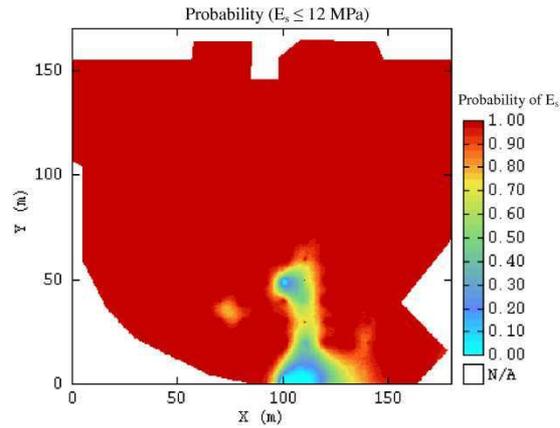
g)

Figure 4-18: Probability of soil modulus for different threshold values of E_s in order to show the location of areas with a high probability to encounter low soil modulus values

A flowchart is provided in Figure 4-19 which illustrates how the methods used in this chapter are linked one to each other. Furthermore, it allows us to see the overall procedure of probabilistic and geostatistics methods integrated into a finite element method. The following results for the superficial geotechnical designs are obtained by using this flow chart.
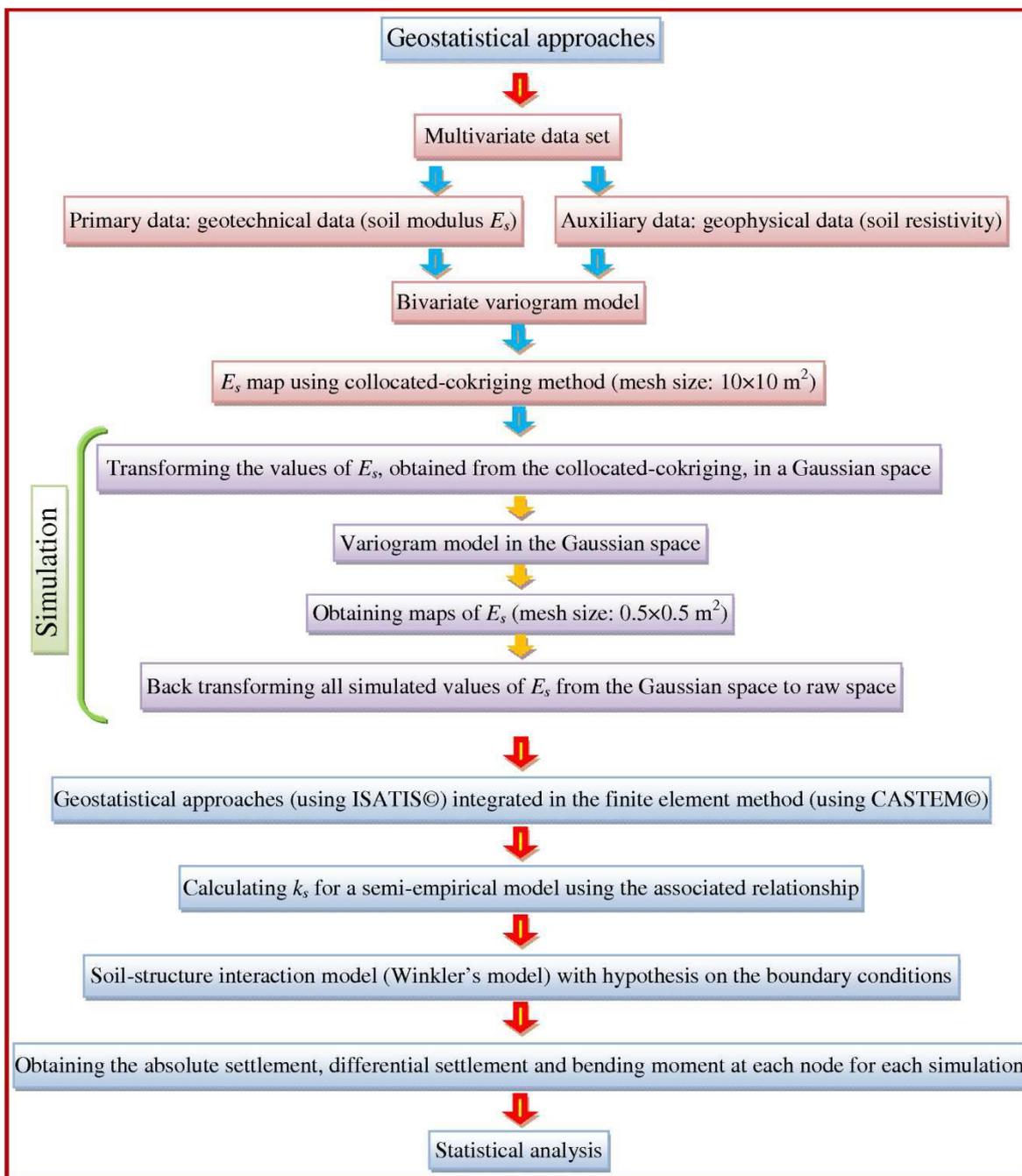
Figure 4-19: Flow chart of the methods used in this chapter to illustrate the overall procedure of the probabilistic and geostatistics methods integrated into a finite element method

4.4. Taking into account of the spatial variability of soil in the superficial geotechnical designs

In our analytical approach it is not possible to consider the soil characteristics as different at each given location along the spread footing and buried pipe axes (see sections

3.2 and 3.3.2). It could be very interesting to take into account the correlation length of soils parameters along the pipe axis or spread footing to characterize spatial variability of soil. Such an approach could be performed with the coupling of the finite element method with geostatistical methods, what is described for the superficial geotechnical designs in the ensuing sections.

Some authors (for example Elachachi et al. 2004, Niandou et al., 2009) have shown that the influence of the spatial variability of soil properties is the most important on the settlement and the bending moment when the spatial correlation length of soil is approximately equal to the length of the structure. This is not the case in this study where the considered lengths of the structures (10 m for the spread footing and 50 m for the buried pipe) are rather favorable compared to the correlation length identical with geophysics (37 m).

In the following, the spatial variability of Young's soil modulus is only taken into account and the spatial variability of soil parameters (v_s: Poisson's ratio of soil, L: length of low stiffness zone of soil beneath the pipe) and structure parameters (b and h respectively width and height of the spread footing, d: external diameter of the pipe, E_c: Young's modulus of the buried pipe or the spread footing) are not considered in the computations.

4.4.1. Taking into consideration of the spatial variability of soil modulus in the spread footing design (one dimensional model, 1D)

For taking into account of the spatial variability of soil modulus, we consider three different locations of a spread footing with a length of 10 m on the construction site (Figure 4-20). The soil parameters, the load, the mechanical property and the geometrical dimensions of this spread footing are identical to those previously studied in previous chapters (chapter 2 and 3). For each location of spread footing, the values of Young's soil modulus are obtained at each node from the 1000 simulations results using ISATIS© software. From these values of E_s, the different values of subgrade reaction modulus for each semi-empirical model are obtained using relationship from Table 2-4. These values of subgrade reaction modulus are introduced in the finite element method using one dimensional model to obtain the maximum differential settlements and the maximum bending moments for each semi-empirical model at each location. These computations are

performed with the CASTEM© software (Verpaux et al. 1988) using the Winkler model. Finite element modeling of a spread footing of 10 m has twenty elements with 21 nodes with free ends as boundary conditions (Figure 4-21).
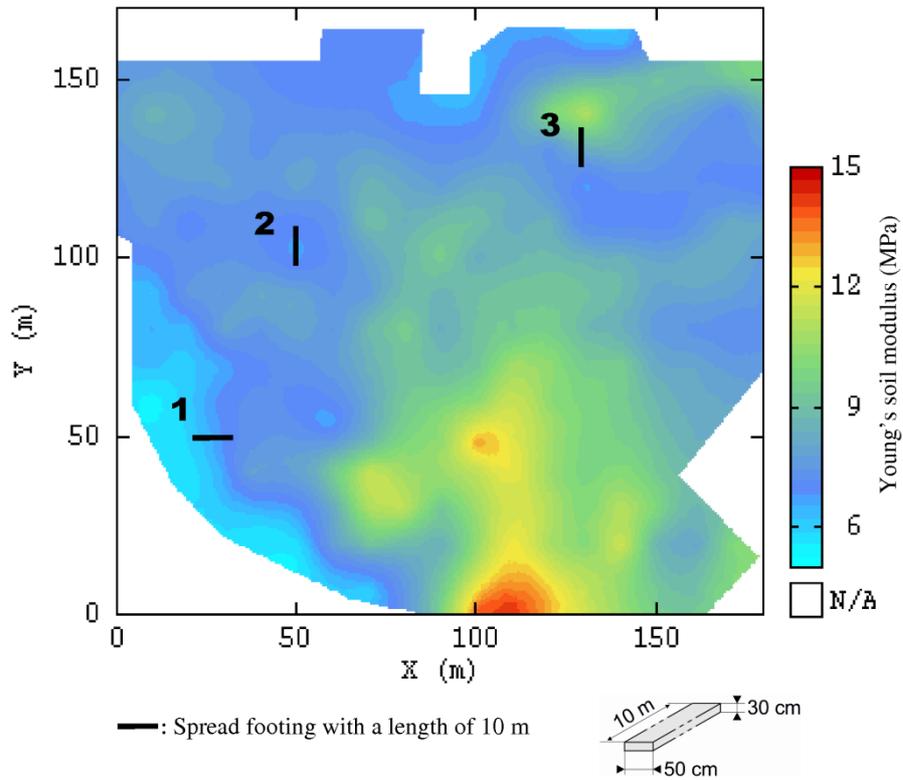
Figure 4-20: Three different locations of a spread footing with a length of 10 m on the construction site
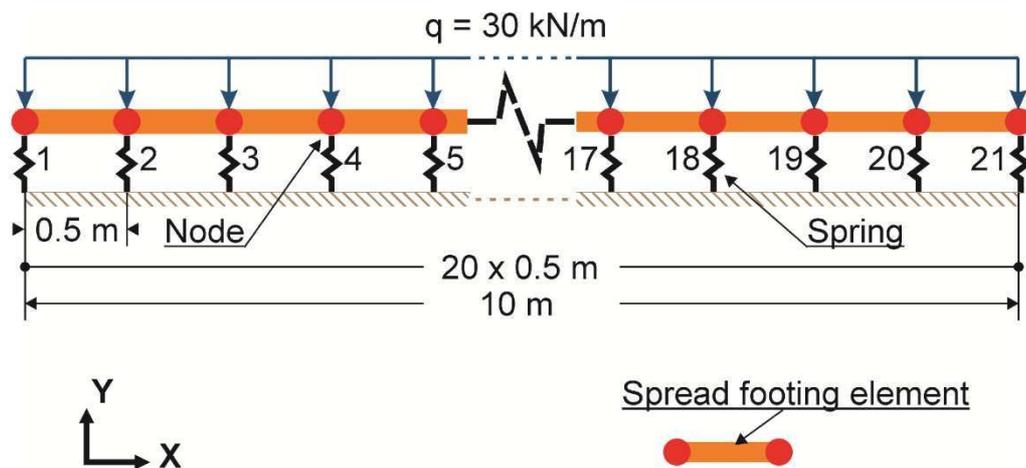
Figure 4-21: Finite element modelling of a spread footing of 10 m with free ends as boundary conditions(one dimensional model, 1D)

These results can be then statistically analyzed to better understand the behavior of a spread footing in the presence of spatial variability on the construction site. This is described in the following.

For a preliminary evaluation, Figure 4-22 depicts the data distribution for the 20000 soil modulus values for the three different locations of a spread footing in the case of the study site. For the soil modulus probability between 5% and 95%, the intervals of soil modulus values for the locations (1), (2) and (3) are respectively [5.41, 8.26], [5.86, 8.06] and [6.43, 11.29] MPa. The values of soil modulus in the locations (1) and (2) are nearly close together while the values of soil modulus in the locations (3) are greater and wider compared to the latter.
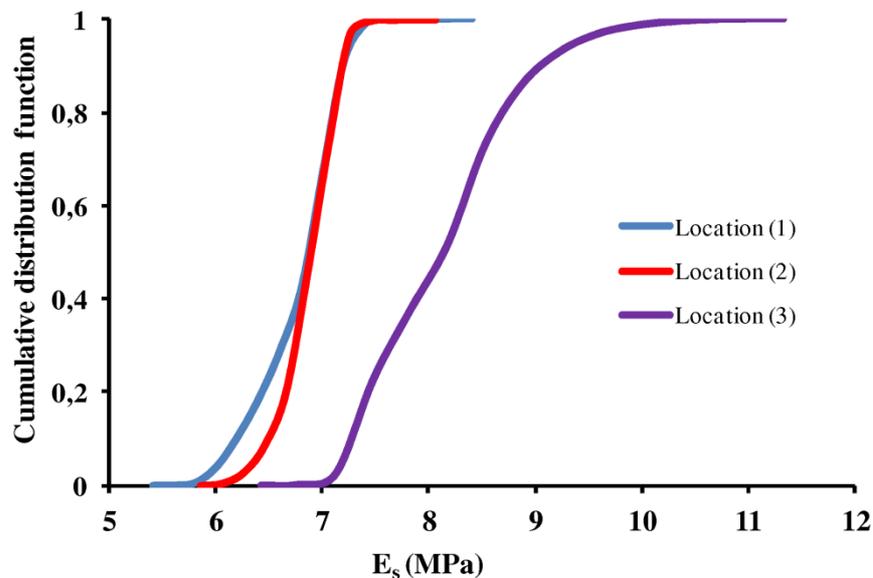
Figure 4-22: Cumulative distribution function of soil modulus for the three different locations of a spread footing in the case of the study site

To illustrate finite element results and the influence of geostatistical simulations, Figure 4-23a and Figure 4-23b respectively show the deformation and the bending moment along a spread footing length of 10 m for the first three simulations in the case of Vesic model for the location 3.
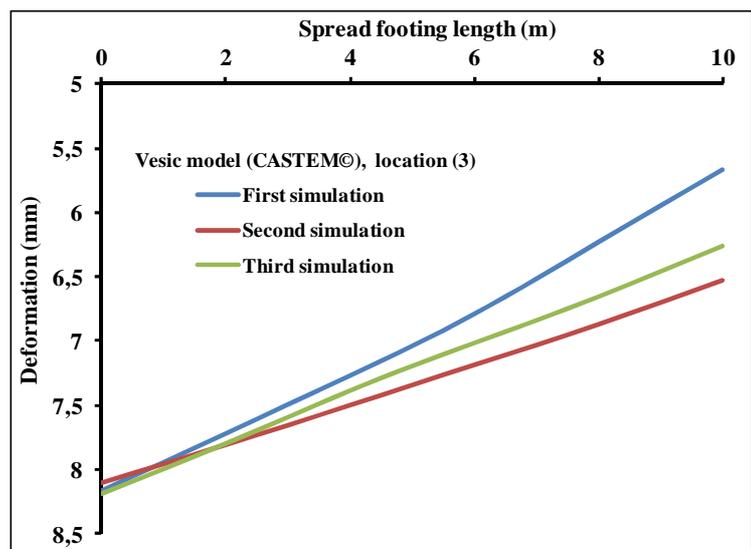
a)
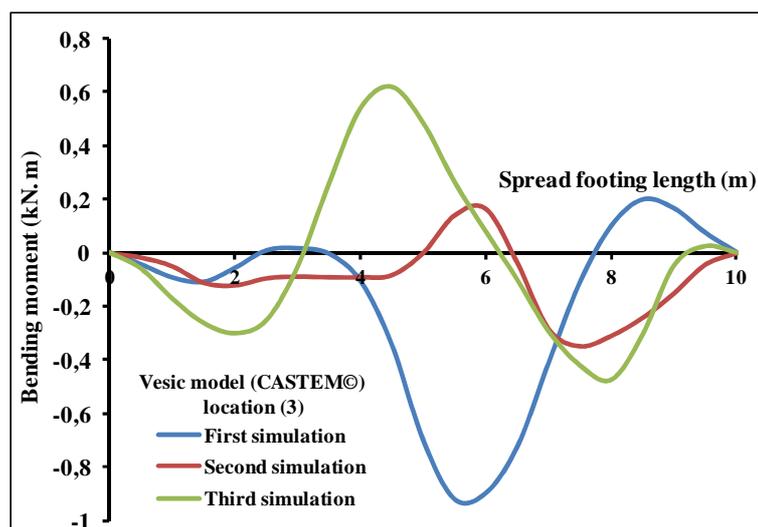
b)

Figure 4-23: a) Deformation and b) Bending moment along a spread footing length of 10 m for the first three simulations in the case of Vesic model

Figure 4-24a and Figure 4-24b respectively depict the deformation and the bending moment along a spread footing length of 10 m for the first simulation and for the four semi-empirical models for the location 3. Ménard's model gives the lowest values of the maximum deformation and the maximum bending moment and Vesic's model gives the greatest values. Biot's and Vlassov's models give approximately the same values.
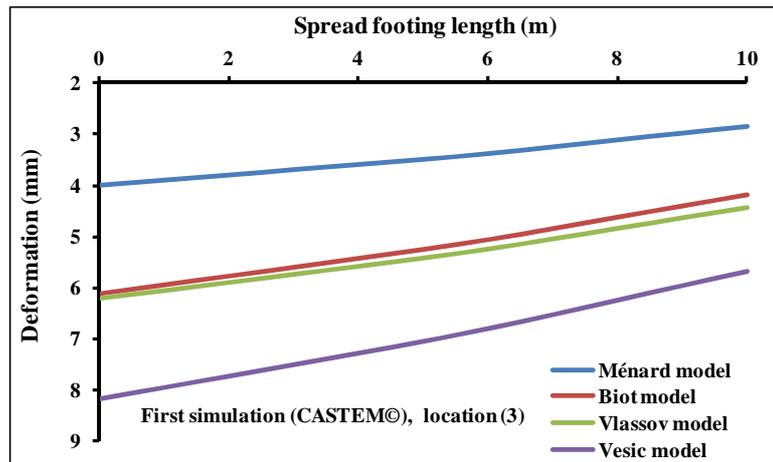
a)
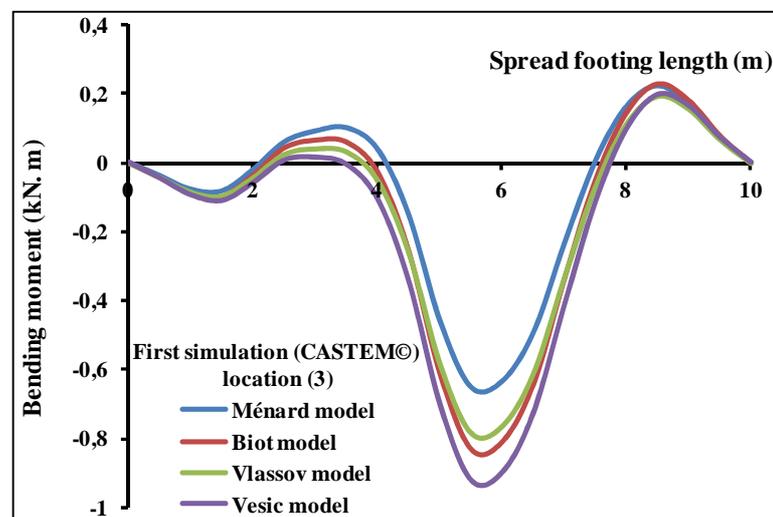
a)

Figure 4-24: a) Deformation and b) Bending moment along a spread footing length of 10 m for the first simulation and for the four semi-empirical models

In order to describe the behavior of a spread footing for these three different locations, the results obtained for the maximum differential settlement and the maximum bending moment are shown in the form of cumulative distribution function for the four studied semi-empirical models (Figure 4-25, and Figure 4-26).
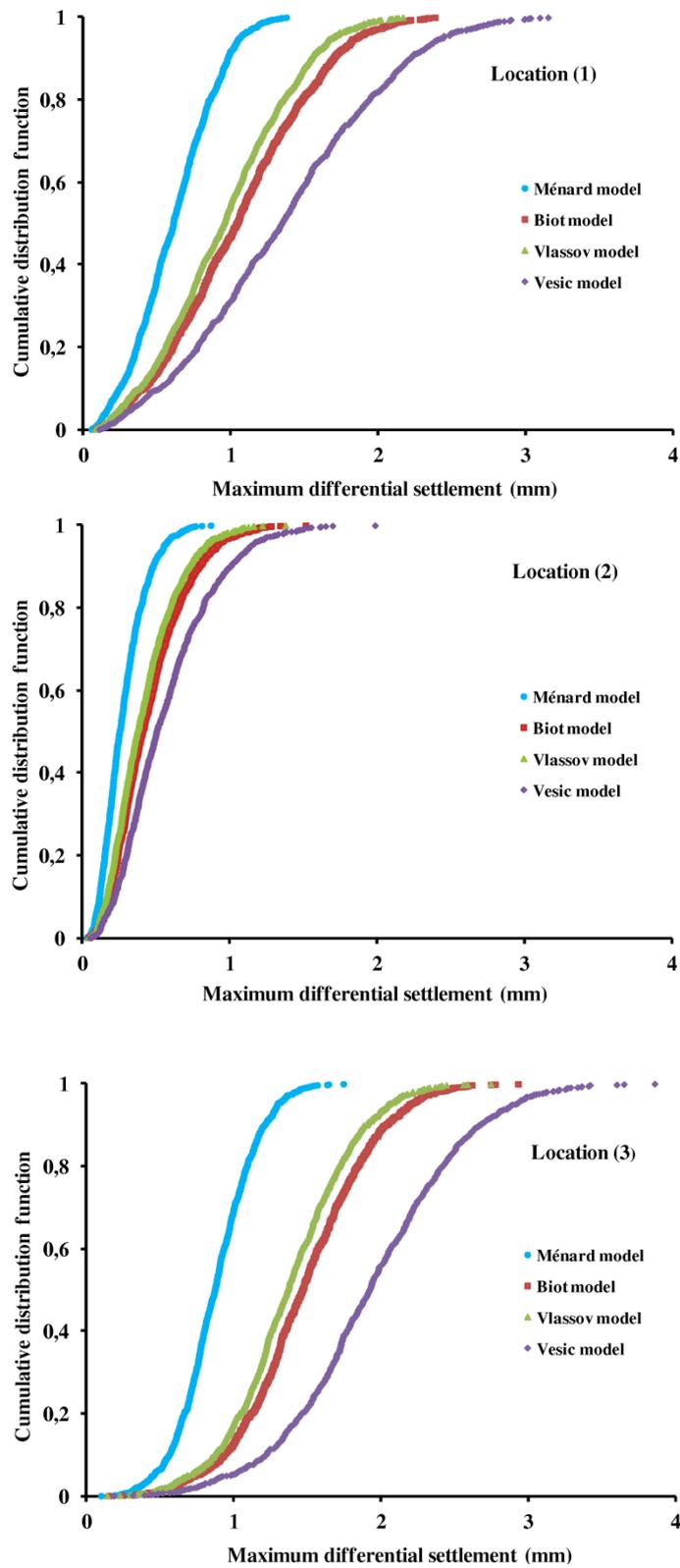
Figure 4-25: Cumulative distribution function of the maximum differential settlement for the three different locations, in the case of the study site for the four semi-empirical models
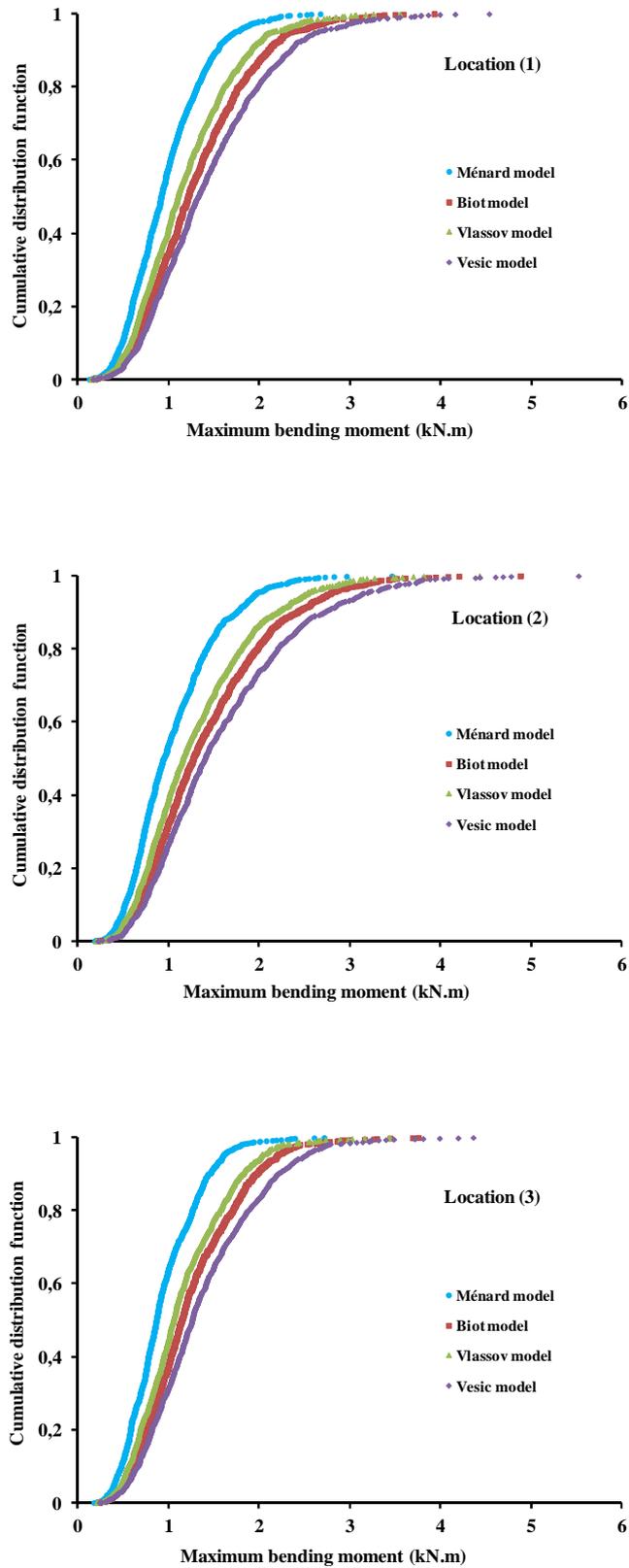
Figure 4-26: Cumulative distribution function of the maximum bending moment for the three different locations, in the case of the study site for the four semi-empirical models

For the probability of the maximum differential settlement between 5% and 95%, the intervals of the maximum differential settlements for the locations (1), (2) and (3) are respectively [0, 3], [0, 2] and [0, 4] mm (Figure 4-25). For these locations, Vesic's model gives the greatest values of the maximum differential settlements and Ménard's model gives the lowest values. Biot's and Vlassov's models give almost the same value of the maximum differential settlements.

For instance, in the case of location (1), the probabilities to obtain a maximum differential settlement lower than 1 mm for the Ménard, Biot, Vlassov and Vesic models are respectively 31%, 46%, 55% and 92%. The latter in the case of location (2) for the four semi-empirical models is almost 100%. Finally for the last location, these probabilities for the Ménard, Biot, Vlassov and Vesic models are respectively 6%, 13%, 17% and 70% (Figure 4-25) showing that the range of E_s (larger for the location (3)) as important as the presence of low values of E_s (location (1)). All in all, the obtained results provide insight regarding the stochastic analysis in the field of geotechnical engineering and show the importance of the spatial variability of soil modulus in the outcomes of a probabilistic assessment.

Similar observations can be made with regard to the distributions of the maximum bending moment (Figure 4-26) showing again the importance of the spatial variability of soil parameters on the longitudinal behavior of a spread footing.

For completing this section, the cumulative distribution functions of the maximum differential settlement and the maximum bending moment for the two extreme semi-empirical models (Ménard's and Vesic's models) and for the three different locations are shown in Figure 4-27 and Figure 4-28 in order to illustrate the importance of the semi-empirical model choice whatever the location.

As shown in Figure 4-28a, we obtain almost the same values of the cumulative distribution function for the different location for the Ménard model. The same interpretation is also true for the Vesic model (Figure 4-28b). However, for probabilities between 5% and 95%, the interval of the maximum bending moment values for the Vesic model is greater and wider than the Ménard model.

Finally, the results obtained here show, whatever the location of a spread footing on the construction site and whatever the considered semi-empirical model, the probability of having the critical values of the maximum differential settlement and the maximum

bending moment remains low. Of course, this conclusion is limited to a considered spread footing on the construction site in this section.

a)

b)
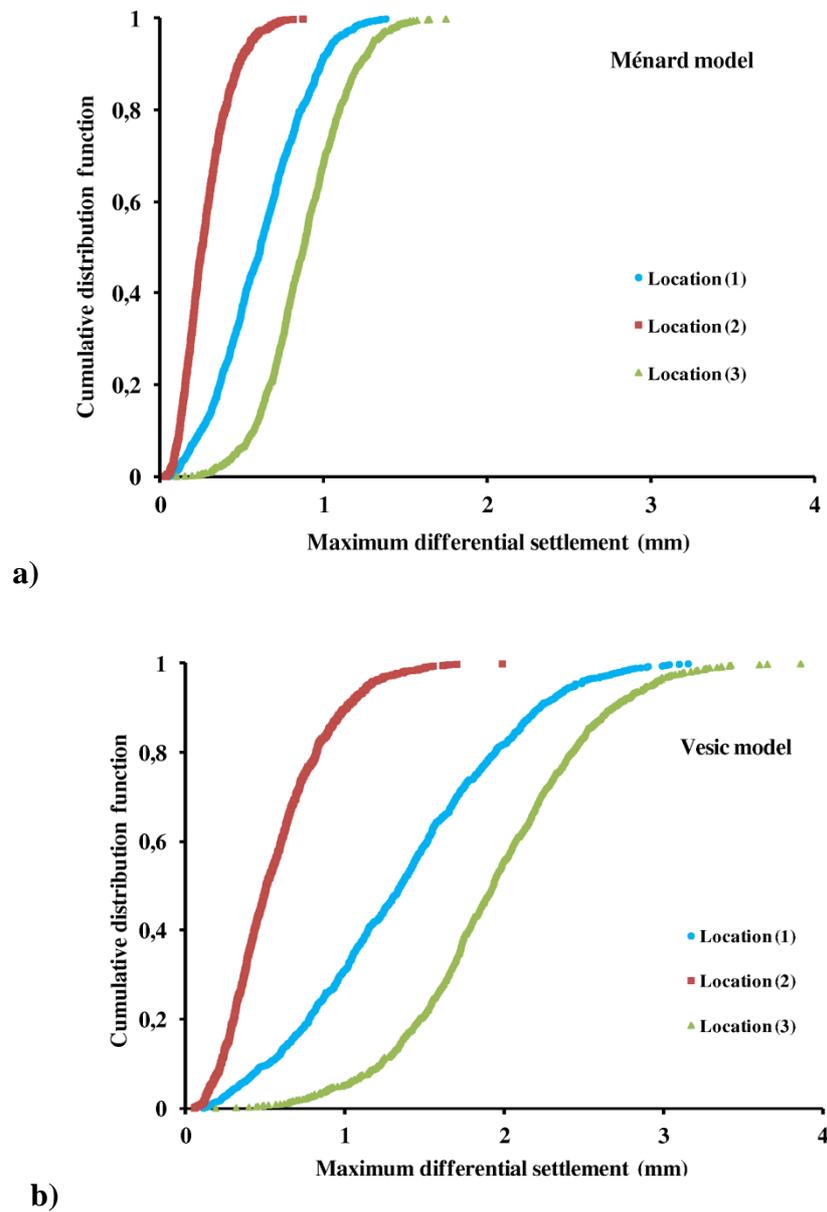
Figure 4-27: Cumulative distribution function of the maximum differential settlement for the three different locations, in the case of the study site for the two extreme semi-empirical models: a) Ménard's model and b) Vesic's model

a)

b)
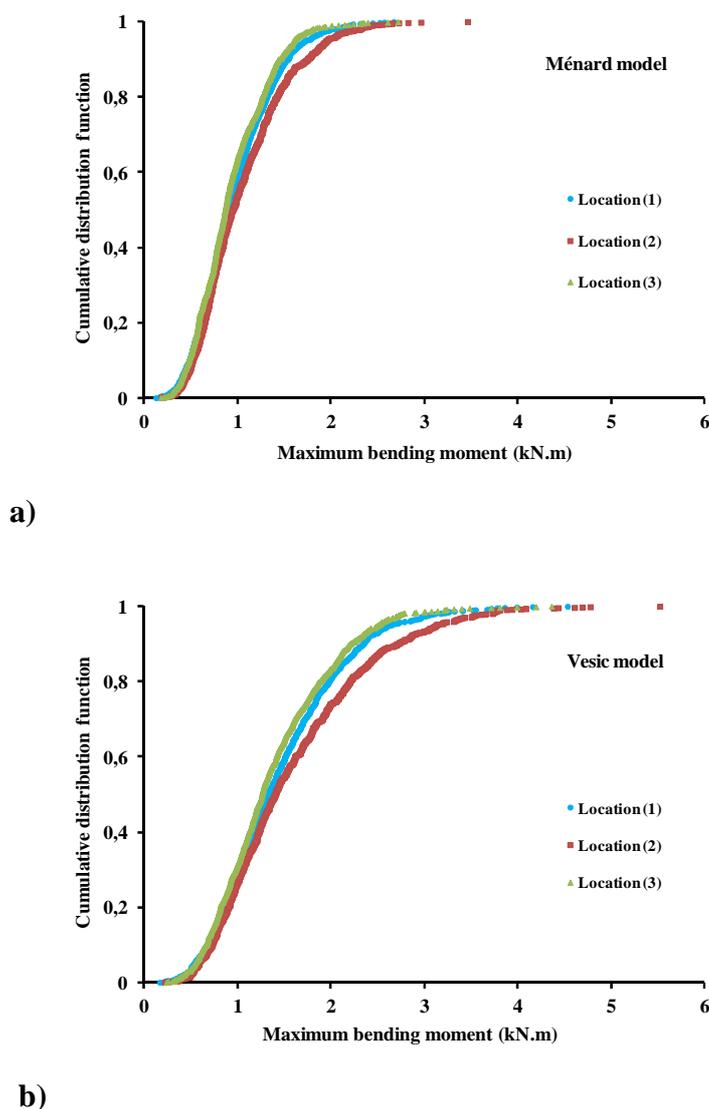
Figure 4-28: Cumulative distribution function of the maximum bending moment for the three different locations, in the case of the study site for the two extreme semi-empirical models: a) Ménard's model and b) Vesic's model

4.4.1.1. Comparison between analytical and numerical results (for a spread footing)

The objective is to compare the results obtained by the previous numerical method with those obtained by the analytical method presented in chapter three in order to show the influence of the spatial variability on the results. We cannot compare directly the obtained results here (from the probabilistic and geostatistics methods integrated into a finite element method using CASTEM© software) to those resulting from analytical methods (Figure 3-1b, c and d), since there are not great significant difference between the soil

reaction modulus values in the case of the study site for a length of 10 m (Figure 4-8). Obtained results here, can only be compared to those from analytical methods in the case 1 (Figure 3-1a) where we have a spread footing resting with free ends on an elastic soil with only an absolute settlement and no bending moment. In the following, this comparison is performed for a spread footing of 10 m at location (3).

Starting from the numerical method (ISATIS© and CASTEM© softwares) and considering the 1000 simulations of twenty values of the soil reaction modulus beneath the spread footing, we obtain the mean ($E[\overline{\Delta}]$), variance ($Var[\overline{\Delta}]$) and then the coefficient of variation ($CV[\overline{\Delta}]$) of the absolute settlement for each semi-empirical model (Table 4-2).

In the analytical method, the spatial variability of Young's soil modulus is not considered and the mean of this modulus is considered as constant beneath a spread footing. The coefficient of variation of the absolute settlement can be obtained from the analytical method from theory or calculated from these 1000 simulations as explained in the following:

- Analytical method from theory: for each simulation we obtain from twenty values of Young's soil modulus under the spread footing the mean E_s, and from the 1000 simulations mean ($E[\overline{E_s}]$), variance ($Var[\overline{E_s}]$) and then the coefficient of variation ($CV[\overline{E_s}]$) respectively equal to 8.136 MPa, 0.0353 (MPa)^2 and 0.0231. The coefficient of variation of k_s (CV_{ks}) can be calculated for each semi-empirical model from Equation 2-8 ($CV_{ks}=\eta_{Es}.CV_{Es}$, the values of η_{Es}, depends on each semi-empirical model, are reported in Table 2-5). Calculation of the coefficient of variation of settlement for these four semi empirical models is very straightforward: $CV_T[\Delta]= CV_{ks}$ as we showed in chapter three in the case 1 (Figure 3-1a). Values are also reported in the Table 4-2.

- Analytical method from 1000 simulations: the mean of soil modulus is obtained for each simulation as previously. From this value, the associated value of k_s and the associated absolute settlement for each simulation and for each semi-empirical model are calculated. Then the mean (*E[Δ]*), variance (*Var[Δ]*) and coefficient of variation of the absolute settlement (*CV[Δ]*) are obtained from 1000 simulations and for each semi-empirical model. These values are reported in the Table 4-2.

As can be seen from the Table 4-2, the values of the coefficient of variations obtained from these two analytical methods are nearly same. These two analytical methods give the same results as one would expect.

The difference between $E[\overline{\Delta}]$ and $Var[\overline{\Delta}]$ from the numerical simulation and $E[\Delta]$ and $Var[\Delta]$ from the analytical analysis is due to the influence of the intrinsic spatial variability of E_s along the spread footing. Then, it can be written (Equation 4-3):

$$E[\overline{\Delta}] = E[\Delta] + E[\Delta_u], \quad Var[\overline{\Delta}] = Var[\Delta] + Var[\Delta_u]$$

Equation 4-3

where $\overline{\Delta}$: settlement from the total spatial variability, Δ: settlement from the analytical method (E_s is constant) and Δ_u: settlement from the intrinsic spatial variability (E_s is variable) as shown in Figure 4-29:

Table 4-2: Comparison of the maximum settlement between analytical and numerical methods for a spread footing of 10 m at location (3).

Statistical parameters	**Ménard**	**Vesic**	**Biot**	**Vlassov**	Considered methods
$E[\overline{\Delta}]$ (mm)	3.960	8.119	6.073	6.178	Numerical methods (ISATIS© and CASTEM©)
$Var[\overline{\Delta}]$ (mm)^2	0.0193	0.1012	0.0580	0.0492	
$CV[\overline{\Delta}]$	0.0351	0.0392	0.0396	0.0360	
$CV_T[\Delta]$	0.0231	0.0254	0.0254	0.0231	Analytical method (obtained from theory)
$CV[\Delta]$	0.0230	0.0249	0.0255	0.0230	Analytical method (obtained from 1000 simulations)
$E[\Delta]$ (mm)	3.513	7.131	5.320	5.481	
$Var[\Delta]$ (mm)^2	0.0065	0.0314	0.0184	0.0159	
$E[\Delta]/E[\overline{\Delta}]$	88.7%	87.8%	87.6%	88.7%	Contribution to the estimated settlement
$Var[\Delta]/Var[\overline{\Delta}]$	33.7%	31%	31.7%	32.3%	Contribution to the variability of settlement

$E[\overline{\Delta}], Var[\overline{\Delta}], CV[\overline{\Delta}]$ *are respectively the mean, variance and coefficient of variation of the absolute settlement from numerical methods, $CV_T[\Delta]$: coefficient of variation of the absolute settlement using analytical method (obtained from theory), $E[\Delta]$, $Var[\Delta]$ and $CV[\Delta]$: are respectively the mean, variance and coefficient of variation of the absolute settlement using analytical method (obtained from 1000 simulations). $\overline{\Delta}$: settlement from the total spatial variability, Δ: settlement from the analytical method (E_s is constant)*
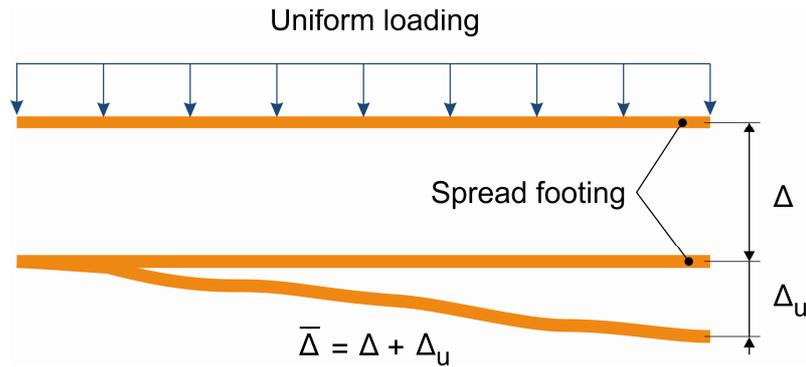
Figure 4-29: Schematical definition of $\overline{\Delta}$: the settlement from the total spatial variability, Δ: settlement from the analytical method and Δ_u: settlement from the intrinsic spatial variability

The results of the comparison of the settlement between analytical and numerical methods for a spread footing of 10 m at locations (1) and (2) can be found in appendix 2.

For the different location, it can be calculated the contribution of the absolute settlement Δ to the total settlement $\overline{\Delta}$ and the contribution of the variance of the absolute settlement to the total variance respectively from ratios $E[\Delta]/E[\overline{\Delta}]$ and $Var[\Delta]/Var[\overline{\Delta}]$.

In the case of location 3, the contribution of the absolute settlement to the total settlement is about 88% and the contribution of the variance of the absolute settlement to the total variance is close to 32%. The latter value shows the great influence (68%) of the spatial variability of E_s along the spread footing (intrinsic spatial variability) in the variance of $\overline{\Delta}$. This influence is reported, on average, on the settlement with a contribution of the intrinsic spatial variability on the total settlement of 12%.

Location 2, where variability of E_s is the lowest compared to others locations, gives a very low contribution of the intrinsic spatial variability on the settlement (3%). The contribution of the variance of the intrinsic spatial variability on the variance of the settlement remains important (52%). Location 1, where the variability of E_s is greater than for location 2, shows a very important influence of the intrinsic spatial variability on the variance of the total settlement (85%).

Note that for all locations under study, all contributions are almost the same, whatever the semi-empirical model considered for k_s.

All these results show the influence of the spatial variability of E_s along the spread footing in the case of a spread footing with free ends even when the correlation length is greater than the length of the spread footing.

4.4.2. Taking into consideration of the spatial variability of soil modulus in the buried pipe design

For taking into account of the spatial variability of soil modulus, we consider a buried concrete pipe of 100 m with manholes at both ends on the construction site (Figure 4-30). The soil parameters, the load, the mechanical property and the geometrical dimensions of this buried concrete pipe are identical to those previously studied in previous chapters (chapter 2 and 3). The values of Young's soil modulus are obtained at each node from the 1000 simulations results using ISATIS© software. From these values of E_s, the different values of subgrade reaction modulus for each semi-empirical model are obtained using relationship from Table 2-8. These values of subgrade reaction modulus are introduced in the finite element method using one dimensional model to obtain the maximum differential settlements and the maximum bending moments for each semi-empirical model. These computations are performed with the CASTEM© software using the Winkler model. Finite element modeling of a buried pipe of 100 m has 200 elements with 201 nodes with fixed ends as boundary conditions (Figure 4-31).
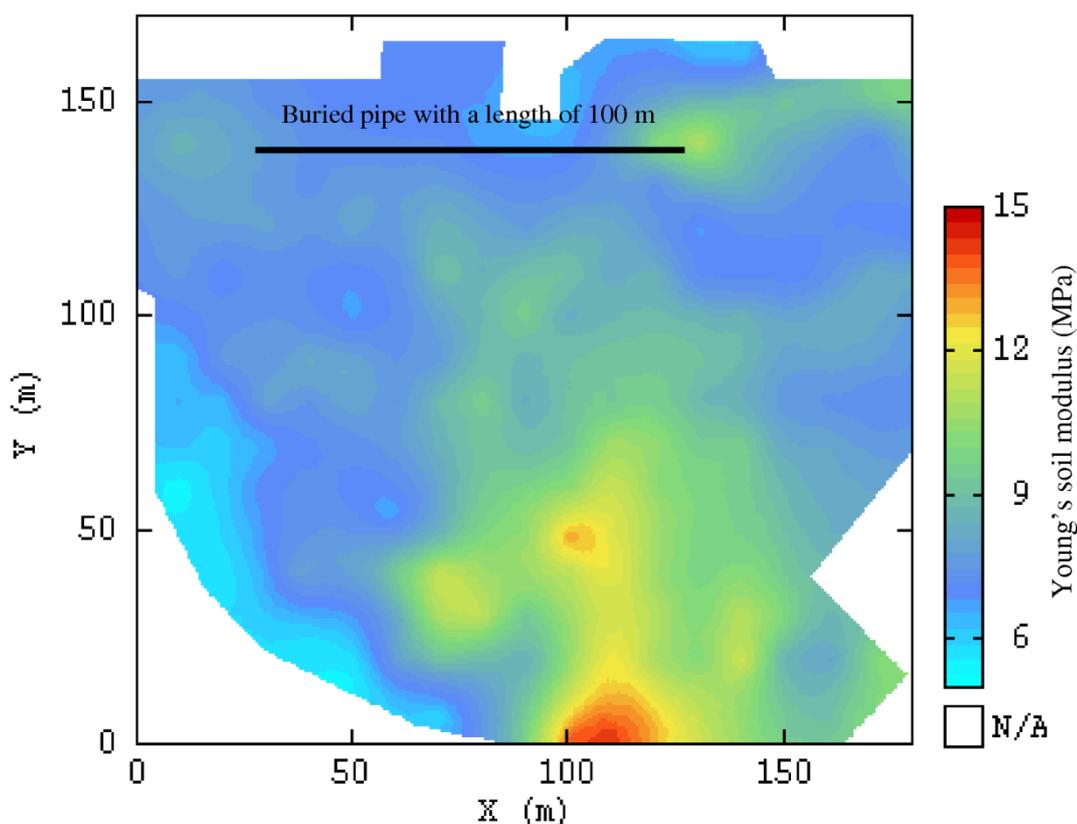
Figure 4-30: Location of a buried concrete pipe with a length of 100 m on the construction site
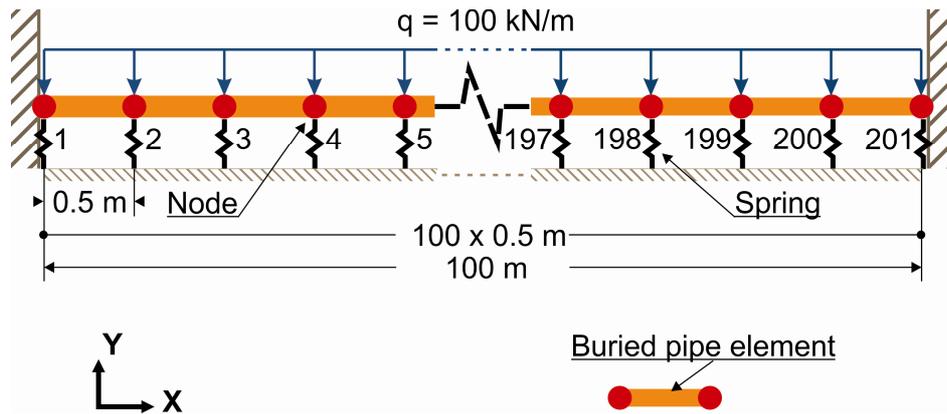
Figure 4-31: Finite element modelling of a buried pipe of 100 m with fixed ends as boundary conditions(one dimensional model, 1D)

As in the case of a spread footing, the obtained results can be then statistically analyzed to better understand the behavior of a buried concrete pipe in the presence of spatial variability on the construction site. In the following, this statistical analysis is performed for the two extreme semi-empirical models (Vesic's and Matsubara's models) since these two models include the values of the k_s and CV_{ks} for the other semi-empirical models (Biot, Meyerhof, Kloppel and Selvadurai, Figure 2-11 and Figure 2-16).

For a preliminary evaluation, Young's soil modulus along a buried pipe of 100 m (Figure 4-30) for the first 100 simulations is shown in Figure 4-32 to show the variation of soil modulus beneath the buried pipe.
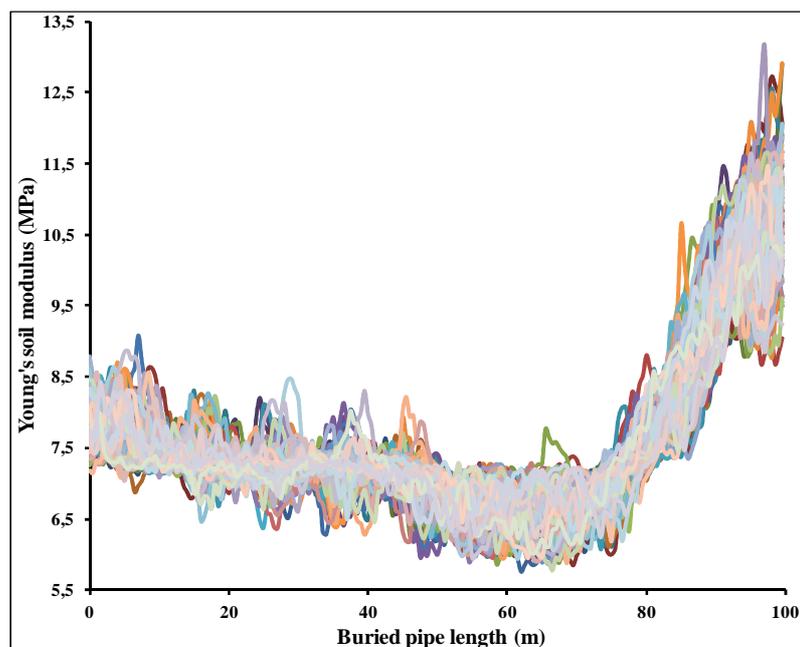
Figure 4-32: Young's soil modulus along a buried pipe of 100 m (Figure 4-30) for the first 100 simulations

Figure 4-33 shows the data distribution for the 200000 soil modulus values for the location of a buried pipe in the case of the study site. For the soil modulus probability between 5% and 95%, the interval of soil modulus values for this location is [6.4, 10.3] MPa (Figure 4-33b).
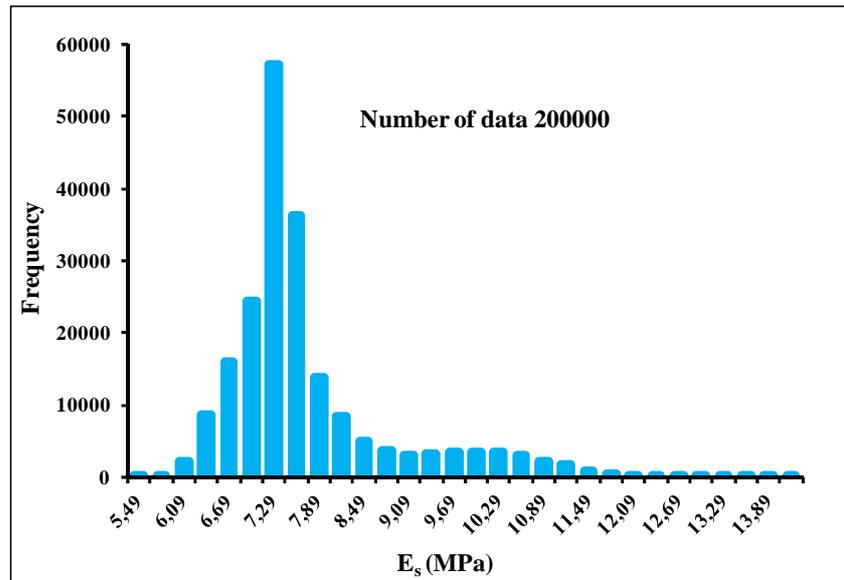
a)
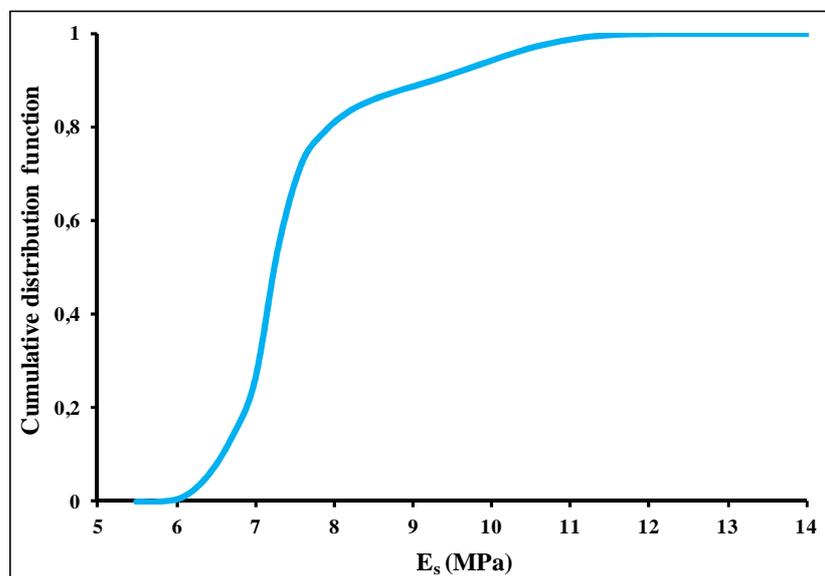
b)

Figure 4-33:a) Histogram and b)Cumulative distribution function of soil modulus for the location of buried pipe (Figure 4-30) in the case of the study site

Some preliminary calculated results obtained using the finite element method (CASTEM©) for this location are shown in Figure 4-34 and Figure 4-35. Figure 4-34a and Figure 4-34b respectively show the deformation and the bending moment along a buried pipe with a length of 100 m for the first three simulations in the case of Vesic model.

a)

b)
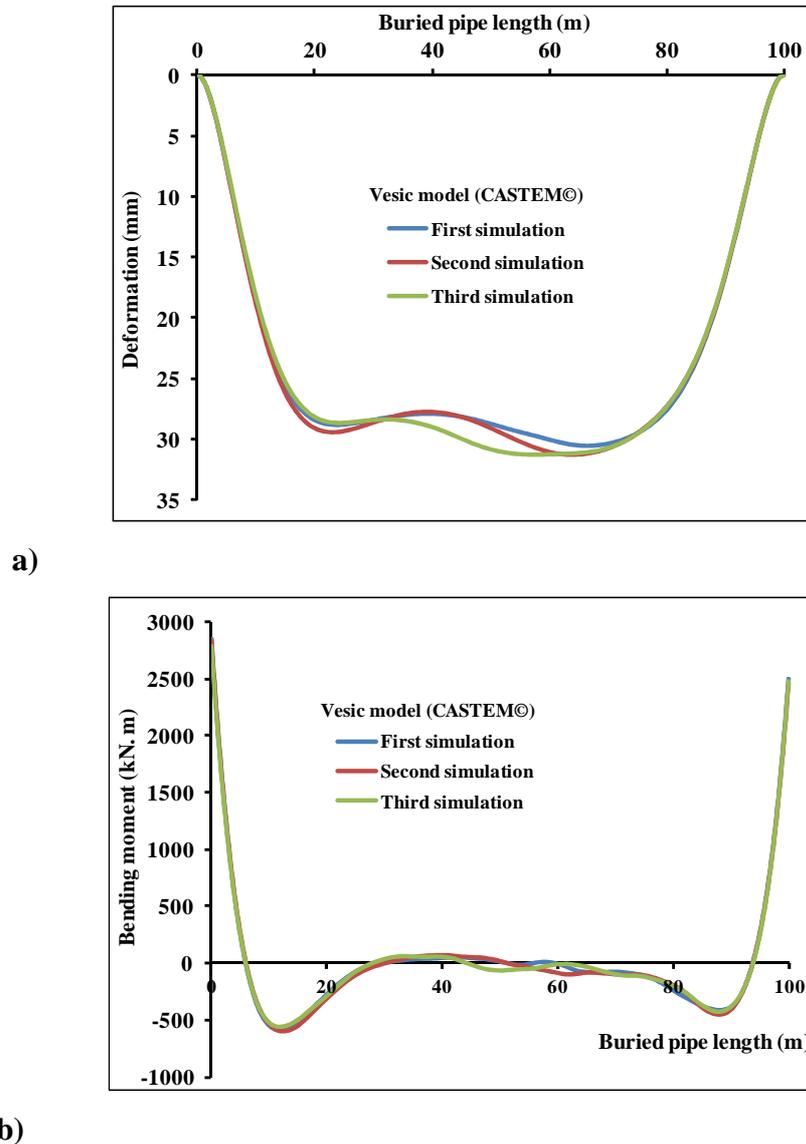
Figure 4-34: a)Deformation and b) Bending moment along a buried pipe of 100 m for the first three simulations in the case of Vesic model

Figure 4-35a and Figure 4-35b respectively show the deformation and the bending moment along a buried pipe for the first simulation and for the two extreme semi-empirical models. As expected, the Vesic model gives the greater values of the maximum deformation and the maximum bending moment than the Matsubara model.

a)

b)
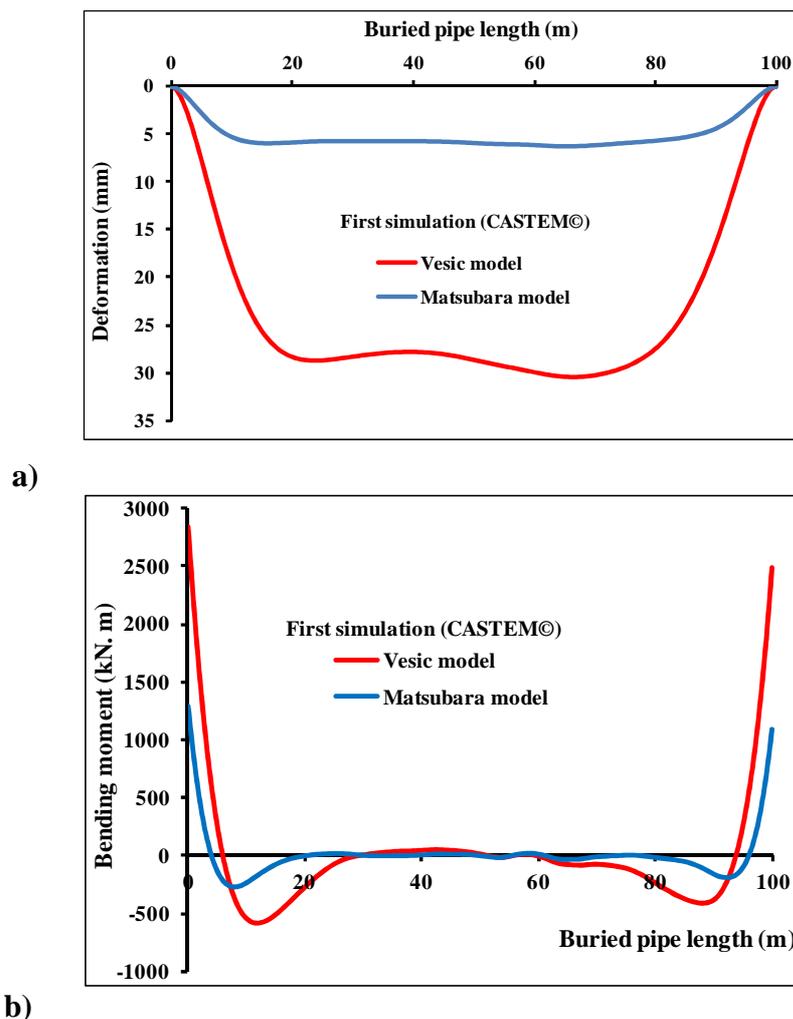
Figure 4-35: a) Deformation and b) Bending moment along a buried pipe of 100 m for the first simulation and for the two extreme semi-empirical models

In order to explain the behavior of a buried concrete pipe for this location, the results obtained for the maximum differential settlement and the maximum bending moment are transformed in the form of cumulative distribution function for these two semi-empirical models (Figure 4-36 and Figure 4-37).

For the probability of the maximum differential settlement between 5% and 95%, the intervals of the maximum differential settlements for the Matsubara and Vesic models are respectively [6, 6.7] and [30, 32.5] mm (Figure 4-36). As can be seen, there is a large difference between the values of these two intervals. For example, the probability to obtain a maximum differential settlement lower than 6.7 mm for the Matsubara model is equal to 95% while this probability for the Vesic model and for a maximum differential settlement less than 29.5 mm is equal to 0%, illustrating the importance of the choice of a semi-

empirical model and the importance of the spatial variability of soil parameters on the longitudinal behavior of a buried pipe.

Similar interpretation can be made with regard to the distributions of the maximum bending moment (Figure 4-37).
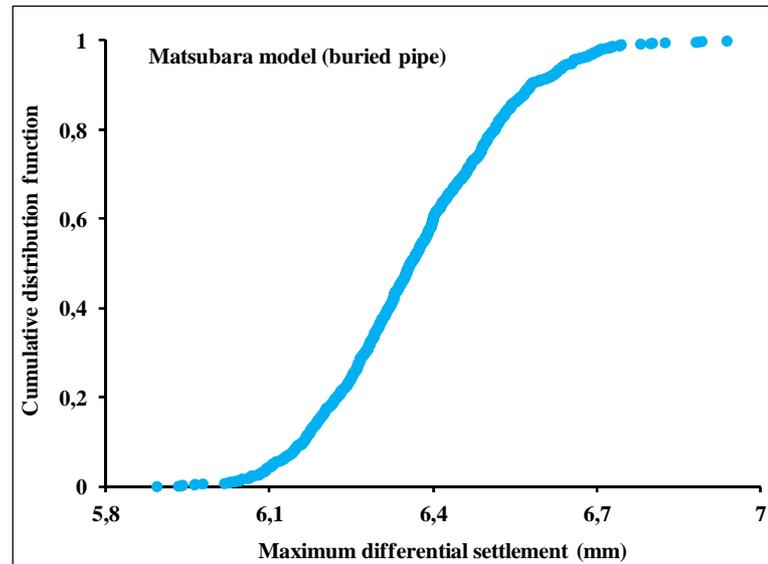
a)
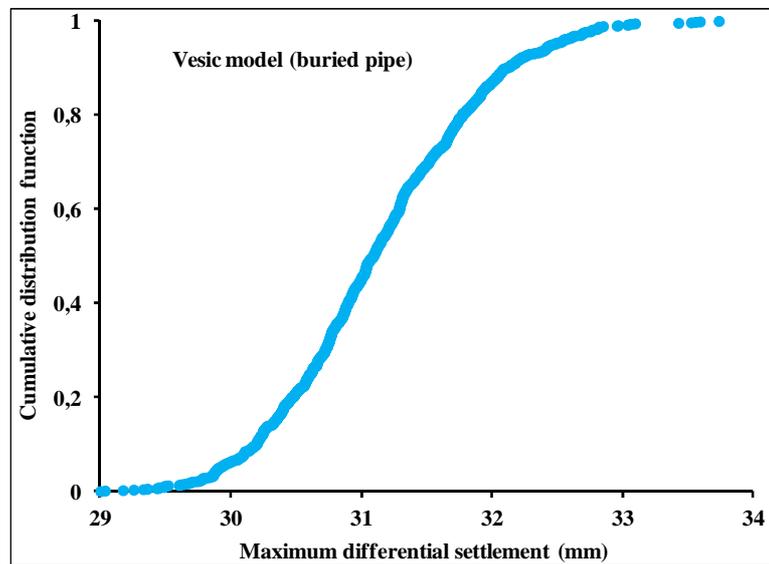
b)

Figure 4-36: Cumulative distribution function of the maximum differential settlement for a buried pipe of 100 m in the case of the study site for the two extreme semi-empirical models: a) Matsubara model b)Vesic model
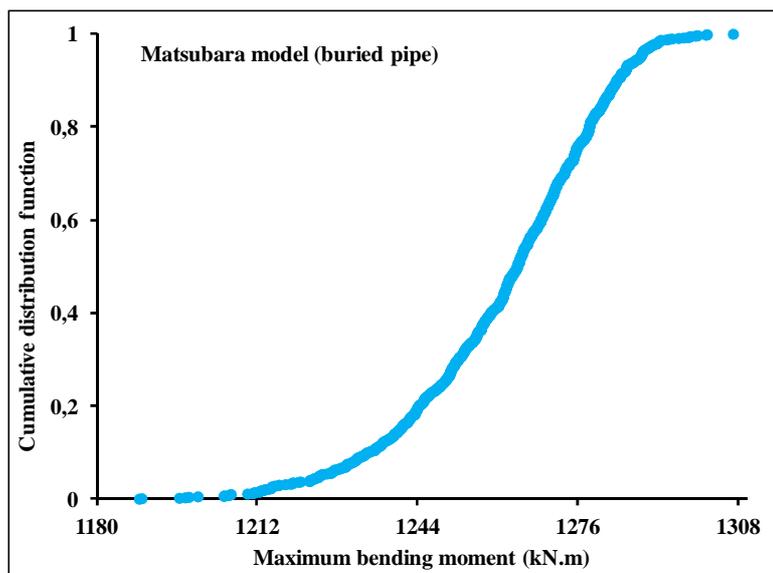
a)
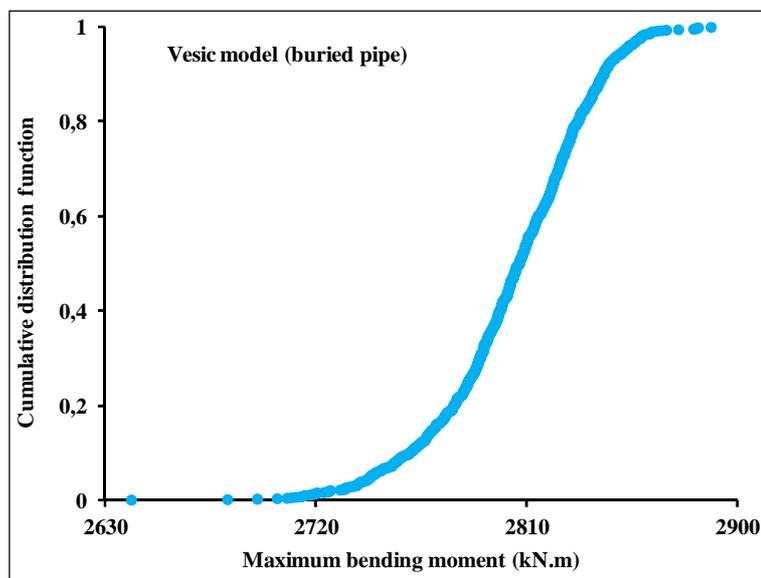
b)

Figure 4-37: Cumulative distribution function of the maximum bending moment for a buried pipe of 100 m in the case of the study site for the two extreme semi-empirical models: a) Matsubara model b)Vesic model

It can be noted that this site does not present zone of weak soil ($E_s \leq 2$ MPa). The maximum calculated counter slope, for the Vesic model, is about 1/1000 and the maximum bending moment is far lower than the elastic maximum bending moment. The probability of failure, for this buried pipe, is then very low on this site.

4.4.2.1. Comparison between analytical and numerical results (for a buried pipe)

In this section we compare the results obtained by the previous numerical method with those obtained by the analytical method presented in chapter three in the case of a buried pipe of 100 m in order to show the influence of the spatial variability on the maximum settlement and the maximum bending moment. As it was shown in chapter three for a low stiffness zone length greater than 50 m (Figure 3-28) the uncertainty of CV_L is equal to zero then we take into account only the uncertainty of k_s (CV_{ks}). In the following, this comparison is performed for the buried concrete pipe at the considered location on the construction site (Figure 4-30).

Starting from the numerical method (ISATIS© and CASTEM© softwares) and considering the 1000 simulations of 200 values of the soil reaction modulus beneath the buried pipe, we obtain the mean ($E[\overline{\Delta}]$), variance ($Var[\overline{\Delta}]$) and then the coefficient of variation ($CV[\overline{\Delta}]$) of the maximum total settlement for the Matsubara and Vesic models (Table 4-3).

As it was previously mentioned, in the analytical method, the spatial variability of Young's soil modulus is not considered and the mean of this modulus is considered as constant beneath a buried pipe. The coefficient of variation of the maximum total settlement can be obtained from the analytical method from theory or calculated from these 1000 simulations as explained in the following:

- Analytical method from theory: for each simulation we obtain from 200 values of Young's soil modulus under the buried pipe the mean E_s, and from the 1000 simulations mean ($E[\overline{E_s}]$), variance ($Var[\overline{E_s}]$) and then the coefficient of variation ($CV[\overline{E_s}]$) respectively equal to 7.544 MPa, 0.0053 (MPa)^2 and 0.0096. The coefficient of variation of k_s (CV_{ks}) can be calculated for each semi-empirical model from Equation 2-8 ($CV_{ks}=\eta_{Es}.CV_{Es}$, the values of η_{Es}, depends on each semi-empirical model, are reported in Table 2-9). Calculation of the coefficient of variation of settlement for these two semi empirical models is very straightforward: $CV_T[\Delta]= CV_{ks}$ as we showed in chapter three (Figure 3-27). Values are also reported in the Table 4-3.

- Analytical method from 1000 simulations: the mean of soil modulus is obtained for each simulation as previously. From this value, the associated value of k_s and the associated maximum settlement for each simulation and for each semi-emprical model are calculated. Then the mean ($E[\Delta]$), variance ($Var[\Delta]$) and coefficient of variation of the absolute settlement ($CV[\Delta]$) are obtained from 1000 simulations and for each semi-empirical model. These values are reported in the Table 4-3.

As can be seen from the Table 4-3, the values of the coefficient of variations obtained from these two analytical methods are almost same and as expected give the same results.

Table 4-3: Comparison of the maximum settlement between analytical and numerical methods for a buried pipe of 100 m at considered location on the construction site.

Statistical parameters	Matsubara	Vesic	Considered methods
$E[\overline{\Delta}]$ (mm)	6.366	31.128	Numerical methods (ISATIS© and CASTEM©)
$Var[\overline{\Delta}]$ (mm)^2	0.0272	0.5797	
$CV[\overline{\Delta}]$	0.0259	0.0245	
$CV_T[\Delta]$	0.0096	0.0106	Analytical method (obtained from theory)
$CV[\Delta]$	0.0096	0.0104	Analytical method (obtained from 1000 simulations)
$E[\Delta]$ (mm)	5.489	26.673	
$Var[\Delta]$ (mm)^2	0.0028	0.0776	
$E[\Delta]\big/E[\overline{\Delta}]$	86.2%	85.7%	Contribution to the estimated settlement
$Var[\Delta]\big/Var[\overline{\Delta}]$	10.3%	13.4%	Contribution to the variability of settlement

$\overline{\Delta}$: *Maximum settlement from the total spatial variability*, Δ: *Maximum settlement from the analytical method (E_s is constant)*

The difference between $E[\overline{\Delta}]$ and $Var[\overline{\Delta}]$ from the numerical simulation and $E[\Delta]$ *and* $Var[\Delta]$ from the analytical analysis is due to the influence of the intrinsic spatial variability of E_s along the buried pipe.

For this location, it can be calculated the contribution of the maximum settlement Δ to the maximum total settlement $\overline{\Delta}$ and the contribution of the variance of the maximum settlement to the total variance respectively from ratios $E[\Delta]\big/E[\overline{\Delta}]$ and $Var[\Delta]\big/Var[\overline{\Delta}]$.

The contribution of the maximum settlement to the maximum total settlement is about 86% and the contribution of the variance of the maximum settlement to the total variance is close to 12%. The latter value shows the great influence (88%) of the spatial variability of E_s along the buried pipe (intrinsic spatial variability) in the variance of $\overline{\Delta}$. This influence is reported, on average, on the maximum settlement with a contribution of the intrinsic spatial variability on the maximum total settlement of 14%.

With the same methodology as in the case of maximum settlement, comparison of the maximum bending moment between analytical and numerical methods for the considered buried pipe is presented in Table 4-4.

Table 4-4: Comparison of the maximum bending moment between analytical and numerical methods for a buried pipe of 100 m at considered location on the construction site.

Statistical parameters	Matsubara	Vesic	Considered methods
$E\left[\overline{M}\right]$ (kN.m)	1260.97	2803.72	Numerical methods (ISATIS© and CASTEM©)
$Var\left[\overline{M}\right]$ (kN.m)^2	384.17	1071.62	
$CV\left[\overline{M}\right]$	0.0155	0.0117	
$CV_T[M]$	0.0048	0.0053	Analytical method (obtained from theory)
$CV[M]$	0.0048	0.0052	Analytical method (obtained from 1000 simulations)
$E[M]$ (kN.m)	1036.24	2284.26	
$Var[M]$ (kN.m)^2	24.97	142.38	
$E[M]\big/E\left[\overline{M}\right]$	82 .2%	81.5%	Contribution to the estimated bending moment
$VarM\big/Var\left[\overline{M}\right]$	6.5%	13.3%	Contribution to the variability of bending moment

$E\left[\overline{M}\right], Var\left[\overline{M}\right], CV\left[\overline{M}\right]$ *are respectively the mean, variance and coefficient of variation of the maximum bending moment from numerical methods, $CV_T[M]$: coefficient of variation of the maximum bending moment using analytical method (obtained from theory), E[M], Var[M] and CV[M]: are respectively the mean, variance and coefficient of variation of the maximum bending moment using analytical method (obtained from 1000 simulations).*

Again, the difference between $E\left[\overline{M}\right]$ and $Var\left[\overline{M}\right]$ from the numerical simulation and *E[M]* and *Var[M]* from the analytical analysis is due to the influence of the intrinsic spatial variability of E_s along the buried pipe.

For this location, it can be calculated the contribution of the maximum bending moment M to the maximum total bending moment $\overline{M}$ and the contribution of the variance of the maximum bending moment to the total variance respectively from ratios $E[M]/E[\overline{M}]$ and $Var[M]/Var[\overline{M}]$.

The contribution of the maximum bending moment to the maximum total bending moment is about 82% and the contribution of the variance of the maximum bending moment to the total variance is close to 10%. The latter value shows again the great influence (90%) of the spatial variability of E_s along the buried pipe (intrinsic spatial variability) in the variance of $\overline{M}$. This influence is reported, on average, on the maximum bending moment with a contribution of the intrinsic spatial variability on the maximum total bending moment of 18%.

As in the case of continuous spread footing, it is shown that the spatial variability of soil properties adds a significant part of uncertainty in the differential settlement and the bending moment.

4.5. Summary and conclusions

In this chapter the geological conditions of a studied construction site and available data from the geotechnical and geophysical investigations were presented. Appropriate geostatistical methods were used to improve the quality of geotechnical data and bring more information to the soil spatial variability at the construction site. We showed how to improve one's knowledge of the mechanical characteristics at the construction site by using a combination of geotechnical and geophysical information and employing collocated co-kriging. This information was then coupled with a finite element method (CASTEM© software) to take into account the influence of the spatial variability of soil modulus on the maximum differential settlements and the maximum bending moments for the considered superficial geotechnical designs (continuous spread footing and buried pipe) at the construction site. The analysis of these statistical and geostatistical results makes it possible to develop decision support tools and to describe the longitudinal behavior of superficial geotechnical designs when they are located at different positions on the construction site. A comparison of analytical and numerical results shows the importance of the influence of the spatial variability of soil modulus and the importance of the choice

of the semi-empirical model on the behavior of these superficial geotechnical designs. It also shows that the uncertainty on differential settlement and bending moment is always more important when the spatial variability of soil properties is considered.

Finally, the results obtained here show, for continuous spread footings (for residential houses) and buried pipes, that the longitudinal behavior of the structure is as important as the transverse behavior. Specific consideration is required to adapt the design of individual houses and buried pipes to a construction site whose soil properties are characterized by spatial variability.

Chapter 5

General conclusion and future research directions

5. General conclusion and future research directions

5.1. General summary and conclusions

In geotechnical designs, the soil beneath structure exhibits spatial heterogeneities resulting from the history of its deposition and aggregation processes, which occur in different physical and chemical environments. This inherent or natural variability can be very important in the behavior of the superficial geotechnical systems inducing differential settlements, whose consequences on structural response can be harmful: local failures, cracking in beams or walls, leakage in sewers. The uncertainty can also exist in structure mechanical and geometrical parameters.

The main objective of this thesis was to take into consideration:

- uncertainty in the mechanical properties of soil,
- spatial variability in the mechanical properties of soil,
- uncertainty in structure mechanical properties,
- uncertainty in structure geometrical parameters

in order to estimate the uncertainty in differential settlement and bending moment of two superficial geotechnical works: continuous spread footing and buried concrete or steel pipe.

Arriving at a realistic model, for example using Mohr-Coulomb or Cam-Clay models, is complicated in foundation analysis by the extreme difficulty of acquiring the exact property parameters of soil. Thus, we chose to use Winkler's analytical approach with only one parameter (subgrade soil reaction modulus) to model the soil-structure interaction instead of modeling the subsoil in all its complexity, which seems, from a practical point of view, to be appropriate for superficial geotechnical designs.

Eight semi-empirical models which give the coefficient of subgrade reaction were studied by considering soil and structure uncertainties. The FOSM and SOSM methods were used on these semi-empirical models to determine the coefficient of variation of soil reaction modulus. Results obtained using the FOSM method for the spread footings show the major effects of the uncertainties of soil modulus, Poisson's ratio and the width of the continuous spread footing on the uncertainty of the coefficient of subgrade reaction. For the latter, results for the buried pipes show the major effects of the uncertainties of soil modulus, the external diameter of buried concrete or steel pipe and Poisson's ratio of soil

on the uncertainty of the coefficient of subgrade reaction (k_s). We showed that if the additional amount of accuracy resulting from the SOSM method was insignificant then the FOSM method alone would be sufficient to correctly estimate the coefficients of variation of k_s.

We proposed, for each model semi-empirical, simplified expressions that take into account the minimum parameters for determining the coefficient of variation of soil-reaction modulus. These different relationships give to the practitioner a quick estimate of the uncertainty of the soil-reaction modulus.

We then studied the incorporation of uncertainty of k_s in the Winkler analytical model, using simplified expressions and the influence of this uncertainty on the differential settlement and bending moment in the longitudinal direction of spread footings and buried pipelines. The FOSM method was used again on the analytical solution of a beam on an elastic foundation from Winkler's hypothesis and with different boundary conditions.

Results from the FOSM method, for a spread footing, show that the uncertainties of the differential settlement (CV_Δ) and the bending moment (CV_M) are very different depending on the length of a spread footing and the boundary conditions considered in order model a zone of weak soil at the construction site. Whatever for the differential settlement or bending moment, the obtained results concerning the probability of the serviceability limit state (P_{SLS}) show the importance of the choice of semi-empirical model and the boundary conditions. For the semi-empirical model and the boundary conditions selected, when the uncertainty on the value of k_s is high, the probability of the serviceability limit state can be exceeded even if the soil has good mechanical properties.

Results in the case of buried pipes show two things. The uncertainties of the differential settlement and the bending moment are very different depending on the length of the low stiffness zone beneath the buried pipe and its value of E_s. Additionally, these uncertainties are more influenced by the length of the low stiffness zone than the value of the subgrade reaction modulus. From a practical point of view, this indicates that an accurate knowledge of soil is more important in determining low stiffness zone lengths than properties of soil in case of soil reconnaissance for buried pipes.

In the case where the choice of a suitable semi-empirical model for the estimation of the uncertainty on k_s is not straightforward, a global uncertainty approach is proposed. This approach includes the uncertainties from each semi-empirical model and can be used to

verify whether the maximum values exceed the serviceability values for the ultimate limit state.

A comparison between the FOSM and Monte Carlo analysis results was performed and the results were similar. This is to be expected given the low non-linearity of the model.

In our analytical approach it was not possible to consider the soil characteristics as different at each given location along the spread footing and buried pipe axes. We coupled the finite element method (CASTEM© software) with geostatistical methods (ISATIS©), in order to take into account the correlation length of soils parameters along the pipe axis and spread footing to characterize the spatial variability of soil.

It was shown, using data from a real construction site, how the combination of the geotechnical and geophysical information can improve by using collocated cokriging knowledge of the mechanical characteristics of the site. The analysis of these statistical and geostatistical results makes it possible to describe the behavior of the superficial geotechnical designs when they are constructed on different locations at the construction site. A comparison between analytical and numerical results shows the importance of the influence of the spatial variability of soil modulus and the importance of the choice of the semi-empirical model on the behavior of these superficial geotechnical systems. It also shows that the uncertainty on differential settlement and bending moment is always more important where the spatial variability of soil properties are considered.

Finally, the results obtained here show, in the case of continuous spread footings for residential houses and buried pipes, the importance of the longitudinal behavior of these structures and the significance of uncertainty in their design. Specific consideration is required to adapt the design of individual houses and buried pipes to a construction site whose soil properties are characterized by spatial variability.

5.2. Future research directions

Based on the work performed in this research, the following directions for future work can be proposed:

a) The same work can now be studied with different analytical models taking into account more parameters such as Vlassov & Pasternak models with two parameters, or Kerr's model with three parameters, in order to compare the uncertainties on the differential

settlement and the bending moment from these models with those obtained from the Winkler model in this study.

b) Development of the analytical model can be performed considering three different zones of soil beneath the considered superficial geotechnical systems. Furthermore, this would help us to choose suitable boundary conditions for these geotechnical systems in our analytical computations since the boundary conditions have a strong influence on the uncertainty of differential settlement and bending moment.

c) Shrinkage-swelling phenomena in clay soils have their origins in the mineralogical composition and texture of the soil. These predisposing factors, associated with strong climatic variations and a succession of intensely dry periods in particular, have been responsible for numerous natural disasters in superficial geotechnical systems in France. It would be interesting to take into consideration these phenomena with associated uncertainties for their design.

d) We can study, at a real construction site, the effect of joints in a buried concrete pipe along a low stiffness zone length, and compare the results with those obtained in this thesis which did not consider joints.

e) In this thesis, the uncertainties of the geometrical parameters, the width and the height of spread footing and the external diameter of buried pipe are only taken into account in the estimate of the coefficient of variation of the subgrade reaction modulus. These uncertainties were not considered in the calculation of the moment of inertia of the cross section of these structures. It would be interesting to also consider the uncertainties of these parameters in the calculation of the moment of inertia in the deformation equation for these structures.

f) In this study, only the uncertainty of Young's soil modulus was considered in a geostatitical approach coupled with a finite element method. The uncertainties of geometrical parameters of spread footings and buried pipes can also be considered in a geostatistical approach in order to propose a complete reliability analysis for these structures.

j) We can take into account the uncertainty related to the spatial variation of the load for the buried pipes.

h) We can extend the study of the effects of the uncertainties of soil and structure parameters on the differential settlements and the bending moments for superficial geotechnical systems in two or three dimensions.

References

References

Adler RJ., 1981. ″The geometry of random fields″. Chichester, New York, John Wiley & Sons.

Alfaro M., 1979. ″Etude de la robustesse de fonctions aléatoires″. Thèse de doctorat, E.N.S. des mines de Paris, France.

Al-sanad HA., Ismael NF., Brenner RP., 1993. ″Settlement of circular and ring plates in very dense calcareous sands″. Journal of Geotechnical Engineering, ASCE, Volume 119(4), pp. 622-638.

Andrieux C., Chrétien M., Denis A., Fabre R., Lataste JF., 2011. ″Shrinkage and swelling of clay soil, Comparison between laboratory and in situ measurements″. European Journal of Environnemental and Civil Engineering, Volume 5, pp. 819-838.

Ang AHS., Tang, WH., 1984. ″Probability concepts in engineering planning and design″. Vol. 2: Decision, risk, and reliability. John Wiley & Sons Inc., New York, N.Y.

ASTM, 1994. ″Test method for bearing capacity of soil for static load on spread footings″. D 1194-94, Annual Book of ASTM Standards, 4.08. American Society for Testing and Materials, West Conshocken, PA.

Auvinet G., Mellah R., Masrouri F., Rodriguez JF., 2005. ″La méthode des éléments finis en géotechnique″. Revue Française de Géotechnique, N°93, 4ième trimestre, pp. 67-79.

Avramidis IE., Morfidis K., 2006. ″Bending of beams on three-parameter elastic foundation″. International Journal of Solids and Structures, Volume 43(2), pp. 357-375.

Bacconnet C., 1991. ″Géostatistique et géotechnique, application à la reconnaissance des sols″. Thèse de doctorat, Université Blaise Pascal – Clermont II, France.

Baecher GB., Christian JT., 2003. ″Reliability and statistics in geotechnical engineering″. John Wiley & Sons.

Balkaya M., Moore ID., Saglamer A., 2012a. ″Study of non-uniform bedding due to voids under jointed PVC water distribution pipes″. Geotextiles and Geomembranes, October, Volume 34, pp. 39-50.

Balkaya M., Moore, I., and Sağlamer, A., 2012b. ″Study of nonuniform bedding support because of erosion under cast iron water distribution pipes″. Journal of Geotechnical and Geoenvironmental Engineering, 138(10), pp. 1247–1256. doi: 10.1061/(ASCE)GT.1943-5606.0000689.

Benjamin JR., Cornell CA., 1970. ″Probability statistic and decisions for civil engineers″. Mc Graw Hill, New York. USA.

Benson AK., Payne KL., Stubben MA., 1997. ″Mapping groundwater contamination using dc resistivity and VLF geophysical method, a case study″. Geophysics, Volume 62, pp. 80–86.

Biot MA., 1937. ″Bending of infinite beams on an elastic foundation″. Journal of Applied Mechanics, the American Society of Mechanical Engineers, Volume 59: A1–A7.

Bjerrum L., 1963. ″Discussion on proceedings of the european conference of soils mechanics and foundations engineering″. Norwegian Geotech Inst. Publ., No 98, Oslo, Norway, Volume 3, pp.1-3.

Bourges M., Mari JL., Jeannée N., 2012. ″A practical review of geostatistical processing applied to geophysical data: methods and applications″. European Association of Geoscientists & Engineers, Geophysical Prospecting, Volume 60, Issue 3, pp. 400–412.

Bowles JE., ″Foundation analysis and design″. New York: McGraw-Hill Book Co; 1988.

Braga A., Malagutti W., Dourado J., Chang H., 1999. ″Correlation of electrical resistivity and induced polarization data with geotechnical survey standard penetration test measurements″. Journal of Environmental and Engineering Geophysics Volume 4, pp.123–130.

Brockwell PJ., Davis RA., 1987. ″Time series: theory and methods″. Springer-Verlag, New York.

Bruxer J., 2011. ″Uncertainty analysis of Lake Erie Net Basin Supplies as computed using the residual method″. dissertation, McMaster University, Hamilton, Ontario, Canada.

Buco J., Emeriault F., Kastner R., 2008a. ″3D numerical analyses of the soil variability impact on longitudinal behavior of buried pipes″. 12th IACMAG, Goa, India, 1-6 October, pp. 3827- 3834.

Buco J., Emeriault F., Kastner R., 2008b. ″Full-scale experiment determination of concrete pipe joint behavior and its modeling″. Journal of Infrastructure Systems, Volume 14(3).

Buco J., Emeriault F., Le Gauffre P., Kastner R., 2006. ″Statistical and 3D numerical identification of pipe and bedding characteristics responsible for longitudinal behaviour of buried pipes″. ASCE Conference Pipelines, Chicago, USA.

Cassan M., 1978. ″Les essais in situ en mécanique des sols″. Tome II. Editions Eyrolles, Paris.

Chilès JP., Blanchin R., 1995. ″Contribution of geostatistics to the control of the geological risk in civil-engineering projects: the example of the Channel Tunnel″. In Application of Statistics and Probability, Lemaire, Favre & Mébarki (eds), Blakeme, Rotterdam.

Chilès JP., Delfiner P., 1999. ″Geostatistics: modeling spatial uncertainty″. Wiley Series in Probability and Statistic. Wiley.

Cho SE., 2007. ″Effects of spatial variability of soil properties on slope stability″. Engineering Geology, N°92, pp. 97-109.

Cho SE., Park HC., 2010. ″Effect of spatial variability of cross-correlated soil properties on bearing capacity of strip footing″. International Journal for Numerical and Analytical Methods in Geomechanics, Volume 34, pp.1-26, DOI: 10.1002/nag.791.

Chowdhury RN., 1984. ″Recent developments in landslide studies: probabilistic methods″. In Proceedings of the 4th International Symposium on Landslides, Toronto, Ont., September 16-21. Canadian Geotechnical Society, Volume 1, pp. 209–228.

Christakos G., 1992. ″Random field models in earth sciences″. San Diego, Academic Press.

Christakos G., 2000. ″Modern spatiotemporal geostatistics″. New York, Oxford University Press.

Christakos G., Hristopulos DT., 1998. ″Spatiotemporal environmental health modeling: a tractatus stochasticus″. Boston, MA, Kluwer Academic Publishers.

Cosenza P., Marmet E., Rejiba F., Cui YJ., Tabbagh A., Charlely Y., 2006. ″Correlation between geotechnical and electrical data: a case study at Garchy in France″. Journal of Applied Geophysics, Volume 60, pp. 165–178.

Council on tall buildings and urban habitat, committee 43, 1993. ″Semi-Rigid connections in steel frames″. New York: McGraw-Hill.

Dawson KD., Baise LG., 2005. ″Three-dimensional liquefaction hazard analysis using geostatistical interpolation″. Soil Dynamics and Earthquake Engineering, Volume 25 (5), pp. 369–381.

Deck O., Singh A., 2012. ″Analytical model for the prediction of building deflections induced by ground movements″. International Journal for Numerical and Analytical Methods in Geomechanics, Volume 36(1), pp. 62-84.

Denis A., Elachachi SM., Niandou H., 2011. ″Effects of longitudinal variability of soil on a continuous spread footing″. Engineering Geology, Volume 122(3-4), pp. 179-190

Denis, A., Marache, A., Obéllianne, T., Breysse, D., 2002. ″Electrical resistivity borehole measurements: application to an urban tunnel site″. Journal of Applied Geophysics Volume 50 (3), pp. 69–81.

Det Norske Veritas (DNV), 2007. ″Statistical representation of soil data″. Recommended practice DNV-RP-C207, printed in Norway

Dettinger MD., Wilson JL., 1981. ″First order analysis of uncertainty in numerical models of groundwater flow″. 1, Mathematical development, Water Resour. Res., Volume 17(1), pp. 149-161.

Deutsch CV., 2002. ″Geostatistical reservoir modeling″. Oxford University Press, Oxford, N.Y.

Deutsch CV., Journel AG., 1998. ″GSLIB geostatistical soft- ware library″. Oxford University Press, Oxford, New York.

Dowd PA., 2003-2004. ″MINE5280 Non-linear Geostatistics″. Notes on MSc. in Mineral Resources and Environmental Geostatistics, University of Leeds, Leeds, U.K.

Dubost J., Denis A., Marache A., Breysse D., 2011. ″Effect of uncertainties in soil data on settlement of soft columnar inclusions″. Engineering Geology, Volume 121(3-4), pp. 123-134, doi:10.1016/j.enggeo.

Dubost J., Denis A., Marache A., Chanson M., 2007. ″Probabilistic FEM analysis of railway-platform settlements″. In: Pande, G.N., Pietruszczak, S. (Eds.), International Symposium on Numerical Model in Geomechanics, NUMOG X. Taylor & Francis, Rhodes, Greece, pp. 525–530.

Dubreuilh J., 1976. ″Contribution à l'étude sédimentologique de système fluviatile Dordogne-Garonne dans la région bordelaise″. Thèse de doctorat, Université Bordeaux 1, France.

Duncan JM., 2000. ″Factors of safety and reliability in geotechnical engineering″. Journal of Geotechnical and Geoenvironmental Engineering, Volume 126(4), pp. 307-316.

Dutta SC., 2000. ″Seismic torsional behavior of elevated tanks for improved code provisions: elastic behavior″. J Inst Engrs (India), Volume 80, pp.169–81.

Dutta, SC., Roy R., 2002. ″A critical review on idealization and modeling for interaction among soil-foundation-structure system″. Computers and Structures, Volume 80, pp. 1579-1594.

Einstein H., Baecher GB., 1982. ″Probabilistic and statistical methods in engineering geology, Problem statement and introduction to solution″. Rock Mech., Suppl., Volume 12, pp. 47-61.

Einstein H., Baecher GB., 1983. ″Probabilistic and statistical methods in engineering geology; specific method and example - part 1: exploration″. Rock Mechanics and Rock Engineering Volume 16, pp. 39–72.

El Gonnouni M., Riou Y., Hicher PY., 2005. ″Geostatistical method for analysing soil displacement from underground urban construction″. Geotechnique, Volume 55, N°2, pp. 171- 182.

Elachachi SM., Breysse D., Benzeguir H., 2011. ″Soil spatial variability and structural reliability of buried networks subjected to earthquakes″. Computational Methods in Applied Sciences, Volume 22, pp. 111-127, doi: 10.1007/978-90-481-9987-7-6.

Elachachi SM., Breysse D., Denis A., 2012. ″The effect of soil spatial variability on reliability of rigid buried pipes″. Computers and Geotechnics, Volume 43, pp. 61-71.

Elachachi SM., Breysse D., Houy L., 2004. ″Longitudinal variability of soils and structural response of sewer networks″. Computers and Geotechnics, Volume 31, pp. 625-641.

Elkadi AS., Huisman M., 2002. ″3D-GIS geotechnical modelling of tunnel intersection in soft ground: the Second Heinenoord Tunnel, Netherlands″. Tunnelling and Underground Space Technology, N°17, pp. 363-369.

Elkateb T., Chalaturnyk R., Robertson PK., 2003. ″An overview of soil heterogeneity: quantification and implications on geotechnical field problems″. Can Geotech J, Volume 40(1), pp. 1-15.

El-Ramly H., 2001. ″Probabilistic and quantitative risk analysis for earth slopes″. PhD thesis, university of Alberta, Edmonton, Alta.

Emeriault F., Breysse D., Kastner R., Denis A., 2004. ″Geotechnical survey and mechanical parameters in urban soils: modelling soil variability and inferring representative values using the extension of Lyon subway lined as case study″. Canadian Geotechnical Journal, Volume 41, pp. 773-786.

Endres AL., Clement, WP., 1998. ″Relating cone penetrometer test information to geophysical data: a case study″ . Symposium on the Application on Geophysics and Engineering and Environmental Problems (SAGEEP98), Chicago. USA.

Eurocode 1 (EC1), 1991. ″Basis of design and actions on structures″. ENV.

Evans M., Hastings N., Peacock B., 2000. ″Statistical distributions″. 3rd edn. New York: Wiley.

Fenton GA., Griffiths DV., 2002. ″Probabilistic foundation settlement on spatially random soil″. Journal of Geotechnical and Geoenvironmental Engineering Volume 128(5), pp. 381-390.

Fenton GA., Griffiths DV., 2003. ″Bearing capacity prediction of spatially random c- φ soils″. Can Geotech J Volume 40, pp. 54-65.

Fenton GA., Griffiths DV., Williams MB., 2005. ″Reliability of traditional retaining wall design″. Geotechnique, Volume 55, N°1, pp. 55-62.

Fenton GA., Vanmarcke E., 1990. ″Simulation of random fields via local average subdivision″. Journal of Engineering Mechanics, Volume 116(8), pp. 1733-1749.

Filonenko-Borodich MM., 1940. ″Some approximate theories of elastic foundation Uchenyie Zapiski Moskovskogo Gosudarstvennogo Universiteta [in Russian] Mekhanica″. pp. 46:3-18.

Frantziskonis G., Denis A., 2003. ″Complementary entropy and wavelet analysis of drilling-ability data″. Mathematical Geology, Volume 35 (1), pp. 89-103.

Gorbunov-Posadov GI., 1949. ″Beams and plates on elastic base (in Russian) Moscow″. USSR: Stroizdat.

Graettinger AJ., Dowding CH., 1999. ″Directing exploration with 3D FEM sensitivity and data uncertainty″. Journal of Geotechnical and Geoenvironmental Engineering Volume 125 (11), pp. 959–967.

Griffiths DV., Fenton GA., 2000. ″Influence of soil strength spatial variability on the stability of an undrained clay slope by finite elements″. In: Slope stability. Geotechnical Special Publications No. 101, ASCE, pp. 184-193.

Griffiths DV., Fenton GA., 2007. ″Probabilistic methods in geotechnical engineering″. Published:[S.l.]: Springer Wien NewYork, , ISBN:9783211733653- 3211733655, International Centre for Mechanical Sciences.

Harr ME., 1977. ″Mechanics of particulate media-a probabilistic approach″. MacGraw-Hill.

Harr ME., 1987. ″Reliability based design in civil engineering″. Dover Publications Inc.

Hasofer AM., Lind NC., 1974. ″An exact and invariant first-order reliability format″. Journal of the Engineering Mechanics Division, ASCE 100, pp. 111-121.

Hetenyi M., 1946. ″Beams on elastic foundations″. University of Michigan Press.

Hetenyi M., 1950. ″A general solution for the bending of beams on an elastic foundation of arbitrary continuity″. J Appl Phys, Volume 21, pp. 55-8.

Houy L., Breysse D., Denis A., 2005. ″Influence of soil heterogeneity on load redistribution and settlement of a hyperstatic three-support frame″. Geotechnique, Volume 55(2), pp.163-170.

Huang An-bin, April 2008. ″Geotechnical and geophysical site characterization″. ISBN: 9780415469364, Proceedings of the Third International Conference on Site Characterization ISC'3, Taipei, Taiwan, Editors: Huang, An-Bin, Mayne, Paul W., Publisher:Taylor & Francis Group, Subject: Civil, Series: Balkema: Proceedings and Monographs in Engineering, Water and Earth Sciences, Pages: 249.

Huijbregts CJ., Davis JC., Mc Cullagh MJ., (Eds.), 1975. ″Regionalized variables and quantitative analysis of spatial data″. Display and Analysis of Spatial Data. John Wiley, New York.

Hwang, D., Karami, HA., Byun, DW., 1998. ″Uncertainty analysis of environmental models within GIS environments″. Computers & Geosciences, Volume 24 (2), pp. 119–130.

Imanzadeh S., Denis A., Marache A., 2011. ″Estimation de la variabilité du module de réaction pour l'étude du comportement des semelles filantes sur sol élastique″. 29èmes rencontres universitaires de Génie Civil – AUGC, Tlemcen, Algérie, pp. 145-154.

Imanzadeh S., Denis A., Marache A., 2013a. "Effect of uncertainty in soil and structure parameters for buried pipes". Geotechnical and Geophysical Site Characterization 4 – Coutinho & Mayne (eds) © 2013 Taylor & Francis Group", pp. 1847-1853, London, ISBN 978-0-415-62136-6.

Imanzadeh S., Denis A., Marache A., 2013b. "Simplified uncertainties analysis of buried steel pipes on elastic foundation in the presence of low stiffness zones". Computers and Geotechnics, pp. 62-71.

Isaaks EH., Srivastava RM., 1989. "An introduction to applied geostatistics". Oxford University Press, New York. pp. 560.

jaksa MB., Brooker PI., Kaggwa WS., 1997. "Inaccuracies associated with estimating random measurement errors". ASCE Journal of Geotechnical and Geoenvironmental Engineering, Volume 123 (5), pp. 393–401.

Jaksa MB., 1995. "The influence of spatial variability on the geotechnical design properties of a stiff, overconsolidated clay". Thesis of the University of Adelaide, Australia.

Jaksa MB., Fenton GA., 2002. "Assessment of fractal behavior of soils". In: Proc. Int. Conf. on Probabilistics in GeoTechnics: Technical and Economic Risk Estimation, Eds: Pöttler, R., Klapperich and Schweiger H., Graz Austria, United Engineering Foundation, New York, pp. 47–54.

Jimenez R., Sitar N., 2009. "The importance of distribution types on finite element analyses of foundation settlement". Computers and Geotechnics, Volume 36(3), pp. 474–483.

Journel A., 1989. "Fundamentals of geostatistics in five lessons, short course in geology". Volume 8, American Geophysical Union,Washington, D.C.

Journel AG., 1977. "Géostatistique minière". Centre de Géostatistique, Fontainebleau, France.

Journel AG., Huijbregts JCH., 1978. "Mining geostatistics". Academic Press, London, pp.600.

Kerr AD., 1964. "Elastic and viscoelastic foundation models". J Appl Mech Trans ASME, Volume 31(4), pp. 491–8.

Kerr AD., 1965. "A study of a new foundation model". Acta Mechanica, Volume I (2), pp.135–147.

Khalfaoui S., Mezghache 2005. "Évaluation géostatistique de la maille de reconnaissance géotechnique de l'aérodrome de Batna (N-E algérien) ". Revue Française de Géotechnique, n°111, 2ème trimestre.

Kloppel K., Glock D., 1979 "Theoretische und experimentelle untersuchungen zu den traglastproblemen beigewiecher, in die erde eingebetteter rohre". Veröffentlichung des Instituts Statik und Stahlbau der Technischen Hochschule Darmstadt, H-10.

Kolmogorov AN., 1941 "Interpolirovanie i ekstrapolirovanie statsionamykh sluchainykh posledovate1'nostei (Interpolated and extrapolated stationary random sequences)". Iivestiya AN SSSR, seriya matematicheskaya 5, No. 1.

Koutsourelakis S., Prevost JH., Deodatis G., 2002. "Risk assessment of an interacting structure-soil system due to liquefaction". Earthquake Eng Struct Dyn, Volume 31:851-79.

Krige DG., 1951. "A statistical approach to some basic mine evaluation problems on the Witwatersrand", 1. Chem. Metall. and Mining Soc. of 5.Afr., Volume 52, pp. 119-39.

Krige DG., 1966. "Two-dimensional weighted moving average trend surface for ore evaluation". S. Afr. Inst, of Mining and Metall, Volume 66, pp. 13-38.

Krige, DG., Guarascio M., Camisani-calzolari FA., 1989. "Early South African geostatistical techniques in today's perspective", in Armstrong m., (ed.) Geostatistics, volume I (Kluwer, Dordrecht) pp. 1-19.

Kulhawy FH., 1992. "On the evaluation of soil properties". ASCE Geotech. Spec. Publ., Volume 31, pp. 95-115.

Kulhawy FH., Roth MS., Grigoriu MD., 1991. "Some statistical evaluation of geotechnical properties". In Proceedings of the 6th International Conference on Applications of Statistics and Probability in Civil Engineering, Mexico City, Volume 2, pp. 705–712.

Kunstmann H., Kinzelbach W., Siegfried T., 2002. "Conditional first-order second-moment method and its application to the quantification of uncertainty in groundwater modelling". Water Resources Research, Volume 38(4), pp.6-1 to 6-15.

Lacasse S., Nadim F., 1996. "Uncertainties in characterizing soil properties in uncertainty in the Geologic Environment: From Theory to Practice". ShacklefordCD, NelsonPP, RothMJS (eds). ASCE Geotechnical Special Publication No. 58. ASCE: New York, pp. 49–75

References

Lacasse S., Nadim F., 1997. "Uncertainties in characterizing soil properties". Norwegian Geotechnical Institute, Oslo, Norway, Volume, 201, pp. 49–75.

Lacasse S., Nadim F., 2007. "Probabilistic geotechnical analyses for offshore facilities". Georisk: Assessment and Management of Risk for Engineered Systems and Geohazards, Volume 1, N°1, pp. 21-42.

Largueche F., 2006. "Estimating soil contamination with kriging interpolation method". American Journal of Applied Sciences, DOI:10.3844/ajassp.2006.1894.1898, pp. 1894-1898.

Laslett GM., Mcbratney AB., Pahl PJ., Hutchinson MF., 1987. "Comparison of several spatial prediction methods for soil pH", 1. Soil Sci., Volume 38, pp. 325-41.

Lenz, J., Baise, LG., 2007. "Spatial variability of liquefaction potential in regional mapping using CPT and SPT data". Soil Dynamics and Earthquake Engineering, Volume 27 (7), pp. 690–702.

Li KS., Lumb P., 1987. "Probabilistic design of slopes". Canadian Geotechnical Journal Volume 24, pp. 520–535.

Limpert E., Stahel W., Abbt M., 2001. "Log-normal distributions across the sciences: keys and clues". BioScience, Volume 51(5), pp. 341–52.

Low BK., 2005. "Reliability-based design applied to retaining walls". Geotechnique, Volume 55, N°1, pp. 63-75.

Low BK., 2008. "Efficient probabilistic algorithm illustrated for a rock slope". Rock Mech Rock Eng, Volume 41(5), pp.715–34.

Lumb P., 1966. "The variability of natural soils". Canadian Geotechnical Journal, Volume 3, pp. 74-97.

Madsen HO., Krenk S., Lind NC., 1986. "Methods of structural safety". Prentice-Hall, Englewood Cliffs, N.J.

Magnan JP., Deroy JM., 1982. "Analyse graphique des tassements observés sous les ouvrages". Bull. liaison Labo P. et Ch., N°109, pp. 45-52.

Major G., Ross-Brown DM., Kim H-S. 1978. "A general probabilistic analysis for three-dimensional wedge failures". In Proceedings of the 19th U.S. Symposium on Rock Mechanics, Stateline, Nev., 1–3 May, pp. 45–56.

Marache A., Dubost J., Breysse D., Denis A., Dominique S., 2009a. "Understanding subsurface geological and geotechnical complexity at various scales in urban soils using a 3D model". Georisk, Volume 3 (4), pp. 192–205.

Marache A., Breysse D., Piette C., Thierry P., 2009b. "Geological and geotechnical modeling at the city scale using statistical and geostatistical tools". The Pessac case (France). Engineering Geology, Volume 107(3-4), pp. 67-76.

Marcotte D., 2003. "Cours de géostatistique minière". Document de cours de l'École Polytechnique de Montréal.

Massih DSYA., Soubra AH., Low BK., 2008. "Reliability-based analysis and design of strip footings against bearing capacity failure". Journal of Geotechnical and Geoenvironmental Engineering, Volume 134, N°7, ASCE, pp. 917-928.

Matheu EE., Suarez LE., 1996. "Eigenvalue analysis of structures with flexible random connections". Struct Engng Mech, Volume 4(3), pp. 277–301.

Matsubara K., Hoshiya M., 2000. "Soil spring constants of buried pipelines for seismic design". J Eng Mech ASCE; Volume 126(1), pp. 76–83.

Melchers RE., 2002. "Structural reliability analysis and prediction". 2nd ed. Chichester: John Wiley & Sons.

Mendes RM., Lorandi R., 2008. "Analysis of spatial variability of SPT penetration resistance in collapsible soils considering water table depth". Engineering Geology, Volume 101, pp. 218–225.

Meyerhof GG., Baikie LD., 1963. "Strength of steel sheets bearing against compacted sand backfill". Highway research board proceedings 30.

Monnet J., Ploto P., 2008. "Méthodes de reconnaissance croisées pour l'analyse de stabilité des digues soumises à érosion interne". Studia Geotechnica et Mechanica, Volume XXX, No. 1-2, pp.21-30.

Morfidis K., 2007. "Exact matrices for beams on three-parameter elastic foundation". Computers and Structures, Volume 85, pp. 1243-1256.

Nascimento V., Simoe A., 1957 "Relation between CBR and modulus of strength". Proc. 4th Int. Conf. on Soil Mechanic and Foundation Engineering, London, pp. 166-168.

Nguyen VU., Chowdhury RN., 1985. "Simulation for risk analysis with correlated variables". Géotechnique, Volume 35, pp. 47-58.

Niandou H., Breysse D., 2007. "Reliability analysis of a piled raft accounting for soil horizontal variability". Computers and Geotechnics, Volume 34, pp. 71–80.

Niandou H., La Borderie C., Breysse D., 2009 "Influence de l'hétérogénéité tridimensionnelle des sols sur un radier". 27èmes rencontres universitaires de Génie Civil – AUGC.

Nobahar A., 2003. "Effects of soil spatial variability on soil-structure interaction". PhD Thesis, Memorial University, St. John's, NL.

Nobahar A., Popescu R., 2000. "Spatial variability of soil properties-effects on foundation design". Proceedings of 53rd Canadian geotechnical conference, Montreal, Québec. Volume 2, pp. 1139-1144.

Norme NF P 16-341, 1990. "Evacuations, assainissement. Tuyaux circulaires en béton armé et non armé pour réseaux d'assainissement sans pression". Définitions, spécifications, méthode d'essai, marquage, conditions de réception.

Nour A., Slimani A., Laouami N., 2002. "Foundation settlement statistics via finite element analysis". Comput Geotechn, Volume 29, pp. 641–72.

Okeagu B., Abdel-Sayed G., 1984. "Coefficients of soil reaction for buried flexible conduits". Journal of Geotechnical Engineering, ASCE, Volume 110(7), pp. 908-922.

Oskooi B., Pedersen LB., 2005. "Comparison between VLF and RMT methods. A combined tool for mapping conductivity changes in the sedimentary cover". Journal of Applied Geophysics Volume 57, pp. 227–241.

Paice GM., Griffiths DV., 1996. "Fenton GA. Finite element modeling of settlements on spatially random soil". J Geotechn Eng., Volume 122(9), pp. 777–9.

Paice GM., Griffiths DV., Fenton GA., 1994. "Influence of spatially random soil stiffness on foundation settlement". In Proceedings of the Conference on Vertical and Horizontal Deformation of Foundations and Embankments, Part 1 (of 2), College Station, Tex., pp. 628–639.

Paikowsky GS., 2002. "Load and resistance factor design (LRFD) for deep foundation. Foundation design codes in view of international harmonization and performance". IWS Kamakura, Japan, 10–12 April, pp.59-94.

Palisade Corporation, 1996. "@Risk: Risk analysis and simulation add-in for Microsoft Excel or Lotus 1–2–3", NY.

Papadrakis M., Papadopoulos V., Lagaros N., 1996. "Structural reliability analysis of elastic-plastic structures using neural networks and Monte Carlo simulation". Comput Methods Appl Mechan Eng, Volume 136(1), pp. 145-63.

Park HJ., West TR., Woo I., 2005. "Probabilistic analysis of rock stability and random properties of discontinuity parameters". Intersate Highway 40, Western North Carolina, USA. Engineering Geology Volume 79, pp. 230–250.

Parsons RL., Frost JD., 2002. "Evaluating site investigation quality using GIS and geostatistics". Journal of Geotechnical and Geoenvironmental Engineering, Volume 128, N°6, pp. 451-461.

Parzen E., 1964. "Stochastic processes". San Francisco, Holden-Day.

Pasternak PL., 1954. "On a new method of analysis of an elastic foundation by means of two foundation constants (in Russian)". Gosudarstvennoe Izdatelstvo Literaturi po Stroitelstvu i Arkhitekture. Moscow: USSR.

Pate-Cornell ME., 1987. "Risk uncertainties in safety decisions. Reliability and risk analysis in civil engineering". In Proceedings of the ICASP5, the 5th International Conference on the Application of Statistics and Probability in Soil and Structural Engineering, Vancouver, B.C. Volume 1, pp. 538–545.

Phoon KK., 1995. "Reliability-based design of foundations for transmission line structures". Ph.D. dissertation, Cornell University, Ithaca, N.Y.

Phoon KK., Kulhawy FH., 1999a. "Evaluation of geotechnical property variability". Canadian Geotechnical Journal, Volume 36, pp. 625-639.

Phoon KK., Kulhawy FH., 1999b "Characterization of geotechnical variability". Canadian Geotechnical Journal, Volume 36, pp. 612–624.

Phoon KK., Kulhawy FH., 2005. "Characterisation of model uncertainties for laterally loaded rigid drilled shafts". Géotechnique Volume 55(1), pp. 45–54.

Popescu R., 1995. "Stochastic variability of soil properties: data analysis, digital simulation, effects on system behavior". PhD Thesis, Princeton University, Princeton, NJ;

Popescu R., Deodatis G., Nobahar A., 2002. "Bearing capacity of heterogeneous soils-a probabilistic approach". In: Proceedings of 55th Canadian geotechnical conference, Niagara Falls, ON, pp. 1021–1028.

Popescu R., Deodatis G., Nobahar A., 2005. "Effects of random heterogeneity of soil properties on bearing capacity". Probabilistic Engineering Mechanics, Volume 20, pp. 324–341.

Popescu R., Prevost JH., Deodatis G., 1997. "Effects of spatial variability on soil liquefaction: some design recommendations". Geotechnique, Volume 47(5), pp. 1019-36.

Raspa G., Moscatelli M., Pio Stigliano F., Patera A., Marconi F., Folle D., Vallone R., Mancini M., Cavinato GP., Milli S., Coimbra Leite Costa JF., 2008. "Geotechnical characterization of the upper Pleistocene–Holocene alluvial deposits of Roma (Italy) by means of multivariate geostatistics: cross-validation results". Engineering Geology, Volume 103 (3–4), pp. 251–268.

Sadrekarimi J., Akbarzad M., 2009. "Comparative study of methods of determination of coefficient of subgrade reaction". Electronic Journal of Geotechnical Engineering, Volume 14, Bund. E

Sap 2000 NonLinear Version 6.11, 1995. "Integrated finite element analysis and design of structures". Berkeley, California, USA: Computers and Structures, Inc.

Schiel F., 1942. "Der Schwimmende Balken". Z wandte Math Mech, Volume 22, pp. 255–62.

Seefeld S., Stockwell WR., 1999. "First-order sensitivity analysis of models with time-dependent parameters: an application to PAN and ozone". Atmospheric Environment, Volume 33 (18), pp. 2941–2953.

Selvadurai APS., 1985. "Soil–pipeline interaction during ground movement". In Bennett FL, Machemehl JL, editors, Arctic, Civil Engineering in the Arctic offshore. ASCE speciality conference, San Francisco, pp. 763–73

Shinozuka M., 1983. "Basic analysis of structural safety". Journal of Structural Engineering, ASCE, Volume 109(3), pp. 721–740.

Silva JL., El Debs MK., Beck AT., 2008. "Reliability evaluation of reinforced concrete pipes in crack opening limit state". Revista DAE, Volume 1(4), pp. 314–30.

Sitharam TG., Samui P., 2007. "Geostatistical modelling of spatial and depth variability of SPT data for Bangalore". Geomechanics and Geoengineering, Volume 2 (4), pp. 307–316.

Sivakumar Babu GL., Srivastava A., Murthy DSN., 2006. "Reliability analysis of bearing capacityof shallow foundation resting on cohesive soil". Canadian Geotechnical Journal Volume 43 (2), pp. 217–223.

Spies BR., 1989. "Depth of investigation in electromagnetics sounding methods". Geophysics, Volume 54, pp. 872–888.

Spies BR., 1996. "Electrical and electromagnetic borehole measurements: a review". Surveys in Geophysics Volume 17, pp. 517–556.

Srivastava A., Sivakumar Babu GL., 2009. "Effect of soil variability on the bearing capacity of clay and in slope stability problems". Engineering Geology, Volume 108, pp. 142–152.

Srivastava A., Sivakumar Babu GL., Haldar S., 2010. "Influence of spatial variability of permeability property on steady state seepage flow and slope stability analysis". Engineering Geology, Volume 110, pp. 93–101.

Stavridis LT., 2000. "Simplified analysis of layered soil-structure interaction". Journal of Structure Engineering (ASCE), Volume 128(2), pp. 224-230.

Taylor DW., 1964. "Fundamentals of soil mechanics". New York: John Wiley and Sons.

Terzaghi KV., 1955. "Evaluation of coefficient of subgrade reaction". Geotechnique, Volume 5(4), pp. 297-326.

Thierry P., Breysse D., 2006. Avec la collaboration de Vanoudheusden E., Marache A., Dominique S., Rodière B., Bourgine B., Regaldo Saint Blancard P., Piette C., Rivet F., Fabre R., "Projet RIVIERA: RIsque en VIlle, Equipement, Réseaux, Archéologie". Rapport final, 55085-FR, pp. 245, 3 annexes.

Tiktak A., Leijnse A., Veissenberg H., 1999. "Uncertainty in a regional-scale assessment of cadmium accumulation in the Netherlands". Journal of Environmental Quality, Volume 28 (2), pp. 461–470.

Tobutt DC., 1982. "Monte Carlo simulation methods for slope stability". Computers and Geosciences, Volume 8, pp. 199-208.

US. Army Corps of Engineers, 1997. "Engineering and design introduction to probability and reliability methods for use in geotechnical engineering". Engineering Technical Letter No. 1110-2-547. Department of the Army, Washington, D.C.

Uzielli M., Nadim F., Lacasse S., Kaynia AM., 2008. "A conceptual framework for quantitative estimation of physical vulnerability to landslides". Engineering Geology, Volume 102, pp. 251-256

Vallabhan CVG., Das YC., 1991. "Modified Vlassov model for beams on elastic foundation". J Geotech Engng, Volume 117(6), pp. 956–66.

Vanmarcke EH., 1977. "Probabilistic modeling of soil profiles". ASCE Journal of Geotechnical Engineering Volume 103 (11), pp. 1227–1246.

Vanmarcke EH., 1980. "Probabilistic stability analysis of earth slopes". Engineering Geology, Volume 16, pp. 29–50.

Vanmarcke EH., 1983. "Random fields: analysis & synthesis". MIT Press, Cambridge.

Vargas-Guzman JA., Yeh TCJ., 1999. "Sequential kriging and cokriging: two powerful geostatistical approaches". Stochastic Environmental Research and Risk Assessment, Volume 13, pp. 416-435.

Verpaux P., Charras T., Millard A., 1988. "Castem2000: une approche moderne du calcul des structures". In Calculs de Structures et Intelligence Artificielle, edited by J. Fouet, P. Ladevèze and R. Ohayon, (Pluralis).

Vesic AB., 1961. "Beams on elastic subgrade and Winkler's hypothesis". Proc. 5th International Conference on Soil Mechanic and Foundation Engineering, pp. 845-850.

Villavicencio AG, Breul P., Bacconnet C., Boissier D., Espinace AR., 2011. "Estimation of the variability of tailings dams properties in order to perform probabilistic assessment". Geotechnical and Geological engineering, Volume 29, issue 6, pp. 1073-1084.

Vlassov VZ., Leontiev NN., 1960. "Beams, plates and shells on an elastic foundation (in Russian)". Moscow, USSR: Fizmatgiz.

Vlassov VZ., Leontiev NN., 1966. "Beams, plates, and shells on elastic foundations". Translated from Russian, Israel Program for Scientific Translations. Jerusalem.

Wackernagel H., 2006. "Multivariate geostatistics: An Introduction with applications". third edition, Springer, New York.

Wang CM., Iang YX., Wang Q., 2001. "Axisymmetric buckling of reddy circular plates on Pasternak foundation". J Eng Mech ASCE, Volume 127(3), pp. 254–259.

Winkler E., 1867. "Die lehre von der elasticitaet und festigkeit". Prag: Dominicus.

Wolff TF., 1996. "Probabilistic slope stability in theory and practice". In Proceedings of the Conference on Uncertainty in the Geologic Environment, Uncertainty 96, Part 1 (of 2), Madison, Wis., pp. 419–433.

Xu W., Tran TT., Srivastava RM., Journel AG., 1992. "Integrating seismic data in reservoir modeling: the collocated cokriging alternative". In the proceedings of 67th annual technical conference of the society of petroleum engineering (Washington, 1992), no. 24742 in SPE, pp. 833-842.

Yoon GL., Lee KW., Chae YS., Kim DH., Kim HY., 2007. "Spatial variability of undrained shear strength of marine clay from geostatistical approach". In Applications of Statistics and Probability in Civil Engineering, Kanda, Takada & Furuta (Eds), pp. 109-116.

Zevgolis IE., Bourdeau PL., 2010. "Probabilistic analysis of retaining walls". Computers and Geotechnics, Volume 37, pp. 359–373.

Zhang LM., Tang WH., Ng CWW., 2001. "Reliability of axially loaded driven pile groups". J Geotech Geoenviron Eng ASCE, Volume 127(12), 1051-60.

Ziaie Moayed R., Naeini SA., 2006. "Evaluation of modulus of subgrade reaction in gravely soils based on standard penetration test (SPT)". Proceedings of the Sixth International Conference on Physical Modelling in Geotechnics, 6th ICPMG, Hong Kong, Chapter 115.

Ziaie-Moayed R., Janbaz M., 2009. "Effective Parameters on Modulus of Subgrade Reaction in Clayey Soils". Journal of Applied Sciences, Volume 9, pp. 4006-4012. DOI: 10.3923/jas.2009.4006.4012.

Appendices

Appendix 1

1. Reliability analysis for a continuous spread footing by the hypothesis of a log-normal distribution
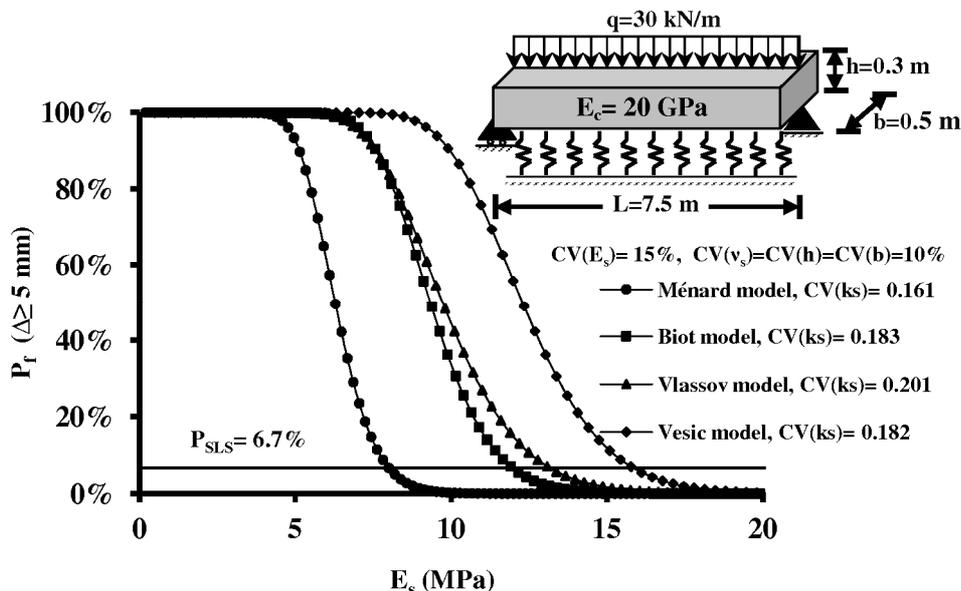

Fig. 1: *Estimation of the probability of failure (P_f) as function of E_s for a maximum differential settlement of a spread footing with simply supported at two ends as boundary conditions (for the four semi-empirical models).*
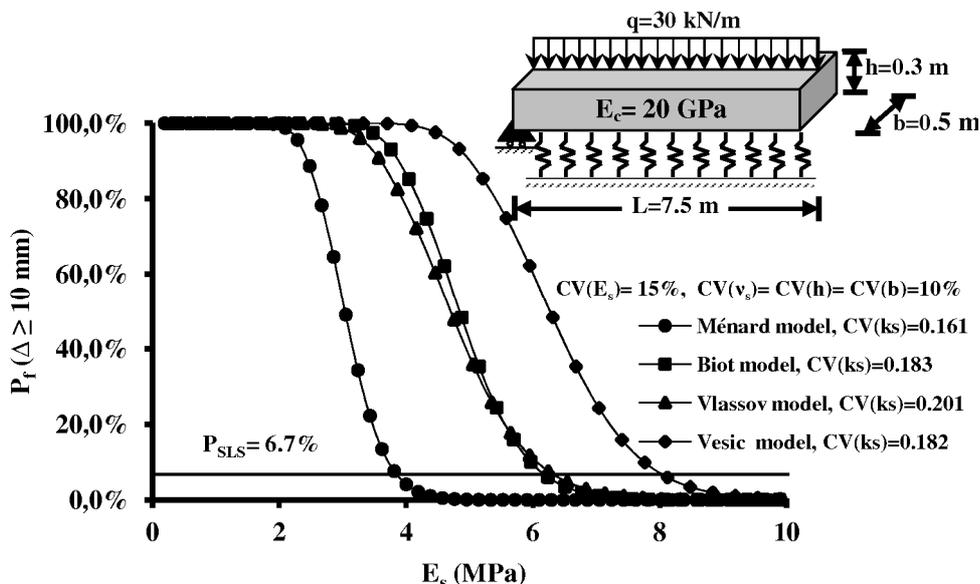

Fig. 2: *Estimation of the probability of failure (P_f) as function of E_s for a maximum differential settlement of a spread footing with simply supported at one end as boundary conditions (for the four semi-empirical models).*
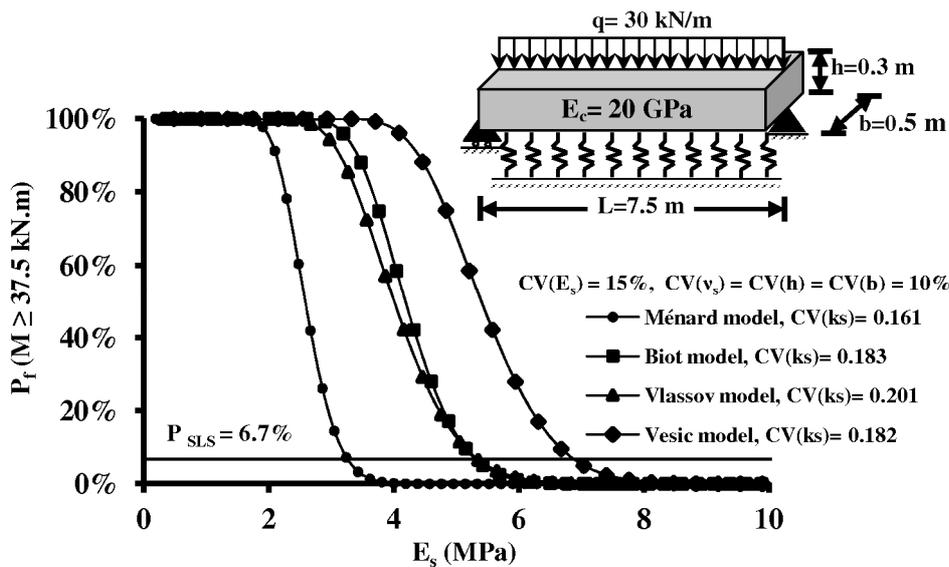
Fig. 3: *Estimation of the probability of failure (P_f) as function of E_s for a maximum elastic bending moment of a spread footing with simply supported at two ends as boundary conditions (for the four semi-empirical models).*
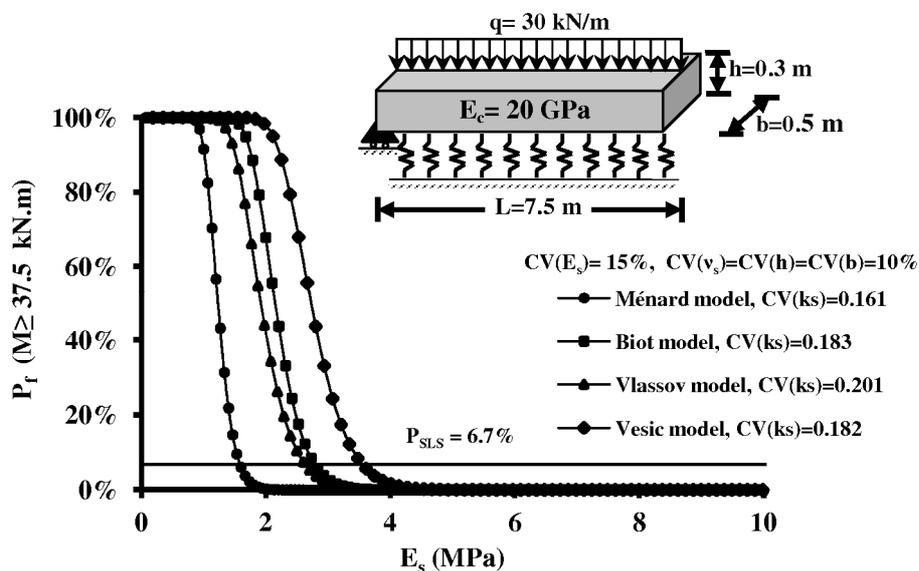

Fig. 4: *Estimation of the probability of failure (P_f) as function of E_s for a maximum elastic bending moment of a spread footing with simply supported at one end as boundary conditions (for the four semi-empirical models).*
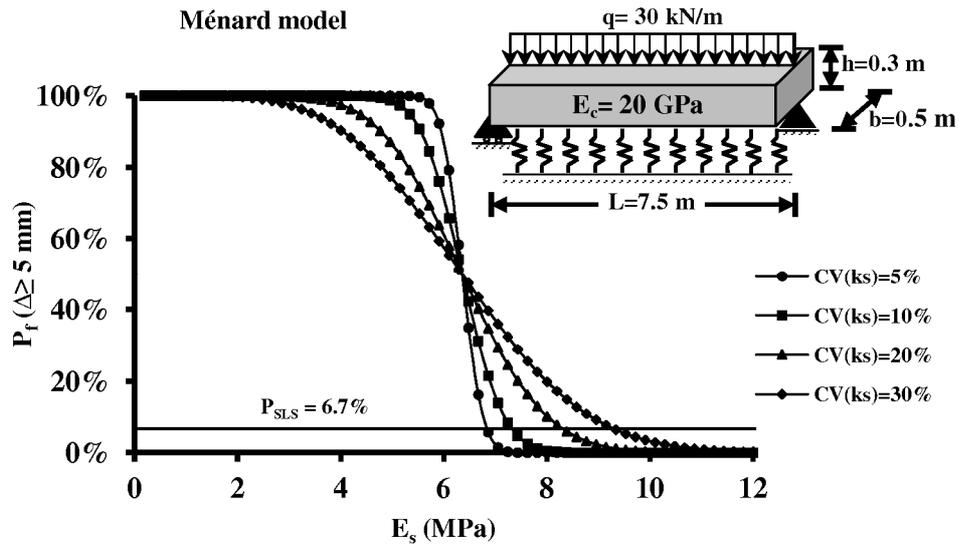
Fig. 5: *Probability of failure (P_f) for a maximum differential settlement of a spread footing with simply supported at two ends as boundary conditions for different values of CV_{ks} (Ménard's model).*
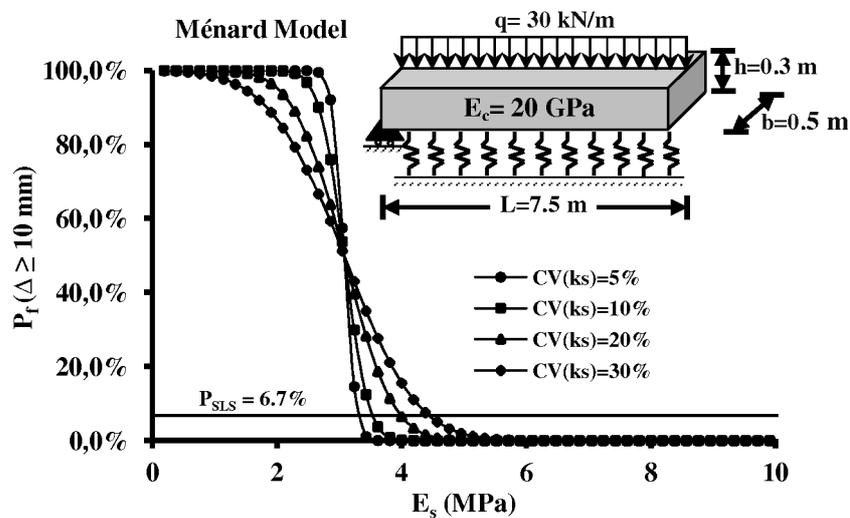
Fig. 6: *Probability of failure (P_f) for a maximum differential settlement of a spread footing with simply supported at one end as boundary conditions for different values of CV_{ks} (Ménard's model)*

243

2. Buried pipes (continuous buried steel pipes and buried concrete pipes)

2.1. Estimation of the uncertainty of the differential settlement and bending moment (for a continuous buried steel pipe)
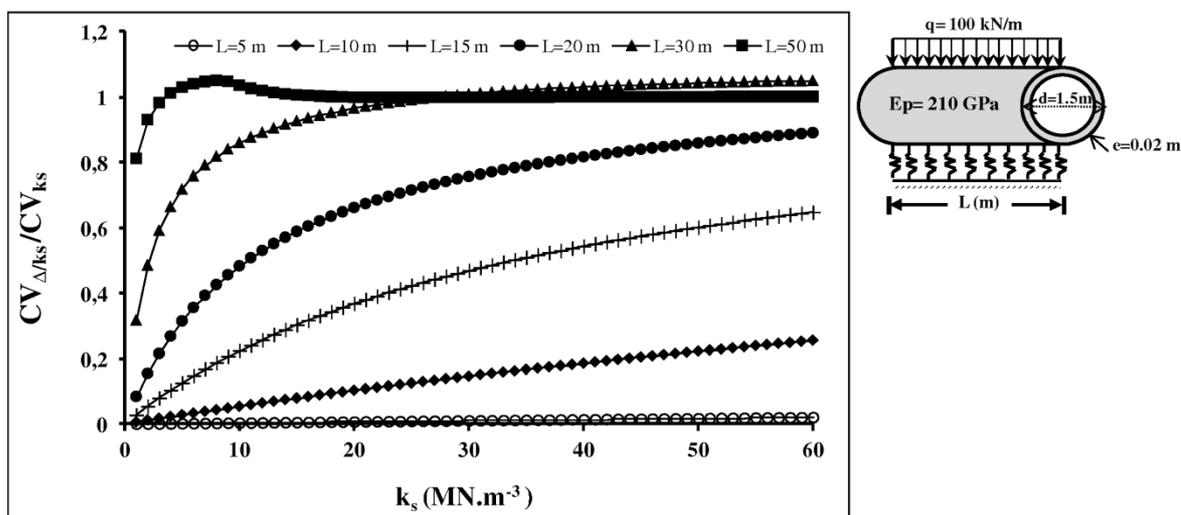
**Fig. 7:** *Influence of the uncertainty of k_s on the uncertainty of the maximum differential settlement for the different low stiffness zone lengths (L) ($CV_{\Delta/ks}$: coefficient of variation of the differential settlement with respect to k_s, CV_{ks}: coefficient of variation of k_s).*
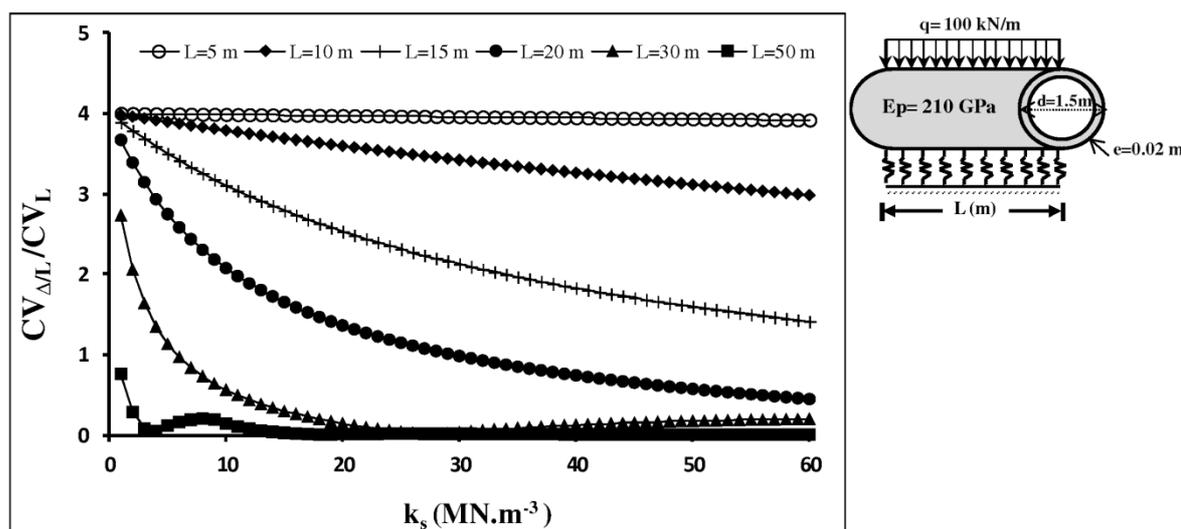
Fig. 8: *Influence of the uncertainty of L on the uncertainty of the maximum differential settlement for the different low stiffness zone lengths (L) ($CV_{\Delta/L}$: coefficient of variation of the differential settlement with respect to L, CV_L: coefficient of variation of L).*
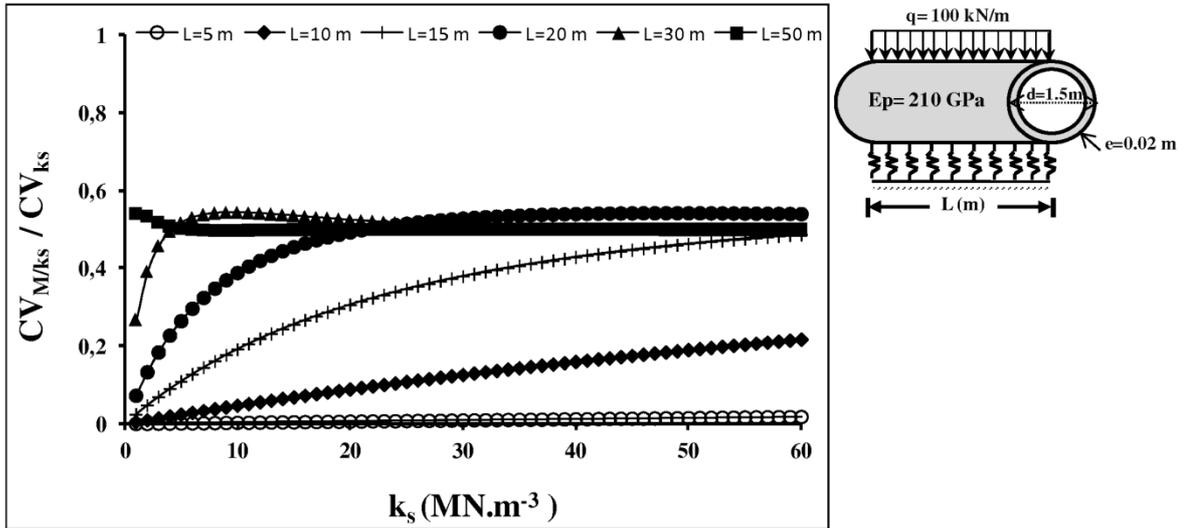
Fig. 9: *Influence of the uncertainty of k_s on the uncertainty of the maximum bending moment for the different low stiffness zone lengths (L) ($CV_{M/ks}$: coefficient of variation of the bending moment with respect to k_s).*
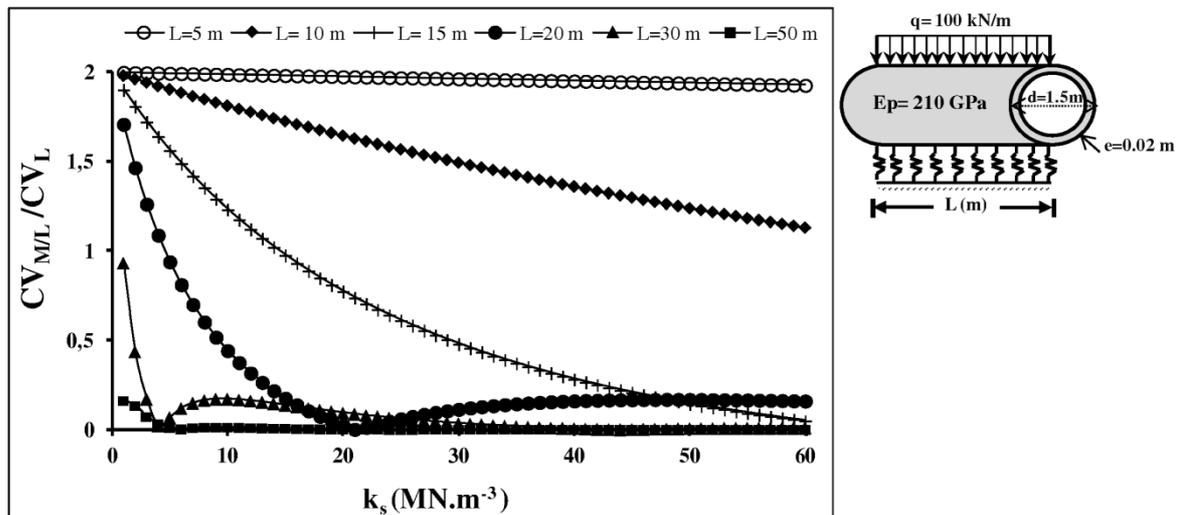

Fig. 10: *Influence of the uncertainty of L on the uncertainty of the maximum bending moment for the different low stiffness zone lengths ($CV_{M/L}$: coefficient of variation of the bending moment with respect to L).*

## 2.2. Reliability analysis for a buried concrete pipe by the hypothesis of a log-normal distribution
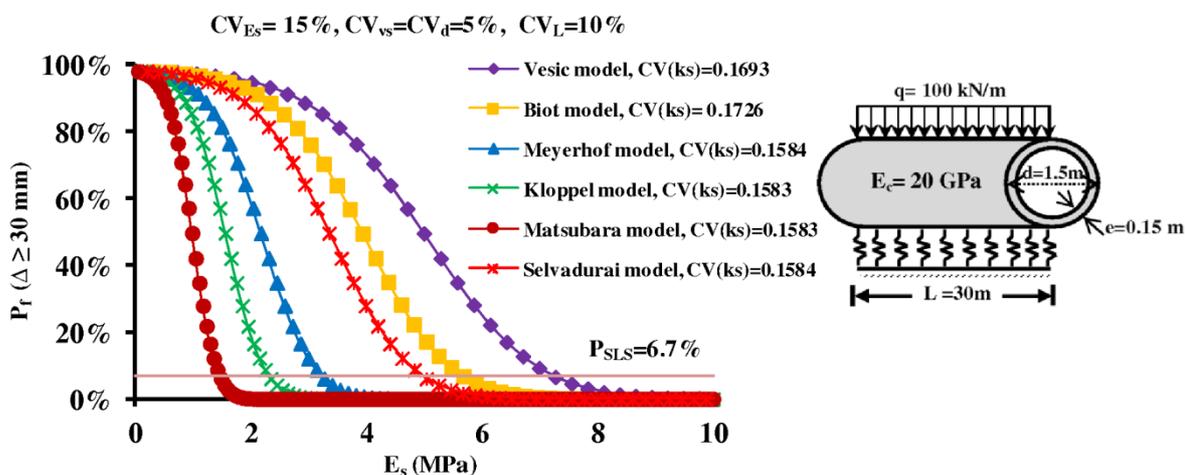
Fig. 11: *Estimation of the probability of failure (P_f) as function of E_s for a maximum differential settlement of a buried pipe (for the six semi-empirical models).*
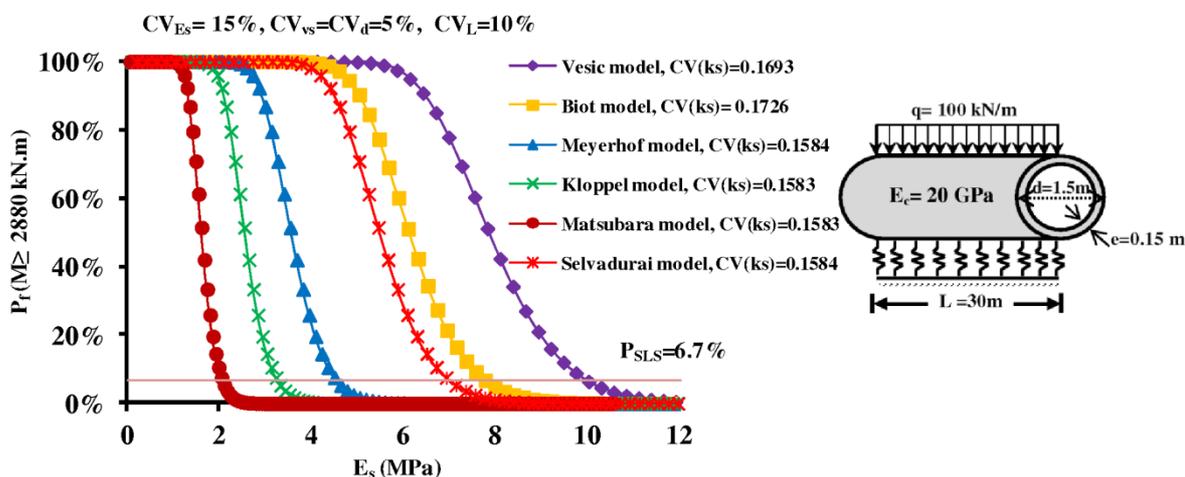

Fig. 12: *Estimation of the probability of failure (P_f) as function of E_s for a maximum elastic bending moment of a buried pipe (for the six semi-empirical models and for a maximum elastic stress of concrete equal to 10 MPa).*
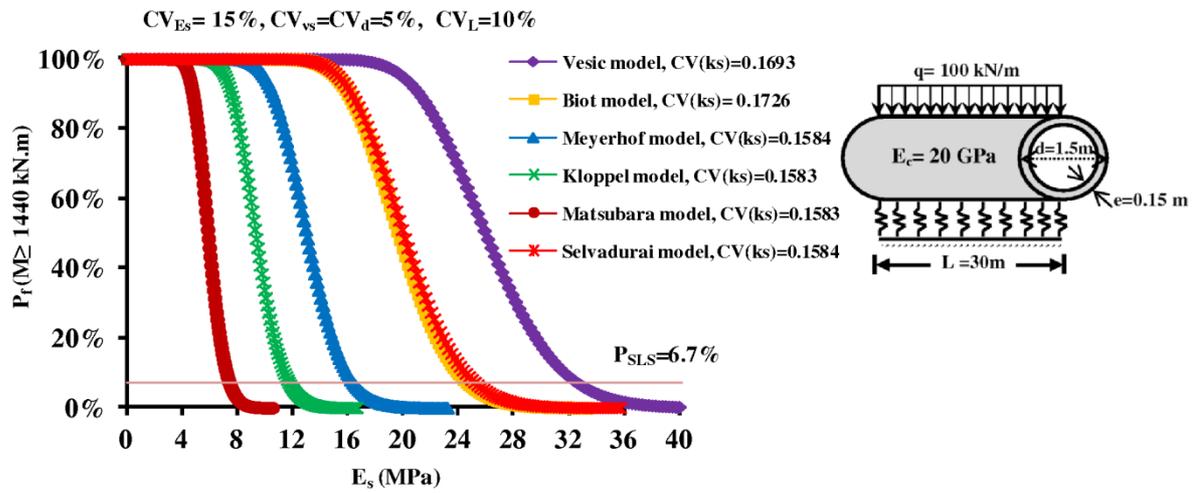
Fig. 13: *Estimation of the probability of failure (P_f) as function of E_s for a maximum elastic bending moment of a buried pipe (for the six semi-empirical models and for a maximum elastic stress of concrete equal to 5 MPa).*
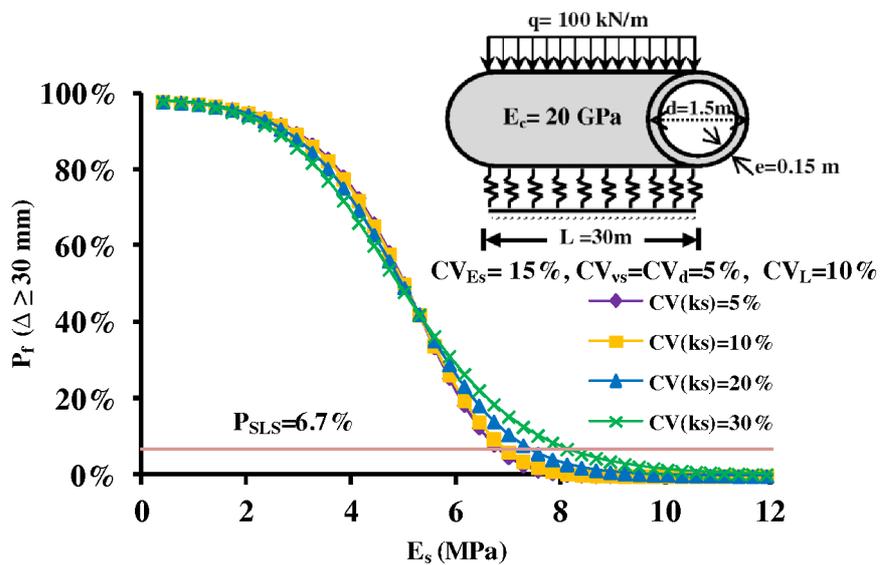

Fig. 14: *Probability of failure (P_f) for a maximum differential settlement of a buried pipe for different values of CV_{ks} (Vesic's model)*
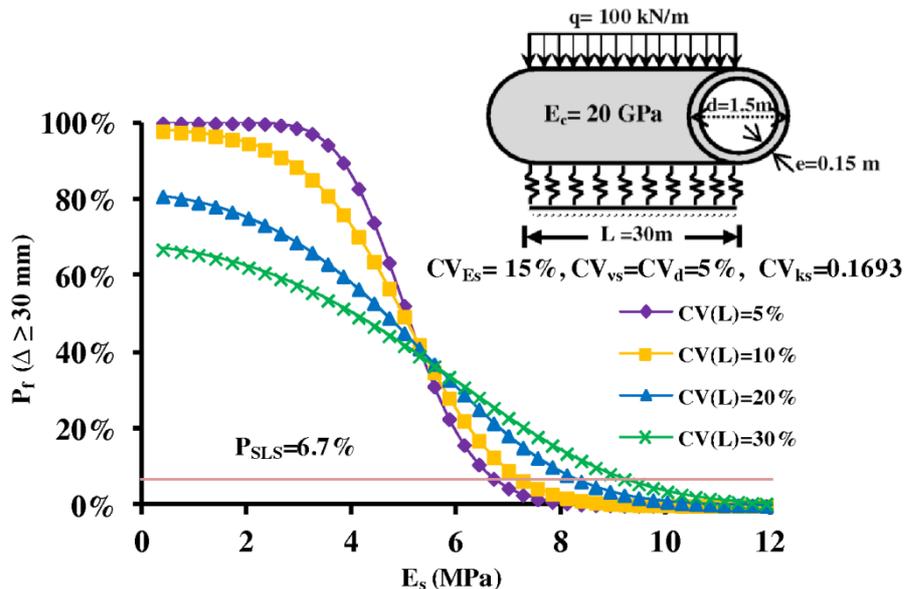
Fig. 15: *Probability of failure (P_f) for a maximum differential settlement of a buried pipe for different values of CV_L (Vesic's model)*
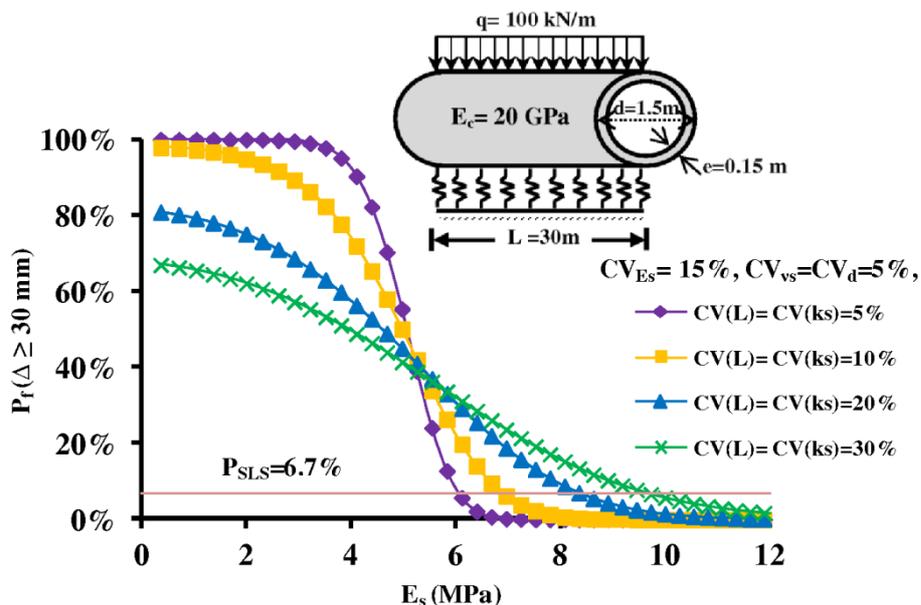

Fig. 16: *Probability of failure (P_f) for a maximum differential settlement of a buried pipe for different values of CV_ks and CV_L (Vesic's model)*

2.3. Application to global uncertainty analysis (for a continuous buried steel pipe)
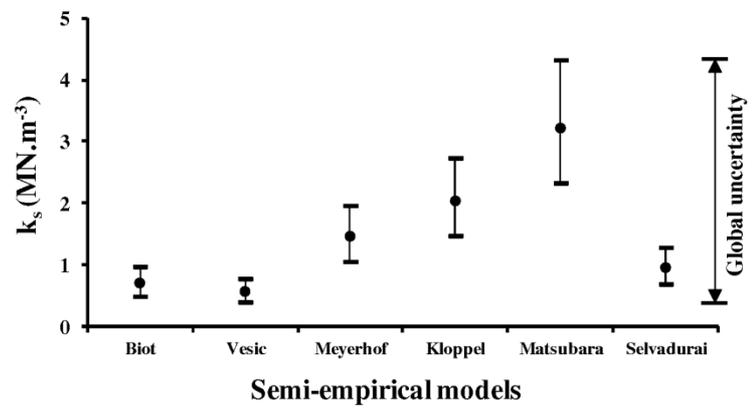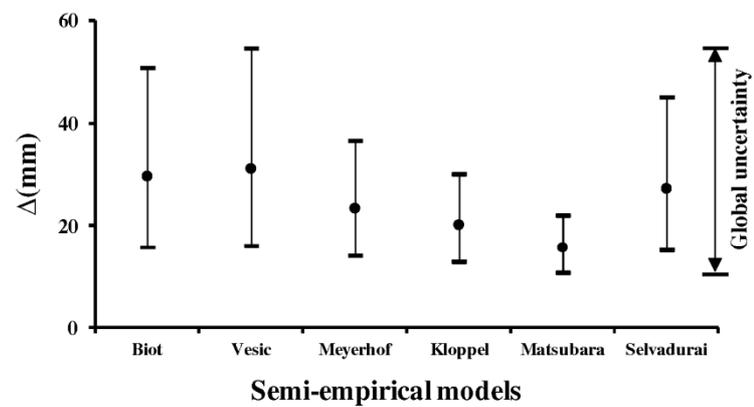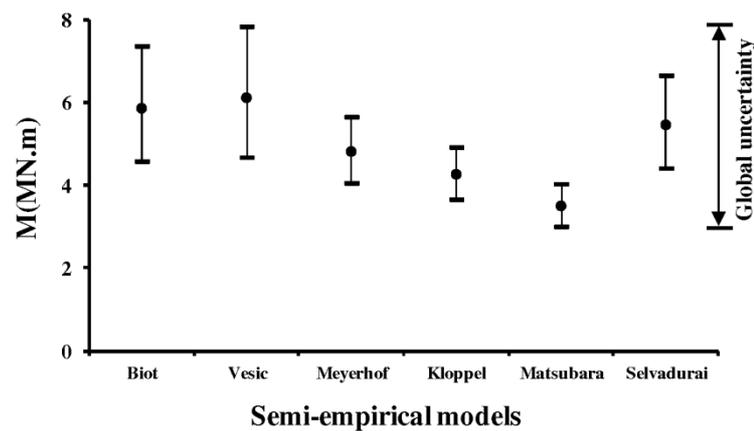
Fig. 17: *Global uncertainties for the a) Subgrade reaction modulus k_s, b) Maximum differential settlement Δ and c) Maximum bending moment M by considering 95% confidence bound for each semi-empirical model with log-normal distribution ($E_s=2$ MPa, $E_p=210$ GPa, $v_s=0.3$, $d=1.5$ m, $e=0.02$ m, $L=30$ m, $q=100$ kN/m, $CV_{Es}=15\%$, $CV_L=10\%$, $CV_d=CV_{vs}=CV_{Ep}=5\%$).*

249

Appendix 2

Table 1: Comparison of the settlement between analytical and numerical methods for a spread footing of 10 m at location (1)

Statistical parameters	**Ménard**	**Vesic**	**Biot**	**Vlassov**	Considered methods
$E[\overline{\Delta}]$ (mm)	4.566	9.446	7.104	7.116	Numerical methods (ISATIS© and CASTEM©)
$Var[\overline{\Delta}]$ (mm)^2	0.060	0.304	0.180	0.148	
$CV[\overline{\Delta}]$	0.0536	0.0584	0.0597	0.0540	
$CV_T[\Delta]$	0.0228	0.0251	0.0251	0.0228	Analytical method (obtained from theory)
$CV[\Delta]$	0.0229	0.0247	0.0254	0.0229	Analytical method (obtained from 1000 simulations)
$E[\Delta]$ (mm)	4.209	8.667	6.499	6.567	
$Var[\Delta]$ (mm)^2	0.009	0.046	0.027	0.023	
$E[\Delta]/E[\overline{\Delta}]$	92.2%	91.7%	91.5%	92.3%	Contribution to the estimated settlement
$Var[\Delta]/Var[\overline{\Delta}]$	15%	15.1%	15%	15.5%	Contribution to the variability of settlement

$E[\overline{\Delta}], Var[\overline{\Delta}], CV[\overline{\Delta}]$ *are respectively the mean, variance and coefficient of variation of the absolute settlement from numerical methods, $CV_T[\Delta]$: coefficient of variation of the absolute settlement using analytical method (obtained from theory), $E[\Delta]$, $Var[\Delta]$ and $CV[\Delta]$: are respectively the mean, variance and coefficient of variation of the absolute settlement using analytical method (obtained from 1000 simulations). The mean, variance and coefficient of variation of E_s for the location (1) are respectively $E[\overline{E_s}]$ =6.791 MPa, $Var[\overline{E_s}]$=0.024 (MPa)^2 and $CV[\overline{E_s}]$=0.0228. $\overline{\Delta}$: settlement from the total spatial variability, Δ: settlement from the analytical method (E_s is constant).*

Table 2: Comparison of the settlement between analytical and numerical methods for a spread footing of 10 m at location (2)

Statistical parameters	**Ménard**	**Vesic**	**Biot**	**Vlassov**	Considered methods
$E[\overline{\Delta}]$ (mm)	4.280	8.800	6.609	6.667	Numerical methods (ISATIS© and CASTEM©)
$Var[\overline{\Delta}]$ (mm)^2	0.0195	0.092	0.056	0.046	
$CV[\overline{\Delta}]$	0.0326	0.0344	0.0357	0.0322	
$CV_T[\Delta]$	0.0231	0.0254	0.0254	0.0231	Analytical method (obtained from theory)
$CV[\Delta]$	0.0234	0.0253	0.0260	0.0234	Analytical method (obtained from 1000 simulations)
$E[\Delta]$ (mm)	4.160	8.558	6.415	6.490	
$Var[\Delta]$ (mm)^2	0.0095	0.047	0.028	0.023	
$E[\Delta]/E[\overline{\Delta}]$	97.2%	97.3%	97.1%	97.3%	Contribution to the estimated settlement
$Var[\Delta]/Var[\overline{\Delta}]$	48.7%	51.1%	50%	50%	Contribution to the variability of settlement

The mean, variance and coefficient of variation of E_s for the location (2) are respectively $E[\overline{E_s}]$ =6.872 MPa, $Var[\overline{E_s}]$ =0.0253 (MPa)^2 and $CV[\overline{E_s}]$ =0.0231